Synthesis and *In vitro* Evaluation of Triphenylethylene and Naphthalimide Derivatives for Anticancer Activity

A thesis submitted in the fulfillment of the

requirement for the degree of

Doctor of Philosophy

by

Sudesh Rani

(Regn. No. 901509020)

Under the supervision of

Dr. Kamaldeep Paul

(Professor)

SCHOOL OF CHEMISTRY AND BIOCHEMISTRY

THAPAR INSTITUTE OF ENGINEERING AND TECHNOLOGY

PATIALA-147004

PUNJAB

May 2021

Certificate

It is certified that the work contained in the thesis entitled "**Synthesis and *In vitro* Evaluation of Triphenylethylene and Naphthalimide Derivatives for Anticancer Activity**" by Sudesh Rani in fulfilment of the degree of Doctor of Philosophy, is an authentic record of candidate's own independent and original research work carried out under my supervision in the School of Chemistry and Biochemistry, Thapar Institute of Engineering and Technology, Patiala, Punjab-India. The material embodied in this thesis has not been submitted in part or full to any other University or Institute for the award of any degree.

Dr. Kamaldeep Paul 16/6/21

(Supervisor)

Professor

School of Chemistry and Biochemistry,

Thapar Institute of Engineering and Technology,

Patiala – 147004, Punjab (India)

Dr. Susheel Mittal 21/6/21

(Head, SCBC)

Sr. Professor

School of Chemistry and Biochemistry,

Thapar Institute of Engineering and Technology,

Patiala – 147004, Punjab (India)

Candidate's Declaration

I hereby declared that the presented work in the thesis entitled "**Synthesis and *In vitro* Evaluation of Triphenylethylene and Naphthalimide Derivatives for Anticancer Activity**" in fulfillment of the degree of Doctor of Philosophy is the outcome of research work carried out by me under the supervision of Dr. Kamaldeep Paul, Associate Professor, School of Chemistry and Biochemistry, Thapar Institute of Engineering & Technology, Patiala, Punjab (India). This work has not been submitted in part or whole to any other University or Institute for the award of any degree.

Sudesh Rani
Reg. No. 901509020
School of Chemistry and Biochemistry,
Thapar Institute of Engineering and Technology,
Patiala – 147004, Punjab (India)

Dr. Kamaldeep Paul 1/6/21
(Supervisor)
Professor
School of Chemistry and Biochemistry,
Thapar Institute of Engineering and Technology,
Patiala – 147004, Punjab (India)

Acknowledgment

I may halt for a while to record my gratefulness to all those who have made a contributed to the successful completion of this thesis. Above all, I express my gratitude to the family members for their blessings and support. I acknowledge the gratitude towards my respected supervisor Dr. Kamaldeep Paul, Associate professor, School of Chemistry and Biochemistry (SCBC), Thapar Institute of Engineering & Technology, Patiala (Punjab, India), for the opportunity to work in his group. His inspiring guidance, academic support, encouragement, and motivation made this work possible. I thank him for his help in the writing this dissertation, other research articles and for improving me at scientific communication and style.

I express my gratitude to Director (Thapar Institute of Engineering & Technology, Patiala), Dr. Rafat Siddique (Dean of Research and Sponsored Projects), Prof. O. P. Pandey (former Dean RSP), Dr. Susheel Mittal (Head, SCBC), Dr. Amjad Ali (Former Head, SCBC), Prof. Bonamali Pal (Former Head, SCBC) for all facilities which have been immensely helpful in completing my work.

I am also thankful to all my respected teachers of the School of Chemistry and Biochemistry (SCBC) and my doctoral committee members Dr. Satnam Singh, Dr. Manmohan Chhibber, Dr. Mondem Sudhakra Reddy, for their valuable suggestion and motivation at every step during my whole thesis work.

During my Ph.D. studies, I had the opportunity to work in close collaborations with other research groups. I want to express my sincere thank to Dr. Vijay Luxami for her initial days of co-operation and for inspiring me to learn spectroscopy studies. I thank her group members, especially Dr. Gulshan Kumar, Dr. Richa Rani, for their support and discussion.

Time flew by in the company of good friends, and therefore, a special thanks to Iqubal Singh, Richa Bansal, Ruhi Mehta, Aastha Palta, Dinesh Singla, Rekha Thakur, Saurabh Gupta, Rohini Gupta, Geetika Rani, Palak Sharma, and Nandan Sarkar. I want to extend the thanks to other colleagues Mandeep Kaur and Konpal Raheja, for creating a great work atmosphere and help at different stages during my course study. I extend my gratitude to other research scholars Anju Gahalawat, Raviza, Yuvraj Garg, Anirudh Sharma, Aadil Bathla, Santosh Kumar Rath, and others not mentioned by name for their support and encouragement. I express my warm thanks to

my colleagues and friends who spent and enjoyed scientific and social activities with me. I now have a forever collection of stories and a lot of everlasting memories to tell.

I would also like to thank Dr. Baldev Singh and Gurpreet Singh for their scientific and non-scientific help during my Ph.D. studies.

Another round of thanks for friends away from here; Yadwinder Singh, Perminder Kaur, Gurdeep Singh, Harish Kumar Goyal, Sidharth Sharma, Navpreet Kaur, Niffali Mittal, Priya Gupta, Parveen Kumar, and Tejinder Sharma for a laugh whenever possible.

I want to thank Sakshi Bhardwaj, who always encouraged and helped me in tough times. I appreciate her compassion, understanding, and what she did for me.

I acknowledge the help of Mr. Mayank Sharma, office staff, and Chander Singh Thakur, Chandar Shekhar, Hemant Sharma, and Vishwanath Dass, technical staff of School of Chemistry and Biochemistry, for their support in various aspects.

I extend my thankful acknowledgment to SAI Labs, Thapar Institute of Engineering & Technology, Patiala; SAIF Lab, Panjab University, Chandigarh; CIL, IIT Ropar; Imtech, Chandigarh for providing experimental instrumentation. I extend my gratitude to Mr. Mukesh Aggarwal, SAI Labs, Thapar Institute of Engineering & Technology, Patiala, during NMR/CHNS data collection. I am also thankful to National Cancer Institute, the USA, for anticancer activity.

I thankfully acknowledge Thapar Institute of Engineering & Technology, Patiala, for providing teaching assistantship during my course.

Finally, none of this would have been possible without the constant love, support, guidance, and patience of all my family members. I owe my gratitude to my respected Father-Mother and Uncle-Aunty, whose blessings, belief, and encouragement have shown me the path to pursue goals in my life. I thank my brothers for everything they have done for me. And a special thanks to my sister, who always stands for me. They all have been amazing and have always been there for me. I cannot thank them enough. Thank you for your everlasting love and support.

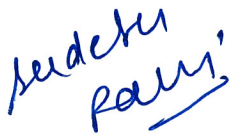

Dedication

I want to dedicate this thesis to my elder sister Geeta Gandhi, who always inspires and gives me strength; who provided moral, spiritual, emotional and financial support. Today what I am, it is only possible due to your support. Your belief in me and other chit-chat deepen me with positivity and, thus, made this journey possible.

Abbreviations

Å	Angstrom
μM	Micromolar
5-FU	5-Fluorouracil
ADP	Adenosine diphosphate
ACN	Acetonitrile
AF	Amonafide
Ala	Alanine
ArH	Aromatic hydrogen
Arg	Arginine
Asn	Asparagine
ATP	Adenosine triphosphate
R-B(OH)$_2$	Boronic acid
BSA	Bovine serum albumin
CDCl$_3$	Deuterated chloroform
COSY	Co-relation spectroscopy
DMF	Dimethylformamide
DMSO-d_6	Hexadeuterodimethyl sulfoxide
DNA	Deoxyribonucleic acid
Et-OH	Ethyl alcohol
ER	Estrogen receptor
FRET	Föster resonance energy transfer
GI%	Growth Inhibition

GI_{50}	Median growth inhibition concentration
Gly	Glycine
H-bonding	Hydrogen bonding
HPLC	High-performance liquid chromatography
HSA	Human serum albumin
IC_{50}	Median inhibition concentration
IPA	Isopropyl alcohol
LC_{50}	Median lethal concentration
Leu	Leucine
LOD	Limit of detection
Lys	Lysine
Met	Methionine
mg	Milligram
MG-MID	Mean graph mid-point
min	Minutes
MH	Molecular hybridization
MTT	3-(4,5-Dimethylthiazol-2-yl)-2,5-diphenyl tetrazolium bromide
NCI	National cancer institute
NMR	Nuclear magnetic resonance
NOE	Nuclear Overhausser effect
NT	Not treated
$Pd(PPh_3)_2Cl_2$	Bis(triphenylphosphine)palladium(II)chloride
$Pd(PPh_3)_4$	Tetrakis(triphenylphosphine)palladium(0)

PDB	Protein data bank
Phe	Phenylalanine
ppm	Parts per million
Py	Pyridine
SAR	Structure-activity relationship
SDS	Sodium dodecyl sulfate
Ser	Serine
SERM	Selective estrogen receptor modulator
TAM	Tamoxifen
TBAI	Tetrabutylammonium iodide
TGI	Total growth inhibition concentration
Thr	Threonine
THF	Tetrahydrofuran
TOPO-II	Topoisomerase-II enzyme
TPE	Triphenylethylene
TPE-naph	Triphenylethylene-naphthalimide
TPSA	Total polar surface area
Trp	Tryptophan
Tyr	Tyrosine
USA	United States America
UV	Ultra-violet
Val	Valine
Zn	Zinc

Content

INTRODUCTION

Cancer is a cluster of diseases that accounts for the leading cause of mortality globally. The incidence of cancer continues to increase in developing as well as developed countries.[1] According to World Health Organization (WHO) report, about 17.0 million cancer cases were diagnosed and 9.5 million died from cancer worldwide in 2018.[2] It was also estimated that over 19.3 million cases of cancer were diagnosed and that 10 million people died from this disease in 2020.[3] The most significant number of deaths are caused due to lung cancer (18.4%) followed by colorectal cancer (9.2%), liver cancer (8.3%), stomach cancer (7.7%), and female breast cancer (6.9%).[3] Moreover, it has been reported that about 12.7 million cancer cases and 7.6 million cancer deaths are estimated to have occurred in 2008.[4] Thus, the new figures indicated that the incidence of cancer and mortality are increasing at an alarming rate. Researchers have made considerable progress in drug discovery in the past decades but inefficient in bringing novel drugs for clinical evaluation.[5] Therefore, cancer remains one of the most promising challenges in the 21st century despite many therapeutic successes.

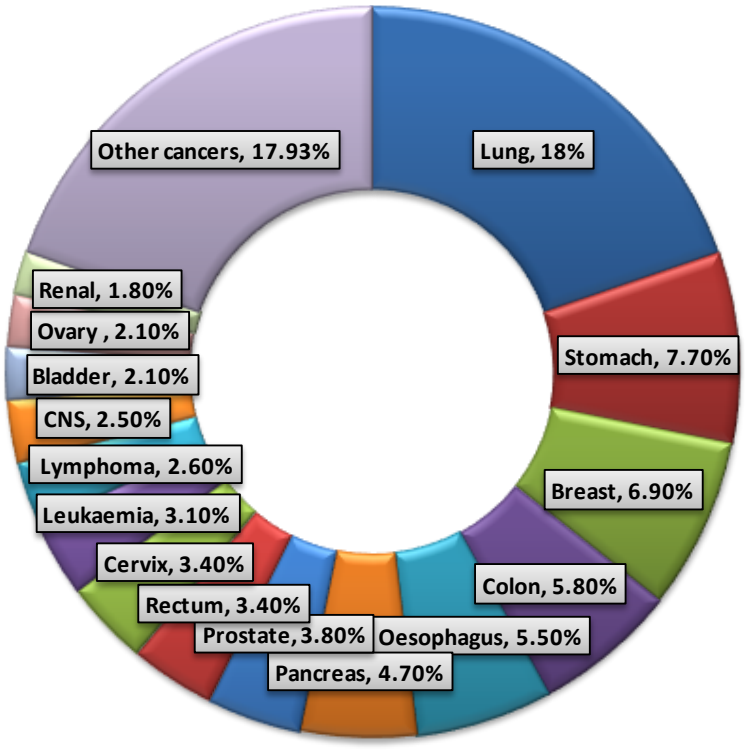

Figure 1: Worldwide percentage of mortality rates due to cancer in 2020[3]

At present, the traditional paradigm in cancer therapy targets DNA or inhibiting the pathways which mediate and regulate the cell division or replication and transcription of DNA.[6] Although for cancer drug development in pharmaceuticals, inhibition of TOPO-II enzymes has long attracted interest. Type II topoisomerase regulates DNA topology by making a double-stranded break in one DNA duplex, transporting another DNA segment through this break, and then resealing it.[7] A number of genetic factors emerged in cancer therapy, between the susceptibility of cancer cells and lack of autophagic machinery.[8] The efficacy of conventional prescribed antineoplastic drugs is often limited due to their high toxicity to normal cells, acquired resistance after long term drug administration, and difficulty in delivery of existing drugs to target sites.[9] To improve drug perfusion, potency and oral bioavailability, and to develop a new set of potential target with optimal physicochemical profile, immense efforts have been devoted. Chemotherapeutic agents efficiency and specificity towards cancer cells has also been improved by synthesizing the compounds through systematic strategies and molecular hybridization techniques.[10] In the last decades, the "one drug multiple targets" approach has also attracted significant attention in drug discovery.[11] Several aromatic and heterocyclic functionalities such as triphenylethylene and naphthalimide analogues have been reported in the literature possessing excellent anticancer activity.[12,13]

The aromatics and heterocycles are of great interest in pharmaceuticals and medicinal chemistry.[14] Tri/tetra aryl or hetero aryl substituted ethylene compounds (**Figure 2**) belong to a class of drug called Selective Estrogen Receptor Modulator (SERM).[15] These have substantial

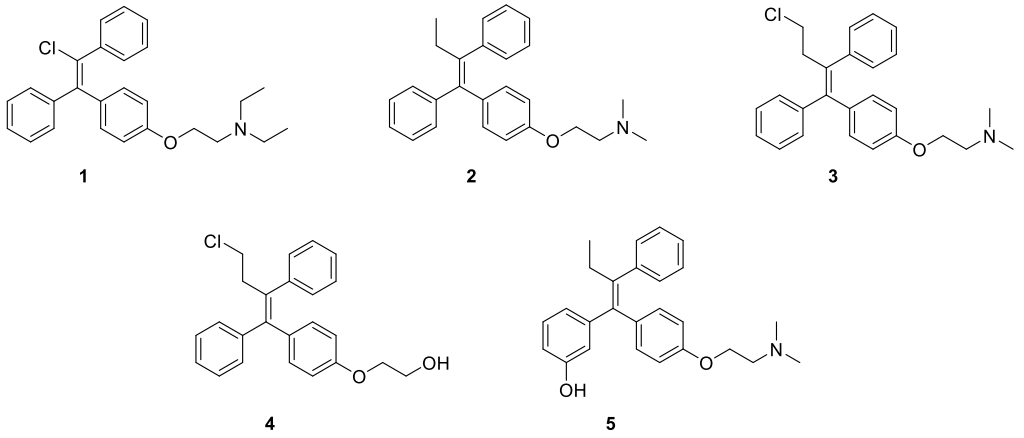

Figure 2: Structure of triphenylethylene drugs; clomiphene (**1**), tamoxifen (**2**), toremifene (**3**), ospemifene (**4**) and droloxifene (**5**)

significance as anticancer drugs such as tamoxifen (**2**), and its analogues clomiphene (**1**), toremifene (**3**), ospemifene (**4**) and droloxifene (**5**) etc.[16] Tamoxifen (**2**) is a prodrug acting as both a competitive antagonist to the estrogen receptor in breast cells as well as partial agonist to endometrial cells.[17] Due to its partial agonist behaviour, it should be modified, therefore, various aryl substituted olefins have attracted the attention of numerous researchers over many years. Substituted olefins have been studied extensively due to their wide range of pharmacological applications.

Introduction of heteroatoms such as oxygen, nitrogen and sulfur in the core structure of aromatic or aliphatic carbon moieties formulate compounds showing pharmacological and biological activities. Various components such as vitamins, antibiotics, alkaloids, hormones, synthetic drugs, and dyes contain heterocyclic and aromatic ring systems. Naphthalimide is a class of heterocycles, constituting π-deficient planar aromatic structure and a versatile pharmacophore with diverse biological applications in pharmaceuticals such as anticancer, analgesic, antiviral, and antibacteria.[18] The biological potential of naphthalimides has been explored through different mechanisms. Naphthalimides exert antiproliferative activity due to their ability to intercalate between base pairs of DNA (DNA-intercalation), minor groove binding and inhibit topoisomerase. Besides acting as anticancer agents, naphthalimides, due to high absorption coefficient, high fluorescence quantum yield and high photostability, are employed as protein sensor probes. These immense pharmacological significances and photophysical properties of naphthalimides prompted us to synthesize new derivatives of low toxicity and high potency.

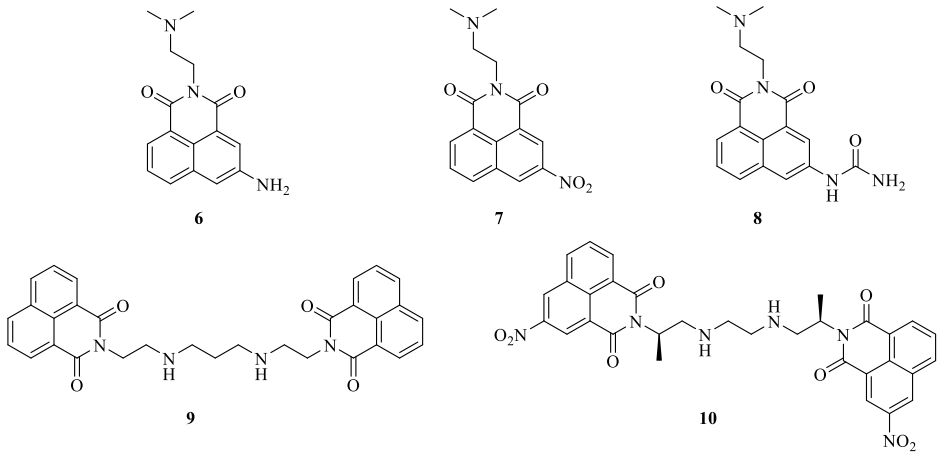

Figure 3: Structures of biological-active naphthalimide; amonafide (**6**), mitonafide (**7**), UNBS5162 (**8**), elinafide (**9**) and bisnafide (**10**).

In the quest for potent anticancer agents, we had designed and synthesized triphenylethylene and naphthalimide analogues. These newly synthesized derivatives have been evaluated for their anticancer activity against 60 human cancer cell lines. Further, the mechanism of their cytotoxicity has been explored through TOPO-II inhibition. Also the binding interactions of these moieties with human serum albumin and bovine serum albumin have been studied through spectroscopy techniques. To determine the interaction of synthesized derivatives with enzymes/serum albumins, molecular docking studies have been performed. In this dissertation, the work accomplished is categorized into the following parts:

Chapter 1: Review of literature
Chapter 2: Triphenylethylene analogues
Chapter 3: Triphenylethylene-naphthalimide conjugates
Chapter 4: Benzothiazole appended naphthalimides

CHAPTER 1
REVIEW OF LITERATURE

Marketed drugs with incredible versatility and optimal physicochemical properties are the fundamental pillars of medicinal chemistry. Since the discovery of anticancer agents, triphenylolefins and heterocycles are intense areas of research. Extensive reports on the development of triphenylethylene and naphthalimide analogues as anticancer agents have been reported in the literature.

1.1 Biological activity of triphenylethylene based compounds

Christoudolu *et al.* in 2013 synthesized a novel series of tamoxifen derivatives bearing amide group as a side chain and evaluated their anticancer activity against MCF-7 (breast cancer), HeLa (cervix adenocarcinoma), and MSTO-211H (biphasic mesothelioma) cell lines.[19] The *E*/*Z* stereochemical assignments of compounds **11a-g** and **12a-g** were made on the basis of the 2D-NOESY experiment. The mechanism of cytotoxicity has been explored by topoisomerase-I and -II inhibition assay. Analogue **11b** (GI_{50} = 2.9 μM) was found to be 4-times more potent towards MCF-7 cell line than reference drug tamoxifen (GI_{50} = 12.0 μM) while **12b** exhibited potency against HeLa cell line with GI_{50} value of 6.7 μM. Analogue **11g** substituted with piperidine displayed promising anticancer activity against MSTO-211H with GI_{50} value of 2.3 μM. Compound **12d** substituted with *N*,*N*-dimethylamino group (*Z*-isomer) exhibited two times more potency than **11d** (*E*-isomer) towards MCF-7, HeLa and MSTO-211H cell lines. It has been observed that compounds **11a-g** and **12a-g** exerted more activity towards HeLa and MSTO-211H cell lines when compared to tamoxifen but less effective than 4-OH tamoxifen.

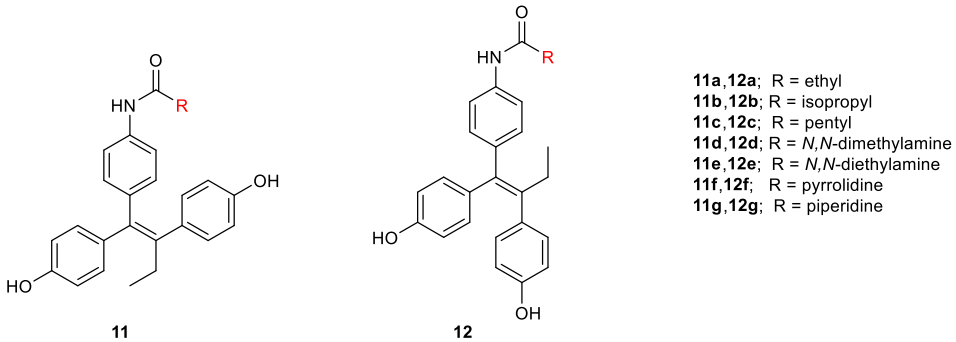

Christoudolu *et al.* synthesized derivatives of 4-(1,2-diarylbut-1-en-1-yl)isobutyranilide as topoisomerase-II inhibitor and evaluated their potency to inhibit estrogen-dependent (MCF-7)

and estrogen-independent (HeLa) cancer cell lines.[20] When methoxy group to compound **14a** (MCF-7, GI_{50} > 30.0 μM; HeLa, GI_{50} = 28.1 μM) is incorporated at R_1 position, led to **14b** (MCF-7, GI_{50} = 27.9 μM; HeLa, GI_{50} = 10.1 μM)) with improved anti-proliferative activity. When OBn group is introduced at R_3 position to **13b** as in **13d**, it renders to increase in inhibition potency by 7-folds towards HeLa cell line. Compound **13e** substituted with methoxy group at R_1 position and chloride atom at R_2 and R_3 positions, was found to be the most potent inhibitor towards HeLa cell line while growth inhibition towards MCF-7 cell line is same as reference drug tamoxifen. Analogue **13g**, hydroxyl group positioned at R_3 position displayed improved activity by 4-folds towards MCF-7 and 3-folds against HeLa cell line compared to **13b**. Thus, the presence of hydroxy and chloro substituent at R_3 position enhances the cytotoxicity, whereas hydroxy or methoxy group at R_1 position showed reduce antiproliferative activity, which revealed that substituents attached to phenyl rings affect the anticancer activity.

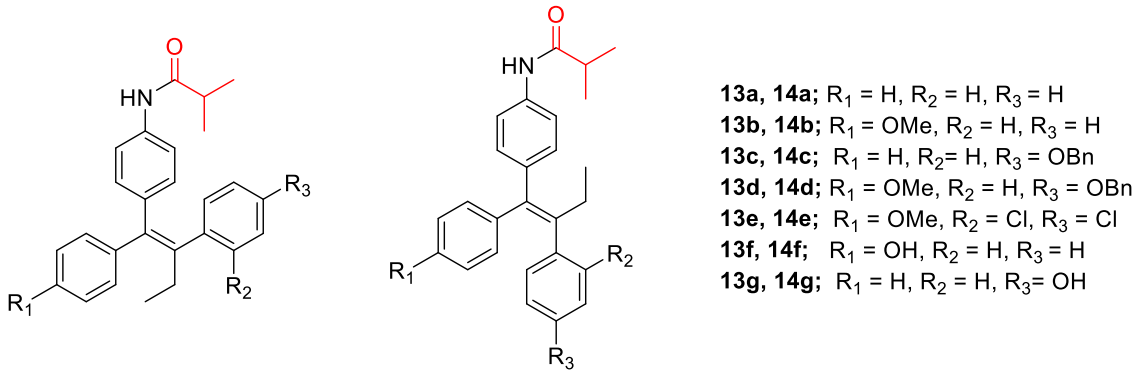

13 **14**

Marty *et al*. had synthesized a series of tamoxifen analogues by replacing the ethyl group of tamoxifen with methylene (1*H*-1,2,4-triazole) as potent antibreast cancer agents.[21] Compound **15f** (GI_{50} = 0.23 μM) displayed improved antiproliferative activity when compared to tamoxifen (GI_{50} = 0.24 μM) against MDA-MB-231 cell line. Compound **15g** (GI_{50} = 0.12 μM) retained similar inhibition tendency against SiHa cell line (human cervical cancer) as reference drug (GI_{50} = 0.12 μM). It is demonstrated that the basicity of side chain of triazole substituted tamoxifen derivatives affects the anticancer activity.

Shoda *et al.* reported the synthesis of tamoxifen analogues with a long alkyl side chain as selective estrogen down regulator.[22] Preliminary compounds **16a-f** and **17a-c** were screened for their tendency to inhibit Estrogen receptor alpha protein in MCF-7 breast cancer cell line. Compound **16c** (IC_{50} = 3.4 nM) bearing fluoro at the alkyl terminal had manifested 2-fold

enhanced inhibition potency when compared to 4- OH-tamoxifen. When the fluoro of **16c** is replaced with hydroxy substituent, it led to **16d** (IC_{50} =

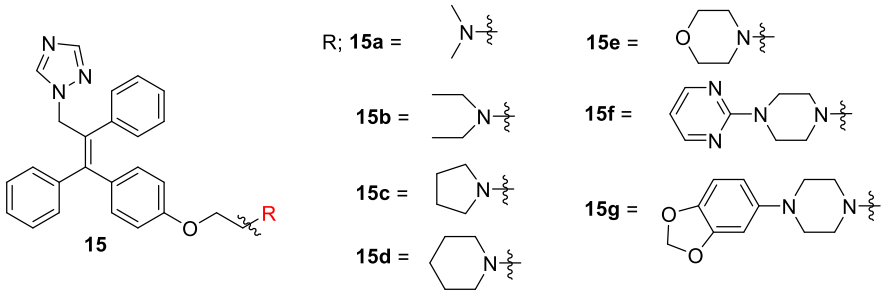

210 nM) with loss of inhibition activity. When chain length in **16a** (IC_{50} = 53 nM) is increased as in **16e** (IC_{50} = 11 nM), the antiproliferative activity enhanced by 5-folds. Among analogues **17a-c**, only **17b** (IC_{50} = 14 nM) elicited better ER-α inhibition efficiency compared to **17a** (IC_{50} = 151 nM) and **17c** (IC_{50} > 100,000 nM). Analogues **16a**, **17a**, **16e,** and **17b** exhibited better binding affinity than reference drug 4-OH-tamoxifen with western blotting analysis. It revealed that the length of the alkyl chain and terminal group attached to side chains play a crucial role in the inhibition of ER-α protein in MCF-7 cell line and on their relative binding affinity.

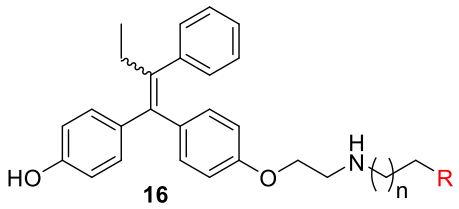

16a; n = 7, R = H
16b; n = 9, R = H
16c; n = 9, R = F
16d; n = 9, R = OH
16e; n = 13, R = H
16f; n = 15, R = H

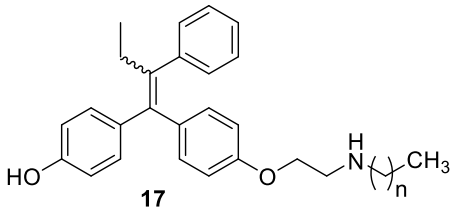

17a; n = 5
17b; n =11
17c; n = 17

Sharma and co-workers designed and synthesized a series of triphenylethylene derivatives by incorporating short alkyl chain instead of *O*-dimethylaminoethyl side chain.[23] Compound **18** displayed remarkable anticancer activity against MCF-7 and MD-MBA-231 cell lines with IC_{50} values of 16.9 and 11.4 μM, respectively. Among oxalimide **20a-c**, derivative **20a** (IC_{50} = 11.5 μM) having benzylamine retained similar inhibition potency as compound **18** towards MD-MBA-231 cell line. Analogue **20b** bearing morpholine displayed less potent inhibition activity against MD-MBA-231 cell line with IC_{50} = 20.0 μM. Derivatives **19a-c** substituted with amido group were found to be less potent than oxalimide analogues **20a-c**.The structure-activity relationship revealed that incorporating the oxalimide group enhanced the potency of triphenylethylene derivatives towards breast cancer cell lines compared to tamoxifen.

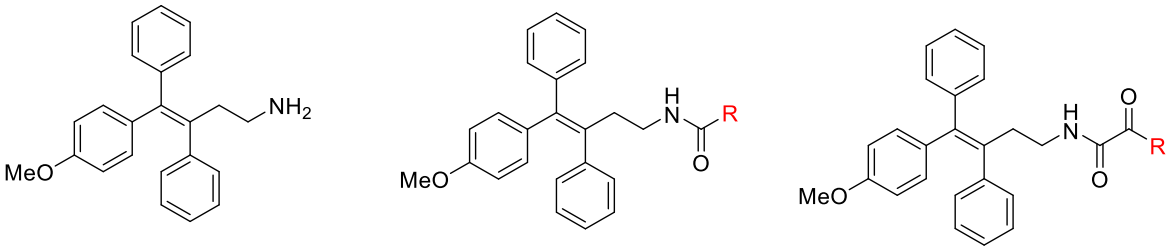

18 **19** **20**

R; **19a, 20a** = benzylamine
19b, 20b = morpholine
19c, 20c = piperidine

Zhao *et al*. had reported the synthesis of novel triphenylethylene derivatives *via* Suzuki-Miyaura coupling approach on *α*,*α*-dibromoalkene and evaluated their efficacy to inhibit aromatase and *α*- and *β*-estrogen receptors.[24] Compound **21d** was found to be the most potent anti-aromatase (IC_{50} = 62.2 nM) when compared to *E*,*Z*-norendoxifen (**23**; IC_{50} = 102.2 nM) and also displayed good inhibition potency against ER-*α* (EC_{50} = 72.1 nM), ER-*β* (EC_{50} = 70.8 nM). Among amino derivatives **22a-d**, **22b** displayed promising potency as aromatase inhibitior with IC_{50} value of 8.8 nM which is close to the value reference drug letrozole (IC_{50} = 5.3 nM). Thus, amino groups at *para* position of 'A' and 'B' rings play important role in the modulation of aromatase inhibitory activity. Structure-activity relationship suggested that the replacement of ethyl side chain with a methyl substituent lowers the potency towards aromatase inhibition. The presence of aminoethoxyl side chain in triphenylethylene derivatives is not significant for aromatase and ER inhibition.

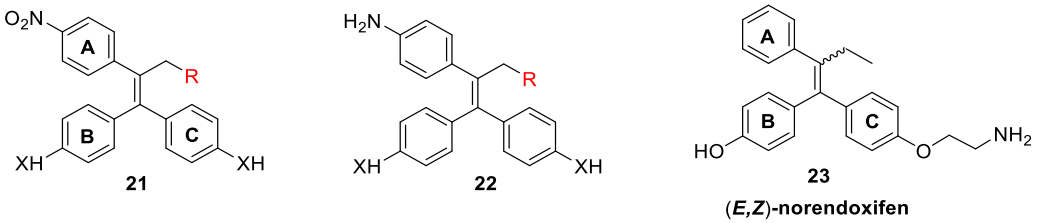

21a, 22a; R = H, X = O
21b, 22b; R= CH_3, X = O
21c, 22c; R = H, X = NH
21d, 22d; R = CH_3, X = NH

Further, to develop more potent norendoxifen analogues and overcome the problem of *E*/*Z*-isomers of norendoxifen, Wei *et al.* synthesized triphenylethylene bisphenol analogues by eliminating the aminoethoxy chain of norendoxifen and evaluated their affinity to inhibit aromatase and bind to ER-*α* and ER-*β*.[25] The imidazole compound **24a** was the most potent aromatase inhibitor with IC_{50} value of 4.77 nM and also retained high binding affinity towards

ER-α and ER-β. Compound **25a** (IC_{50} = 137 nM) with a 1,2,4-triazole side chain showed moderate aromatase inhibitiory activity and weak binding to ER-α and ER-β. It was inferred that compounds containing the imidazole ring (Fe co-ordinating group) showed superior aromatase inhibitory activity in nM range compared to *E*, *Z* norendoxifen, and other synthesized derivatives.

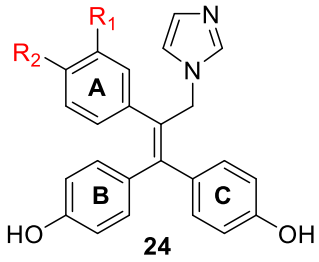

24

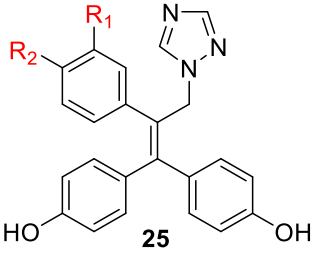

25

24a, 25a; R_1 = H, R_2 = H
24b, 25b; R_1 = H, R_2 = OH
24c, 25c; R_1 = F, R_2 = OH
24d, 25d; R_1 = H, R_2 = NH_2

Ahmed *et al.*, in 2016 synthesized a novel series of tamoxifen analogues as antibreast cancer agent and evaluated their efficacies to bind with ER-α.[26] These analogues featured the same activity as tamoxifen but these are metabolized by a pathway which does not involve the CYP2D6 enzyme. All the derivatives (**26a-l**) have more potency towards MCF-7 breast cancer cell line as compared to tamoxifen (IC_{50} = 4.40 μM). Compound **26f** exhibited the most promising potency on MCF-7 cell line with the GI_{50} value of 0.005 μM. These derivatives were found to be sensitive towards the estrogen receptor-α with IC_{50} values in the nanomolar range. It is demonstrated that ester group at 4-position enhances the anticancer activity towards MCF-7 cell line.

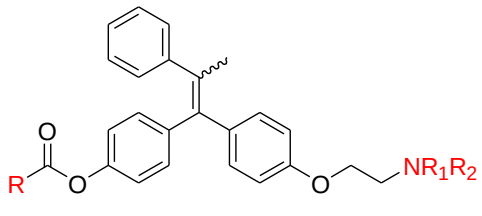

26

	NR_1R_2	R
26a;	$(CH_3)_2$	H
26b:	pyrrolidine	H
26c;	piperidine	H
26d;	$(CH_3)_2$	$COCH_3$
26e;	$(CH_3)_2$	COC_3H_7
26f;	$(CH_3)_2$	COC_9H_{19}
26g;	pyrrolidine	$COCH_3$
26h;	pyrrolidine	COC_3H_7
26i;	pyrrolidine	COC_9H_{19}
26j;	piperidine	$COCH_3$
26k;	piperidine	COC_3H_7
26l;	piperidine	COC_9H_{19}

Ahmed and co-workers reported the synthesis of tamoxifen analogues by substituting one of the phenyl rings with benzyl group and also incorporated ester group at 4-position.[27] Analogue **27b** possessing piperidine exhibited excellent potency against MCF-7 cell lines with GI percentage of 82%, while **27a** displayed 70% growth inhibition towards MCF-7 BUS cell line.

Analogue **27b** displayed antiestrogenic activity with IC_{50} value of 510 *n*M towards MCF-7 cell line and was found to be 5-folds more potent than tamoxifen (IC_{50} = 503 *n*M) towards MCF-7 BUS cell line (IC_{50} = 96 *n*M). Structure-activity relationship implied that the nature of the side group governs the antiproliferative activity.

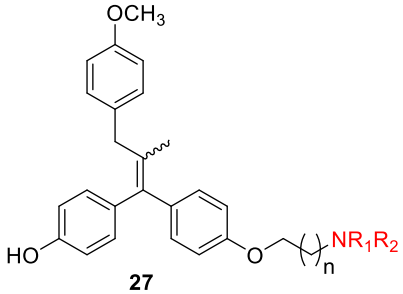

27

27a; n = 2, NR_1R_2 = dimethylamine
27b; n = 1, NR_1R_2 = piperidine

Xia liu Li and co-workers reported the synthesis of trimers of triphenylethylene-coumarin hybrids bearing two amino acid chains and examined their anticancer activity towards HeLa, A549, K562, and MCF-7 cell lines.[28] The trimer **29a** had displayed promising activity towards MCF-7, A549, and HeLa with IC_{50} values of 8.51, 8.38, and 7.99 μM, respectively. Derivative **28a-d** exhibited weak anticancer activity because of their bulky structure. Analogue **29b-d** elicited 2-3 folds less potency as compared to *cis*-platin (MCF-7, IC_{50} = 6.60 μM; A549, IC_{50} = 8.94 μM; HeLa, IC_{50} = 6.09 μM). It is revealed that the flexibility of analogue **29a-d** is responsible for better anticancer activity as compared to compounds **28a-d**.

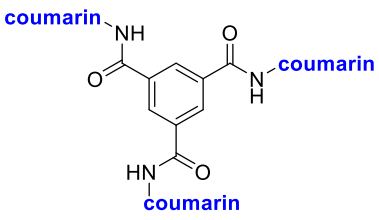

28

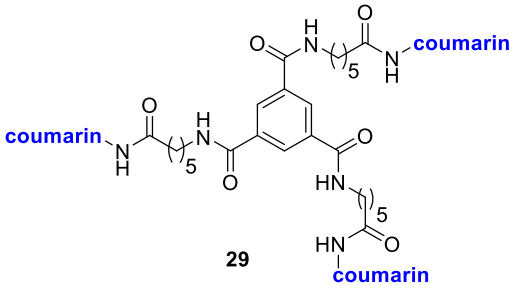

29

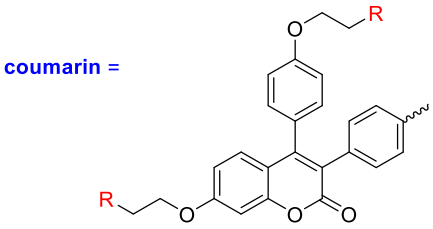

R; **28a, 29a** = piperidine
28b, 29b = morpholine
28c, 29c = pyrrolidine
28d, 29d = *N*,*N*-diethylamine

Kumar *and* co-workers designed and synthesized 1*H*-1,2,3-triazole tagged ospemifene-isatin hybrid (**30a-f**) and evaluated their antiproliferative activity against MCF-7 and MDA-MB-231 cancer cell lines.[29] Derivative **30a** (IC_{50} = 53.10 μM) retained similar inhibition potency as

tamoxifen (IC_{50} = 50.0 μM) against MCF-7 cell line. Analogue **30c** exerted the most promising anticancer activity with IC_{50} value of 1.56 μM against MCF-7 cell line while it exhibited low potency towards MDA-MB-231 (IC_{50} = 48.46 μM). Analogue **30e** bearing fluoro exhibited improved inhibition activity with IC_{50} value of 71.1 μM as compared to tamoxifen (IC_{50} = 75.0 μM) towards MDA-MB-231 cancer cell line. Structure-activity relationships suggested that these hybrids are selectively more active towards MCF-7 cell line and were more potent than tamoxifen.

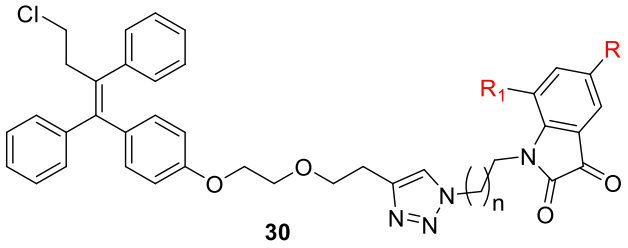

30

30a; R = H, R_1 = H, n = 1
30b; R = CH_3, R_1 = H, n = 2
30c; R = Br, R_1 = Br, n = 1
30d; R = Br, R_1 = Br, n =2
30e; R = F, R_1 = H, n = 3
30f; R= Cl, R_1 = H, n = 2

Catanzaro *et al.* reported the synthesis of tamoxifen analogues by reducing the flexibility of the side chain and discovered a new TPE-xanthene hybrid as anticancer agent.[30] These derivative were evaluated *in vitro* for their antitumor activity towards MCF-7 and MDA-MB-231 breast cancer cell lines. Among the series, conjugate **31** (MCF-7, IC_{50} = 12.4 μM; MDA-MB-231, IC_{50} = 25.4 μM) bearing xanthene moiety displayed promising anticancer activity which is comparable with tamoxifen (MCF-7, IC_{50} = 10.5 μM; MDA-MB-231, IC_{50} = 28.9 μM). Additionally, the TPE core substituted with butinyl side chain was proved to be deleterious (**32**; IC_{50} values approximately to 40 μM). SAR implied that there is decrease in antiproliferative activity of TPE-derivatives on incorporation of rigid butinyl side chain.

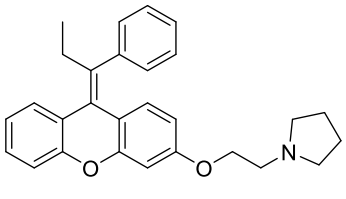

31

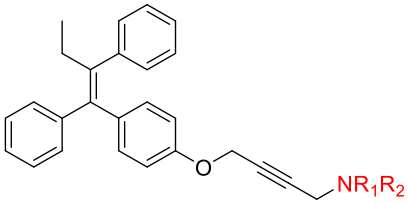

NR_1R_2; **32a** = pyrrolidine
32b = piperidine

Ahmad *et al.* synthesized the benzopyran based triphenylethylene analogues as growth inhibitors of breast carcinoma cells.[31] The newly synthesized derivatives exhibited significant growth inhibition of estrogen receptor positive (MCF-7) and estrogen receptor negative (MD-MBA-231) cell lines with IC_{50} values ranging between 0.55-9.96 μM. Compound **33c** with highest selectivity index towards MCF-7 (4.42) and MD-MBA-231(1.55), was chosen for

mechanistic studies. It is implied that benzopyran coupled with triphenylethylene (TPE) showed enhanced antiproliferative activity when compared to tamoxifen (MD-MBA-231, IC_{50} = 9.96 μM, MCF-7 IC_{50} = 8.12 μM).

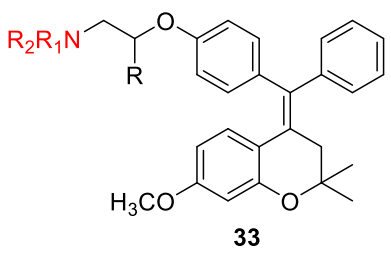

33

	NR_1R_2	R
33a;	*N*,*N*-dimethylamine	H
33b;	*N*,*N*-diethylamine	H
33c;	*N*,*N*-dimethylamine	CH_3
33d;	pyrrolidine	H
33e;	piperidine	H

Luo *et al.* designed and synthesized a novel series of 3-aryl-4-anilino-2*H*-chromen-2-one analogues by substituting with different amines and structural modifications at C-7 position.[32] Antiproliferative activity of analogues **34a-c** has been evaluated against MCF-7 and Ishikawa breast cancer cell lines. Analogues **34a** (IC_{50} = 5.86 μM), **34b** (IC_{50} = 4.31 μM), **34c** (IC_{50} = 7.31 μM) had exhibited potent activity against MCF-7 cell line with IC_{50} values 5.86, 4.31 and 7.31 μM, respectively. Further, analogue **34c** elicited remarkable ER-α binding affinity with relative binding affinity (RBA) value of 2.83%. From the structure-activity relationship, it is indicated that hydroxyl group is the crucial substituent for better ER-α binding. For these TPE analogues, medium size amines are more preferred for improved antitumor activity.

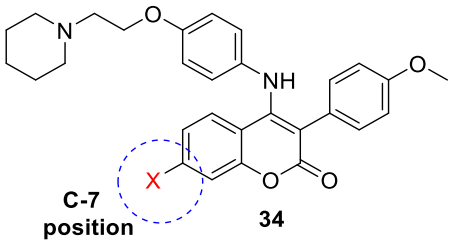

34

X

34a; H

34b; OCH_3

34c; OH

Palermo *et al.* synthesized a novel series of tamoxifen analogues *via* McMurry coupling and used nickel catalyzed three-component approach as ER-α and HD (histone deacetylase) inhibitors.[33] Analogue **35** (IC_{50} = 1.3 μM) displayed similar potency as reference drug 4-OHTam (IC_{50} = 3.3 μM) towards MCF-7 cells but less potent than SAHA (IC_{50} = 0.95 μM). Among the series, **35** showed better inhibition activity towards ER-α; and was the most potent inhibitor of HDAC6 and HDAC3 with IC_{50} values of 0.300 and 0.734 μM, respectively. SAR suggested that flexibility of the side chain governs the anti-proliferative active.

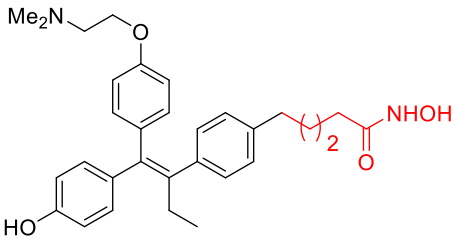

35

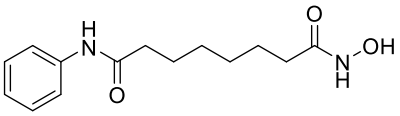

Suberoylanilidehydroxamic acid (SAHA)
HDAC inhibitor

Meegana and co-workers reported the synthesis of combreastatin conjugates substituted with amines using Mukiyama's reagent as antiproliferative agents.[34] Alamar Blue assay was performed to evaluate the cytotoxic effect of analogues **36a-b** on the viability of MCF-7 breast cancer cell line. Compound **36a** had displayed the most potent activity with IC_{50} value of 0.083 μM. On replacing *N*-tolyl group of **36a** with *N*-phenyl substituent, it led to analogue **36b** (IC_{50} = 0.13 μM) with reduced potency. It is implied that incorporating amines to CA-4 (IC_{50} = 0.0039 μM) lowers the anticancer activity of newly synthesized analogues. Moreover, analogue **36a** elicited overall highest potency with a mean GI_{50} value, of 0.41 μM.

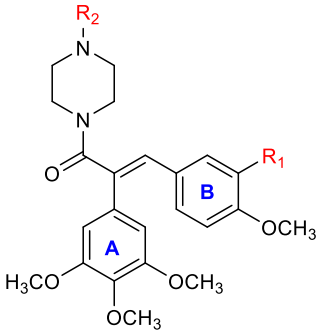

36

36a; $R_1 = NH_2$, $R_2 = C_6H_4$-*p*-CH_3
36b; $R_1 = NH_2$, $R_2 = C_6H_5$

Carr *et al.* in 2020 reported analogues of 4-aryl-4*H*-chromene scaffold by substituting with basic aryl ethers at the C-4 position and various esters at C-3 position as Selective Estrogen Receptor Modulator (SERM).[35] Preliminary, these analogues were evaluated for their anti-breast cancer activity towards MCF-7 cell line. Analogue **37e** was found to be the most potent inhibitor against MCF-7 cell line with IC_{50} value of 2.65 μM. Compound **37e** displayed excellent inhibition towards ER-α while **37d** inhibited both receptors (ER-α and ER-β) selectively with IC_{50} values 0.02 and 0.06 μM, respectively. Analogues **37b** (ER-α, IC_{50} = 0.01 μM and ER-β = 0.170 μM) and **37c** (ER-α, IC_{50} = 0.05 μM and ER-β = 0.22 μM) were found to be as effective inhibitors towards ER-α than ER- β when compared to tamoxifen (ER-α, IC_{50} = 0.070 μM and ER-β = 0.170 μM).

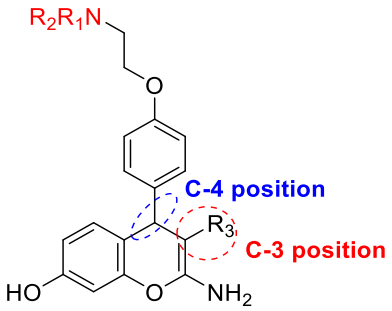

37

37a; NR_1R_2 = pyrrolidine, $R_3 = CO_2(CH_2)_3CH_3$
37b; NR_1R_2 = pyrrolidine, $R_3 = CO_2C(CH_3)_3$
37c; NR_1R_2 = piperidine, $R_3 = CO_2CH_3$
37d; NR_1R_2 = piperidine, $R_3 = CO_2CH_2CH_3$
37e; NR_1R_2 = piperidine, $R_3 = CO_2C(CH_3)_3$
37f; NR_1R_2 = morpholine, $R_3 = CO_2CH_3$

Dheer *et al.* synthesized a series of triphenyl-1,2,3-triazole derivatives as antitumor agents. The selectivity index and antiproliferative activity of analogue **38a-d** were evaluated against MCF-7 and MD-MBA-231 cancer cell lines.[36] Analogue **38d** was found to be sensitive towards MCF-7 cell line with IC_{50} value of 3.95 μM. When the value of n in derivative **38a** (substituted with pyrrolidine; IC_{50} = 7.71 μM), is increased from 2 to 4, it led to compound **38b** (IC_{50} = 4.70 μM) with increased activity. Analogue **38c** manifested highest selectivity index among other derivatives i.e. 9.94. Therefore, it has been selected for the further mechanistic studies.

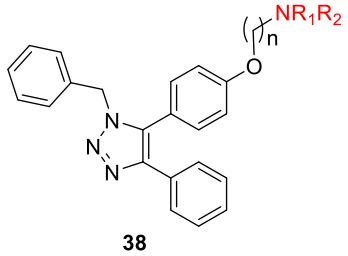

38

38a; n = 2, NR_1R_2 = pyrrolidine
38b; n = 4, NR_1R_2 = pyrrolidine
38c; n = 2, NR_1R_2 = diethylamine
38d; n = 5, NR_1R_2 = piperidine

(B) Naphthalimide Based Derivatives

Xin and co-workers reported the synthesis of 3-nitro-1,8-naphthalimide analogues by substituting with various aliphatic and aromatic amines as anticancer agents.[37] Naphthalimide **39a-f** was inquired *in vitro* for their anticancer activity by MTT assay against SKOV3, A549, HepG2, SMMC-7721, T-24, and HL-7702 cell lines. Analogue **39a** (HepG2, IC_{50} = 9.20 μM; T-24, IC_{50} = 4.13 μM) manifested most potent activity towards HepG2 and T-24 cancer cell lines when compared to reference drug mitonafide (HepG2, IC_{50} = 10.88 μM; T-24, IC_{50} = 5.01 μM). These derivatives displayed lower cytotoxicity to HL-7702 normal cell line. It has also been demonstrated that analogue **39a** inhibits TOPO-I and induces apoptosis by cell cycle arresting at the G-2 stage.

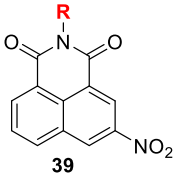

39

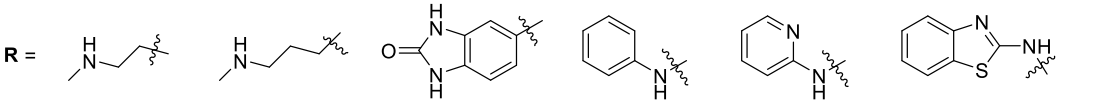

39a 39b 39c 39d 39e 39f

Rong *et al.* in 2018 synthesized derivatives of bis-naphthalimide by substituting various secondary amines at the C-4 position and investigated their cytotoxic activity against HeLa, MCF-7, A549 and MGC-803 cancer cell lines.[38] Analogues **40a** (HeLa, IC_{50} = 2.89 μM; MGC-803, IC_{50} = 0.60 μM) and **40d** (HeLa, IC_{50} = 2.73 μM; MGC-803, IC_{50} = 1.60 μM) exhibited excellent inhibition activity towards HeLa and MGC-803 cell lines. While derivative **40e-f** displayed weak anticancer activity towards all the tested cancer cell lines compared to reference drug amonafide. It is demonstrated that the nature of amine substituted at C-4 position plays a key role in the antiproliferative activity of naphthalimide derivatives.

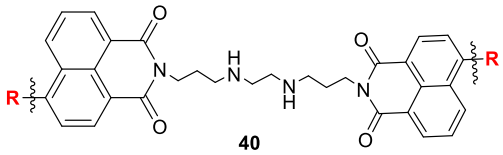

40

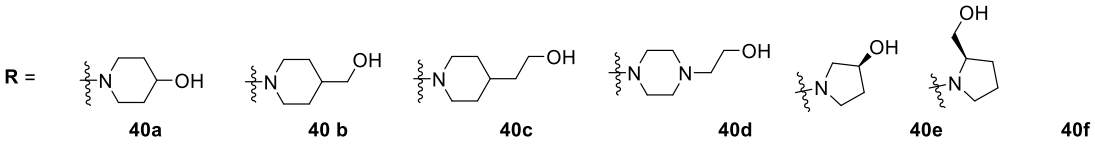

40a 40 b 40c 40d 40e 40f

Espinoza *et al.* synthesized analogues of 5-ethynylarylnaphthalimides *via* Sonogashira coupling reaction and evaluated their anticancer activity towards SK-Br-3 (human breast cancer), HEL (human erythroleukemia) and HL60 (human promyelocytic leukemia) cancer cell lines.[39] On introducing methoxy group at 3-position to phenyl ring, analogue **41b** (SK-Br-3, IC_{50} = 2.0 μM; HEL, IC_{50} = 1.0 μM; HL60, IC_{50} = 1.0 μM) displayed enhanced activity when compared to **41a** (SK-Br-3, IC_{50} = 4.6 μM; HEL, IC_{50} = 1.4 μM; HL60, IC_{50} = 4.6 μM) against cancer cell lines while on incorporation of NO_2 group to **41a**, it led to analogue **41f** with complete loss of activity. When phenyl ring of **41a** is replaced with heterocyclic rings such as furan and thiophene as in **42a** and **42b** displayed similar potency as compared to reference drug amonafide. From the SAR, it is implied that on introducing ethynylaryl group, naphthalimides showed better antiproliferative activity in comparison to amonafide.

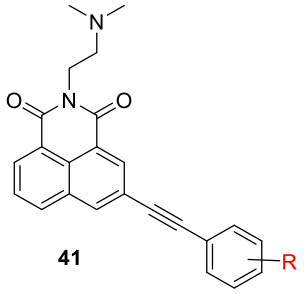

41

41a; R = H
41b; R = 3-OCH_3
41c; R = 3-NO_2

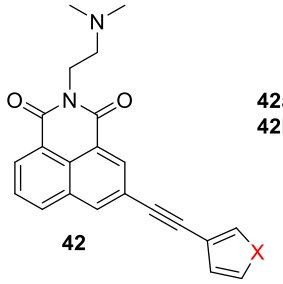

42

42a; X = O
42b; X = S

Yang and co-workers synthesized naphthalimide-urea conjugates and screened their cytotoxicity on A549 lung cancer and HUVEC (human umbilical vein) normal cell line.[40] Furthermore, the binding interaction of obtained compounds with duplex and telomeric G-quadruplex has been studied. Among the derivative **43a-d,** analogue **43d** substituted with phenyl ring showed significant inhibition against A549 cancer cell line with IC_{50} value of 2.98 μM.

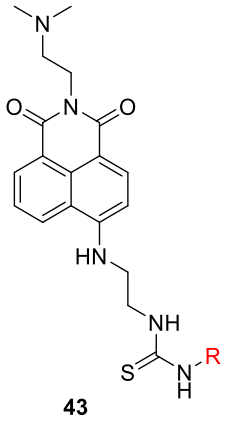

43

43a; R = CH_3
43b; R = C_2H_5
43c; R = C_4H_9
43d; R = C_6H_5

Analogue **43a-c** was found to be 2-folds more active than amonafide (IC_{50} = 8.39 μM). All the compounds showed selectivity towards A549 cancer cell line over HUVEC normal cell line. These naphthalimide conjugates were also able to bind selectively with telomeric G-quadruplex DNA *vs.* duplex DNA.

Johnson *et al.* synthesized aminonaphthalimide hybrids as anticancer and fluorescent cell imaging agents.[41] These obtained compounds (**44a-c**) were screened against K-562 (leukemia) and MCF-7 (breast cancer) cell lines at concentration range 10^{-4} to 10^{-8} M and as a function of exposure time of 24h, 48h, and 72h. After 24h, analogues **44b** (GI_{50} = 15 μM) and **44c** (GI_{50} = 14 μM) displayed significant growth inhibition against K-562 cancer cell line. After 48h, the growth inhibition potency of these analogues increases. After 72h, derivatives **44a** (GI_{50} = 6 μM) and **44b** (GI_{50} = 2.2 μM) manifested promising growth inhibition against K-562 and MCF-7 cell

lines, respectively. From SAR, it is revealed that analogues bearing secondary alkyl amine exhibited enhanced cytotoxicity.

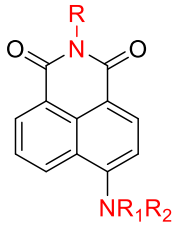

44

	NR_1R_2	R
44a;	piperazine	methyl
44b;	*N*-methylethylenediamine	methyl
44c;	*N*-methylethylenediamine	*N*-methylethylenediamine

Xie and co-workers synthesized naphthalimide polyamine conjugates and evaluated their antitumor activity towards K562, HepG2, HCT16 and SMMC-7721 cancer cell lines.[42] Analogue **45b** (IC_{50} = 10.42 μM) displayed similar inhibition potency as amonafide (IC_{50} = 10.10 μM) against K562 cell line. Derivatives **45c** (IC_{50} = 7.26 μM), **45e** (IC_{50} = 9.76 μM) and **45g** (IC_{50} = 8.75 μM) manifested significant anticancer activity towards HepG2 cell line. Analogue **45g** displayed excellent sensitivity with IC_{50} value of 3.30 μM while **45e** exhibited similar potency towards SMMC-7721 cell line as amonafide (IC_{50} = 10.32 μM). It is implied that the nature of amine at the N-position affects the anticancer activity of naphthalimide conjugates.

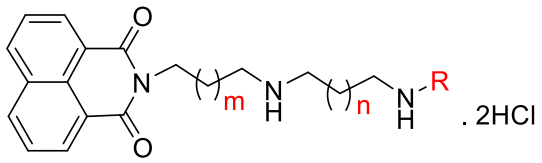

45

45a; m = 1, n = 1, R = ethyl
45b; m = 2, n = 2, R = ethyl
45c; m = 1, n = 1, R = propyl
45d; m = 1, n = 1, R = cyclopropyl
45e; m = 2, n = 1, R = cyclopropyl
45f; m = 2, n = 2, R = cyclopropyl
45g; m = 2, n = 1, R = cyclohexyl

Qian and co-workers synthesized a novel series of naphthalimide conjugates with indomethacin *via* molecular hybridization approach and investigated their antitumor activity towards HeLa (cervical carcinoma), A549 (lung), P388 (leukemia), HL-60 (leukemia), MCF-7 (breast), HCT-8 (ileocecal) and A375 (melanoma) cancer cell lines.[43] Analogues **46b** and **46d** with more linker length displayed promising anticancer activity as compared to **46a** and **46c** (with small linker length). It was inferred that analogues with amide linkage exhibited more cytotoxicity than the ones with ester linkage. It is also demonstrated that length of linker plays crucial role in the anticancer activity of naphthalimide-indomethacin hybrids.

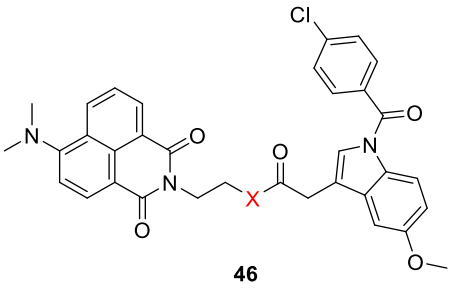

46

46a: X = -O-
46b: X = -O(CH$_2$)$_2$O-
46c: X = -NH-
46d: X = -NH(CH$_2$)$_4$-

Kamal and co-workers synthesized naphthalimide derivatives tagged with benzothiazole/cinnamide moiety as anticancer agents and topoisomerase-IIα inhibitors.[44] Derivatives **47a** and **47b** bearing electron-donating group exhibited improved activity against HT-29 and A549 cell lines while being insensitive towards MCF-7 cancer cell line when compared to amonafide. Analogues **48a** and **48b** exhibited significant activity with IC$_{50}$ values in a range of 3.46–5.08 and 3.71–7.90 μM, respectively, against cancer cell lines. Among naphthalimides tagged with cinnamide, **49b** was found to be most potent, showing selectivity towards HT-29 and A-549 with IC$_{50}$ values 3.80 and 4.79 μM, respectively. Compound **49c** bearing 2,5-difluoro group exhibited better activity than **49d** with 3,5-difluoro. Structure-activity relationship demonstrates that analogue (**48a-b**) having amide bond at C-6 position displayed remarkable anticancer activity.

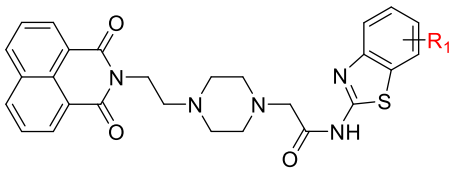

47

47a: R$_1$ = 6-OMe
47b: R$_1$ = 5,6-dimethyl

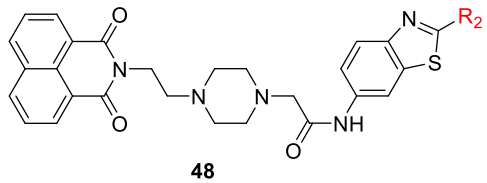

48

48a: R$_2$ = H
48b: R$_2$ = Me

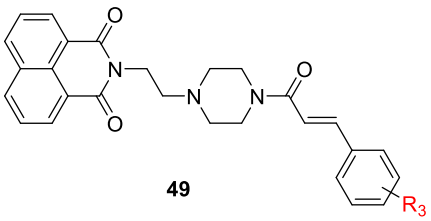

49

49a: R$_3$ = 4-*N*,*N*-dimethyl
49b: R$_3$ = methylene dioxy
49c: R$_3$ = 2,5-difluoro
49d: R$_3$ = 3,5-difluoro

Rong *et al.* synthesized a series of novel bis-naphthalimides and evaluated their inhibition potencies towards HeLa, MCF-7, SGC-7901, and A549 cancer cell lines.[45] Compound **50a** exhibited excellent cytotoxicity towards all the tested cell lines with IC$_{50}$ values of 2.31, 2.94, 0.88 and 1.21 μM, respectively, compared to control drug amonafide. Analogues **50d** (SGC-

7901, IC_{50} = 2.30 μM; A549, IC_{50} = 3.04 μM) and **50e** (SGC-7901, IC_{50} = 2.47 μM; A549, IC_{50} = 0.60 μM) elicited potent activity when compared to their enatiomers **50c** (SGC-7901, IC_{50} = 4.46 μM; A549, IC_{50} = 4.71 μM) and **50f** (SGC-7901, IC_{50} = 23.23 μM; A549, IC_{50} = 1.59 μM) respectively. It is implied that cytotoxicity of the pyrrolidine derived naphthalimides was dependent on the chiral configuration of the pyrrolidine group.

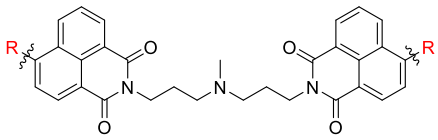

50

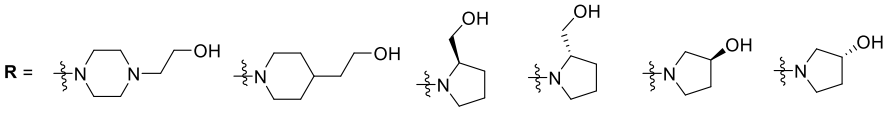

50a **50b** **50c** **50d** **50e** **50f**

Shih and co-workers synthesized naphthalimide analogues by substituting benzazole group at C-4 position as anticancer agent against murine B16F10 melanoma cells.[46] Analogue **51f** manifested promising cytotoxic activity with IC_{50} value of 4.5 μM, while compound **51e** (IC_{50} = 7.8 μM) exhibited less potency than reference drug amonafide (IC_{50} = 6.7 μM). Structure-activity relationship studies demonstrated that the nature of imide substitution alters the cytotoxic properties of these analogues. It is also inferred that the benzazole ring attached to C-4 position enhances the anticancer activity of naphthalimides.

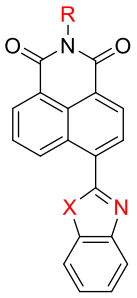

51

51a; R = *n*-Bu, X = O
51b; R = *n*-Bu, X = S
51c; R = CH_2CH_2OH, X = O
51d; R = CH_2CH_2OH, X = S
51e; R = $CH_2CH_2N(CH_3)_2$, X = O
51f; R = $CH_2CH_2N(CH_3)_2$, X = S

Paul and co-workers synthesized naphthalimide-phenanthro[9,10-*d*]imidazole derivatives by substituting primary and secondary amines as anticancer agents as well as topoisomerase-II inhibitors.[47] The synthesized compounds were tested for their anticancer activity against 60 human cancer cell lines at the one-dose concentration (10 μM) by National Cancer Institute, USA. Analogue **52** was discovered to be most cytotoxic with growth inhibition percentage from −55.78 to 94.53 towards 14 cancer cell lines. Further, compound **52** was evaluated for their

cytotoxicity towards A549, MCF-7, and HeLa cancer cell lines at five-dose concentration levels. Analogue **52** exhibited potency against A549, MCF-7, and HeLa cell lines with IC_{50} values of 33.53, 25.33, 28.34 μM, respectively. These results demonstrated that naphthalimide hybrids displayed good antiproliferative activity.

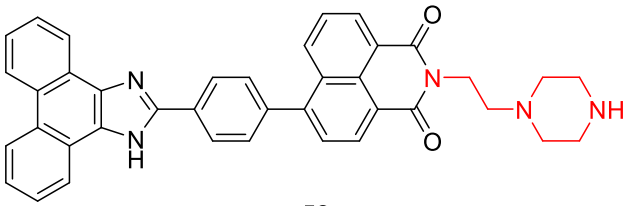

52

Paul and co-workers also reported the naphthalimide-benzimidazole conjugates as potential antiproliferative agents.[48] Analogues **53a** and **53b** were found to be potent against a panel of 60 human cancer cell lines and displayed MG-MID GI_{50} values of 1.43 and 1.83 μM at five-dose concentration levels, respectively. Additionally, **53a** and **53b** were found to be more superior to amonafide (a naphthalimide analog) but inferior to nocadozaole (a benzimidazole analog) towards cancer cell lines. Structure-activity studies indicated that derivatives bearing naphthalimide at position-5 are more active as compared to naphthalimide at position-6 towards cancer cell lines. Moreover, alkyl-based compounds showed better anti-tumoral activity than the aryl ones. In particular, alkyl substituents creating a bit steric hindrance and were noticed to exhibit more promising anticancer activity.

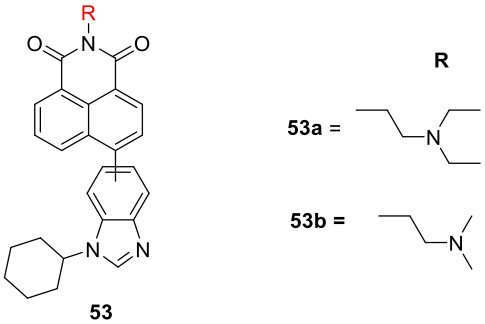

53

Kumar and co-workers reported a novel series of naphthalimide-chalcone/pyrazoline conjugates as antibreast cancer agents and selective estrogen receptor modulators.[49] Analogue **54b** exhibited significant potency compared to **54a (**IC_{50} = 98.11 μM) against MCF-7 cell line with IC_{50} value of 62.23 μM while found to be inactive towards MDA-MB-231 cell line. The cytotoxicity of derivative **54a-b** was also evaluated towards Hek293 normal cell line and found

to be inactive. It is also observed that naphthalimide analogues tagged with chalcone and pyrazoline were found to be less potent than tamoxifen and plumbagin.

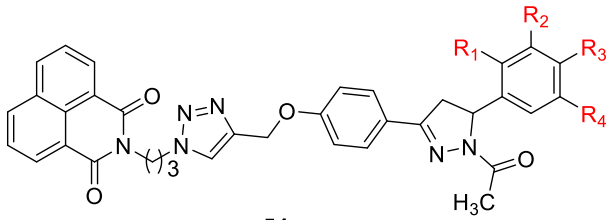

54

54a; $R_1 = R_2 = R_4 = H$, $R_3 = OCH_3$
54b; $R_1 = R_4 = OCH_3$, $R_2 = R_3 = H$

Liang *et al.* reported 3-nitro naphthalimide analogues and evaluated their efficacies towards SMMC-7721, T-24, SKOV-3, and A549 cancer cell lines.[50] Analogues **55a-b**, **56a-b** and **57** were found to be more active than amonafide (IC_{50} = 6.93 μM) against SMMC-7721. Interestingly, analogues **55b** (IC_{50} = 1.05 μM), **56b** (IC_{50} = 1.57 μM) and **57** (IC_{50} = 2.71 μM) displayed high potency when compared to mitonafide (IC_{50} = 3.22 μM) towards SMMC-12 cancer cell line. Analogues **55b**, **56b** and **57** exerted better cytotoxicity as compared to mitonafide with IC_{50} values of 0.83, 0.42, and 0.33 μM, respectively, against T-24 cancer cell lines. Analogue **57** (IC_{50} = 0.27 μM) was found to be the most potent against A549 cell line. It is documented that the nature of imide substitution and amines at C-4 positions modulate the behavior of naphthalimides towards anticancer activity.

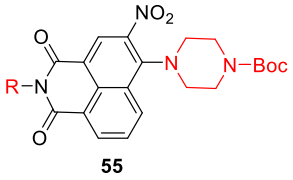

55

55a; R = *N*-methylaminopropyl
55b; R = *N,N*-dimethylaminoethyl

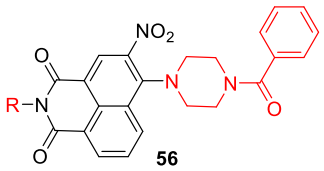

56

56a; R = *N*-methylaminopropyl
56b; R = *N,N*-dimethylaminoethyl

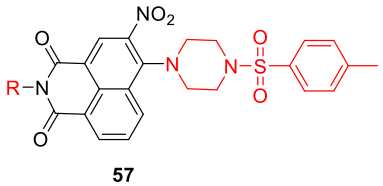

57

R = *N,N*-dimethylaminoethyl

On summarizing, the structure-activity relationship of triphenyl ethylene and naphthalimide derivatives based derivatives has been deduced towards cancer cell lines from the above forementioned literature.

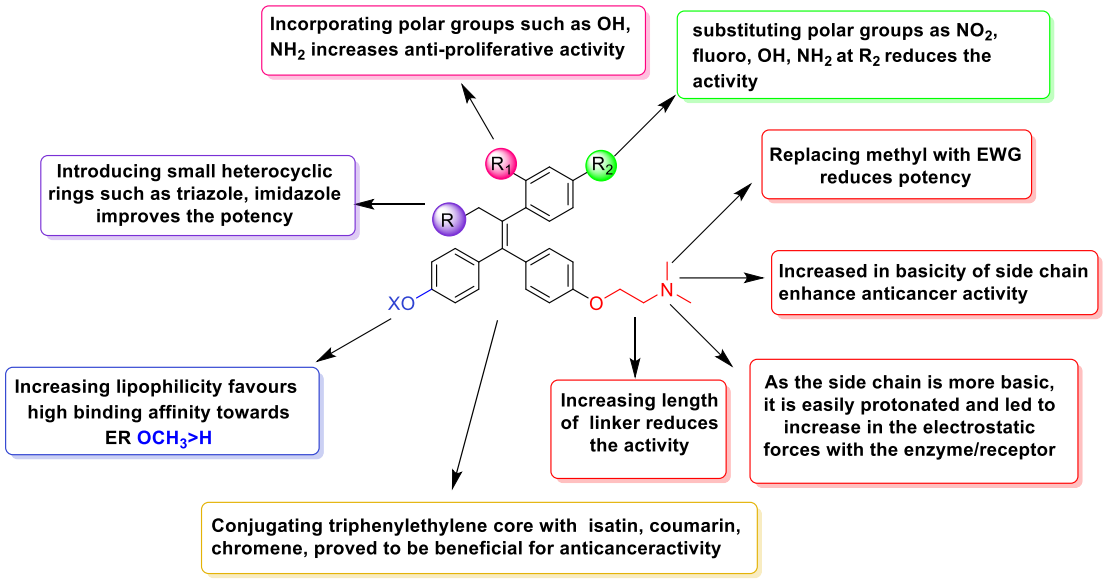

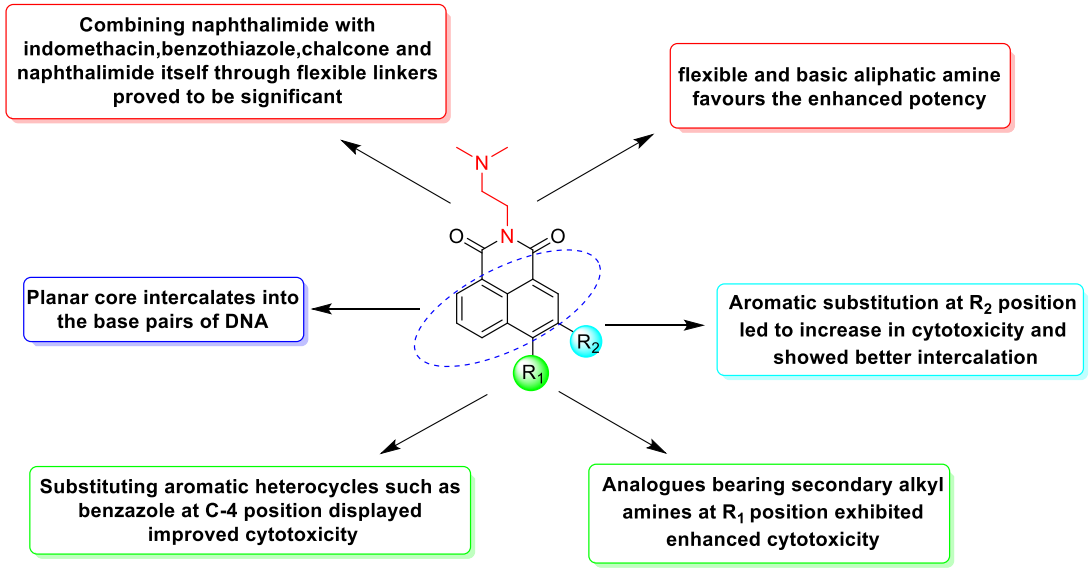

CHAPTER 2
TRIPHENYLETHYLENE ANALOGUES

2.1 Introduction

Triphenylethylene scaffold; tamoxifen is a first-generation Selective Estrogen Receptor Modulator (SERM) having the features of estrogen diethylstilbestrol and emerged as target motif for the treatment of cancer in pharmacotherapy.[51] It is observed to be the first line chemopreventive which is effective at every stage of breast cancer, in premenopausal and postmenopausal women.[52] These days, tamoxifen (*Z* isomer) has been sold as brand name Nolvadex and considered as one of the best-selling medicine for breast cancer.[53] In addition to breast cancer, tamoxifen (triphenylethylene derivative) also exhibits immense pharmacological properties such as antibacterial,[54] antioxidant,[55,56] antifungal,[54] antiangiogenesis,[57] and antiviral properties.[54] Moreover, it reduces the risk of coronary artery disease and bone fractures at some sites.[58] In recent years, tamoxifen analogues have made a significant impact on the pharmacotherapy of estrogen receptor (ER) positive cancer cell lines.

Despite many advantages, the most challenging issue is acquired resistance which often emerges with long-term administration of tamoxifen in patients.[59] Tamoxifen acts as a partial agonist, thus, increasing the risk of endometrium cancer and venous thromboembolism.[60] It is also associated with numerous side effects such as menstrual abnormalities, vaginal dryness, hot flashes, and hepatocytotoxicity.[61-63]

Primarily, tamoxifen ceases the tumour growth either by blocking estrogen receptor or inhibiting estrogen receptor-mediated signaling pathways, which prevent the interaction of transcription factor-ER.[64] As tamoxifen has many sites of action, it targets either cellular DNA through intercalation[65] or by inhibiting the enzymes which promote DNA replication, such as topoisomerase.[66-67] It is a cationic drug and inhibits both β-oxidation and respiration in hepatic mitochondrial cells.[67] This causes cell cycle arrest and leads to programmed cell death (apoptosis).

Through structural-activity relationship studies, it has been observed that the triarylethylene core forms the backbone, which mimics the effect of natural estrogen. It was observed that this core acts as an estrogen agonist and the side-chain attached to the core is responsible for its antagonistic (full/partial) behavior.[68] Recently, endoxifen, one of the metabolites of tamoxifen

has been evaluated in phase I clinical trials for bipolar disorder.[69] Additionally, it has also been reported that substituting one of *N*-methyl group of tamoxifen side chain by *N*-(2,2,2-trifluoroethyl) group loses its potency to inhibit MCF-7 cells.[70] This profound effect shows that the decrease in the basicity of side chain reduces its potency towards cancer cell lines. In recent years, researchers have made considerable progress in the field of drug discovery, but still, drug resistance in cancer treatment remains a frontline intervention. Altogether, to develop structure-activity relationships towards the novel anticancer active triarylethylenes, variation in side-chain attached to its core has gained substantial attention in the literature.

2.1.1 Designing of triphenylethylene analogues

Research has focused on the efforts geared towards the modification of the side chain of tamoxifen. As the basicity of the side chain attached to tamoxifen analogue alters the anticancer properties, we designed and synthesized triphenylethylene analogues bearing amino-isopropanol side chain *via* McMurry coupling reaction.

We have synthesized a new series of triphenylethylene analogues *via* McMurry coupling reaction with variations in the amine side chain and characterized by various spectroscopic techniques. In the newly synthesized triphenylethylene analogues, the ethylene linker of the side chain of tamoxifen is replaced with isopropanol chain, and the methyl substituent is incorporated in place of the ethyl group (**Figure 1**). These compounds were evaluated for their anti-proliferative effect on a panel of 60 human cancer cell lines. To study the molecular targets for cytotoxicity, the effect on topoisomerase-II relaxation is reported for the most cytotoxic derivatives. Furthermore, colorimetric analysis was also performed to investigate the toxicity towards normal cell lines. Docking studies also suggested a plausible explanation of the experimental biological evidences.

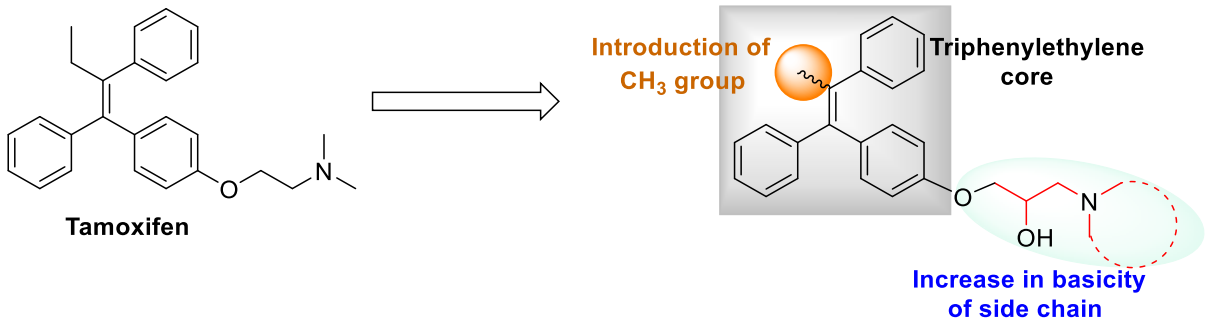

Figure 1: Design of novel triphenylethylene analogue

2.2 Chemistry

To synthesize triphenylethylene scaffolds, a chemical approach was depicted, including McMurry coupling[71] and nucleophilic substitution reaction as shown in **Scheme 1**. The cross-coupled product 4-(1,2-diphenylprop-1-en-yl)phenol (**3**) was easily prepared by the reaction of an equimolar amount of 4-hydroxy benzophenone (**1**) and acetophenone (**2**) *via* McMurry reaction, in a very good yield (80%). Formation of compound **3** in isomeric forms (*E*/*Z*:1:1) was confirmed by the appearance of methyl singlets at δ values 2.14 and 2.10 ppm; and broad singlets of the hydroxy group at δ 4.59 and 4.81 ppm. Subsequently, treatment of compound **3** with epichlorohydrin in the presence of potassium carbonate afforded **4a** and **4b**. The optimized parameters for the formation of intermediate **4a** in major amount are given in **Table 1**. The cyclized and open-chained intermediates **4a** and **4b** were obtained in 3.4:1 and 2:1 ratios of *E*- and *Z*-isomers, respectively. Intermediates **4a** and **4b** were separated by column chromatography and further confirmed by NMR with characteristic signals of the closed epoxy ring (separated signals) and open-chained (merged signals) in the regions 3.38-2.67 and 4.12-3.92 ppm, respectively. Further, the nucleophilic amination was preceded with intermediate **4a** due to its closed ring. Initially, the ring-opening of intermediate **4a** with various amines was carried out using polar solvent ethanol at 60 ^{o}C. But due to competitive epoxy ring-opening by ethanol (solvent) and poor yield of final products, reaction under this condition was impeded, and thus, further optimizations have proceeded with other conditions. Finally, epoxide **4a** was treated with various primary and secondary amines in acetonitrile at reflux conditions to afford corresponding derivatives **5-19** in quantitative yields of 65-85% with varying ratios of *E*- and *Z*-isomers (**Scheme 1**). The statistical mixture of *E*- and *Z*-stereoisomers of triphenylethylene derivatives was obtained and various attempts were made to isolate these isomers but found unsuccessful due to same R_f value in different solvent systems. So, without isolating of *E*- and *Z*-stereoisomers, the synthesized analogs were characterized by ^{1}H NMR, ^{13}C NMR, and mass spectrometry. For instance, ^{1}H NMR of analogue **5** showed the characteristic signals of piperidine at δ values 2.61, 2.51-2.48; and m/z ratio was found to be 428.2. Further, the *E*/*Z* ratio of triphenylethylene derivatives was confirmed by ^{1}H NMR from the integral of respective protons[72] as well as HPLC methodology.[73]

For the correct assignment of phenyl protons of triphenylethylene analogue **12**, Co-relation spectroscopy ($^1H–^1H$ COSY)[71] was carried out. **Figure 2** represents the co-relation between the resonances of protons through bond-coupling. The doublet shift at δ value 6.89 ppm

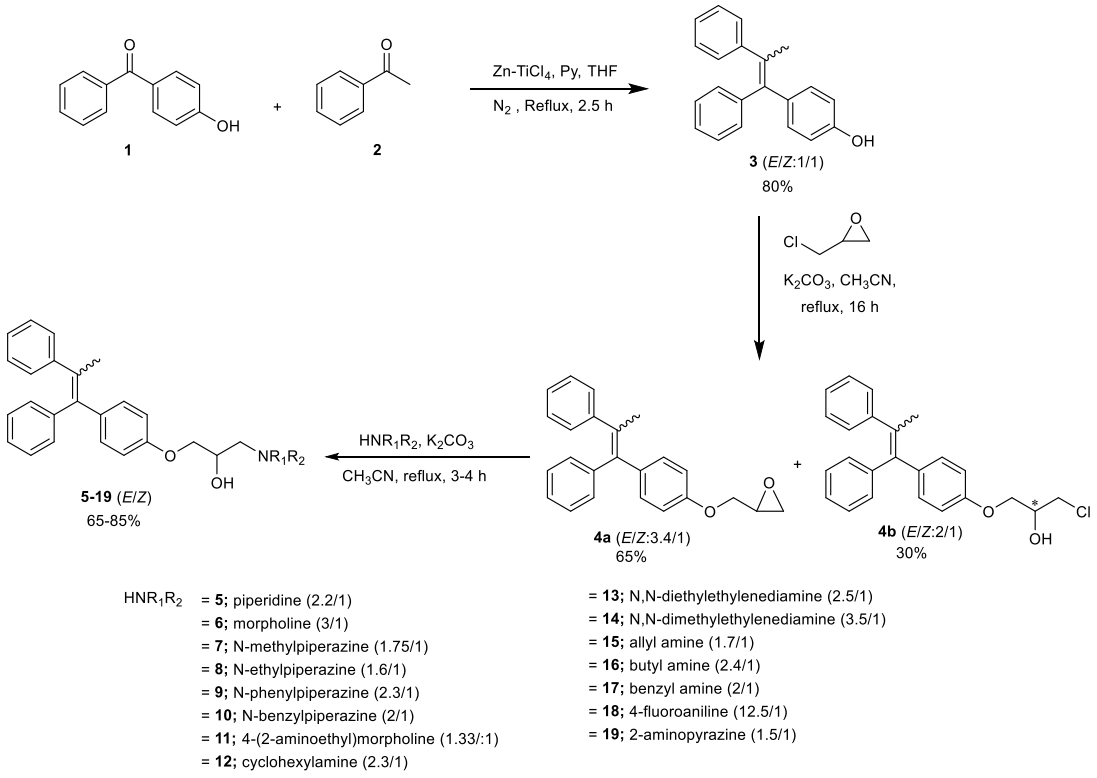

Scheme 1: Synthesis of triphenylethylene analogues with the variation of amines (**5-19**)

Table 1: Optimization of reaction conditions for the formation of intermediate **4a** in the presence of various solvents and bases.

Entry	Base	Solvent	PTC	Temperature	Yield (%)	
					4a	**4b**
1	NaOH	Water	-	rt	-	10
2.	NaOH	Water	-	reflux	-	30
3	NaOH	Water	TBAI	reflux	10	70
4	**K_2CO_3**	**Acetonitrile**	**-**	**reflux**	**65**	**30**
5	K_2CO_3	DMF	-	reflux	30	45

Bold - indicated suitable conditions to obtain **4a**

corresponds to resonances of H_1 and H_2 protons due to the electron-donating effect of the neighboring O (oxygen) atom. The resonance peak at 7.12 ppm stems from protons H_3 and H_4 as it has a strong co-relation with H_1 and H_2. The protons resonating at δ 6.89 ppm showed co-relation with protons resonating at δ 7.01 ppm, which confirmed the presence of another isomer.

After these assignments, the remaining peaks co-relating at δ values at 7.31 and 7.21 ppm, and 6.77 and 6.54 ppm belong to the proton resonances of the unsubstituted phenyl rings.

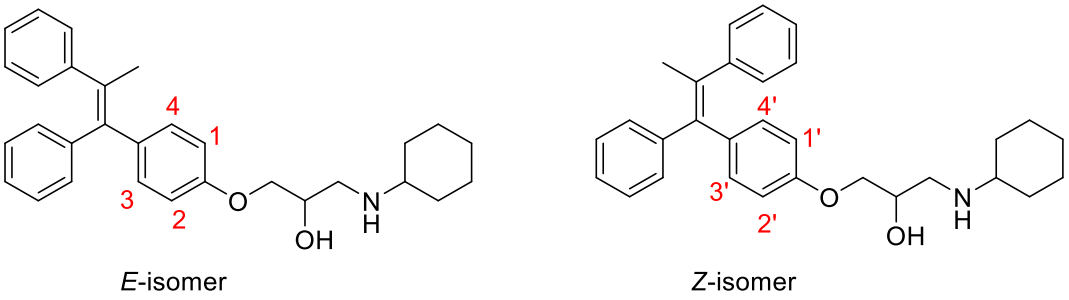

E-isomer *Z*-isomer

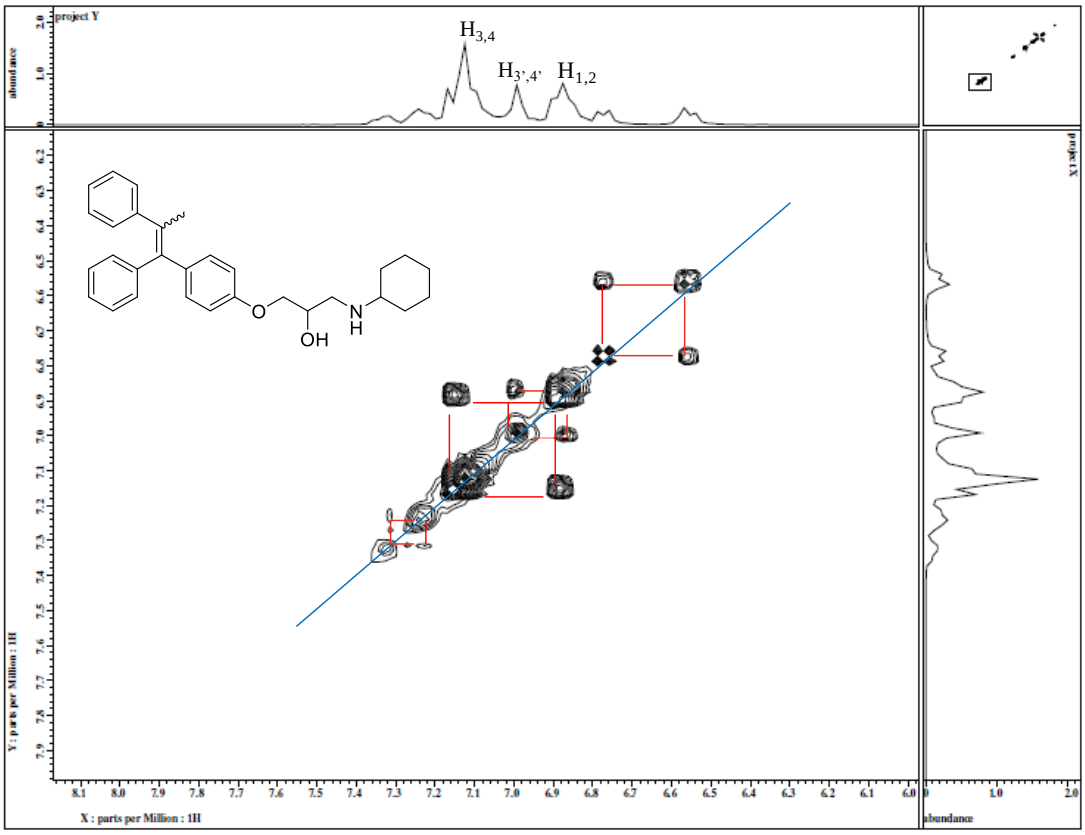

Figure 2: Partial 2D-COSY spectrum of (1-(cyclohexylamino)-3-(4-(1,2-diphenylprop-1-en-1-yl)phe noxy)propan-2-ol (**12**)

Further, the stereochemical assignments of *E*- and *Z*-isomers were also determined on the basis of Nuclear Overhauser Spectroscopy (2D-NOESY) experiments. In the NOE spectrum (**Figure 3**), cross-peaks indicated in blue-circles showed NOE between the methyl group (deshielded protons at δ 2.14 ppm) and one of the aromatic rings at δ value of 7.12 ppm. As well the OCH_2 in side chain at δ 3.83 ppm showed coupling with the phenyl ring of triphenylethylene at δ value 6.89 ppm. These couplings are absent in the case of another isomer (*Z*-isomer, at δ

2.10 ppm). This relationship is also found to be true for tamoxifen as all the protons of *E*-tamoxifen resonated down-field as compared to *Z*-tamoxifen.[74-75] These results can be accounted, if the phenyl ring is present at 90^{o} angle to the ethylene double-bond as well the side-chain and aromatic ring sandwiched between two other phenyl rings experiencing a double shielding effect from their ring-currents.

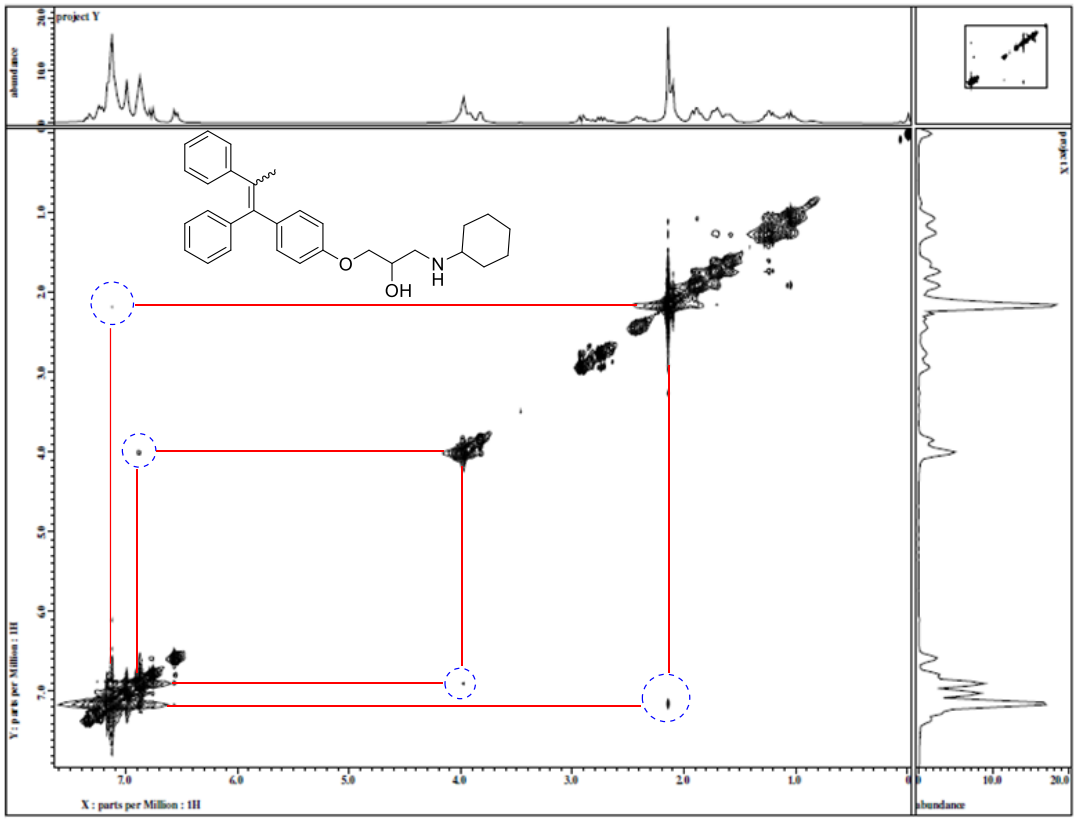

Figure 3: 2D NOE spectrum of 1-(cyclohexylamino)-3-(4-(1,2-diphenylprop-1-en-1-yl)phenoxy)propan-2-ol (**12**)

The ratios of *E*- and *Z*-isomers of triphenylethylene derivatives were confirmed by reverse phase HPLC methodology using C-18 column with a flow rate 1.0 mL/min. As in the case of compound **5**, the chromatogram was recorded at the wavelength 276nm using the mobile phase 0.01M tetrabutylammonium hydrogen sulfate: methanol: acetonitrile (5:10:85; v/v/v). Chromatogram of compound **5** spiked with *E*- and *Z*-isomers is shown in **Figure 4** and was recorded at wavelength 276 nm. The retention times of *E*- and *Z*-triphenylethylene have been found to be 10.14 and 12.41 min., respectively. Thus, ^{1}H NMR spectrum of compound **5** contained CH_3 singlet, centered at δ 2.14 ppm and δ 2.10 ppm was assigned *E* configuration

(retention time of 10.14) and *Z* configuration (retention time of 12.14), respectively. It has been revealed that the ratio of *E/Z*-isomers determined from ^{1}H NMR is corroborated with HPLC as both have the same ratio of isomers, i.e., 2.2:1. The *E/Z* ratios of other derivatives were also determined with the same methodologies.

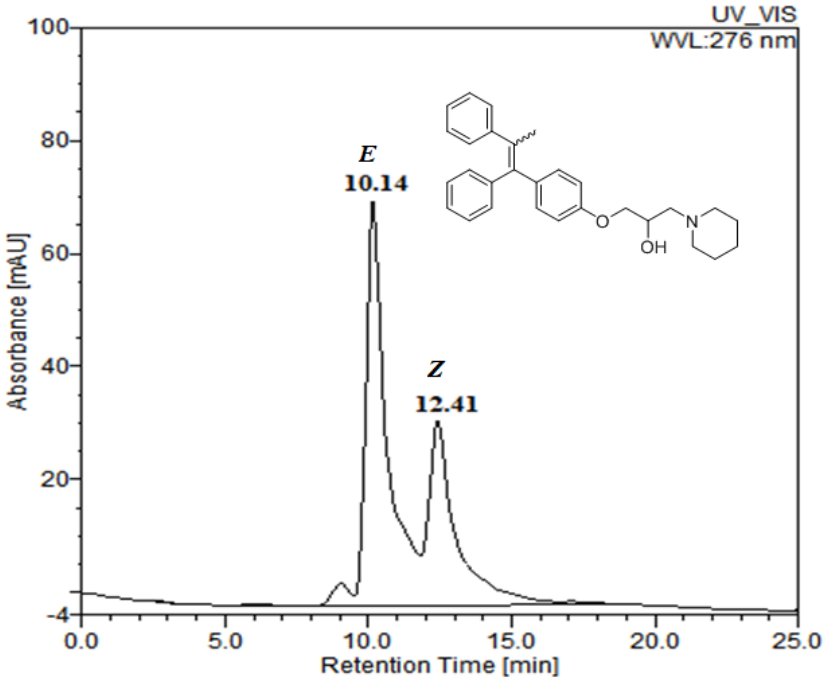

Figure 4: HPLC chromatogram of compound **5** containing a mixture of *E*- and *Z*-isomers.

2.3 Biology

2.3.1 *In vitro* antiproliferative activity

The derivatives of triphenylethylene series **5-19** were chosen by the National Cancer Institute, USA on account of computer modelling techniques for anticancer activity.[76] These compounds were evaluated *in vitro* for antiproliferative assay against a panel of 60-human cancer cell lines at a single dose of 10 μM concentration. And the percentages of growth inhibition (% GI) over these cell lines were determined (**Tables 2** and **3**). Further, the obtained results were also compared with the known drug tamoxifen.

Most of the synthesized triphenylethylene analogues showed an interesting antiproliferative activity with negative values of % growth inhibition indicating higher cytotoxicity towards most of the cancer cell lines. The opposite behavior, as expected, was found for tamoxifen, which shows cytotoxicity towards few cancer cell lines. Moreover, the comparison between the results

obtained and the chemical structures of new derivatives **5-19**, allowed some interesting structure-activity relationships to be discovered. The analogous with secondary amine substituents such as piperidine (**5**), *N*-ethylpiperazine (**8**), and *N*-benzylpiperazine (**10**), and primary amine substituents allylamine (**15**) and 2-aminopyrazine (**19**) showed scarce antiproliferative activity and were considered to be least effective in the series. Increase in lipophilicity in case of analogoues of triphenylethylene with substituents morpholine (**6**), *N*-methylpiperazine (**7**), *N*-phenylpiperazine (**9**), butylamine (**16**), benzylamine (**17**) and 4-fluoroaniline (**18**) increased the antiproliferative activity to some extent. Interestingly, derivatives bearing primary amines 4-(2-aminoethyl)morpholine (**11**), cyclohexylamine (**12**), *N*,*N*-diethylethylenediamine (**13**) and *N*,*N*-dimethylethylenediamine (**14**) rendered the compounds more active, suggesting that hydrophilicity and/or hydrogen bond donor played important roles in cytotoxic effect.

Preliminary, *in vitro* activity revealed that compound **6** inhibited leukemia cancer cell line K-562 and colon cancer cell line HT29 with growth inhibitions of 80.3% and 86.9%, respectively. Compound **7** displayed selectivity towards leukemia cancer cell lines (K-562; GI = 95.8 %, SR; GI = 96.2 %) and colon cancer cell line (HT29; GI = 91.8 %), melanoma cancer cell line (MDA-MB-435; GI = 61.6%) while compound **16** showed cytostatic activity towards leukemia cancer cell line K-562, and colon cancer cell lines HCC-2998, HCT-116, HCT-15, HT29 and KM12, and cytotoxic activity towards RPMI-8226, NCI-H322M, NCI-H522, COLO 205 and U251 cell lines. As it is clear from the data given in tables 2 and 3, due to increase in basicity, compounds **11-13** exhibited excellent cytostatic activity and cytotoxicity towards most of the cancer cell lines and therefore selected to test their anticancer activity at 5-dose concentration levels. Moreover, for most of cancer cell lines, compounds **12** and **13** had more cytotoxicity than tamoxifen, indicating these compounds exhibited high selectivity and activity than tamoxifen and may also act *via* a non-estrogen mechanism.

Table 2 Percentage growth inhibition (GI%) of *in vitro* subpanel tumor cell lines at 10 μM concentration of compounds **5-12**.

Panel	**Cell line**	**5**	**6**	**7**	**8**	**9**	**10**	**11**	**12**
Leukemia	CCRF-CEM	8.64	19.6	24.8	-	**30.0**	4.15	**43.5**	**-33.4**
	HL-60(TB)	4.77	**39.3**	21.4	7.12	**38.9**	10.8	**80.0**	**-57.1**
	K-562	**31.1**	**80.3**	**95.8**	-	**43.7**	6.25	**97.6**	**98.4**
	MOLT-4	5.24	**38.5**	**38.4**	-	**41.0**	-	**59.0**	**-42.0**

	RPMI-8226	4.61	25.0	25.0	-	**42.4**	6.98	**79.8**	**-43.7**
	SR	24.7	**52.8**	**96.2**	2.33	**39.7**	-	**99.3**	**-11.4**
Lung	A549	-	12.8	27.9	-	21.3	-	29.2	**-63.6**
	EKVX	4.16	3.36	10.9	-	21.2	-	17.2	**-32.6**
	HOP-62	-	9.90	18.2	-	-	-	25.1	**-69.7**
	HOP-92	6.16	19.8	**35.4**	2.85	26.1	-	**40.9**	**-89.5**
	NCI-H226	0.76	3.44	-	-	12.5	-	3.88	22.7
	NCI-H23	-	-	5.03	-	25.1	-	16.7	**-80.2**
	NCI-H322M	-	4.48	9.54	-	6.94	-	27.3	**-90.4**
	NCI-H460	-	7.41	29.0	11.6	19.7	-	**82.4**	**-92.0**
	NCI-H522	4.96	26.7	11.0	-	17.0	-	**55.5**	**-54.7**
Colon	COLO 205	-	**30.6**	**37.5**	-	7.80	-	**-64.5**	**-61.8**
	HCC-2998	-	-	9.11	-	-	-	**-59.6**	**-93.3**
	HCT-116	-	**53.7**	-	3.68	25.7	-	-	7.30
	HCT-15	9.85	**46.2**	23.3	-	**38.8**	-	**95.5**	**-88.2**
	HT29	29.6	**86.9**	**91.8**	-	**65.9**	-	**96.8**	**-42.3**
	KM12	-	**36.4**	28.8	-	**31.4**	-	**45.7**	**-82.8**
	SW-620	3.87	11.4	17.7	-	26.7	-	**50.9**	**-85.9**
CNS	SF-295	-	-	2.85	-	-	-	28.8	**-95.4**
	SF-539	-	25.8	15.6	-	8.67	-	27.2	**-97.2**
	SNB-19	-	-	-	5.50	-	-	8.80	**-56.5**
	SNB-75	8.61	8.61	15.3	-	24.7	-	**34.2**	**-93.7**
	U251	3.59	19.9	**35.3**	-	24.2	-	**67.4**	**-58.4**
Melanoma	LOX IMVI	-	12.2	17.6	-	7.89	-	**81.3**	**-99.2**
	MALME-3M	-	24.8	28.5	-	20.0	-	**-71.7**	**-88.6**
	M14	2.68	**-45.1**	3.59	-	10.7	-	7.31	7.51
	MDA-MB-435	-	9.29	**61.6**	-	13.3	8.99	**-63.8**	**-93.8**
	SK-MEL-2	-	1.12	-	-	10.3	-	5.09	**-60.3**
	SKMEL-28	-	10.0	17.4	3.39	-	-	**-86.2**	**-96.4**
	SK-MEL-5	1.04	12.9	9.87	-	17.8	-	**71.0**	**-96.1**
	UAAC-257	-	6.64	16.8	-	8.47	-	**-27.5**	**-62.8**
	UAAC-62	-	3.00	**37.3**	-	12.3	-	**37.3**	**-72.2**
Ovarian	IGROV1	-	3.82	**36.6**	-	9.02	-	**36.6**	**-93.3**
	OVCAR-3	-	9.60	22.1	-	15.3	-	22.1	**-88.3**
	OVCAR-4	1.77	10.7	29.8	-	25.2	-	29.7	**-86.4**
	OVCAR-5	-	12.8	24.8	-	2.30	3.01	24.7	**-91.7**
	OVCAR-8	-	11.5	21.8	1.40	11.6	-	21.8	**-37.3**
	NCI-RES	-	6.78	19.8	-	18.2	-	19.8	**-74.7**
	SK-OV 3	-	8.68	4.57	-	-	-	4.6	**-31.4**
Renal	786-0	-	**32.9**	-	5.97	17.6	-	2.4	-
	A-498	13.5	8.44	14.0	-	-	-	20.1	**31.7**
	ACHN	-	1.16	1.00	-	2.30	4.23	18.6	**-100.0**
	CAKI-1	11.0	19.9	11.2	14.3	17.8	-	**32.1**	**-95.9**
	SN12C	2.91	11.6	10.9	-	22.4	-	23.9	**-91.0**
	TK-10	-	5.68	5.31	-	2.44	-	26.5	**-77.0**
	UO-31	17.4	26.3	22.4	-	**63.2**	-	**30.8**	**-99.8**

Prostate	PC-3	3.23	28.2	16.2	-	22.4	-	**34.5**	**-79.4**
	DU-145	-	1.88	11.0	-	8.36	**30.1**	**32.3**	**-89.1**
Breast	MCF7	14.8	15.8	**30.2**	-	**53.0**	-	**55.4**	**-89.8**
	MDA-MB-231	-	-	-	-	10.2	-	**70.6**	**-90.4**
	HS 578T	6.96	9.19	16.2	-	9.59	-	29.5	**-58.5**
	BT-549	-	6.69	-	-	5.70	10.7	-	-
	T-47D	10.8	**39.7**	5.73	-	**45.2**	-	10.7	**-60.5**
	MDA-MB-468	1.28	14.9	6.56	-	26.2	-	**46.9**	**-79.5**

- indicated inactive, **orange bold** –30-40 %GI, **black bold** – 40-50 %GI, **pink bold** – 50-70 %GI, **blue bold** – 70-100 %GI, **red bold** - cytotoxic

Table 3 Percentage growth inhibition (GI%) of *in vitro* subpanel tumor cell lines at 10 μM concentration of compounds **13-19**.

Panel	**Cell Lines**	**13**	**14**	**15**	**16**	**17**	**18**	**19**	**TAM**
Leukemia	CCRF-CEM	**-18.0**	**69.2**	-	**31.0**	6.47	**32.9**	-	**65.4**
	HL-60(TB)	**-49.1**	**-13.7**	-	**37.0**	6.20	**69.5**	-	**60.4**
	K-562	**-23.0**	**90.0**	2.90	**88.8**	14.9	29.6	17.7	-
	MOLT-4	**-18.5**	**52.0**	-	**31.7**	19.1	**37.4**	-	**66.7**
	RPMI-8226	**-34.9**	**61.3**	-	**-17.7**	-	**37.4**	-	**-28.3**
	SR	**-5.03**	**-1.12**	4.07	23.6	14.6	**30.6**	-	**-18.9**
Lung	A549	**-32.1**	28.6	1.77	11.0	14.0	24.9	-	**50.2**
	EKVX	**82.3**	19.3	1.36	-	17.2	18.8	-	**40.0**
	HOP-62	**-41.8**	22.5	-	4.26	9.26	-	-	**56.9**
	HOP-92	**-9.64**	**50.2**	-	5.49	28.6	-	-	
	NCI-H226	17.1	-	-	3.96	18.5	-	-	7.50
	NCI-H23	**65.3**	9.83	-	12.3	14.0	18.4	14.1	**39.7**
	NCI-H322M	**-1.25**	17.6	-	**-45.5**	4.28	-	-	**34.0**
	NCI-H460	**-81.0**	**78.3**	-	14.2	5.91	7.71	-	**97.6**
	NCI-H522	**-24.0**	27.8	11.8	**-26.2**	20.7	**37.8**	23.0	**53.4**
Colon	COLO 205	**-50.7**	**-47.3**	-	**-37.8**	-	-	-	**-89.0**
	HCC-2998	**-85.5**	**56.6**	-	**91.7**	-	7.30	-	**83.7**
	HCT-116	33.2	21.9	28.8	**82.1**	15.9	25.0	7.02	**73.8**
	HCT-15	**-24.3**	**69.6**	-	**89.3**	5.69	25.7	3.04	**92.4**
	HT29	**-28.6**	**90.3**	-	**60.3**	7.92	12.1	-	**-11.2**
	KM12	**-92.3**	29.6	-	**85.3**	6.54	23.2	6.05	**75.0**
	SW-620	**-69.1**	29.0	-	1.48	3.38	16.6	-	**95.1**
CNS	SF-268	-	-	-	-	-	-	-	**43.3**
	SF-295	**-83.2**	25.4	-	11.3	5.41	-	-	**59.8**
	SF-539	**-83.6**	25.3	6.54	5.35	-	4.09	-	-
	SNB-19	**91.3**	16.3	1.10	19.3	7.77	-	-	**47.4**
	SNB-75	**-87.4**	12.0	-	27.6	20.4	3.70	-	**60.1**
	U251	**-50.8**	**72.8**	-	**-81.5**	4.71	-	-	**95.2**
Melanoma	LOX IMVI	**-83.5**	**72.5**	-	15.8	13.4	13.7	12.1	**-43.9**
	MALME-3M	**-88.8**	**37.8**	4.11	23.8	12.3	7.44	-	**-67.5**

	M14	9.43	17.6	-	-	11.5	8.93	-	**-75.0**
	MDA-MB-435	**88.0**	**92.6**	-	-	8.49	3.48	-	**62.2**
	SK-MEL-2	**-41.5**	2.14	-	2.72	5.85	-	-	**31.5**
	SKMEL-28	**-87.1**	**39.7**	-	6.69	-	-	-	**88.7**
	SK-MEL-5	**-97.0**	24.6	-	-	6.41	2.29	-	**-95.2**
	UAAC-257	**-55.8**	25.4	-	**34.6**	-	-	-	**-64.3**
	UAAC-62	**-82.7**	-	-	23.2	**36.5**	11.4	25.7	-
Ovarian	IGROV1	**-32.0**	23.8	-	22.2	16.2	3.55	12.2	**58.8**
	OVCAR-3	**-70.8**	19.8	-	-	7.40	9.31	-	**47.1**
	OVCAR-4	**-52.4**	27.0	-	**46.1**	20.6	17.4	17.2	**53.7**
	OVCAR-5	**84.3**	13.0	4.33	17.1	2.67	-	-	-
	OVCAR-8	**91.3**	22.1	-	-	6.12	4.04	-	**39.5**
	NCI-RES	**59.4**	7.12	-	18.8	8.36	9.09	-	**56.8**
	SK-OV 3	**-52.7**	-	-	9.09	-		-	**33.2**
Renal	786-0	9.79	9.16	1.87	2.91	-	7.44	-	**-41.0**
	A-498	**-76.2**	17.1	4.04	21.0	-	-	20.7	**35.9**
	ACHN	**-33.5**	20.7	-	23.6	14.8	10.6	3.74	**39.4**
	CAKI-1	**-56.5**	24.2	4.39	-	**35.1**	**72.1**	20.0	**70.9**
	SN12C	**68.7**	13.0	-	**43.5**	13.0	21.1	-	**52.3**
	TK-10	**-28.9**	11.6	2.21	26.2	-	-	-	**48.1**
	UO-31	**-83.6**	**30.5**	8.86	24.1	**42.4**	**57.2**	**30.2**	**59.7**
Prostate	PC-3	**-22.5**	24.2	3.41	**62.2**	19.3	26.4	6.19	**65.6**
	DU-145	**94.6**	22.0	-	-	5.95	3.45	-	**34.6**
Breast	MCF7	**-46.0**	27.1	-	6.81	-	13.4	-	**-10.3**
	MDA-MB-231	**-43.6**	**31.7**	-	-	26.9	29.0	11.7	**54.8**
	HS 578T	**-47.8**	22.5	-	11.4	20.6	-	-	**39.5**
	BT-549	6.02	6.37	-	**86.6**	-	-	-	**30.2**
	T-47D	**-3.36**		-	-	18.9	25.7	18.4	-
	MDA-MB-468	**-65.2**	**42.2**	-	-	8.72	8.97	11.5	**-13.3**

- indicated inactive, **orange bold** –30-40 %GI, **black bold** – 40-50 %GI, **pink bold** – 50-70 %GI, **blue bold** – 70-100 %GI, **red bold** - cytotoxic

Compounds **11-13** were selected by the NCI for further testing for *in vitro* antitumor activity against 60 human tumor cell lines. The median growth inhibition concentration (GI_{50}), total growth inhibition (TGI), and half-maximal lethal concentration (LC_{50}) were measured in micromolar range for each cell line. For K562 human leukemia cancer cell line, compounds **12** and **13** had GI_{50} values of 0.35 μM and 0.52 μM, respectively; represent an activity higher than that of tamoxifen (TAM). Compound **13** also showed excellent activity towards colon cancer cell line HT29 and melanoma cancer cell line LOXIMVI with GI_{50} values of 0.56 μM and 0.43 μM, respectively. The MG MID GI_{50} values of these three compounds against 60 tumor cell lines were compared with known drug TAM as positive control in **Table 4.** Compound **11** showed comparable activity as tamoxifen while compound **12** bearing cyclohexylamine in the side-chain

with GI_{50} value of 1.69 μM, and compound **13** containing *N*,*N*-diethyl ethylenediamine as side chain with GI_{50} value of 1.53 μM, showed enhanced activity as compared to tamoxifen (GI_{50} = 3.76 μM). It is concluded that compounds **12 (**pK_a = 7.65**)** and **13(**pK_a = 7.85) were found to be 2-3 fold more active than tamoxifen.

Table 4: Compounds **11-13** and TAM with median growth-inhibitory (GI_{50}, μM), total growth-inhibitory (TGI, μM), and median lethal concentrations (LC_{50}, μM) of *in vitro* subpanel cancer cell lines.

Compound	Activity (μM)	I	II	III	IV	V	VI	VII	VIII	IX	MIG-MID[a]
11	GI_{50}	2.19	4.19	2.06	2.81	1.87	5.20	2.40	3.57	3.69	**3.10**
	TGI	5.80	12.2	5.50	9.90	3.74	16.3	7.75	12.9	9.08	9.25
	LC_{50}	23.9	36.3	13.7	25.2	8.55	45.8	22.0	38.4	29.0	26.7
12	GI_{50}	1.54	1.70	1.56	1.69	1.81	1.96	1.62	1.67	1.73	**1.69**
	TGI	3.81	3.37	3.30	3.22	3.38	3.43	2.99	3.90	3.58	3.36
	LC_{50}	38.6	5.85	5.64	5.87	6.11	24.0	5.71	6.11	6.73	11.6
13	GI_{50}	1.29	1.50	1.23	1.47	1.28	1.65	1.40	2.40	1.59	**1.53**
	TGI	3.70	3.11	2.85	2.93	2.95	3.27	2.79	4.81	3.54	3.32
	LC_{50}	1.50	5.87	5.93	5.45	5.46	6.04	5.47	6.39	37.2	8.81
TAM	GI_{50}	2.08	4.01	1.88	4.04	2.03	4.70	7.71	4.40	3.05	**3.76**
	TGI	6.42	9.20	5.96	10.6	5.49	11.8	1.19	11.1	10.3	9.01
	LC_{50}	2.90	2.60	1.77	44.1	1.70	2.78	2.59	2.33	2.83	24.4

I, leukemia; II, non-small cell lung cancer; III, colon cancer; IV, CNS cancer; V, melanoma; VI, ovarian cancer; VII, renal cancer; VIII, prostate cancer; IX, breast cancer. [a]Full panel mean-graph midpoint (μM). TAM = Tamoxifen.

2.3.2 MTT assay

To evaluate the cytotoxic effect of compounds **11**, **12** and **13** on human normal cell line Hek293, a colorimetric assay (MTT assay) was performed at five different concentrations of 10^{-4}, 10^{-5}, 10^{-6}, 10^{-7}, and 10^{-8} M. It has been observed that derivative **11** showed only 15.8%, 13.7%, 7.04%, 5.43% and 4.74% cytotoxicity to Hek293 cells whereas compound **12** exhibited 18.9%, 15.1%, 9.13%, 6.34% and 5.29%; and compound **13** displayed 20.1%, 16.5%, 14.9%, 14.6%, 8.08% cytotoxicity to Hek293 cells at above said concentrations (**Figure 5)**. It revealed that the potent compounds **11**, **12,** and **13** showed low cytotoxicity against normal cells and selectively killed the cancer cells. These compounds showed only 20% toxicity to Hek293 cells even at 100 μM concentration.

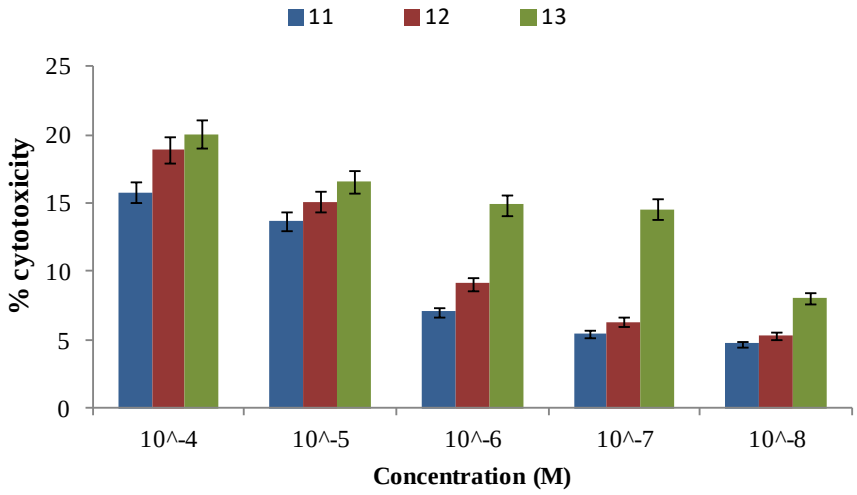

Figure 5: Cytotoxic effect of compounds **11**, **12,** and **13** to human normal cell line (Hek293).

2.3.3 DNA topoisomerase-IIα mediated relaxation activity

Topoisomerase is a class of nucleoenzyme and the enzymatic action of topoisomerase-IIα converts the supercoiled DNA into relaxed form. The inhibition of topoisomerase-II action impairs DNA replication, thus prevents cell growth.[77] Several drugs such as etoposide, idarubicin, daunorubicin, doxorubicin, epipodophyllotoxins, teniposide, and mitoxantrone act as TOPO-II inhibitor. Enzyme topoisomerase-II is mainly expressed in lung cancer, leukemia, malignant lymphoma, breast cancer, and ovarian cancer.[78] The most active triphenylethylene analogues **11**, **12**, and **13** displayed broad-spectrum anticancer-activity towards 60 human cancer cell lines. Therefore, to account for possible mechanism of cytotoxicity, the effect of the most active compounds **11**, **12**, and **13** on the relaxation activity of plasmid DNA catalyzed TOPO-IIα was analyzed. Etoposide (DNA intercalator, TOPO-II inhibitor) was used as a positive control as it also elicited wide spectrum anticancer activity towards various 60 human cancer cell lines. At low concentration, etoposide acts as TOPO-II inhibitor, while at high concentration, it behaves as TOPO-II poison. Supercoiled pHOT1 plasmid DNA was incubated with TOPO-IIα, and 50 μL of compounds **11**, **12,** and **13** in different wells on 1% agarose gel, and DNA relaxation product was resolved by gel electrophoresis (BIO-RAD). **Figure 6** shows the effect of representative compounds (**11, 12**, **13,** and positive control) on the relaxation of plasmid pHOT1 DNA, mediated by topoisomerase-IIα. Among these compounds, compounds **12** and **13** exerted a significant but partial inhibitory effect on topoisomerase-II relaxation at 50 μM concentration, as demonstrated by the appearance of supercoiled DNA. These triphenylethylene analogues bind

with the ATPase-active site of TOPO-II (by acting as a non-competitive inhibitor of ATP) and prevent the binding of two ATP molecules and hydrolysis. The binding and hydrolysis of ATP molecule is the driving force to release DNA in unwound form. The side chain of these triphenylethylene derivatives acts as bronsted-lowry and Lewis acid thus interacts with TOPO-II through these binding sites. Increase in number of binding sites enhances interacting forces such as hydrogen-bonding and van der walls forces with TOP-II. This data revealed that triphenylethylene analogues showed antiproliferative activity through TOPO-II inhibition. Taking into account that compound **11** exerts the low antiproliferative capacity. These data could also suggest the contribution of the inhibition on topoisomerase-II to cytotoxicity.

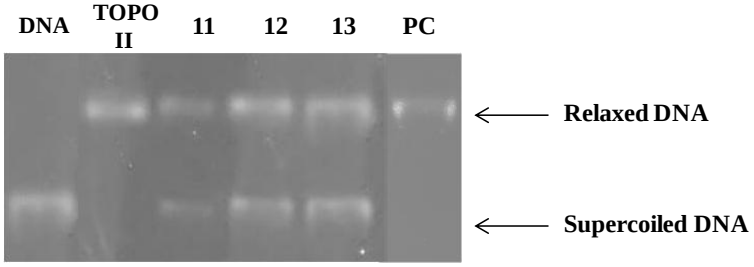

Figure 6: Effect on relaxation activity of supercoiled pHOT1 plasmid DNA by topoisomerase-IIα. Supercoiled plasmid DNA was incubated with topoisomerase-IIα, in the absence (TOPO-II) and in the presence of compounds **11**, **12**, **13,** and etoposide positive control (PC) at 50 μM concentrations.

2.4 Physicochemical properties

Absorption, Distribution, Metabolism, Excretion, and Toxicity (ADMET) predicts the pharmacokinetic behavior of a molecule, and structural modifications in molecule alters its pharmacokinetics and distribution of a drug.[79] To determine the properties and drug-like characteristics of compounds **5-19**, we have carried out the theoretical predictions of ADMET parameters (log P, logD, molecular weight, TPSA, number of hydrogen donors and acceptors, and Lipinski rule violation) using MedChem_designer 5.5 software.[80] If a compound has log P ≤ 5 (octanol-water partition coefficient; defines lipophilicity of neutral/ non-ionizable compounds; logP = logD at any pH), logD (it measures the liopohilicity of ionizable compound at specific pH), TPSA (topological polar surface area) ≤ 140, molecular weight ≤ 500, number of H acceptor (nNO) ≤ 10, number of hydrogen bond donor (nNHOH) ≤ 5, then it is considered to be orally bioavailable drug. S + log P predicts the solubility of the compound in aqueous media, and

higher S + log P value lesser the solubility in an aqueous medium. Compounds with violation of ADMET and Lipinski's rule of five[81] have poor solubility and low absorption. Moreover, violation of two rules of Lipinski's out of five indicates poor bioavailability and occurrence of only passive transportation across membrane. As shown in **Table 5**, it is concluded that compounds selected for *in vitro* anticancer activity displayed good physicochemical properties except **9**, **10**, **17,** and **18** where the violation is due to either higher molecular weight or log P > 5. The antitumor activity of compounds **11-13** also supported the physicochemical parameters where no violation exists.

Table 5: Physicochemical properties of triphenylethylene analogues **5-19** and reference drug tamoxifen

Entry	Diff. coeff.	MlogP	S+logP	S+logD	TPSA	Mol. Wt.	nNO	nNHOH	nviolation
5	0.574	4.568	5.750	4.167	32.70	427.59	3	1	none
6	0.583	3.564	5.061	5.099	41.93	429.56	4	1	none
7	0.564	3.760	4.981	4.002	35.94	442.60	4	1	none
8	0.551	3.953	5.224	3.925	35.94	456.63	4	1	none
9	0.527	4.754	6.584	6.479	35.94	504.67	4	1	1
10	0.516	4.660	6.277	5.890	35.94	518.70	4	1	1
11	0.547	3.165	4.847	3.097	53.96	472.63	5	2	none
12	0.560	4.761	6.247	4.167	41.49	441.62	3	2	none
13	0.539	4.345	5.519	3.051	44.73	458.65	4	2	none
14	0.564	3.956	5.109	5.530	44.73	430.59	4	2	none
15	0.594	4.494	5.081	3.482	41.49	399.54	3	2	none
16	0.574	4.764	5.954	3.819	41.49	415.57	3	2	none
17	0.560	5.129	6.136	5.061	41.49	449.59	3	2	1
18	0.571	5.571	6.797	6.796	41.49	453.56	3	2	1
19	0.583	3.237	4.949	4.949	67.27	437.54	5	2	none
TAM	0.610	5.201	6.642	5.530	12.47	371.52	2	0	1

TAM = Tamoxifen

2.5 Molecular docking

Molecular docking studies were performed to understand the intermolecular interactions between binary complex of topoisomerase-II-DNA (PDB code: 5GWK) and ligands (**11**, **12** and **13**) using AutoDock vina software 4.0 and compared with etoposide.[82] The binding energy scores for ligands **11**, **12**, **13** and etoposide (reference drug) were calculated to be -9.3, -8.6, -7.6 and -9.8 kcal/mol, respectively; suggesting a strong binding affinity of tamoxifen derivatives for the proposed binding sites, although it was not possible to effectively rank the compounds, due to the small binding energy differences observed among them, that are in general lower than the suggested significant threshold (2.5 kcal/mol). These compounds were stabilized in the active

site of TOPO-II through hydrogen bonding, π-π stacking and hydrophobic interactions (**Figure 7**). Compound **11** interacted with residues of TOPO-II *via* Asp463 (*d* = 2.68 Å) through hydrogen bonding, and Gly462, Gly760, Tyr805, Lys614, and Leu616 with van der Waal's forces; backbone of DNA through DT-9 (*d* = 2.08 Å) *via* hydrogen-bonding; DC8, DT9 *via* electrostatic force of attraction, and DC-8 through hydrophobic interactions (**Figure 7a**). Compound **12** is surrounded by only residues of TOPO-II, Glu839 H-bonding (*d* = 2.73 Å) and electrostatic interactions; Phe1003, His759, Pro724 and Arg713 (hydrophobic interaction) (**Figure 7b**). Compound **13** binds with TOPO-II Lys728 (*d* = 2.29 Å) and Ser756 (*d* = 2.63 Å) residues by hydrogen bonds; Glu839, Phe1003 and Pro724 by hydrophobic interactions; stacked DNA bases, DG-7 (*d* = 4.69 Å) by electrostatic charge attractions (**Figure 7c**). On the other hand, etoposide binds with TOPO-II complex *via* Asn770 (*d* = 2.38 Å) and Gln773 (*d* = 2.52 Å)

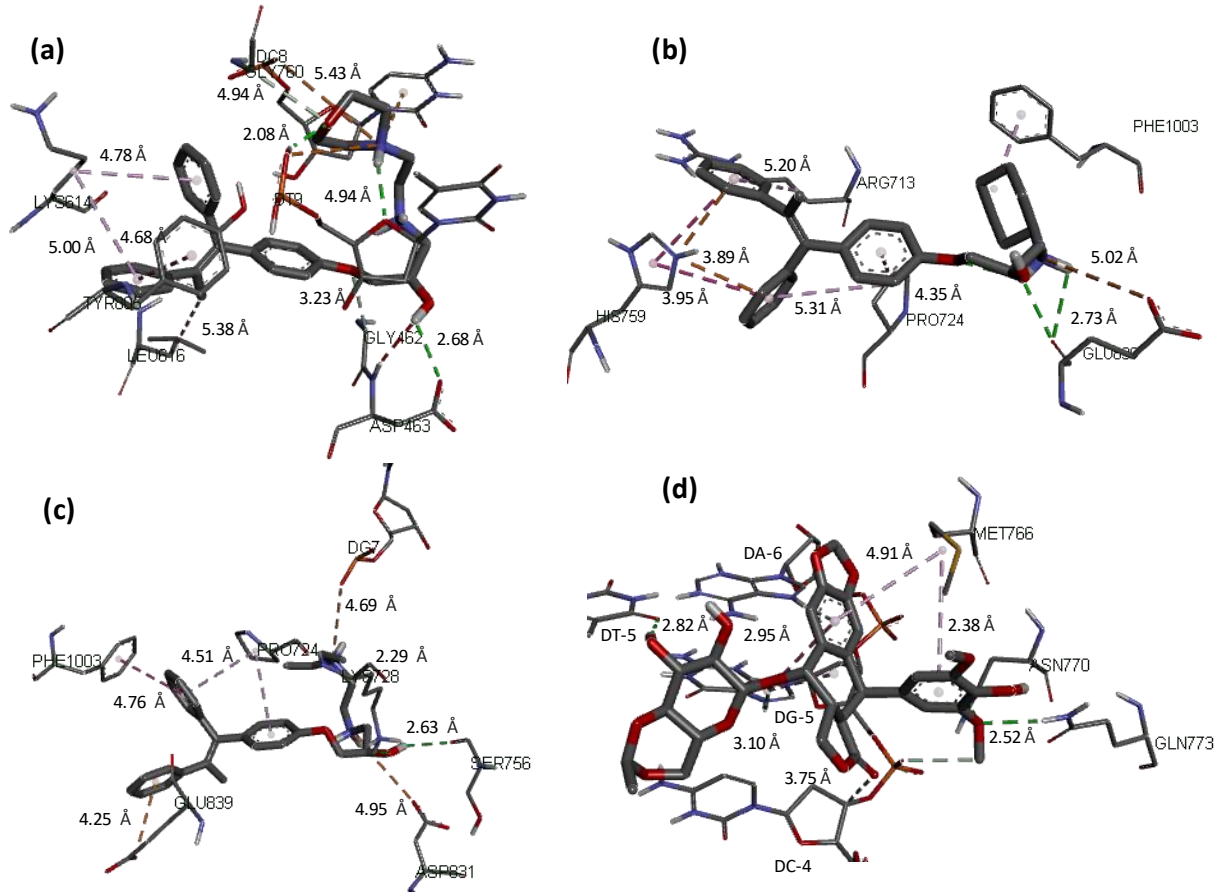

Figure 7: Binding poses showing interactions of compounds **11** (a), **12** (b), **13** (c) and etoposide (d) with TOPO-II-DNA binary complex (PDB code: 5GWK) at pH 7.4.

residues by conventional hydrogen bondings; Met766 through hydrophobic interactions; and sugar back-bone of DNA through DT-5 (*d* = 2.82 Å), DC-4 (*d* = 3.75 Å), DA-6 (*d* = 2.95 Å), and DG-5 (*d* = 3.10 Å) (**Figure 7d).**

Like etoposide, protonated triphenylethylenes **11** and **13** displayed appreciable interactions with TOPO-II as well with DNA except analogue **12** bearing protonated cyclohexylamine. It indicated that triphenylethylene analogues behave as both TOPO-II inhibitor and poison.

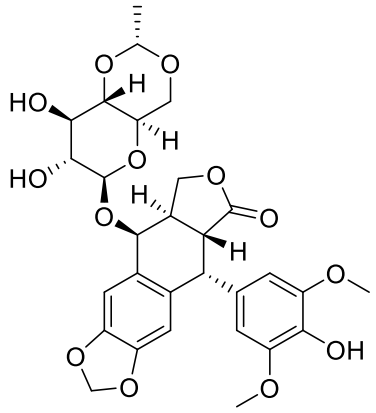

Etoposide

Figure 8: Structure of TOPO-II inhibitor and poison, etoposide

2.6 Conclusion

In this chapter, we have identified a novel series of aminopropan-2-ol based *E/Z*-tamoxifen and characterized by NMR and HPLC spectroscopy. The biological data on 60 different human cancer cell lines at one dose and five dose concentration levels showed interesting activity for most of the described compounds. The presence of primary amines *viz.*, (2-aminoethyl)morpholine (**11**), cyclohexylamine (**12**) and *N*,*N*-diethylethylenediamine (**13**) at the side chain seems to improve the cytotoxic activity due to increase in the ability of hydrogen donor while most of the secondary amines of the tamoxifen skeleton did not affect positively on the cytotoxicity of the compound. MTT assay towards normal cell line Hek293 suggests that these compounds could kill selectively cancer cells and not normal cells. Further, biological experiments pointed out TOPO-II as a possible intracellular target responsible for the cytotoxicity of these compounds. Moreover, a docking study was performed and predicted the binding of compounds with TOPO-II by forming H-bond, van der Waal's interaction and

hydrophobic interaction. Interestingly, notwithstanding the common general triarylskeleton, here reported tamoxifen analogs show a different biological profile with respect to the reference drug, being more cytotoxic on non-estrogenic cell lines and affecting the catalytic activity of the topoisomerase-II. Altogether, these results show various aminopropan-2-ol as an interesting side chain for the development of new anticancer compounds. Altogether, the biological screening results showed triphenylethylene derivatives as an interesting scaffold and gives new insight into the development of novel anticancer drugs.

2.7 Experimental section

All substrates, reagents, and solvents were purchased from Aldrich, Spectrochem, TCI and used without further purification. Reactions were carried out using dry solvent under nitrogen atmosphere. Melting points were determined in open capillaries and were uncorrected. Reactions were monitored by thin-layer chromatography using silica gel GF-254 and visualized by UV light. Column chromatography was performed using silica gel of mesh size 60-120. ^{1}H and ^{13}C NMR were recorded on Jeol spectrometer (400 MHz for ^{1}H and 100 MHz for ^{13}C) using $CDCl_3$ as a solvent. Chemical shifts are reported in parts per million (ppm) with TMS as an internal reference. Mass spectra of the synthesized compounds were observed at Water Micromass-Q-T of Micro. The HPLC chromatograms of synthesized compounds were recorded using Ultimate 3000 HPLC (Thermofisher Scientific) system. The TOPO-II inhibition assay was performed using Gel-Electrophoresis technique (BIO-RAD).

4-(1,2-Diphenylprop-1-en-1-yl)phenol (3)

To a two-necked oven-dried round bottom flask, a suspension of zinc (1.61 g, 25.2 mmol) in 20 mL of dry THF was stirred at 0-5 ^{o}C for 15 minutes. To the stirred suspension, the slow addition of $TiCl_4$ (1.38 mL, 12.6 mmol) was done carefully with the help of a syringe under the inert atmosphere of nitrogen. After the complete addition of $TiCl_4$, the resulting black mixture was stirred at room temperature for 30 minutes and then allowed to reflux for 3 h. The reaction mixture was gradually cooled to 0 ^{o}C and was charged with pyridine (0.5 mL, 6.3 mmol), and further stirred for 15 minutes. A solution of 4-hydroxy benzophenone (0.5 g, 2.5 mmol) and acetophenone (0.29 mL, 2.5 mmol) in dried THF was added slowly to the reaction mixture. The reaction was refluxed for 2.5 h. The reaction was monitored by TLC. After the completion of the reaction, it was quenched by the addition of a 10% aqueous solution of K_2CO_3 till neutralization. Then, the quenched solution was filtered off. From the filtrate, the crude product was extracted

with chloroform. The organic layer was dried over sodium sulfate and the solvent was evaporated. A yellow colored oily product was collected. The crude was purified by column chromatography using eluents hexane-ethyl acetate (97:3) to obtain the desired product. Finally, the chromatographed product was washed with hexane to afford white-colored precipitates of *E/Z* diastereomers.

4-(1,2-Diphenylprop-1-en-1-yl)phenol (3)

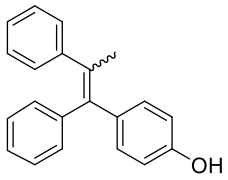

White solid, *E/Z* 1:1; 80% yield; mp. 145-148 ^{o}C; ^{1}H NMR (400 MHz, $CDCl_3$) δ 7.35-7.31 (m, 2H, ArH), 7.23–7.21 (m, 3H, ArH), 7.18-7.05 (m, 12H, ArH), 7.03-6.96 (m, 3H, ArH), 6.89-6.84 (m, 2H, ArH), 6.81-6.77(m, 2H, ArH), 6.75-6.71 (m, 2H, ArH), 6.49-6.45 (m, 2H, ArH), 4.81 (s,1H, OH), 4.59 (s,1H, OH), 2.14 (s, 3H, CH_3), 2.10 (s, 3H, CH_3); ^{13}C NMR (100MHz, $CDCl_3$) δ 154.22, 153.54, 144.32, 144.27, 143.81, 143.42, 138.84, 138.73, 136.21, 135.85, 135.41, 134.95, 132.28, 131.53, 131.02, 130.12, 129.42, 129.40, 128.19, 128.01, 127.93, 127.46, 126.64, 126.19, 126.18, 125.86, 115.00, 114.43 (Ar-C), 23.52 (CH_3), 23.44(CH_3); MS: 287.1 $[M+1]^{+}$.

2-((4-(1,2-Diphenylprop-1-en-1-yl)phenoxy)methyl)oxirane (4)

4-(1,2-Diphenylprop-1-en-1-yl)phenol (1.0 g, 3.5 mmol) **3** was refluxed with epichlorohydrin (2.73 mL, 34.9 mmol) in the presence of potassium carbonate (0.58 g, 4.1 mmol) in acetonitrile for 16 h. After the completion of reaction, the solvent was evaporated under reduced pressure. Then the product was extracted from aqueous layer using $CHCl_3$. On removal of chloroform, the white colored semi-solid product was obtained. The crude was further purified by column chromatography by employing hexane-ethylacetate (98:2) as solvent system.

2-((4-(1,2-Diphenylprop-1-en-1-yl)phenoxy)methyl)oxirane (4a)

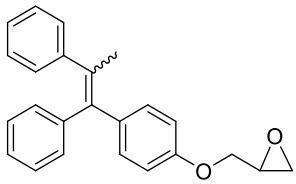

White solid; 65% yield; *E*:*Z* = 3.4:1; mp. 58-62 ^{o}C; ^{1}H NMR (400 MHz, $CDCl_3$) δ 7.35-7.28 (m, 1H), 7.24-7.19 (m, 1H), 7.17-7.08 (m, 10H), 6.90-6.76 (m, 5H), 6.79-6.76 (m, 1H), 6.59-6.54 (m, 1H), 4.22 (dd, 1H, *J* = 11.0, *J* = 3.24 Hz, OCH_2), 4.18 (dd, 1H, *J* = 11.04, *J* = 3.24 Hz, OCH_2), 3.97 (dd, 1H, *J* = 10.60, *J* = 5.64 Hz, OCH_2), 3.82 (dd,1H, *J* = 10.92, *J* = 5.64 Hz, OCH_2), 3.38-3.33 (m, 1H, CH-epoxy), 3.29-3.25 (m, 1H, CH-epoxy), 2.92-2.87 (m, 1H, CH_2-epoxy), 2.86-2.83 (m, 1H, CH_2-epoxy), 2.77-2.73 (m, 1H, CH_2-epoxy), 2.69-2.67 (m, 1H, CH_2-epoxy), 2.14 (s, 3H, CH_3), 2.10 (s, 3H, CH_3); ^{13}C NMR (100 MHz, $CDCl_3$) δ 157.28, 156.61, 144.33, 144.30, 143.86, 143.45, 138.92, 138.80, 136.65, 136.64, 136.23, 135.53, 135.10,

132.17, 131.43, 131.07, 130.17, 129.47, 129.44, 128.26, 128.10, 128.00, 127.54, 126.71, 126.27, 125.94, 114.28, 113.62 (Ar-C), 68.88 (OCH_2), 68.61 (OCH_2), 50.30 (epoxy OCH), 50.20 (epoxy OCH), 44.89 (epoxy OCH_2), 44.86 (epoxy OCH_2), 23.59 (CH_3), 23.53 (CH_3); MS: 343.1 $[M+1]^+$.

1-Chloro-3-(4-(1,2-diphenylprop-1-en-1-yl)phenoxy)propan-2-ol (4b)

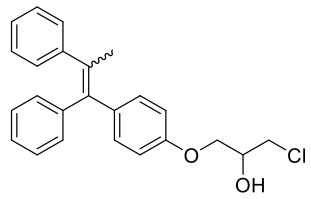

White solid; 30% yield; *E*:*Z* = 2:1; ^{1}H NMR (400 MHz, $CDCl_3$) δ 7.36-7.33 (m, 1H, ArH), 7.27-7.23 (m, 2H, ArH), 7.19-7.04 (m, 9H, ArH), 7.02-7.01 (m, 2H, ArH), 6.93-6.87 (m, 4H, ArH), 6.82-6.77 (m, 1H, ArH), 6.61-6.54 (m, 1H, ArH), 4.43-4.41 (m, 1H, CH-OH), 4.33-4.31 (m, 1H, CH-OH), 4.22-4.15 (m, 2H, OCH_2), 4.12-4.08 (m, 1H, OCH_2), 4.07-3.99 (m, 1H, CHCl), 3.97-3.92 (m, 1H, CHCl), 2.16 (s, 3H, CH_3), 2.12 (s, 3H, CH_3).

1-(4-(1,2-Diphenylprop-1-en-1-yl)phenoxy)-3-aminopropan-2-ol (5-19): To a solution of 2-2-((4-(1,2-diphenylprop-1-en-1-yl)phenoxy)methyl)oxirane **4** (0.10 g, 0.2 mmol) in acetonitrile, K_2CO_3 (0.048 g, 0.35 mmol) was added and the solution was refluxed with various primary and secondary amines (1.4 mmol) for 3-4 h until the completion of reaction. After removal of solvent under reduced pressure, water was added to the reaction mixture and extracted with chloroform. The obtained residues were purified by column chromatography using different ratios of hexane-ethyl acetate as eluents to give compounds **5-19**.

1-(4-(1,2-Diphenylprop-1-en-1-yl)phenoxy)-3-(piperidin-1-yl)propan-2-ol (5)

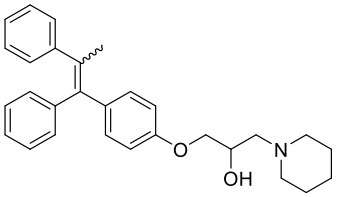

White solid, *E*/*Z* : 2.2/1; Yield 75 %; mp: 125-127 ^oC; ^{1}H NMR (400 MHz, $CDCl_3$) δ 7.35-7.31 (m, 1H), 7.24-7.20 (m, 1H), 7.15-7.07 (m, 9H), 7.02-6.97 (m, 3H), 6.90-6.84 (m, 4H), 6.77-6.74 (m,1H), 6.58-6.54 (m, 1H), 4.12-4.06 (m, 1H, OCH_3), 4.01-3.99 (m, 1H, OCH_3), 3.98-3.97 (m, 1H, OCH) 3.96-3.94 (m, 1H, OCH), 3.85-3.79 (m, 1H, OCH_2), 3.49-3.44 (m, 1H, OCH_2), 2.61 (br, s, 4H, pip-NCH_2), 2.51 (m, 1H, OCH_2), 2.48-2.29 (m, 5H), 2.13 (s, 3H, CH_3), 2.09 (s, 3H, CH_3), 1.53-1.64 (m, 6H, pip-CH_2), 1.46-1.41 (m, 3H,CH_2); ^{13}C NMR (100 MHz, $CDCl_3$) δ 157.50, 144.29, 143.43, 138.91, 136.27, 135.36, 131.20, 131.00, 129.40, 127.90, 127.42, 126.15, 125.82, 114.10 (Ar-C), 70.41 (CH_2-O), 65.35 (C-OH), 61.31 (C-N), 54.81 (pip-NCH_2), 26.07 (CH_2-pip), 24.25 (CH_2-pip), 23.51 (CH_3); MS: 428.2 $[M+1]^+$.

1-(4-(1,2-Diphenylprop-1-en-1-yl)phenoxy)-3-morpholinopropan-2-ol (6)

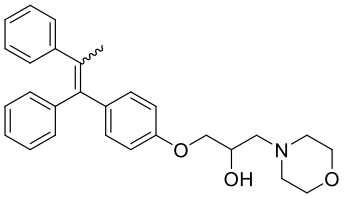

White solid, *E*/*Z* : 3/1; Yield 77 %; mp: 124-127 ^{o}C; ^{1}H NMR (400 MHz, $CDCl_3$) δ 7.91 (br, s, 1H), 7.42-7.25 (m, 5H), 7.13-6.58 (m, 5H), 4.13-3.86 (m, 8H), 4.01 (s, 2H, OCH), 3.74 (s, 8H, morph O-CH_2), 3.06-2.86 (s, 4H), 2.67-2.32(m, 14H), 2.15 (s, 3H, CH_3), 2.11 (s, 3H, CH_3); ^{13}C NMR (100 MHz, $CDCl_3$) δ 157.36, 156.68, 144.29, 144.24, 143.82, 143.39, 138.84, 138.71, 136.41, 136.00, 135.42, 134.96, 132.06, 131.32, 130.99, 130.09, 129.39, 128.16, 128.00, 127.91, 127.44, 126.60, 126.18, 126.15, 125.84, 114.08, 113.45 (Ar-C), 70.13 (OCH_2), 69.88 (OCH_2), 67.10 (morph-OCH_2), 67.08 (morph-OCH_2), 65.43 (OCH), 65.37 (OCH), 61.13 (N-CH_2), 61.05 (N-CH_2), 53.80 (morph-NCH_2), 23.50 (CH_3), 23.44 (CH_3); MS: 430.2 $[M+1]^+$.

1-(4-(1,2-Diphenylprop-1-en-1-yl)phenoxy)-3-(4-methylpiperazin-1-yl)propan-2-ol (7)

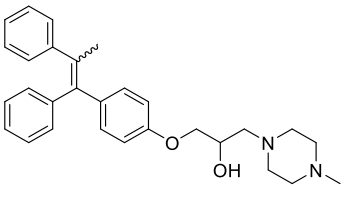

White solid, *E*/*Z* : 1.75/1; Yield 78 %; mp: 132-135 ^{o}C; ^{1}H NMR (400 MHz, $CDCl_3$) δ 7.34-7.30 (m, 1H), 7.23-7.20 (m, 2H), 7.15-7.06 (m, 9H), 7.02-6.95 (m, 3H), 6.90-6.84 (m, 4H), 6.74-6.78 (m, 1H), 6.57-6.54 (m, 1H), 4.12-4.06 (m, 1H, OCH_2), 4.03-4.00 (m, 1H, OCH_2), 3.98 (br, s, 1H, CH), 3.97 (br, s, 1H, CH), 3.84-3.82 (m, 1H, OCH), 2.70-2.40 (m, 14H), 2.28 (s, 3H, N-CH_3), 2.27 (s, 3H, N-CH_3), 2.13 (s, CH_3), 2.09 (s, 3H, CH_3); ^{13}C NMR (100 MHz, $CDCl_3$) δ 157.42, 156.74, 144.29, 144.26, 143.83, 143.40, 138.87, 138.74, 136.35, 135.93, 135.39, 134.92, 132.04, 131.30, 130.99, 130.09, 129.39, 128.16, 128.00, 127.90, 127.43, 126.59, 126.16, 125.82, 114.09, 113.46 (Ar-C), 70.24 (OCH_2), 70.00 (OCH_2), 65.55 (C-OH), 65.48 (C-OH), 60.51 (C-N), 60.44 (C-N), 55.19 (pip-NCH_2), 46.06 (pip-NCH_3), 23.50 (CH_3), 23.43 (CH_3); MS: 443.2 $[M+1]^+$.

1-(4-(1,2-Diphenylprop-1-en-1-yl)phenoxy)-3-(4-ethylpiperazin-1-yl)propan-2-ol (8)

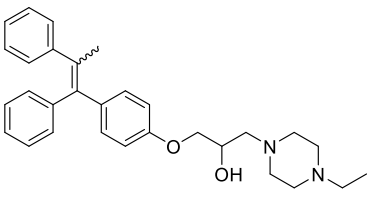

White solid, *E*/*Z* : 1.6/1; Yield 72 %; mp: 136-138 ^{o}C; ^{1}H NMR (400 MHz, $CDCl_3$) δ 7.35-7.31 (m, 1H), 7.24-7.22 (m,1H), 7.16-7.07 (m, 9H), 7.02-6.98 (m, 3H), 6.90-6.86 (m, 4H), 6.78-6.76 (m, 1H), 6.58-6.55 (m, 1H), 4.14-4.08 (m, 1H, OCH_2), 4.05-4.01(m, 1H, OCH_2), 4.00 (s, 1H, CH), 3.98 (s, 1H, CH), 3.85-3.83 (m, 1H, OCH_2), 2.74-2.39 (m,17H), 2.14 (s, 3H, CH_3), 2.11 (s, 2H, CH_3), 1.11-1.08 (m, 5H, N-CH_3); ^{13}C NMR (100 MHz, $CDCl_3$) δ 157.43, 156.73, 144.27, 143.84, 143.41, 138.89, 138.76, 136.35, 135.93, 132.04,

131.00, 130.99, 130.09, 129.39, 128.16, 128.00, 127.90, 127.43, 126.59, 126.16, 125.83, 114.59, 114.10, 113.47 (Ar-C), 70.27 (OCH_2), 70.03 (OCH_2), 65.55 (C-OH), 65.49 (C-OH), 60.55 (NCH_2), 60.48 (NCH_2), 52.82 (pip-NCH_2), 52.33 (pipalkyl-NCH_2), 23.50 (CH_3), 23.44 (CH_3), 11.97 (pipalkyl-CH_3); MS: 457.3 $[M+1]^+$.

1-(4-(1,2-Diphenylprop-1-en-1-yl)phenoxy)-3-(4-phenylpiperazin-1-yl)propan-2-ol (9)

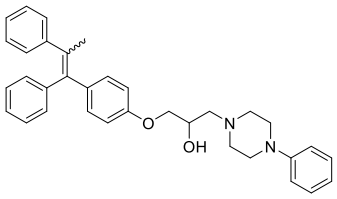

White solid, *E*/*Z* : 2.3/1; Yield 75 %; mp:141-143 ^oC; ^1H NMR (400 MHz, $CDCl_3$) δ 7.35-7.31 (m, 1H), 7.28-7.26 (m, 2H), 7.23-7.21 (m, 1H), 7.16-7.06 (m, 10H), 7.03-6.97 (m, 3H), 6.94-6.83 (m, 9H), 6.79-6.75 (m, 1H), 6.59-6.55 (m, 1H), 4.77 (s, 2H, OH), 4.18-4.11(m, 1H, OCH_2), 4.10-4.04 (m, 1H, OCH_2), 4.02 (s, 1H, OCH), 4.01 (s, 1H, OCH), 3.97-3.96 (m, 1H, OCH_2), 3.87-3.86 (m, 1H, OCH_2), 3.26-3.17 (m, 7H, pip-CH_2), 2.87-2.76 (m, 4H, pip-CH_2), 2.68-2.48 (m, 7H), 2.14 (s, 3H, CH_3), 2.10 (s, 2H, CH_3); ^{13}C NMR (100 MHz, $CDCl_3$) δ 157.28, 156.60, 151.12, 144.14, 143.29, 138.74, 138.61, 136.29, 135.90, 135.31, 134.90, 131.96, 131.22, 130.89, 129.99, 129.87, 129.29, 129.13, 128.79, 128.72, 128.42, 128.34, 128.06, 127.90, 127.80, 127.33, 126.50, 126.07, 125.98, 125.73, 119.91, 116.13, 114.47, 113.98, 113.35 (Ar-C), 70.06 (OCH_2), 69.83 (OCH_2), 65.54 (C-OH), 65.48 (C-OH), 60.52 (NCH_2), 60.45 (NCH_2), 53.28 (pip-NCH_2), 53.25 (pip-NCH_2), 49.26 (pip-NCH_2), 49.23 (pip-NCH_2), 23.40 (CH_3), 23.34 (CH_3); MS: 505.3 $[M+1]^+$.

1-(4-Benzylpiperazin-1-yl)-3-(4-(1,2-diphenylprop-1-en-1-yl)phenoxy)propan-2-ol (10)

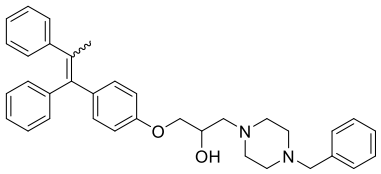

White solid, *E*/*Z* : 2/1; Yield 74 %; mp: 142-144 ^oC; ^1H NMR (400 MHz, $CDCl_3$) δ 7.35-7.30 (m, 8H), 7.27-7.24 (m, 2H), 7.23-7.22 (m, 1H), 7.18-7.06 (m, 10H), 7.03-6.98 (m, 3H), 6.90-6.86 (m, 4H), 6.78-6.75 (m, 1H), 6.57-6.55 (m, 1H), 5.02 (br, s, 2H, OH), 4.15-4.02 (m, 2H, OCH_2), 3.99 (s, 1H, OCH), 3.98 (s, 1H, OCH), 3.53 (s, 2H, benzyl-CH_2), 3.51 (s, 2H, benzyl-CH_2), 2.82-2.39 (m, 1H), 2.14 (s, 3H, CH_3), 2.11 (s, 2H, CH_3); ^{13}C NMR (100 MHz, $CDCl_3$) δ 157.42, 156.74, 144.29, 144.28, 143.85, 143.42, 138.89, 138.76, 137.83, 136.34, 135.93, 135.39, 134.92, 132.07, 131.32, 131.02, 130.12, 129.97, 129.42, 129.37, 129.27, 128.91, 128.39, 128.18, 128.02, 127.93, 127.45, 127.29, 126.62, 126.18, 125.85, 114.59, 114.10, 113.47 (Ar-C), 70.26 (OCH_2), 70.01 (OCH_2), 65.43 (C-OH), 65.36 (C-OH), 62.98 (NCH_2), 60.60 (benzyl-C), 60.53 (benzyl-C), 53.27 (pip-NCH_2), 52.86 (pip-NCH_2), 23.53 (CH_3), 23.47 (CH_3); MS: 519.3 $[M+1]^+$.

1-(4-(1,2-Diphenylprop-1-en-1-yl)phenoxy)-3-((2-morpholinoethyl)amino)propan-2-ol (11)

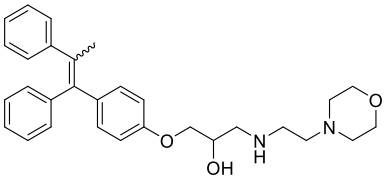

White solid, *E*/*Z* : 1.33/1; Yield 76 %; mp: 137-140 ^{o}C; ^{1}H NMR (400 MHz, $CDCl_3$) δ 7.34-7.31 (m, 2H), 7.24-7.19 (m, 2H), 7.17-7.06 (m, 11H), 7.00-6.97 (m, 3H), 6.89-6.84 (m, 4H), 6.78-6.74 (m, 2H), 6.56-6.52 (m, 2H), 4.16-4.10 (m, 1H, OCH_2), 4.06-4.01 (m, 1H, OCH_2), 4.00-3.95 (m, 2H, OCH), 3.87-3.80 (m, 2H, OCH_2), 3.70-3.65 (m, 7H, morpho-CH_2), 3.15-2.73 (m, 12H), 2.56-2.49 (m, 4H), 2.46-2.43 (m, 7H, morpho-CH_2), 2.13 (s, 3H, CH_3), 2.09 (s, 3H, CH_3); ^{13}C NMR (100 MHz, $CDCl_3$) δ 157.36, 156.68, 144.29, 144.23, 143.82, 143.39, 138.84, 138.70, 136.39, 135.97, 135.41, 134.96, 132.08, 131.33, 130.99, 130.09, 129.98, 129.39, 128.88, 128.53, 128.17, 128.01, 127.91, 127.44, 126.61, 126.10, 125.85, 114.56, 114.07, 113.44 (Ar-C), 70.38 (OCH_2), 70.16 (OCH_2), 68.50 (C-OH), 68.44 (C-OH), 67.09 (morph-OC), 67.00 (morph-OC), 58.26 (ethylene-NC), 53.78 (morph-NC), 53.72 (morph-NC), 51.86 (NCH_2), 51.80 (CH_2), 45.82 (ethylene-NHC), 23.50 (CH_3), 23.46 (CH_3); MS: 473.29 $[M+1]^+$.

1-(Cyclohexylamino)-3-(4-(1,2-diphenylprop-1-en-1-yl)phenoxy)propan-2-ol (12)

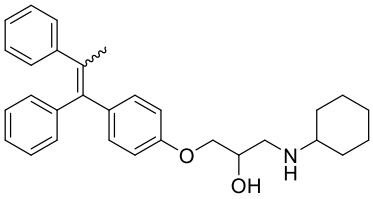

White solid, *E*/*Z* : 2.3/1; Yield 80%; mp: 135-138 ^{o}C; ^{1}H NMR (400 MHz, $CDCl_3$) δ 7.34-7.30 (m, 1H), 7.22-7.20 (m, 1H), 7.16-7.05 (m, 10H), 7.02-6.96 (m, 3H), 6.89-6.83 (m, 4H), 6.78-6.74 (m, 1H), 6.57-6.53 (m, 1H), 4.01-3.87 (m, 4H), 3.83-3.81 (m, 1H, OCH_2), 2.93-2.89 (m, 1H, CH_2), 2.85-2.81 (m, 1H, CH_2), 2.76-2.71 (m, 1H, CH_2), 2.68-2.63 (m, 1H, CH_2), 2.45-2.35 (m, 2H, cyclohexyl-CH), 2.13 (s, 3H, CH_3), 2.03 (s, 3H, CH_3), 1.91-1.84 (m, 4H, cyclohexyl-NCH_2), 1.74-1.68 (m, 4H, CH_2), 1.61-1.57 (m, 4H, cyclohexyl-NCH_2), 1.29-1.19 (m, 4H, CH_2), 1.16-1.00 (m, 4H, CH_2); ^{13}C NMR (100 MHz, $CDCl_3$) δ 157.34, 156.71, 144.29, 144.25, 143.40, 138.86, 138.72, 136.36, 136.29 135.98, 135.88, 135.39, 135.32, 134.99, 134.93, 132.06, 131.31, 130.99, 130.09, 129.39, 128.16, 128.00, 127.90, 127.43, 126.59, 126.16, 125.83, 114.09, 113.45 (Ar-C), 70.46 (OCH_2), 70.24 (OCH_2), 68.53 (C-OH), 68.48 (C-OH), 56.84 (NCH_2), 56.80 (NCH_2), 48.83 (cyclohexyl-NCH), 48.76 (cyclohexyl-NCH), 34.03 (cyclohexyl-C), 33.98 (cyclohexyl-C), 33.79 (cyclohexyl-C), 33.75 (cyclohexyl-C), 26.15 (cyclohexyl-C), 25.11 (cyclohexyl-C), 23.49 (CH_3), 23.44 (CH_3); MS: 442.2 $[M+1]^+$.

1-(Diethylamino)-3-(4-(1,2-diphenylprop-1-en-1-yl)phenoxy)propan-2-ol (13)

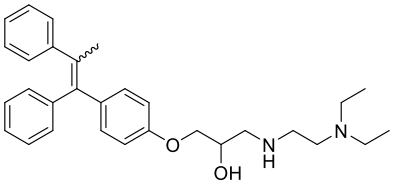

White solid, *E*/*Z* : 2.5/1; Yield 78 %; mp: 130-132 ^{o}C; ^{1}H NMR (400 MHz, $CDCl_3$) δ 7.35-7.31 (m, 1H), 7.24-7.22 (m, 1H), 7.16-7.08 (m, 9H), 7.01-6.96 (m, 3H), 6.90-6.88 (m, 4H), 6.79-6.77 (m, 1H), 6.58-6.56 (m, 1H), 4.09-4.05 (m, 1H, OCH_2), 4.02-3.91 (m, 3H), 3.86-3.79 (m, 1H, OCH_2), 3.32 (br, s, 2H, NH), 2.90-2.69 (m, 6H), 2.58-2.49 (m, 9H), 2.15 (s, 3H, CH_3), 2.12 (s, 1H, CH_3), 1.04-0.98 (m, 9H, *N*,*N*- diethyl CH_3); ^{13}C NMR (100 MHz, $CDCl_3$) δ 157.42, 156.74, 144.31, 144.28, 143.86, 143.42, 138.91, 138.77, 136.32, 135.91, 135.39, 134.92, 132.06, 131.39, 131.31, 131.00, 130.10, 129.41, 129.38, 128.17, 128.02, 127.92, 127.45, 126.68, 126.18, 125.84, 114.12, 113.49 (Ar-C), 70.42 (OCH_2), 70.19 (OCH_2), 68.03 (C-OH), 67.96 (C-OH), 52.31 ($NHCH_2$), 52.26 ($NHCH_2$), 52.00 (ethylene-NCH_2), 51.92 (ethylene-NCH_2), 46.93 (ethylene-$NHCH_2$), 46.85 (*N*,*N*-diethyl CH_2), 23.52 (CH_3), 23.46 (CH_3), 11.42 (N,N-diethyl CH_3); MS: 459.3 $[M+1]^+$.

1-(Dimethylamino)-3-(4-(1,2-diphenylprop-1-en-1-yl)phenoxy)propan-2-ol (14)

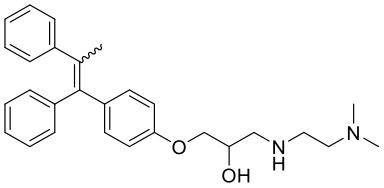

White solid, *E*/*Z* : 3.5/1; Yield 75 %; mp: 127-129 ^{o}C; ^{1}H NMR (400 MHz, $CDCl_3$) δ 7.34-7.30 (m, 1H), 7.22-7.20 (m, 1H), 7.14-7.06 (m, 14H), 7.00-6.95 (m, 3H), 6.88-6.85 (m, 4H), 6.77-6.72 (m, 1H), 6.56-6.54 (m, 1H), 4.06-4.00 (m, 2H, OCH_2), 3.98-3.93 (m, 2H, OCH), 3.82-3.81 (m, 1H, OCH_2), 2.89-2.66 (m, 6H), 2.47-2.29 (m, 5H), 2.22 (s, 6H, dimethyl-NCH_3), 2.20 (s, 2H, dimethyl-NCH_3), 2.13 (s, 3H, CH_3), 2.09 (s, 3H, CH_3); ^{13}C NMR (100 MHz, $CDCl_3$) δ 157.43, 156.73, 144.27, 138.88, 138.75, 136.29, 135.88, 135.37, 134.90, 132.05, 131.30, 131.00, 130.10, 129.95, 129.40, 128.16, 128.01, 127.90, 127.43, 126.59, 126.16, 126.07, 125.82, 114.09, 113.46 (Ar-C), 70.39 (OCH_2), 70.17 (OCH_2), 68.53 (C-OH), 68.47 (C-OH), 59.21 (ethylene-NCH_2), 51.96 (NCH_2), 51.89 (NCH_2), 47.02 (ethylene-NHC), 45.50 (ethylene-NCH_3), 23.50 (CH_3), 23.44 (CH_3); MS: 431.2 $[M+1]^+$.

1-(Allylamino)-3-(4-(1,2-diphenylprop-1-en-1-yl)phenoxy)propan-2-ol (15)

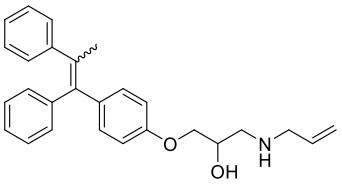

White solid, *E*/*Z* : 1.7/1; Yield 68 %; mp: 120-123 ^{o}C; ^{1}H NMR (400 MHz, $CDCl_3$) δ 7.34-7.31 (m, 1H), 7.23-7.20 (m, 1H), 7.17-7.05 (m, 10H), 7.02-6.95 (m, 3H), 6.89-6.85 (m, 4H), 6.78-6.75 (m, 1H), 6.56-6.52 (m, 1H), 5.91-5.77 (m, 1H, allyl-CH), 5.24-5.12 (m, 2H, allyl CH_2), 4.16-4.07 (m, 1H, OCH_2), 4.05-4.01 (m, 1H, OCH_2), 3.99-3.94 (m, 2H, OCH),

3.87-3.79 (m, 1H, OCH_2), 3.49-3.44 (m, 1H, OCH_2), 3.40-3.17 (m, 2H, allyl-NCH_2), 2.88-2.58 (m, 3H, CH_2), 2.13 (s, 3H, CH_3), 2.10 (s, 2H, CH_3); ^{13}C NMR (100 MHz, $CDCl_3$) δ 157.28, 157.24, 156.59, 156.55, 144.28, 144.24, 143.81, 143.75, 143.39, 138.84, 138.71, 136.47, 136.07, 135.43, 134.99, 134.65, 134.55, 132.23, 132.10, 131.36, 131.00, 130.11, 130.02, 129.40, 128.89, 128.53, 128.18, 128.02, 127.92, 127.45, 126.62, 126.19, 125.85, 118.77 (allyl-CH_2), 114.58, 114.48, 114.10, 113.47 (Ar-C), 70.17 (OCH_2), 70.14 (OCH_2), 68.12 (C-OH), 68.05 (C-OH), 52.31 (NCH_2), 52.26 (NCH_2), 41.10 (allyl-NCH_2), 23.52 (CH_3), 23.46 (CH_3); MS: 400.2 $[M+1]^+$.

1-(Butylamino)-3-(4-(1,2-diphenylprop-1-en-1-yl)phenoxy)propan-2-ol (16)

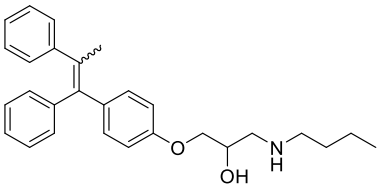

White solid, *E*/*Z* : 2.4/1; Yield 85 %; mp: 119-121 ^oC; ^1H NMR (400 MHz, $CDCl_3$) δ 7.34-7.30 (m, 1H), 7.22-7.20 (m, 1H), 7.15-7.07 (m, 9H), 7.00-6.98 (m, 3H), 6.88-6.86 (m, 4H), 6.71-6.69 (m, 1H), 6.55-6.45 (m, 1H), 4.06 (s, 1H, OCH_2), 3.97-3.96 (m, 2H, OCH), 3.92-3.81 (m, 1H, OCH_2), 3.25-3.16 (m, 1H, OCH_2), 2.86-2.58 (m, 4H, OCH), 2.33-2.29 (m, 3H, butyl-NCH_2), 2.13 (s, 3H, CH_3), 2.09 (s, 2H, CH_3), 1.57-1.43 (m, 3H, butyl-CH_2), 1.36-1.31 (m, 3H, butyl-CH_2), 0.92-0.87 (m, 4H, butyl-CH_3); ^{13}C NMR (100 MHz, $CDCl_3$) δ 157.15, 156.78, 144.24, 144.09, 143.24, 138.69, 138.55, 136.27, 135.31, 135.26, 132.05, 131.93, 131.29, 131.18, 130.84, 129.95, 129.24, 128.01, 127.98, 127.86, 127.81, 127.76, 127.29, 126.46, 126.40, 126.03, 125.94, 125.69, 125.62, 114.98, 114.41, 113.93, 113.29 (Ar-C), 70.28 (OCH_2), 70.06 (OCH_2), 68.00 (C-OH), 67.94 (C-OH), 51.66 (NCH_2), 51.60 (NCH_2), 49.41 (butyl-NCH), 31.90 (butyl-C), 31.54 (butyl-C), 23.35 (CH_3), 20.30 (butyl-C), 14.10 (butyl-C), 13.94 (butyl-C); MS: 416.2 $[M+1]^+$.

1-(Benzylamino)-3-(4-(1,2-diphenylprop-1-en-1-yl)phenoxy)propan-2-ol (17)

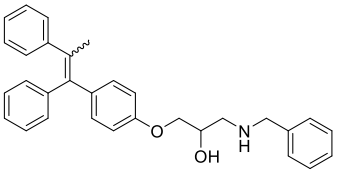

White solid, *E*/*Z* : 2/1; Yield 67 %; mp: 133- 135 ^oC; ^1H NMR (400 MHz, $CDCl_3$) δ 7.34-7.26 (m, 9H), 7.22-7.20 (m, 2H), 7.02-6.98 (m, 3H), 6.89-6.81 (m, 4H), 6.77-6.74 (m, 1H), 6.56-6.53 (m, 1H), 4.10-4.05 (m, 2H, OCH_2), 3.99-3.97 (m, 2H, OCH), 3.84-3.78 (m, 2H,), 3.51 (s, 2H, benzyl-CH_2), 3.49 (s, 1H, benzyl-CH_2), 2.77-2.69 (m, 2H, CH), 2.53-2.47 (m, 2H, CH), 2.13 (s, 3H, CH_3), 2.09 (s, 2H, CH_3); ^{13}C NMR (100 MHz, $CDCl_3$) δ 157.44, 156.70, 144.28, 143.85, 143.43, 138.90, 138.77, 137.97, 136.34, 135.93, 135.39, 134.92, 132.06, 131.32, 131.02, 130.12, 129.97, 129.42, 129.36, 129.20, 128.53, 128.49, 128.37, 128.18, 128.02, 127.93, 127.45, 127.25, 126.60, 126.18, 126.09, 125.85, 114.60, 114.11, 113.48 (Ar-C), 70.27 (OCH_2),

70.03 (OCH_2), 65.50 (C-OH), 65.45 (C-OH), 60.72 (benzyl-C), 60.49 (benzyl-C), 53.45 (NCH_2), 53.14 (NCH_2), 23.53 (CH_3), 23.47 (CH_3); MS: 450.2 $[M+1]^+$.

1-(4-(1,2-Diphenylprop-1-en-1-yl)phenoxy)-3-((4-fluorophenyl)amino)propan-2-ol (18)

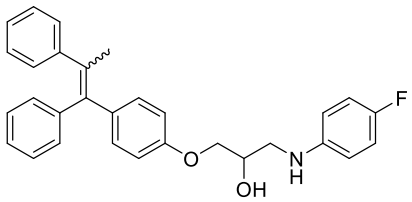

White solid, *E*/*Z* : 12.5/1; Yield 70 %; mp: 134-137 ^oC; ^1H NMR (400 MHz, $CDCl_3$) δ 7.35-726 (m, 1H), 7.17-7.05 (m, 8H), 7.03-6.96 (m, 3H), 6.92-6.84 (m, 6H), 6.63-6.59 (m, 2H), 4.25-4.24 (m, 1H, OCH_2), 4.10-4.02 (m, 2H, OCH), 3.98-3.91 (m, 1H, OCH_2), 3.49-3.43 (m, 1H, CH), 3.40-3.36 (m, 1H, CH), 3.29-3.22 (m, 1H, CH), 2.13 (s, 3H, CH_3), 2.10 (s, 3H, CH_3); ^{13}C NMR (100 MHz, $CDCl_3$) δ 157.04, 144.48, 144.17, 143.34, 138.74, 136.79, 135.56, 131.45, 130.99, 129.40, 127.95, 127.49, 126.25, 125.91, 115.97, 115.75, 114.34, 114.26, 114.10 (Ar-C), 70.06 (OCH_2), 68.83 (C-OH), 47.34 (NCH_2), 23.51 (CH_3); MS: 453.2 $[M+1]^+$.

1-(4-(1,2-Diphenylprop-1-en-1-yl)phenoxy)-3-(pyrazin-2-ylamino)propan-2-ol (19)

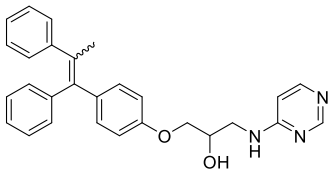

White solid, *E*/*Z* : 1.5/1; Yield 65 %; mp: 148-150 ^oC; ^1H NMR (400 MHz, $CDCl_3$) δ 7.35-7.31 (m, 2H), 7.22 (m, 1H), 7.14-7.09 (m, 12H), 7.01-6.99 (m, 4H), 6.90-6.86 (m, 3H), 6.80-6.78 (m, 2H), -6.72-6.74 (m, 2H), 4.78 (br, s, 1H, NH), 4.55 (br, s, 1H, NH), 4.22 -3.95 (m, 3H), 2.54-2.40 (m, 2H, CH_2), 2.14 (s, 1H, CH_3), 2.10 (s,

CHAPTER 3
TRIPHENYLETHYLENE-NAPHTHALIMIDE CONJUGATES

3.1 Introduction

NA topoisomerase II (TOPO-II) is a class of nucleoenzyme that regulates replication, recombination, and repair of DNA.[83] It is a homo-dimer with three catalytic subunits that catalyze the cleavage of dsDNA, reunites the phosphodiester bonds and release unwound DNA through C-gate to initiate replication.[84] TOPO-II is expressed in various malignancies, therefore an effective target to treat broad-spectrum cancer.[85] TOPO-II inhibitors have applications in cancer therapy, but still, drug resistance in cancer treatment remains a frontline intervention. To maximize the efficacy of anticancer drugs and develop multitarget drug candidates, combinational principle/molecular hybridization (MH) is found to be the effective way to design the drug target.[86-87] The success of triphenylethylene (such as tamoxifen; marketed drug) and naphthalimides (such as amonafide in the clinical trial) provoked to synthesize their conjugates in the area of cancer therapy.[12-13] In pharmaceuticals, a pioneering drug tamoxifen has attracted the attention of researchers over many years.[15] As an anticancer agent, it resists tumor formation by blocking estrogen receptor or interacting with factors which impair DNA replication.[64] On account of the partial agonistic character of tamoxifen,[17] extensive efforts have been devoted to endow new triarylethylene analogues as potent anticancer agents with increase in efficacy and toxicological profile. Moreover, adopting the methodology of molecular hybridization, coupling of triphenylethylene analogue (tamoxifen) with various pharmacophores such as coumarin and xanthene manifested significant anticancer activity.[88-89]

On the other hand, naphthalimides exert antiproliferative activity due to their ability to intercalate into the base pairs of DNA or groove binding.[47] Naphthalimide analogue such as amonafide has reached in phase II clinical trials and displayed promising anticancer activity.[90] But apparently, further clinical development of this moiety was impeded due to its neurological toxicity, poor physicochemical property, and poor therapeutic index.[91-92] Thus, researchers have made efforts toward modifying imide position and substituents at the C-4 position of naphthalene ring. Rao *et al*. have synthesized naphthalimide-benzothiazole/cinnamide derivative as anticancer agent against lung and colon cancer cell lines and inhibited the topoisomerase-II

activity,[44] whereas Lu *et al*. reported a series of C-4 naphthalimide-benzothiazole conjugates with potent inhibitory activity towards murine melanoma cell lines.[45] These promising anticancer activities of naphthalimide and triphenylethylene analogues have prompted us to develop novel structural hybrids evading drug-resistance.

3.1.1 Designing of triphenylethylene-naphthalimide conjugates

Variation of amines at C-1 and C-4 positions has a significant impact on the anticancer activity of naphthalimides. We designed target hybrid by reducing the flexibility as depicted in **Figure 1** by conjugating amino-substituted triphenylethylene scaffold to 4-substituted naphthalic anhydride without any linker. Rigidity due to the presence of aromatic substitution of naphthalimide is rarely known in the literature. With this methodology, we have also targeted to reduce the flexibility of side chain of tamoxifen (triphenylethylene analogue). To the best our knowledge, no report on triphenylethylene-naphthalimide (TPE-naph) hybrids has been explored as anticancer agents in drug discovery.

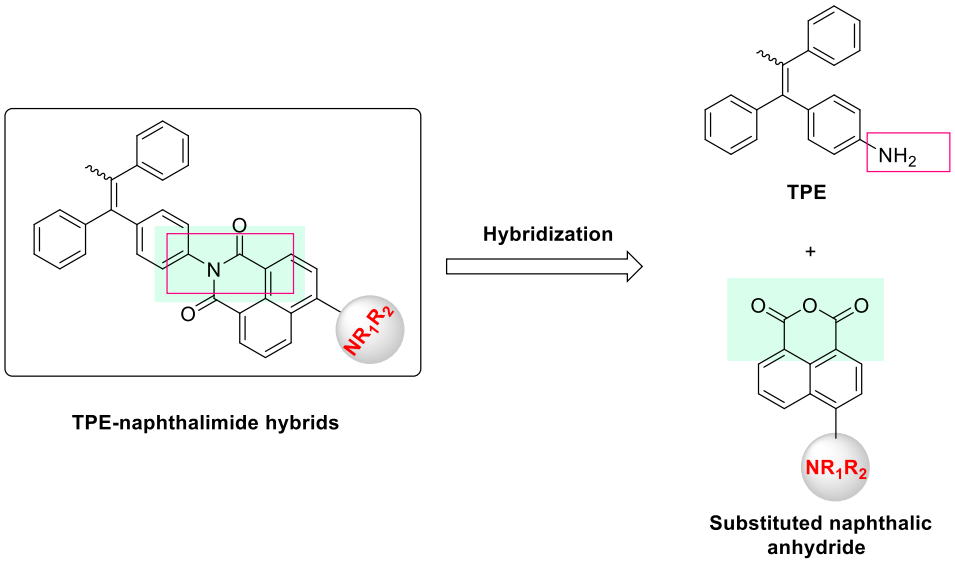

Figure 1: Molecular hybridization of TPE with naphthalic anhydride

Herein, a series of triphenylethylene-naphthalimide hybrids substituted with various primary and secondary amines were synthesized and evaluated for their cytotoxicity against 60 human cancer cell lines. As the triphenylethylene and naphthalimide derivatives are observed as topoisomerase inhibitors, therefore the mechanism of cytotoxicity of the most potent TPE-naphthalimide hybrid **7** was elucidated through topoisomerase-II (TOPO-II) inhibition assay. Further, molecular modeling was performed to determine the interactions between TOPO-II and

TPE-naphthalimide hybrids supporting the plausible experimental data. The transportation behavior of human serum albumin (HSA) for the most potent TPE-naph hybrid has also been studied with UV-Vis and fluorescence spectroscopy techniques.

3.2 Chemistry

A series of triphenylethylene-naphthalimide hybrid was synthesized *via* multistep reactions, including molecular hybridization methodology (**Scheme 1**). Initially, McMurry reaction[71] was employed using the precursor 4-amino benzophenone (**1**) and acetophenone in the presence of Zn and $TiCl_4$ in anhydrous THF to afford homo-coupled and cross-coupled products in isomeric form. The cross-coupled product 4-(1,2-diphenylprop-1-en-1-yl)aniline (**2**) was isolated through column chromatography in isomeric form (*E*/*Z*: 1/6) in 60% yield. ^{1}HNMR spectrum of analogue **2** showed two methyl singlets at δ values 2.18 and 2.10 ppm with varying proton ratios; and the broad splitting pattern of sixteen aromatic protons, which confirmed the formation of *E*/*Z* diastereomers. Subsequently, treatment of acenaphthene (**3**) with *N*-bromosuccinimide in DMF at room temperature furnished intermediate **4** in 97% yield. Further, oxidation of intermediate **4** was accomplished by refluxing of $K_2Cr_2O_7$ in acetic acid to obtain 6-bromo-1*H*,3*H*-benzo[*de*]isochromene-1,3-dione (**5**) in 72% yield. To obtain intermediate **6**, optimization of reaction conditions was followed and shown in **Table 1** where good yield of **6** was obtained in the presence of additive $Zn(OAc)_2$ in ethanol. Zinc-acetate is a Lewis acid, it accepts the electrons from oxygen atom of carbonyl group and facilitates the attack of amine more easily by enhancing the electrophilicity of carbonyl carbon. Further, the nature of solvent affects the rate of reaction where non-polar and aprotic solvents such as toluene and pyridine reduce the solvation of nucleophile while polar and protic solvents of optimum *p*H such as ethanol (behave as a weak acid and weak base) increase the solvation and nucleophilicity of amine. Entry 2, in which acetic acid is used as solvent, lowers the nucleophilicity of amine as it is more acidic (*p*H = 3.0-3.5). So, *p*H of solvent plays important role in the formation of intermediate 6-bromo-2-(4-(1,2-diphenylprop-1-en-yl)phenyl)-1*H*-benzo[*de*]isoquinoline-1,3(2*H*)-dione (**6)**. Finally, intermediate **6** was obtained in quantitative yield on refluxing of compound **2** to a stirred solution of **5** in zinc acetate and ethanol for 15 h. The signals of aromatic protons of naphthalene in the region δ 8.67-8.08 ppm; and the methyl singlets of TPE molecule at δ values 2.21 and 2.13 ppm confirmed the formation of hybrid intermediate **6**. Further, compound **6** was refluxed with primary or secondary amine in the presence of potassium carbonate and DMF for 2-3 h to obtain

isomeric products **7-21** in good yields. Attempts were made to separate *E*- and *Z*-isomers from mixture by column and preparative chromatography were unsuccessful. Without separation of *E*- and *Z*-isomers, these synthesized compounds were characterized by NMR and mass spectrometry. Appearance of multiplets of morpholine in regions δ 4.04-3.99 ppm and 3.29-3.24 ppm confirmed the formation of analogue **7**. The signals at δ values 67.0 and 53.5 ppm of morpholine in ^{13}C NMR further confirmed the assigned structure. The *E*/*Z* ratio of TPE-naph was determined by ^{1}H NMR from the respective integral of methyl protons and HPLC methodology.

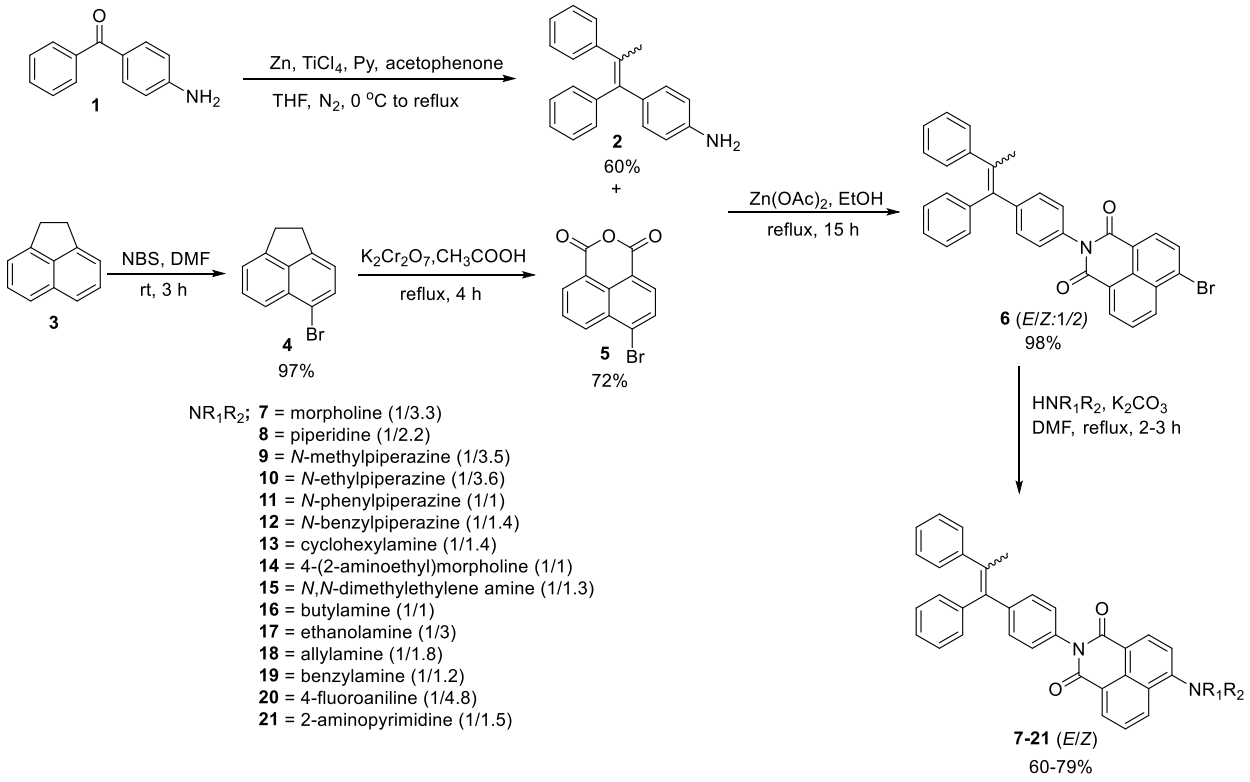

Scheme 1: Synthesis of triphenylethylene-naphthalimide conjugates with the variation of amines (**7-21**)

Table 1: Optimization of reaction conditions for the formation of derivative 6-bromo-2-(4-(1,2-diphenylprop-1-en-yl)phenyl)-1*H*-benzo[*de*]isoquinoline-1,3(2*H*)-dione (**6**).

entry	Solvent	base	additive	time (h)	yield (%)
1.	EtOH	-		24	-
2.	Toluene	-		24	-
3.	Acetic acid	-		24	-
4.	Pyridine	-	$Zn(OAc)_2$	5	25
5.	IPA	K_2CO_3		24	-

6.	EtOH	K_2CO_3		24	-
7.	**EtOH**	**-**	**$Zn(OAc)_2$**	**15**	**98**
8.	Toluene	K_2CO_3		24	-
9.	CAN	K_2CO_3		24	-
10.	Toluene	DIPEA		20	-

The stereochemical assignments of *E*- and *Z*-configurations were given on the basis of Nuclear Overhauser Effect Spectroscopy (NOESY).[74-75] The NOESY spectrum of analogue **7** is given in the **Figure 2**. The cross-peaks in the blue-circles represent dipolar coupling between the spins of methyl protons and the aromatic protons of TPE-naphthalimide conjugate. It has been observed that methyl protons at δ value 2.15 ppm couples with the protons of α-phenyl ring which is shielded than the protons of the α'-phenyl ring, indicated that α-phenyl ring and methyl group lie close in the space (**Figure 3**). Therefore, it is concluded that protons of *Z*-isomer of TPE-naphthalimide conjugate were found to be more shielded than *E*-isomer, and this relationship also holds good for tamoxifen.

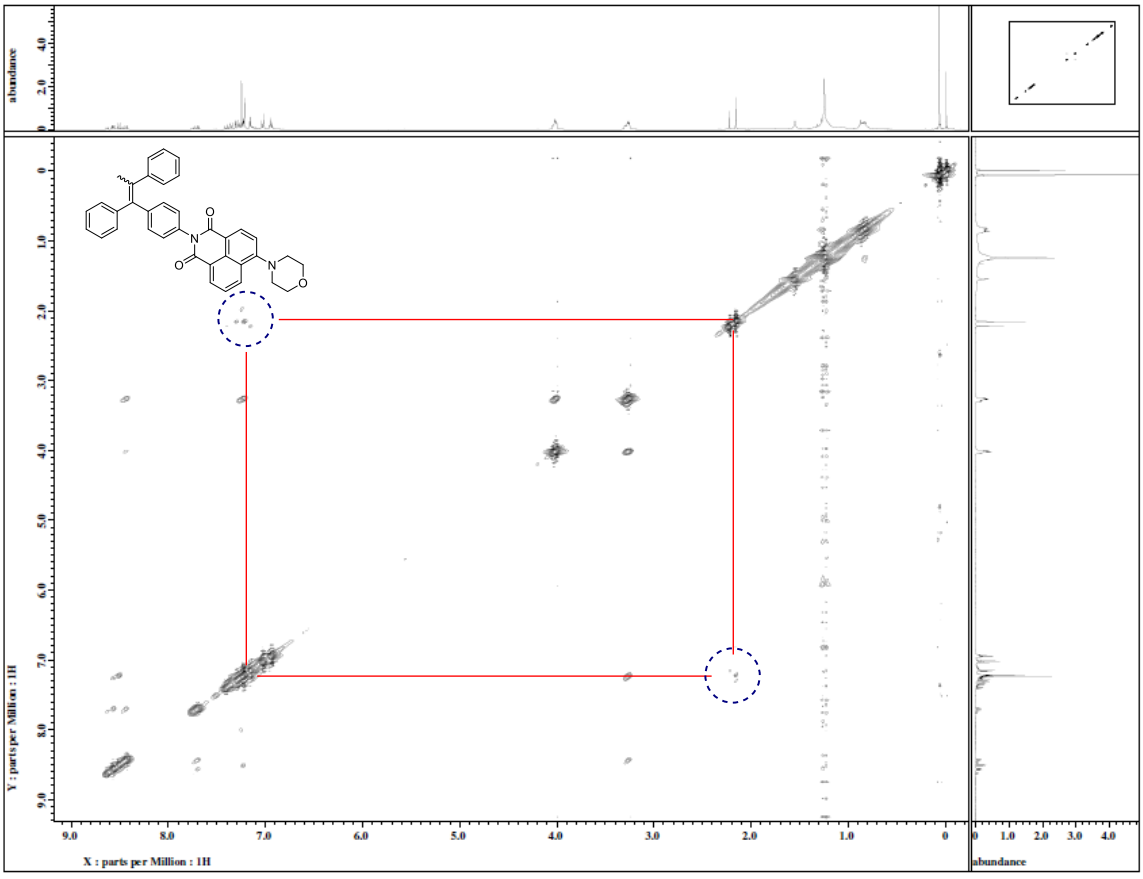

Figure 2: 2D-NOE spectrum of 2-(4-(1,2-diphenylprop-1-en-1yl)phenyl)-6-morpholino-1*H*-benzo[*de*]isoquinoline-1,3(2 *H*)-dione (**7**)

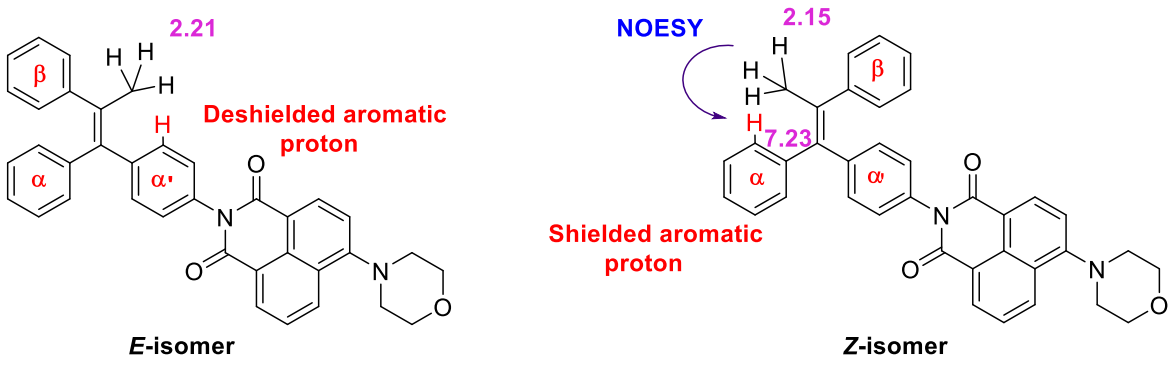

Figure 3: Structures of *E*- and *Z*-isomers of TPE-naphthalimide conjugate **7**

Reverse-phase high performance liquid chromatography (RP-HPLC) method has been developed for the determination of *E*- and *Z*-isomers of TPE-naph conjugates using C-18 column.[73] The wavelength used was 400 nm and the mobile phase was comprised of 0.01 M tetrabutylammoniumhydrogensulfate: acetonitrile (30:70; v/v) with flow rate 1.0 mL/min. **Figure 4** represents the HPLC separation of *E*- and *Z*-isomers of analogue **7** with retention times

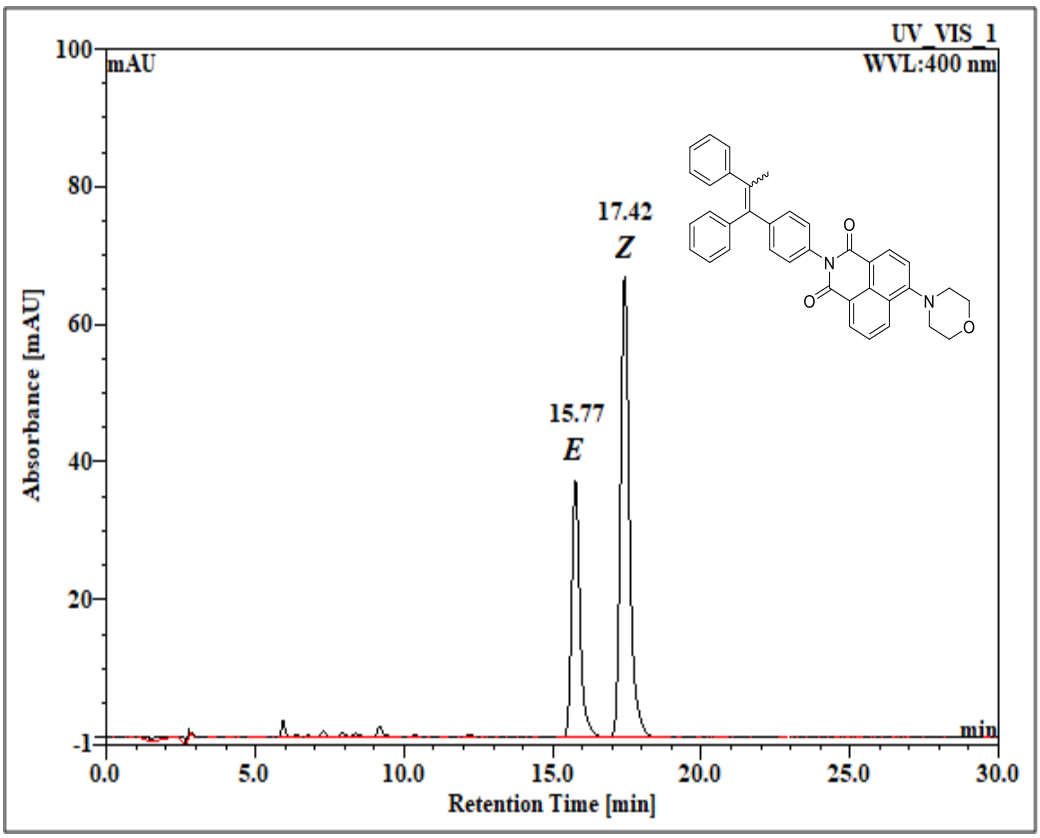

Figure 4: HPLC chromatogram of TPE-naph conjugate **7** containing a mixture of *E*- and *Z*-isomers

singlets at δ values 2.21 and 2.15 ppm due to CH_3 groups which were assigned *E*- (retention time 15.77 min) and Z-configurations (retention time 17.42 min), respectively. The signal identities were established on the basis of retention times of compound **7** obtained from chromatogram. Further, the ratio of *E*- and *Z*-isomers of analogue **7** calculated from ^{1}H NMR is same as that determined from HPLC methodology, i.e. 1:3.3. *E/Z* ratios of other isomers were also observed with same methodologies.

3.3 Biology

3.3.1 *In vitro* antiproliferative activity

Preliminary, *in vitro* antiproliferative activity of compounds (*E/Z)* **7-21** at single dose concentration (10 μM) was evaluated against 60 human cancer cell lines by National Cancer Institute (NCI), Bethesda, USA (**Table 2**).[76] Among tested compounds, derivative **7** possessing morpholine group displayed excellent percentage growth inhibition against almost all cancer cell lines. Compound **7** exhibited good cytotoxicity towards non-small lung (HOP-92, GI = 78.7%; NCI-H23, GI = 78.4%), CNS (SF-295, GI = 71.5%) and ovarian (OVCAR-3, GI = 75.1%) cancer cell lines (**Figure 5**). It was inferred that compound **7** elicited improve cytotoxic potency towards NCI-H23 (non-small lung), OVCAR-3 (ovarian) and MDA-MB-231 (breast cancer) cell lines in comparison to amonafide. When the morpholinyl group of analogue **7** was replaced with piperidine moiety, it led to compound **8** with complete loss of antiproliferative activity which indicated that increased lipophilicity reduces cytotoxicity towards cancer cell lines. Compound **9** (GI = -9.19%) with methyl piperazine was found to be potent against SR leukemia cancer cell line when compared to amonafide (GI = 91.9%). Analogue **9** also exerted excellent anticancer activity towards K-562 (leukemia cancer) cell line with growth inhibition of 90.8% (**Figure 5**). It has also been observed that compound **10** substituted with *N*-ethyl piperazinyl group showed lower activity when compared to **9** having *N*-methyl piperazinyl substituent that also proved that cytotoxicity is dependent upon lipophilicity. Derivative **11** (*N*-phenyl piperazine) displayed weak anticancer activity with average percentage inhibition < 40% except for UO-31 (renal cancer) cell line, while derivative belonging to *N*-benzyl piperazine (**12)** did not show any significant inhibition due to the presence of bulky amine.

On the other hand, compounds **13** (cyclohexylamine), **15** (*N*,*N*-dimethylethylene diamine) and **17** (ethanolamine) with primary amines were least effective against cancer cell lines. Compound **14** bearing 4-(2-aminoethylene)morpholine was found to be sensitive towards

leukemia (K-562, MOLT-4, RPMI-8226, SR), non-small lung (EKVX), colon (HCT-116, HCT-15), ovarian (OVCAR-4) and breast (MCF-7, T-47D) cancer cell lines with GI > 50%. Analogues **16** (GI = 40.4%) and **18** (GI = 45.4%) with respective butylamine and allylamine displayed selectivity towards UO-31 renal cancer cell line.

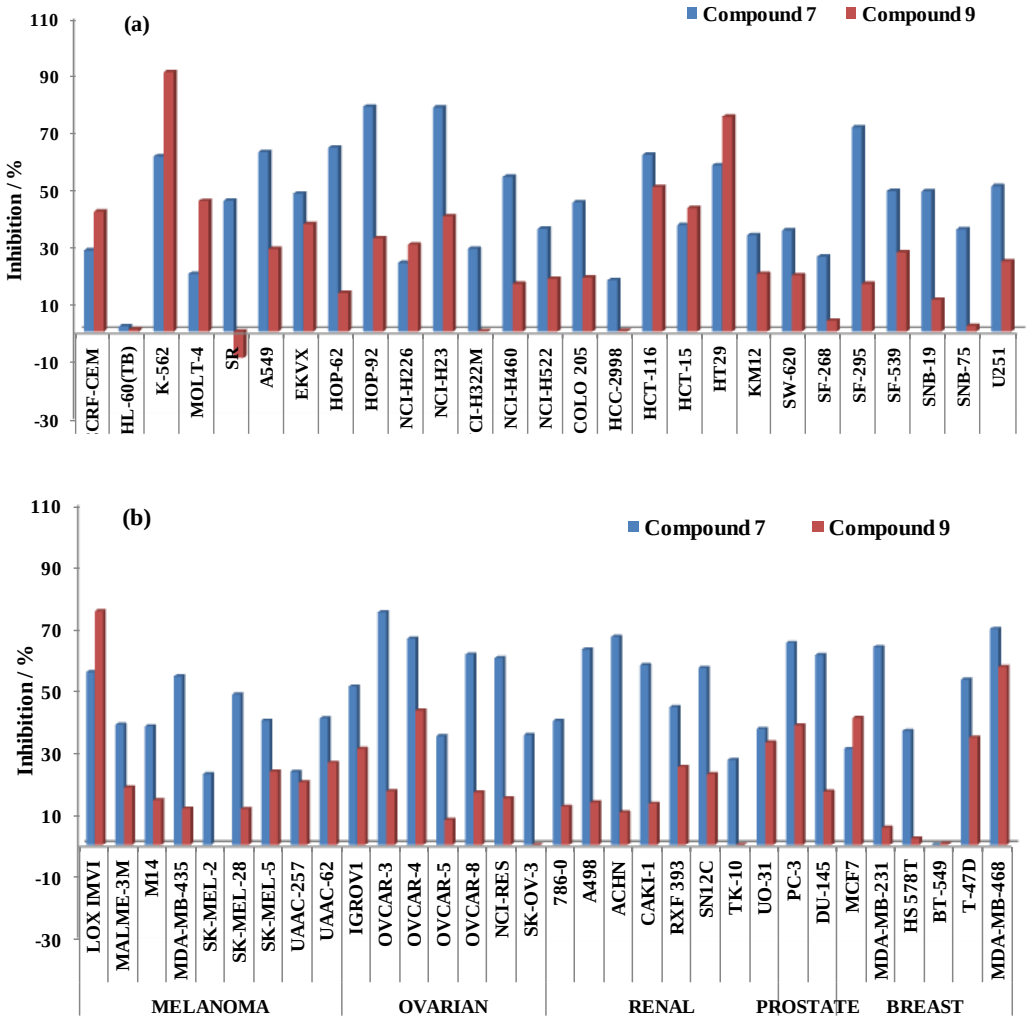

Figure 5: Comparison of anticancer activity between compound **7** and **9** against *in vitro* panel of (A) leukemia, non-small lung, colon, CNS cancer cell lines, and (B) melanoma, ovarian, renal, prostate, breast cancer cell lines

Table 2: Growth inhibition percentages of TPE-naph conjugates **7-21** against a panel of 60 human cancer cell lines at a single dose concentration of 10 μM.

Cell line	7	8	9	10	11	12	13	14	15	16	17	18	19	20	21	AF
Leukemia Cancer																
CCRF-CEM	28.4	17.1	**42.0**	29.7	1.50	10.4	11.2	**34.3**	-	6.6	16.5	15.0	-	20.8	2.88	**86.4**
HL-60(TB)	1.87	-	0.74	-	-	10.9	8.72	16.3	-	1.30	-	-	10.9	3.69	-	**98.3**
K-562	**61.3**	23.8	**90.8**	**68.7**	0.41	18.6	16.7	**56.5**	4.46	15.1	19.4	25.2	-	**67.9**	-	**96.5**
MOLT-4	20.2	8.00	**45.7**	23.4	6.26	10.9	7.6	**56.1**	11.2	9.66	27.0	14.4	14.2	19.2	5.4	**-2.1**
RPMI-8226	-	-	-	-	5.16	18.9	-	**55.3**	-	-	2.27	10.7	11.1	**32.5**	-	**98.2**
SR	**45.8**	27.1	**-9.19**	**83.5**	-	18.5	18.6	**65.5**	12.6	10.3	13.9	-	-	**63.1**	-	**91.9**
Non-Small Lung Cancer																
A549	**62.8**	10.1	28.9	14.0	-	2.63	4.58	28.6	-	4.78	-	17.0	16.4	14.3	4.33	**88.0**
EKVX	**48.3**	21.0	**37.6**	23.7	20.3	3.0	12.9	**54.4**	9.15	**31.1**	-	**41.3**	7.35	**43.8**	4.21	**54.8**
HOP-62	**64.4**	13.6	13.9	7.22	11.1	4.99	-	16.0	4.91	-	-	1.51	24.7	13.3	3.56	**66.0**
HOP-92	**78.7**	**32.3**	**32.6**	26.6	18.6	8.38	21.2	25.5	6.39	17.5	12.0	18.9	-	28.5	9.90	NT
NCI-H226	24.0	13.5	**30.4**	19.0	15.2	3.14	7.71	**35.3**	12.3	1.93	-	-	11.0	18.8	9.39	**-30.3**
NCI-H23	**78.4**	20.7	**40.3**	21.4	15.8	12.2	15.2	**37.7**	3.84	8.69	-	16.9	10.8	25.0	1.45	**68.5**
NCI-H322M	29.0	0.86	-	-	5.96	5.02	-	7.81	-	3.19	-	4.08	10.2	2.45	4.51	**70.6**
NCI-H460	**54.2**	11.4	16.7	7.23	2.33	-	-	25.5	-	-	-	1.22	2.42	9.39	-	**-6.0**
NCI-H522	**36.0**	21.6	18.5	11.1	16.0	11.7	9.24	28.1	7.78	10.9	21.4	11.4	-	17.1	17.8	**-28.3**
Colon Cancer																
COLO 205	**45.2**	19.0	18.9	11.1	3.71	3.52	4.14	23.1	0.26	-	-	-	-	5.92	1.97	**73.8**
HCC-2998	18.0	-	0.24	-	6.21	-	-	9.12	-	-	-	-	-	-	-	**84.6**
HCT-116	**61.9**	26.5	**50.6**	**32.8**	15.4	11.8	14.9	**62.6**	6.49	11.4	-	3.06	-	**41.4**	6.31	**86.3**
HCT-15	**37.3**	14.6	**43.2**	28.4	5.00	5.61	3.43	**58.2**	3.02	-	-	7.25	-	**52.9**	-	**88.2**
HT29	**58.1**	22.9	**75.1**	**62.0**	9.69	13.6	13.5	**54.2**	-	-	-	4.06	-	**61.4**	-	**90.8**
KM12	**33.7**	10.8	20.2	10.1	4.34	7.37	8.76	27.5	6.69	4.13	-	9.47	-	13.7	5.18	**71.2**
SW-620	**35.4**	**35.4**	19.8	6.91	5.72	9.15	5.73	16.8	2.43	-	-	-	8.52	13.9	-	**79.0**
CNS Cancer																
SF-295	**71.5**	6.45	16.7	7.74	3.69	-	0.83	**34.6**	-	8.88	-	17.0	-	16.05	-	**78.9**
SF-539	**49.2**	27.0	27.7	20.6	9.49	4.73	-	27.1	-	-	-	1.59	3.82	20.8	-	**66.6**
SNB-19	**49.1**	17.2	11.1	3.98	2.63	18.0	3.01	4.72	-	-	-	4.73	1.38	-	2.27	**75.5**
SNB-75	**35.8**	29.5	1.95	6.04	12.9	0.56	15.5	**43.3**	1.04	-	-	-	3.24	-	-	**-5.6**
U251	**50.9**	-	24.6	14.0	-	7.33	-	27.3	-	-	-	2.72	5.42	12.1	-	**81.6**
Melanoma Cancer																
LOX IMVI	**55.8**	10.9	**75.4**	**41.4**	-	-	4.57	-	-	-	-	-	0.53	17.9	-	**93.8**

MALME-3M	38.8	5.12	18.6	10.7	6.03	-	-	11.8	-	-	-	-	-	15.0	-	82.6
M14	38.3	8.26	14.4	9.91	7.61	5.34	8.79	24.7	7.06	11.4	-	13.4	3.68	11.6	11.1	58.0
MDA-MB-435	56.5	4.52	11.8	2.43	-	2.76	1.74	14.2	-	-	-	-	10.9	5.73	-	66.3
SK-MEL-2	22.9	6.63	-	-	3.38	-	-	6.92	-	-	-	-	-	4.89	-	70.9
SKMEL-28	48.6	6.81	11.6	2.75	-	-	3.98	26.0	-	2.57	-	-	-	9.71	-	NT
SK-MEL-5	40.1	11.1	23.7	10.8	-	3.82	3.43	37.5	3.95	-	-	6.95	-	7.74	11.0	91.2
Ovarian Cancer																
UAAC-62	40.8	23.8	26.5	13.8	-	14.2	21.7	18.8	6.81	22.0	-	39.6	-	12.4	14.1	86.7
IGROV1	51.1	30.2	31.0	19.1	10.3	12.0	19.4	33.5	23.6	12.7	-	13.1	19.7	32.2	26.9	-39.9
OVCAR-3	75.1	-	17.3	8.6	37.1	2.75	7.18	25.3	-	-	-	-	5.22	4.82	-	43.8
OVCAR-4	66.6	17.3	43.4	30.1	1.46	11.4	10.0	76.4	-	8.77	-	14.9	-	27.9	-	-5.8
OVCAR-5	35.1	5.65	8.15	5.64	-	-	1.17	14.2	-	-	-	-	-	10.8		52.8
OVCAR-8	61.5	25.7	17.2	8.45	6.95	1.23	0.37	14.7	-	-	-	3.11	-	6.97		NT
NCI-RES	60.3	12.6	15.1	7.91	-	2.23	-	17.7	-	1.47	-	5.71	4.97	7.37		67.7
SK-OV 3	35.5	6.97			7.64	-	11.7	10.7	-	-	-	-	2.09	-		63.1
Renal Cancer																
786-0	40.0	-	12.4	6.28	-	-	-	25.7	-	-	-	-	-	11.4		74.3
A-498	63.1	4.43	13.7	4.46	1.36	6.66	32.0	6.66	-	5.84	-	31.5	-	-		58.2
ACHN	67.1	10.4	10.5	4.18	-	-	5.33	22.4	8.11	-	-	19.1	-	12.9	7.68	-30.3
CAKI-1	58.1	26.1	13.3	4.71	11.2	22.2	26.8	28.5	16.3	12.4	-	16.6	5.20	13.5	-	97.0
RXF293	44.5	6.77	25.2	17.8	15.5	-	-	54.0	16.3	-	-		15.5	26.6	-	81.7
SN12C	57.1	12.6	22.8	20.7	3.89	6.37	8.69	16.9	4.47	8.64	-	16.4	-	20.3	5.91	69.1
TK-10	27.5	-	-	-	-	-	-	-	-	-	-	-	8.02		40.1	67.1
UO-31	37.5	28.8	33.1	23.2	45.1	26.3	32.5	42.7	33.0	40.4	31.3	45.4	-	39.5	-	-26.8
Prostate Cancer																
PC-3	65.2	34.4	38.6	24.8	12.6	13.6	20.1	49.6	13.4	11.7	25.0	21.8	31.2	28.6	-	87.4
DU-145	61.3	22.6	17.2	4.97	-	1.06	3.92	8.93	-	1.47	-	9.36	17.9	9.34	-	95.5
Breast Cancer																
MCF7	31.0	2.66	41.0	31.9	3.61	3.42	9.42	51.1	-	6.84	-	20.1		41.6	-	92.0
MDA-MB-231	63.9	19.2	5.53	-	6.90	-	2.72	19.0	-	-	-	2.75	10.1	-	-	43.0
HS 578T	36.7	34.0	2.07	1.42	11.2	11.7	5.11	12.6	-	-	-	-	3.94	5.84	-	42.4
BT-549	-	4.39	0.44	-	3.21	-	-	32.0	6.02	-	-	-	4.05	11.0	-	53.1
T-47D	53.3	39.0	34.7	25.3	8.97	20.0	26.1	69.5	7.99	26.7	-	37.2		34.9	-	87.6
MDA-MB-468	69.7	31.7	57.5	24.4	-	-	-	45.4	1.88	-	28.4	-	24.0	29.7	-	NT

NT- not treated, - indicated inactive, **orange bold** - 30-40% GI, **black bold** – 40-50 % GI, **pink bold** – 50-70 % GI, **blue bold** – 70-100 % GI, **red bold** - cytotoxic , AF = Amonafide

Among derivatives **19**, **20** and **21** substituted with aromatic amines, only analogue **20** with 4-fluoroaniline showed significant activity against leukemia cancer cell line (K-562, GI = 67.9%; SR, GI = 63.1%) and colon cancer cell lines (HCT-15, GI = 52.9%; HT-29, GI = 61.4%). This might be attributed to the presence of fluoro at *para*-position of aniline. Thus, TPE-naph conjugates with secondary amines displayed promising percentage growth inhibition than analogues bearing primary amines. It was inferred that in the present series, compounds **7-21** were found to be more sensitive towards leukemia and colon cancer cell lines. Moreover, from structure-activity relationship studies, it is demonstrated that increasing lipophilicity and bulkiness of substituent attached to C-4 position of naphthalimide ring resulted in decrease in cytotoxic activity. Therefore, the nature and size of amine influenced the anticancer activity of TPE-naph conjugates.

3.3.2 DNA topoisomerase-IIα mediated relaxation activity

Topoisomerase-II (TOPO-II) plays a key role in the segregation of strands of dsDNA which lead to replication resulting in the proliferation of cell.[93] Therefore, to evaluate the mechanism of cytotoxicity of TPE-naph hybrids, we targeted to evaluate the poisoning effect of analogue **7** (with broad-spectrum anticancer activity) on the topoisomerase-IIα using supercoiled pHOT1 plasmid DNA. Etoposide, a well-known DNA-intercalator was used as positive control at 100 μM. **Figure 6** represents the inhibitory effect of hybrid **7** on the relaxation of plasmid DNA mediated by TOPO-II at three different concentrations, i.e., 25 μM, 50 μM, and 100 μM.

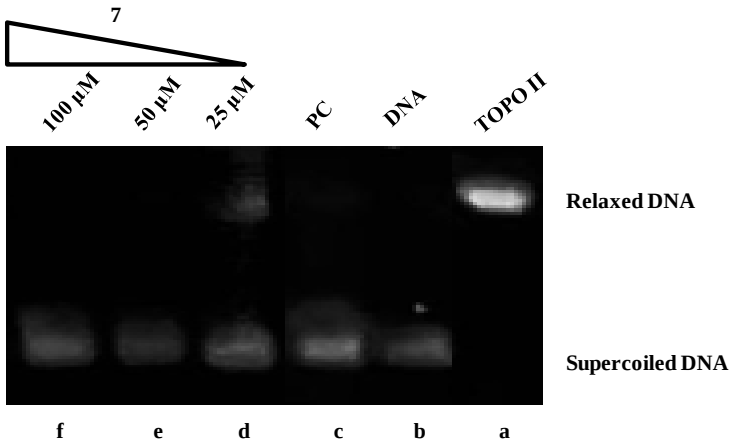

Figure 6: Effect of TPE-naph **7**on the relaxation of supercoiled plasmid DNA topoisomerase-II. Supercoiled DNA (lane b) was incubated with topoisomerase II in the absence (lane a) and

presence of analogue **7** at 25 μM (lane d), 50 μM (lane e), 100 μM (lane f), and etoposide was used as a positive control at 100 μM (lane c)

Compound **7** induces partial inhibitory activity at 25 μM and complete inhibition at 50 μM and 100 μM. It has revealed that the poisoning of TOPO-II by hybrid compound **7** is concentration-dependent and suggested a possible mechanism of cytotoxicity through topoisomerase-II inhibition.

3.3.3 Human Serum Albumin (HSA) studies

Human Serum Albumin (HSA) is a major extracellular plasma protein in blood and features the specific binding site for transportation and deposition of drugs. The binding behavior of the drug towards HSA could modulate its key pharmacodynamic and pharmacokinetic properties like efficacy, metabolism, and drug distribution.[94] Various promising drugs due to their high binding affinity towards HSA were found to be futile. Henceforth, the binding interaction studies have been done between HSA and the biologically active molecules to insight drug-likeliness properties as well as explore screening of molecules in drug discovery. Thus, to analyze the interaction between most active TPE-naph **7** and human serum albumin, *in vitro* studies were carried out *via* UV-visible absorption and fluorescence emission techniques.

UV-visible spectroscopy is a reliable tool employed to determine the structural alterations in protein and investigate the formation of complex on drug binding. In this study, the absorption band of HSA at 280 nm (7 μM, ε = 38700 $M^{-1}cm^{-1}$) was recorded in phosphate buffer (0.1M) at *p*H 7.4. The band at 280 nm corresponds to the aromatic ring of amino acid residues Trp-214, Tyr-411 and Phe-403 in HSA protein. On incremental addition of compound **7**, enhancement in the absorption band of HSA was observed with appearance of a new band at 400 nm (**Figure 7a**). The maximum peak of absorption remains unaltered which indicates that analogue **7** binds with cavity of HSA through non-covalent interactions. This is evident by the existence of π-π stacking interactions between the aromatic rings of analogue **7** and tryptophan, tyrosine and phenylalanine residues in the binding cavity of HSA.[95] In order to evaluate the binding affinity of TPE-naph with HSA, the binding constant (K_b) was calculated from a plot of $1/A\text{-}A_o$ versus 1/Q using Benesi–Hildebrand equation[96] and the ratio of intercept to slope was found to be equal to 1.4×10^4 M^{-1} (**Figure 8**).

Fluorescence spectroscopy is the technique which explores the binding interactions of drug and protein. Under physiological conditions, the fluorescence spectrum of human serum

albumin of **7** in phosphate buffer (*p*H 7.4) was recorded with an excitation wavelength of 280 nm. The fluorescence spectrum of HSA exhibited an emission band at 340 nm due to tryptophan residue. With the incremental addition of compound **7**, the emission band of HSA at 340 nm was consistently quenched, which revealed some changes around Trp-214 of HSA (**Figure 7b**). The λ_{max} of emission of HSA displayed hypsochromic shift by 5 nm (from 340 nm to 335 nm). It indicated that analogue **7** interacts with hydrophobic cavity of HSA.

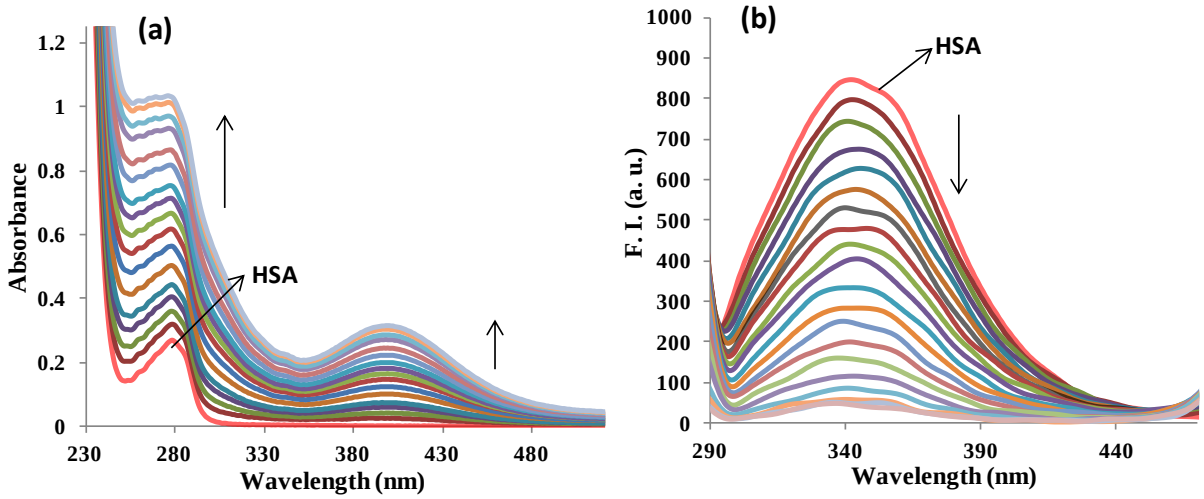

Figure 7: Effect of incremental addition of analogue **7** on (a) UV-Vis absorption and (b) fluorescence emission of HSA (7 μM) in phosphate buffer (*p*H = 7.4).

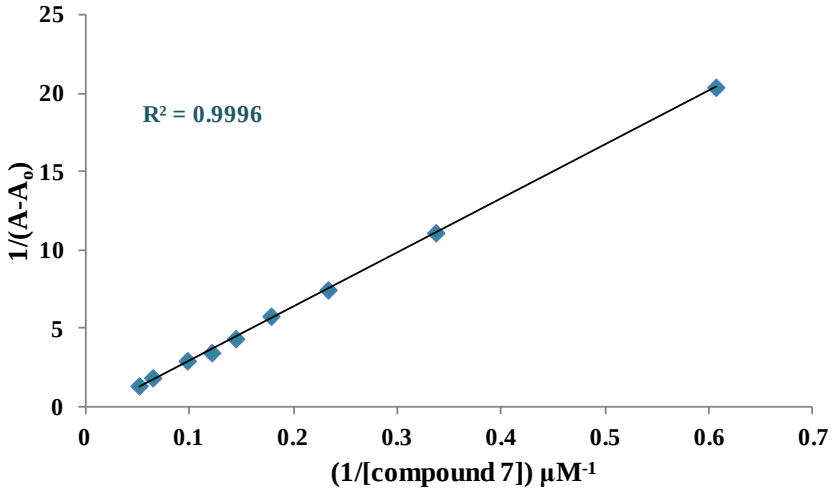

Figure 8: Plot of 1/(A – A_0) *vs.* 1/[compound **7**] for absorption spectra of HSA in phosphate buffer

The quenching of the emission band of human serum albumin upon incremental addition of **7,** results from either dynamic or static quenching. Further, Stern-Volmer equation was

employed to evaluate Stern-Volmer constant, K_{sv} and the bimolecular collision constant, K_q which explicates the binding mode of **7** to HSA (**Figure 9a**).[97] From the linear plot of regression curve of F_o/F versus [Q], K_{sv} and K_q were calculated to be 6.8×10^4 M^{-1} and 1.6×10^{13} $M^{-1}s^{-1}$, respectively. As the bimolecular collision constant (K_q) for HSA : TPE-naph system is greater than diffusion limiting quenching in water[98] i.e. 2×10^{10} M^{-1} s^{-1} which suggested the nature of quenching in the present case is static i.e. formation of analogue **7** and HSA complex in ground state.[99]

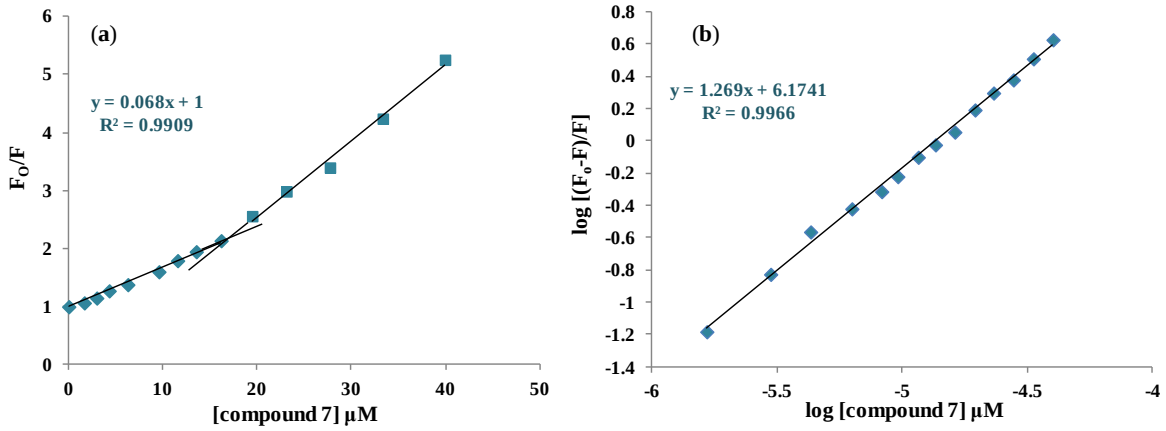

Figure 9: (a) Stern-Volmer plot of F_0/F *versus* [compound **7**] for determination of quenching constant and (b) modified Stern-Volmer plot of log $[(F_o - F)/F]$ *versus* log [compound **7**] for determination of number of binding sites by fluorescence spectrometer titration of HSA with **7** in PBS buffer (*p*H = 7.4) at 298K.

Further, the binding constant and the number of binding sites were determined using modified Stern-Volmer equation from the plot of log$[(F_o\text{-}F)/F]$ versus log[compound **7**] which give K_b and n as intercept and slope, respectively.[100] The binding constant of compound **7** toward HSA was calculated to be 1.4×10^4 M^{-1} and the number of binding sites per HSA was nearly one that revealed strong binding interaction among HSA and TPE-naph (**Figure 9b**).

To determine the spontaneity for formation of complex between conjugate **7** and HSA, change in free energy has been calculated that was found to be -8.4 kcal/mol by employing Gibb's free energy equation.[48] The negative value of ΔG demonstrates spontaneity and existence of hydrophobic interaction among HSA:TPE-naph.

3.3.4 Life-time fluorescence technique

The quenching of HSA emission by TPE-naph is either due to static or dynamic quenching mechanism. In order to have better understanding of quenching mechanism, time-resolved fluorescence experiment was carried out with deltaflex™ spectrometer.[101] **Figure 10** represents life-time decay profile of HSA (7 μM) in the absence and presence of different concentrations of compound **7**. The average lifetime triexponential values were calculated using the equation 1. Upon addition of 14 μM of analogue **7**, the life-time of HSA decrease is marginal (5.06 to 4.80 ns). As depicted from **Table 3**, at higher concentration (21-35 μM) of conjugate **7**, reduction in lifetime of HSA is more pronounced. Although the steady state fluorescence experiment demonstrates the possibility of static quenching but life-time fluorescence revealed that other phenomena of quenching may also exist i.e. dynamic quenching. From above results, it was inferred that both the static as well as dynamic quenching might be responsible for the interaction of analogue **7** to HSA.

$$\tau_{avg} = \alpha_1\tau_1 + \alpha_2\tau_2 + \alpha_3\tau_3 \quad (1)$$

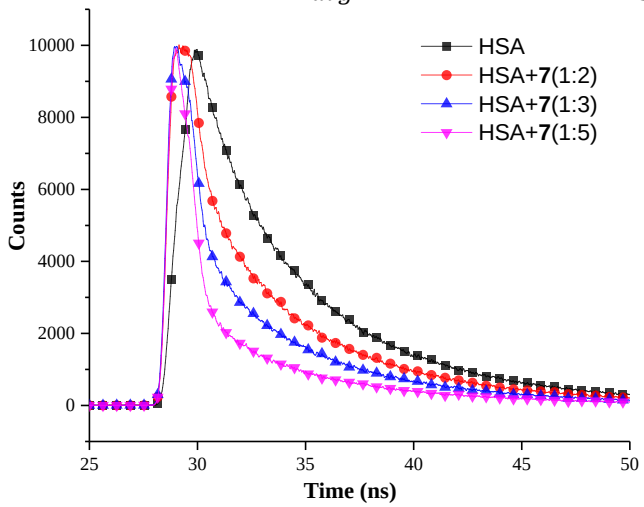

Figure 10: Fluorescence decay profile of HSA on addition of different concentrations of **7** in phosphate buffer (*p*H = 7.4)

Table 3: Fluorescence decay profile of HSA and compound **7**

System	Conc.	$\tau_{1\,(ns)}$	$\tau_{2(ns)}$	$\tau_{3\,(ns)}$	α_1	α_2	α_3	τ_{av}	χ^2
HSA		3.64	6.97	1.17	0.26	0.70	0.02	5.06	1.01
HSA-**7**	1:2	3.65	7.47	0.51	0.35	0.60	0.04	4.80	1.11
	1:3	4.19	7.94	0.64	0.42	0.45	0.12	4.10	1.39
	1:5	3.47	7.83	0.43	0.32	0.53	0.13	2.11	1.23

3.4 Molecular docking

To identify the target site of *E*- and *Z*-isomers of TPE-naph analogue **7** meditating cytotoxicity either through inhibition of catalytic function of TOPO-II (inhibitor; without damage of DNA) or by stabilizing the DNA-topo-II complex through covalent bond (TOPO-II poison; damage DNA), docking studies have been performed using TOPO-II-DNA complex (PDB ID: 5GWK) binary complex *via* Autodock vina 4.0 software.[82] From docking studies, the binding energy scores *E*- and *Z*-isomers for analogue **7** and reference drug etoposide were calculated to be -11.3, -11.3 and -9.8 kcal/mol, respectively. It was observed that *E*- and *Z*-isomers of conjugate **7** exhibited better binding affinity than reference drug etoposide while these bind only with amino acid residues of TOPO-II. It demonstrates the existence of strong intermolecular forces between the ligand and TOPO-II. **Figure 11** represents the 3-D docked structures of compound **7** (*E*-isomer**,** (**a**); *Z*-isomer, (**b**) and etoposide (**c**) with TOPO-II-DNA complex. From the binding pattern, it was inferred that *E*-isomer of **7** interacts with the active sites of TOPO-II-DNA complex *via* Thr618 (*d* = 2.23 Å) through conventional-hydrogen bonding; Tyr805, Lys611,

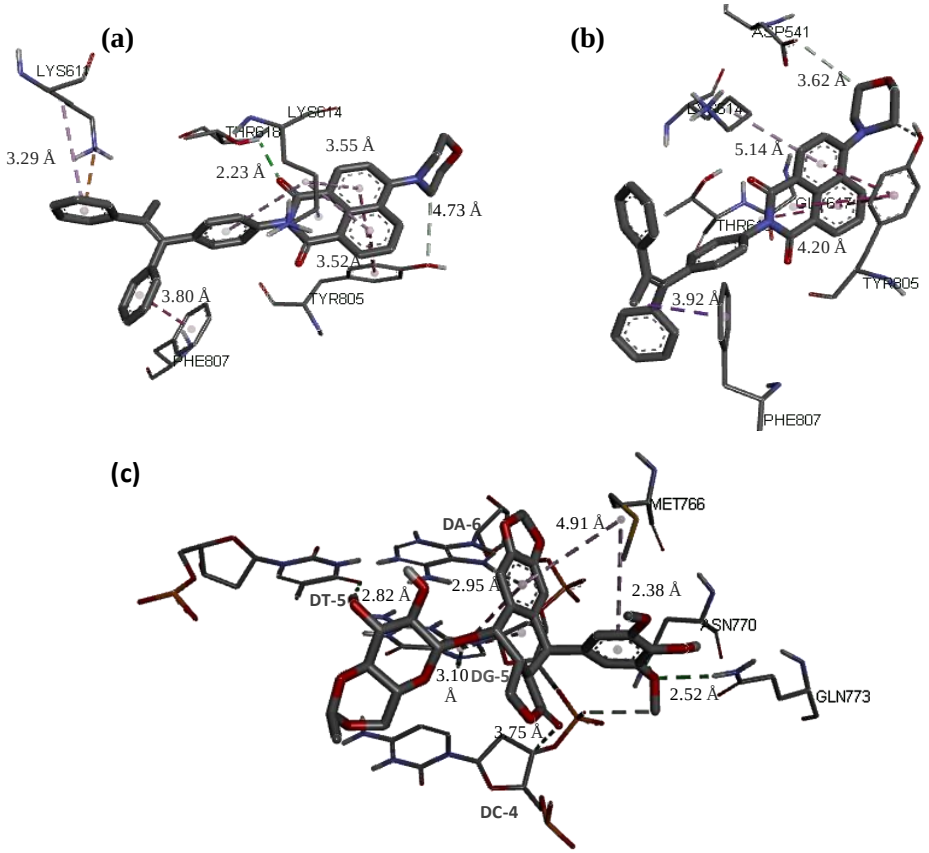

Figure 11: 3-D docked structures of compound **7** (a) *E*-isomer, (b) *Z*-isomer, and (c) etoposide

Lys614 and Phe807 residues through alkyl-alkyl and π-alkyl hydrophobic interactions while *Z*-isomer of analogue **7** showed non-conventional hydrogen bonding (Asp541 and Tyr805) and hydrophobic interactions (Gly617, Thr618, Lys614 and Phe807) with topoisomerase-II-DNA complex (PDB code: 5GWK)

On the other hand, etoposide binds with TOPO-II complex *via* Asn770 (d = 2.38 Å) and Gln773 (d = 2.52 Å) residues by conventional hydrogen bondings; Met766 through hydrophobic interactions; and sugar back-bone of DNA through DT-5 (d = 2.82 Å), DC-4 (d = 3.75 Å), DA-6 (d = 2.95 Å) and DG-5 (d = 3.10 Å). The results of docking studies are consistent with our experimental data and proved that TPE-naph conjugate inhibit TOPO-II without the generation of DNA damage.

3.5 Conclusion

A novel series of triphenylethylene-naphthalimide conjugates has been synthesized by substituting different amines at the C-4 position of naphthalimide ring and evaluated for their cytotoxicity towards sixty human cancer cell lines. Preliminary results indicated that TPE-naph conjugates were found to be more sensitive towards leukemia and colon subpanels at one-dose concentration (10 μM). Among synthesized analogues, only compound **7** bearing morpholinyl group exhibited excellent activity. It was also observed that the increase in lipophilicity of substituent lowers the cytotoxicity of TPE-naph hybrids towards cancer cell lines. More importantly, TPE-naph derivatives substituted with secondary amines exhibited better cytotoxicity. Thus, SAR studies revealed that the nature and bulkiness of substituent play key roles in antiproliferative activity of TPE-naph. The most active compound **7** inhibited the activity of TOPO-II at 50 μM concentration significantly. It suggested the plausible mechanism of cytotoxicity through TOPO-II inhibition; and also supported by docking results. The docking results analyzed the preferential binding sites of TPE-conjugate **7** with TOPO-II-DNA complex. It was observed that oxygen atoms of naphthalimide and phenyl rings of triphenylethylene interact only with TOPO-II through hydrogen bonding and π-π stacking hydrophobic forces with binding affinity -11.3 kcal/mol. Moreover, the interaction of **7** with human serum albumin indicated the binding constant in order of 10^4 M^{-1} which is the evident of drug likeness properties of these analogues. Thus, the present work highlights the approaches employed to design and synthesize new molecular framework (triphenylethylene–naphthalimide conjugates) as

therapeutic template to target TOPO-IIα for anticancer activity. These results extended a new route to design and develop efficient drug candidates as anticancer agent.

3.6 Experimental section

All the chemicals and reagents were commercially available from Spectrochem, Aldrich (Sigma-Aldrich), TCI and used without further purification. Analytical TLC was performed using spectrochem silica gel (GF-254) pre-coated plates and visualized TLC under UV light or by iodine indicator. ^{1}H NMR and ^{13}C NMR spectra were carried out on Jeol spectrometer 400 MHz and 100 MHz, and Bruker 500 MHz and 125 MHz, respectively, using deuterated solvents ($CDCl_3$ and DMSO-d_6). Using TMS as an internal reference, chemical shifts (δ) and coupling constants (J) were recorded in ppm and Hz, respectively. Melting points were determined on equiptronics melting point apparatus and were uncorrected. UV-Vis and fluorescence studies were accomplished on Shimadzu and Varian Cary Eclipse fluorescence spectrophotometer, respectively. The time-resolved fluorescence studies were carried out using deltaflex^{TM} spectrometer. High Resolution Mass Spectra (HRMS) of the synthesized compounds were observed at Waters Q-TOF of Micromass.

4-(1,2-Diphenylprop-1-en-1-yl)aniline (2)

Titanium tetrachloride (2.77 mL, 25.30 mmol) was added gradually to a suspension of Zn (3.24 g, 50.75 mmol) in dry THF (40 mL) under the atmosphere of nitrogen at 0 ^{o}C. Subsequently, the resulting black mixture was allowed to reflux for 3 h to produce titanium reagent. After refluxing, the obtained titanium reagent was cooled to 0 ^{o}C and charged with pyridine (1.02 mL, 12.7 mmol). Then, a solution of acetophenone (0.59 mL, 5.07 mmol) and 4-amino benzophenone (1 g, 5.07 mmol) in THF was added dropwise to reaction mixture at 0 ^{o}C and stirred for 30 min. The reaction mixture was heated to reflux for 2.5 h. The completion of reaction was monitored by TLC. On completion, 10% aq. soln. of K_2CO_3 was poured into the cooled reaction mixture and stirred vigorously for 10 min. On stirring, a black mass was separated out that removed by vacuum filtration. The crude product was extracted from the filtrate with ethyl acetate. The extracted organic layer was dried over Na_2SO_4 and the solvent was evaporated. Further, the resulting brownish-yellow oil was purified by column chromatography (hexane/ethylacetate 97:3) to provide a desired cross-coupled product (**2**) in diasteromeric isomers.

4-(1,2-Diphenylprop-1-en-1-yl)aniline (2)

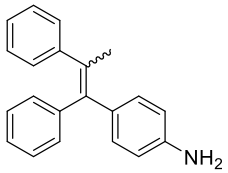

E/Z : 1/6; yield 60%; mp. 142-144 ^{o}C; ^{1}H NMR (400 MHz, $CDCl_3$): δ 7.35-7.32 (m, 2H, ArH), 7.26-7.23 (m, 3H, ArH), 7.17 (br, s, 3H, ArH), 7.13-7.09 (m, 2H, ArH), 7.04-6.96 (m, 1H, ArH), 6.91-6.88 (m, 1H, ArH), 6.67-6.65 (m, 2H, ArH), 6.36-6.33 (m, 2H, ArH), 3.48 (s, 2H, NH_2), 2.18 (s, 3H, CH_3), 2.10 (s, 3H, CH_3); ^{13}C NMR (100 MHz, $CDCl_3$): δ 144.6, 144.2, 144.1, 144.0, 139.1, 134.1, 134.0, 133.6, 132.2, 130.1, 129.5, 129.4, 128.1, 127.9, 127.8, 126.5, 126.0, 114.3 (ArC), 23.4 (CH_3); ESIMS: *m/z* 286.2 $(M+H)^+$.

5-Bromo-1,2-dihydroacenaphthylene (4)[102]

To a suspension of acenaphthene (3 g, 19.4 mmol) in DMF, a solution of *N*-bromosuccinimide (4.15 g, 23.35 mmol) in 30 mL of DMF was added slowly at room temperature. The solution was stirred vigorously for 3 h. The reaction was quenched by adding 300 mL of cold water into solution, and brown colored precipitates were obtained on filtration. The crude was recrystallized to obtain pure 5-bromo-1,2-dihydroacenaphthylene (**4**) in 97% yield, (observed mp: 54-56 ^{o}C, literature mp 52 ^{o}C).

4-Bromo-1,8-naphthalic anhydride (**5**)[103]

Potassium dichromate (6.31 g, 21.45 mmol) was added slowly to a solution of 5-bromo acenaphthene **4** (1 g, 4.2 mmol) in glacial acetic acid at 0 ^{o}C. The mixture was stirred for 10 min at room temperature and then allowed to reflux for 4 h. The cooled reaction mixture was poured into 500 mL of water and filtered to provide green colored precipitates. The excess chromium salt left in residue was removed by washing with boiled water. After washing, white colored solid (**5**) was obtained in 72% yield (mp: 221-224 ^{o}C).

6-Bromo-2-(4-(1,2-diphenylprop-1-en-1-yl)phenyl)-1*H*-benzo[*de*]isoquinoline-1,3(2*H*)-dione (6)

To a two necked round-bottom flask, 4-bromo-1,8-naphthalic anhydride (**5**) (1g, 3.61 mmol) and zinc acetate (0.95 g, 4.3 mmol) were dispersed in 15 mL of ethanol under the inert atmosphere. To the stirred reaction mixture, 4-(1,2-diphenylprop-1-en-1-yl)aniline (**2**) (0.52 g, 1.81 mmol) was added and heated to reflux for 15 h. After completion of reaction, the hot filteration of the suspension was carried out and repeatedly washed with ethanol. The crude was purified by column chromatography (hexane:chloroform; 8:2) to obtain a yellow colored pure product (**6**).

6-Bromo-2-(4-(1,2-diphenylprop-1-en-1-yl)phenyl-1*H*-benzo[*de*]isoquinoline-1,3(2*H*)-dione (**6**)

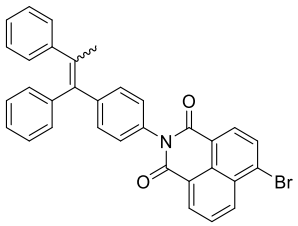

E/Z : 1/2; 98% yield; ^{1}H NMR (400 MHz, $CDCl_3$): δ 8.67-8.64 (m, 1H, ArH), 8.62-8.59 (m, 2H, ArH), 8.44-8.42 (d, *J* = 7.88 Hz, 1H, ArH), 8.37-8.35 (d, *J* = 7.88 Hz, 1H, ArH), 8.14-8.12 (d, *J* = 7.92 Hz, 1H, ArH), 8.10-8.08 (d, *J* = 7.92 Hz, 1H, ArH), 7.97-7.89 (m, 2H, ArH), 7.43-7.37 (m, 4H, ArH), 7.31-7.29 (d, *J* = 7.96 Hz, 4H, ArH), 7.23-7.22 (m, 2H, ArH), 7.16-7.10 (m, 4H, ArH), 7.08-7.02 (m, 4H, ArH), 6.97-6.95 (m, 3H, ArH), 2.21 (s, 3H,CH_3), 2.13 (s, 3H, CH_3); ^{13}C NMR (100 MHz, $CDCl_3$ + DMSO-d_6): δ 163.7, 163.6, 163.5, 143.7, 143.6, 143.5, 143.2, 143.1, 142.7, 138.4, 138.3, 136.6, 136.5, 133.7, 133.6, 132.8, 132.3, 132.2, 131.5, 131.4, 131.3, 131.2, 130.8, 130.7, 130.6, 130.5, 130.0, 129.9, 129.3, 129.2, 128.5, 128.4, 128.3, 128.1, 127.9, 127.7, 127.6, 126.8, 126.6, 123.3, 123.2, 122.4, 122.3 (ArC), 23.6 (CH_3), 23.5 (CH_3); ESIMS: *m/z* 544.0 $(M+H)^+$.

6-Amino subsituted-2-(4-(1,2-diphenylprop-1-en-1-yl)phenyl)-1*H*-benzo[*de*]isoquinolin-1,3(2*H*)-diones (7-21)

A mixture of 6-bromo-2-(4-(1,2-diphenylprop-1-en-1-yl)-1*H*-benzo[*de*]isoquinoline-1,3(2*H*)-dione (**6**) (0.2 g, 0.37 mmol) and corresponding primary or secondary amine (1.1 mmol) was refluxed for 2-3 h in the presence of potassium carbonate (0.06 g, 0.44 mmol) in 10 mL of DMF. The reaction mixture was allowed to cool and poured in water (50 mL) to obtain precipitates. Then, the mixture was filtered off to get corresponding solid crude product of 6-amino subsituted-2-(4-(1,2-diphenylprop-1-en-1-yl)-1*H*-benzo[*de*]isoquinoline-1,3(2*H*)-diones (**7-21**) which was purified by column chromatography over silica gel using hexane and chloroform as eluents.

2-(4-(1,2-Diphenylprop-1-en-1yl)phenyl)-6-morpholino-1*H*-benzo[*de*]isoquinoline-1,3(2*H*)-dione (7)

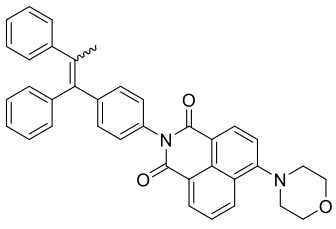

Yellow solid, *E*/*Z* : 1/3.3; Yield 77 %; mp: 236-240 ^{o}C; ^{1}H NMR (400 MHz, $CDCl_3$): δ 8.63-8.61 (dd, 1H, ^{2}J = 7.28 Hz, ^{3}J = 0.92 Hz, ArH), 8.58-8.55 (m, 1H, ArH), 8.51-8.49 (d, 1H, *J* = 8.00 Hz, ArH), 8.48-8.45 (m, 1H, ArH), 8.44-8.41 (m, 1H, ArH), 7.76-7.74 (m, 1H, ArH), 7.72-7.68 (m, 1H, ArH), 7.41-7.34 (m, 3H, ArH), 7.30-7.25 (m, 4H, ArH), 7.23-7.21 (m, 5H, ArH), 7.16-7.11 (m, 2H, ArH), 7.03-7.00 (m, 3H, ArH), 6.95-6.92 (m, 3H, ArH), 4.04-3.99 (m, 5H, morph-OCH_2), 3.29-3.24 (m, 5H, morph-NCH_2), 2.21 (s,

1H, CH_3), 2.15 (s, 3H, CH_3); ^{13}C NMR (100 MHz, $CDCl_3$): δ 164.7, 164.5, 164.2, 164.1, 156.0, 155.9, 144.0, 143.7, 143.3, 143.1, 142.8, 138.7, 138.6, 136.5, 136.4, 133.1, 133.0, 132.9, 131.7, 131.5, 131.1, 131.0, 130.5, 130.4, 130.3, 129.4, 128.5, 128.3, 128.2, 127.9, 127.6, 127.5, 126.7, 126.6, 126.3, 126.2, 126.1, 126.0, 123.5, 117.2, 115.2, 115.1 (ArC), 67.0 (morph-OCH_2), 53.5 (morph-NCH_2), 23.6 (CH_3), 22.9 (CH_3); HRMS (TOF MS): m/z calculated $C_{37}H_{30}N_2O_3$ $[M+1]^+$ 551.2256, found 551.2330.

2-(4-(1,2-Diphenylprop-1-en-1yl)phenyl)-6-(piperidin-1-yl)-1*H*-benzo[*de*]isoquinoline1,3(2*H*)-dione (8)

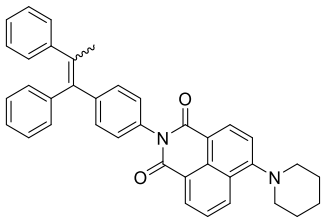

Yellow solid, *E*/*Z* : 1/2.2; Yield 72 %; mp: 235-238 °C; ^1H NMR (400 MHz, $CDCl_3$): δ 8.61-8.59 (m, 1H, ArH), 8.54-8.51 (m, 1H, ArH), 8.47-8.45 (d, *J* = 7.28 Hz, 1H, ArH), 8.44-8.42 (m, 1H, ArH), 8.40-8.38 (m, 1H, ArH), 7.41-7.33 (m, 3H, ArH), 7.30-7.26 (m, 4H, ArH), 7.22-7.17 (m, 5H, ArH), 7.15-7.08 (m, 4H, ArH), 7.03-6.99 (m, 3H, ArH), 6.95-6.92 (m, 3H, ArH), 3.28-3.20 (m, 6H, pip-NCH_2), 1.92-1.84 (m, 6H, pip-CH_2), 1.76-1.70 (m, 3H, pip-CH_2); ^{13}C NMR (100 MHz, $CDCl_3$): δ 163.9, 163.7, 163.4, 163.2, 156.7, 156.6, 143.0, 142.7, 142.5, 142.3, 142.0, 141.8, 137.7, 137.6, 135.4, 132.2, 132.0, 130.7, 130.5, 130.4, 130.1, 130.0, 129.4, 129.3, 128.4, 127.4, 127.2, 127.1, 126.9, 126.7, 126.5, 125.7, 125.6, 125.4, 125.0, 124.5, 124.4, 122.3, 114.9, 113.9, 113.8 (ArC), 53.6 (pip-NCH_2), 28.7 (pip-CH_2), 25.3 (pip-CH_2), 23.4 (CH_3), 22.6 (CH_3); HRMS (TOF MS): m/z calculated $C_{38}H_{32}N_2O_2$ $[M+1]^+$ 549.2464, found 549.2538.

2-(4-(1,2-Diphenylprop-1-en-1-yl)phenyl)-6-(4-methylpiperazin-1-yl)-1*H*-benzo[*de*]isoquinoline-1,3(2*H*)-dione (9)

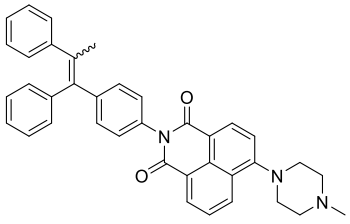

Yellow solid, *E/Z :* 1/3.5; Yield 78 %; mp: 239-242 °C; ^1H NMR (400 MHz, $CDCl_3$): δ 8.62-8.60 (m, 1H,ArH), 8.56-8.54 (m, 1H, ArH), 8.49-8.47 (d, *J* = 8.08 Hz, 1H, ArH), 8.46-8.44 (m, 1H, ArH), 8.42-8.40 (m, 1H, ArH), 7.74-7.72 (m, 1H, ArH) 7.70-7.66 (m, 1H, ArH), 7.41-7.33 (m, 3H, ArH), 7.30-7.25 (m, 4H, ArH), 7.22-7.20 (m, 5H, ArH), 7.16-7.07 (m, 3H, ArH), 7.03-7.00 (m, 3H, ArH), 6.95-6.92 (m, 3H, ArH), 3.32-3.30 (m, 5H, pip-NCH_2), 2.74-2.73 (m, 5H, pip-NCH_2), 2.44 (s, 1H, pip-NCH_3), 2.42 (s, 3H, pip-NCH_3), 2.21 (s, 1H, CH_3), 2.15 (s, 3H, CH_3); ^{13}C NMR (400 MHz, $CDCl_3$ + DMSO-

d_6): δ 164.4, 163.9, 156.4, 156.3, 143.6, 143.2, 142.9, 138.4, 136.4, 131.3, 131.2, 130.8, 130.1, 130.0, 129.2, 128.3, 128.1, 127.8, 126.8, 126.6, 126.1, 125.7, 123.3, 123.2, 116.4, 116.3, 115.0 (ArC), 55.0 (pip-NCH_2), 53.0 (pip-NCH_2), 52.9 (pip-NCH_2), 46.2 (NCH_3), 46.1 (NCH_3), 23.6 (CH_3); HRMS (TOF MS): m/z calculated $C_{38}H_{33}N_3O_2$ $[M+1]^+$ 564.2573, found 564.2646.

2-(4-(1,2-Diphenylprop-1-en-1-yl)phenyl)-6-(4-ethylpiperazin-1-yl)-1*H*-benzo[*de*]isoquinoline-1,3(2*H*)-dione (10)

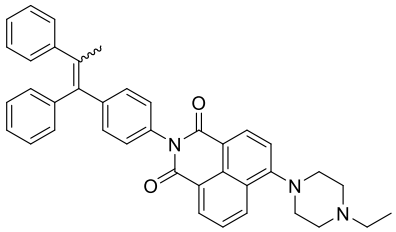

Yellow solid, *E/Z* : 1/3.6; Yield 74 %; mp: 240-243 ^oC; ^1H NMR (400 MHz, $CDCl_3$): δ 8.62-8.57 (m, 1H, ArH), 8.55-8.53 (m, 1H, ArH), 8.49-8.46 (m, 1H, ArH), 8.44-8.40 (m, 1H, ArH), 8.24-8.22 (m, 1H, ArH), 7.77-7.71 (m, 1H, ArH), 7.69-7.65 (m, 1H, ArH), 7.40-7.33 (m, 3H, ArH), 7.30-7.26 (m, 4H, ArH), 7.22-7.19 (m, 5H, ArH), 7.15-7.09 (m, 2H, ArH), 7.04-6.99 (m, 3H, ArH), 6.98-6.92 (m, 3H, ArH), 3.31 (br, s, 4H, pip-NCH_2), 2.77 (br, s, 4H, pip-NCH_2), 2.60-2.53 (m, 3H, NCH_2), 2.21 (s, 1H, CH_3), 2.14 (s, 3H, CH_3), 1.19-1.14 (m, 4H, NCH_3); ^{13}C NMR (400 MHz, $CDCl_3$ + DMSO-d_6): δ 164.5, 163.9, 156.3, 143.8, 143.6, 143.5, 143.3, 143.2, 142.9, 138.5, 138.4, 138.3, 136.5, 136.4, 133.2, 132.8, 131.5, 131.4, 131.3, 131.2, 130.9, 130.8, 130.6, 130.1, 130.0, 129.3, 129.2, 128.1, 127.9, 127.7, 127.5, 126.7, 126.5, 126.1, 125.7, 123.1, 116.3, 114.9 (ArC), 53.0 (pip-NCH_2), 52.9 (pip-NCH_2), 52.7 (ethyl-NCH_2), 52.3 (pip-NCH_2), 23.6 (CH_3), 23.5 (CH_3), 12.0 (ethyl-CH_3); HRMS (TOF MS): m/z calculated $C_{39}H_{35}N_3O_2$ $[M+1]^+$ 578.2729, found 578.2800.

2-(4-(1,2-Diphenylprop-1-en-1-yl)phenyl)-6-(4-phenylpiperazin-1-yl)-1*H*-benzo[*de*]isoquinoline-1,3(2*H*)-dione (11)

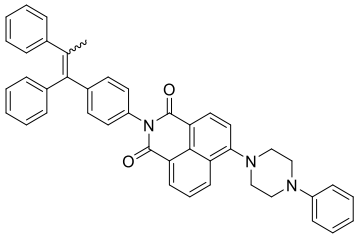

Yellow solid, *E/Z* : 1/1; Yield 79 %; mp: 245-248 ^oC; ^1H NMR (500 MHz, $CDCl_3$): δ 8.66-8.64 (d, *J* = 7.25 Hz, 1H, ArH), 8.60-8.58 (m, 2H, ArH), 8.54-8.52 (d, *J* = 7.85 Hz, 2H, ArH), 8.50-8.48 (d, *J* = 8.40 Hz, 1H, ArH), 7.78-7.71 (m, 2H, ArH), 7.43-7.41 (d, *J* = 8.35 Hz, 2H, ArH), 7.39-7.28 (m, 15H, ArH), 7.24-7.21 (m, 4H, ArH), 7.17-7.16 (m, 4H, ArH),7.13-7.10 (m, 1H, ArH), 7.06-7.03 (m, 8H, ArH), 6.96-6.92 (m, 6H, ArH), 3.55-3.50 (m, 8H, pip-NCH_2), 3.48-3.44 (m, 8H, pip-NCH_2), 2.23 (s, 3H, CH_3), 2.17 (s, 3H, CH_3); ^{13}C NMR (100 MHz, $CDCl_3$): δ 164.7, 164.6, 164.3, 164.1, 156.1, 156.0, 151.1,

143.7, 143.6, 143.3, 143.1, 142.8, 138.6, 136.5, 132.9, 131.7, 131.5, 131.1, 131.0, 130.3, 130.2, 129.4, 129.3, 128.2, 128.1, 127.9, 127.7, 126.7, 126.6, 126.4, 126.3, 126.1, 126.0, 125.9, 123.6, 123.5, 120.5, 117.2, 117.1, 116.6, 116.5, 115.2 (ArC), 53.2 (pip-NCH_2), 53.1 (pip-NCH_2), 49.7 (pip-NCH_2), 49.6 (pip-NCH_2), 23.7 (CH_3), 23.6 (CH_3); HRMS (TOF MS): m/z calculated $C_{43}H_{35}N_3O_2$ $[M+1]^+$ 626.2729, found 626.2809.

6-(4-Benzylpiperazin-1-yl)-2-(4-(1,2-diphenylprop-1-en-1-yl)phenyl)-1*H*-benzo[*de*]isoquinoline-1,3(2*H*)-dione (12)

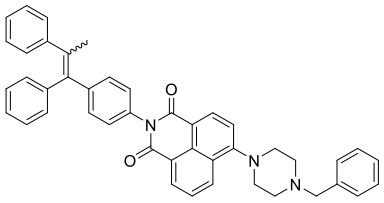

Yellow solid, *E/Z* : 1/1.4; Yield 75 %; mp: 246-249 ^oC; ^1H NMR (400 MHz, $CDCl_3$) δ 8.62-8.60 (d, *J* = 7.2 Hz, 1H, ArH), 8.55-8.53 (d, *J* = 7.80 Hz, 2H, ArH), 8.49-8.40 (m, 3H, ArH), 7.72-7.64 (m, 2H, ArH), 7.41-7.32 (m, 11H, ArH), 7.31-7.22 (m, 10H, ArH), 7.18-7.14 (m, 5H, ArH), 7.11-7.07 (m, 2H, ArH), 7.05-7.00 (m, 5H, ArH), 6.95-6.92 (m, 4H, ArH), 3.67 (s, 2H, benzyl-CH_2), 3.65 (s, 2H, benzyl-CH_2), 3.32-3.29 (m, 7H, pip-NCH_2), 2.78 (br, s, 7H, pip-NCH_2), 2.22 (s, 3H, CH_3), 2.15 (s, 3H, CH_3). ^{13}C NMR (100 MHz, $CDCl_3$): δ 164.8, 164.6, 164.3, 164.1, 144.0, 144.0, 143.7, 143.7, 143.6, 143.6, 143.3, 143.3, 143.1, 142.8, 140.06, 138.82, 138.77, 138.66, 138.65, 138.07, 138.03, 136.4, 136.4, 133.1, 133.1, 133.1, 133.0, 132.9, 131.8, 131.7, 131.7, 131.7, 131.6, 131.4, 131.1, 131.1, 130.9, 130.7, 130.6, 130.3, 130.3, 130.2, 129.4, 129.4, 129.4, 129.4, 129.3, 128.5, 128.5, 128.4, 128.2, 128.1, 128.1, 127.9, 127.9, 127.7, 127.7, 127.5, 127.4, 126.7, 126.7, 126.6, 1263, 126.2, 125.9, 125.9, 125.8, 125.8, 123.4, 130.9, 130.2, 129.41, 128.5, 128.4, 128.2, 128.1, 127.9, 127.7, 127.5, 126.3, 125.9, 125.8, 123.4 (ArC), 65.4 (benzyl CH_2), 65.3 (benzyl CH_2), 53.1 (pip-CH_2), 53.1 (pip-CH_2), 53.1 (pip-CH_2), 23.6 (CH_3), 23.6 (CH_3); HRMS (TOF MS): m/z calculated $C_{44}H_{37}N_3O_2$ $[M+1]^+$ 640.2886, found 640.2960.

6-(Cyclohexylamino)-2-(4-(1,2-diphenylprop-1-en-1-yl)phenyl)-1*H*-benzo[*de*]isoquinoline-1,3 (2*H*)-dione (13)

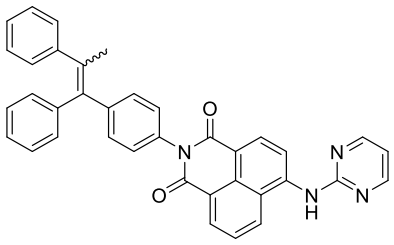

Yellow solid, *E/Z* : 1/1.4; Yield 71 %; mp: 238-242 ^oC; ^1H NMR (400 MHz, $CDCl_3$): δ 8.63-8.61 (d, *J* = 7.24 Hz, 1H, ArH), 8.57-8.55 (d, *J* = 7.16 Hz, 1H, ArH), 8.50-8.42 (m, 2H, ArH), 8.13-8.07 (m, 1H, ArH), 7.70-7.59 (m, 2H, ArH), 7.41-7.34 (m, 4H, ArH), 7.31-7.28 (m, 5H, ArH), 7.23-7.22 (m, 5H,

ArH), 7.17-7.07 (m, 6H, ArH), 7.05-7.01 (m, 5H, ArH), 6.96-6.94 (m, 4H, ArH), 3.64 (br, s, 2H, cyclohexyl-NH), 3.14 (s, 1H, cyclohexyl-CH), 3.11 (s, 1H, cyclohex yl-CH), 2.23 (s, 3H, CH_3), 2.16 (s, 3H, CH_3), 1.88-1.85 (m, 3H, cyclohexyl-CH_2), 1.76-1.72 (m, 2H, cyclohexyl-CH_2), 1.42-1.33 (m, 7H, cyclohexyl-CH_2), 1.29-1.28 (m, 2H, cyclohexyl-CH_2), 1.25--1.21 (m, 6H, cyclohexyl-CH_2); ^{13}C NMR (100 MHz, $CDCl_3$): δ 165.0, 164.8, 164.3, 164.2, 148.7, 148.6, 144.1, 143.7, 143.4, 143.3, 143.0, 142.8, 138.8, 138.7, 136.4, 136.3, 134.9, 134.8, 133.6, 131.7, 131.6, 131.5, 131.2, 131.1, 130.9, 130.6, 130.5, 130.4, 130.3, 129.4, 128.5, 128.3, 128.2, 128.1, 127.9, 127.7, 127.6, 127.5, 126.8, 126.7, 126.6, 126.5, 126.2, 126.1, 125.9, 124.7, 124.6, 123.4, 123.3, 120.3, 120.2 (ArC), 51.8 (cyclohexyl-CH), 32.8 (cyclohexyl-CH_2), 25.7 (cyclohexyl-CH_2), 24.9 (cyclohexyl-CH_2), 23.7 (CH_3), 23.6 (CH_3); HRMS (TOF MS): m/z calculated $C_{39}H_{34}N_2O_2$ $[M+1]^+$ 563.2620, found 563.2693.

2-(4-(1,2-Diphenylprop-1-en-1-yl)-6-((2-morpholinoethyl)amino)-1*H*-benzo[*de*]isoquinolin e-1,3(2*H*)-dione (14)

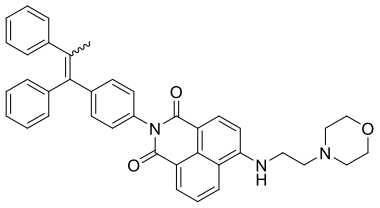

Yellow solid, *E/Z* : 1/1.; Yield 62 %; mp: 249-252 ^{o}C; ^{1}H NMR (500 MHz, $CDCl_3$): δ 8.65-8.64 (d, *J* = 7.20 Hz, 1H, ArH), 8.59-8.57 (d, *J* = 7.25 Hz, 1H, ArH), 8.52-8.50 (d, *J* = 8.3 Hz, 1H, ArH), 8.46-8.44 (d, *J* = 8.35 Hz, 2H, ArH), 8.18-8.12 (m, 2H, ArH), 7.71-7.64 (m, 2H, ArH), 7.41-7.35 (m, 4H, ArH), 7.32-7.28 (m, 5H, ArH), 7.23-7.20 (m, 4H, ArH), 7.17-7.10 (m, 6H, ArH), 7.04-7.00 (m, 5H, ArH), 6.96-6.95 (m, 4H, ArH), 6.37 (br, s, 1H, NH), 6.33 (br, s, 1H, NH), 3.79 (br, s, 8H, morph-OCH_2), 3.47-3.40 (m, 4H, ethyl-$NHCH_2$), 2.86-2.80 (m, 4H, ethyl-CH_2), 2.59 (br, s, 8H, morph-NCH_2), 2.23 (s, 3H, CH_3), 2.17 (s, 3H, CH_3); ^{13}C NMR (100 MHz, $CDCl_3$): δ 165.0, 164.8, 149.7, 149.6, 144.1, 143.7, 143.3, 142.8, 138.8, 138.7, 136.4, 136.3, 135.0, 134.8, 134.3, 133.5, 131.6, 131.5, 131.2, 131.1, 131.0, 130.9, 130.3, 130.2, 129.4, 128.5, 128.2, 128.1, 127.9, 127.7, 127.5, 126.7, 126.6, 126.2, 125.9, 125.2, 125.1, 125.0, 123.4, 123.3, 120.6, 120.5, 120.1, 110.3 (ArC), 67.1 (morph-OC), 67.0 (morph-OC), 56.0 (aliphatic-NC), 55.9 (aliphatic-NC), 53.2 (ethyl-NC), 53.1 (ethyl-NC), 23.7 (CH_3), 23.6 (CH_3); HRMS (TOF MS): m/z calculated $C_{39}H_{35}N_3O_3$ $[M+1]^+$ 594.2678, found 594.2750.

6-((2-(Dimethylamino)ethylamino)-2-(4-(1,2-diphenylprop-en-1-yl)phenyl)-1*H*-benzo[*de*]isoquinoline-1,3(2*H*)-dione (15)

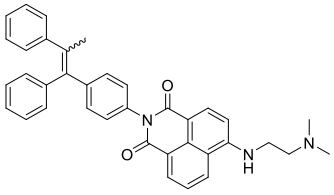

Yellow solid, *E/Z* : 1/1.3; Yield 68 %; mp: 233-235 ^{o}C; ^{1}H NMR (500 MHz, $CDCl_3$): δ 8.61-8.59 (d, *J* = 7.15 Hz, 1H, ArH), 8.54-8.53 (d, *J* = 7.25 Hz, 1H, ArH), 8.50-8.48 (d, *J* = 8.30 Hz 1H, ArH), 8.44-8.42 (d, *J* = 8.30 Hz, 1H, ArH), 8.30-8.25 (m, 2H, ArH), 7.63-7.56 (m, 2H, ArH), 7.40-7.35 (m, 4H, ArH), 7.31-7.28 (m, 5H, ArH), 7.23-7.20 (m, 5H, ArH), 7.17-7.09 (m, 5H, ArH), 7.05-7.01 (m, 4H, ArH), 6.96-6.93 (m, 3H, ArH), 3.91-3.88 (m, 4H, ethyl -NCH_2), 3.83-3.80 (m, 4H, ethyl-NCH_2), 3.43 (s, 4H, CH_3), 3.41 (s, 6H, CH_3), 2.23 (s, 3H, CH_3), 2.16 (s, 3H, CH_3); ^{13}C NMR (100 MHz, $CDCl_3$): δ 165.1, 164.9, 164.5, 164.4, 149.9, 149.8, 144.0, 143.7, 143.4, 143.3, 142.9, 142.8, 138.8, 138.6, 136.4, 134.8, 134.7, 134.4, 133.6, 131.6, 131.5, 131.1, 130.8, 130.3, 130.2, 129.3, 128.5, 128.2, 128.1, 127.9, 127.8, 127.5, 126.7, 126.6, 126.2, 125.9, 125.2, 125.1, 122.8, 120.9, 110.0 (ArC), 59.0 (ethyl-$NHCH_2$), 45.0 (ethyl-NCH_2), 44.8 (ethyl-NCH_2), 40.1 (NCH_3) 40.0 (NCH_3), 23.7 (CH_3), 23.6 (CH_3); HRMS (TOF MS): m/z calculated $C_{37}H_{33}N_3O_2$ $[M+1]^+$ 552.2573, found 552.2645.

6-(Butylamino)-2-(4-(1,2-diphenylprop-1-en-yl)phenyl)-1*H*-benzo[*de*]isoquinoline-1,3(2*H*)-dione (16)

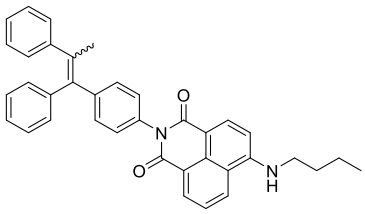

Yellow solid, *E/Z* : 1/1; Yield 60 %; mp: 245-248 ^{o}C; ^{1}H NMR (500 MHz, $CDCl_3$): δ 8.64-8.62 (m, *J* = 7.20 Hz, 1H, ArH), 8.59-8.56 (m, 1H, ArH), 8.52-8.49 (m, 1H, ArH), 8.48-8.44 (m, 1H, ArH), 8.14-8.06 (m, 2H, ArH), 7.72-7.59 (m, 2H, ArH), 7.41-7.35 (m, 3H, ArH), 7.31-7.28 (m, 5H, ArH), 7.23-7.23 (m, 5H, ArH), 7. 17-7.08 (m, 6H, ArH), 7.06-7. 02 (m, 4H, ArH), 6.96-6.92 (m, 3H, ArH), 6.78-6.72 (m, 2H, ArH), 4.16 (br, s, 2H, NH), 3.45-3.41 (m, 4H, butyl-NCH_2), 2.23 (s, 3H, CH_3), 2.16 (s, 3H, CH_3), 1.86-1.77 (m, 4H, butyl-CH_2), 1.73-1.67 (m, 4H, butyl-CH_2), 0.89-0.86 (m, 4H, butyl-CH_2); ^{13}C NMR (100 MHz, $CDCl_3$): δ 165.0, 164.9, 164.5, 164.4, 164.3, 164.2, 150.0, 149.9, 149.8, 144.2, 144.1, 143.8, 143.7, 143.4, 143.3, 142.9, 142.8, 138.9, 138.8, 138.7, 138.6, 136.4, 136.3, 136.2, 135.1, 135.0, 134.9, 134.4, 134.3, 133.6, 133.5, 131.6, 131.1, 130.9, 130.3, 130.2, 129.4, 128.5, 128.3, 128.2, 128.1, 127.9, 127.7, 127.5, 126.7, 126.6, 126.4, 126.3, 125.9, 124.9, 124.8, 124.7, 124.6, 123.4, 123.3, 120.3, 120.2, 110.1, 110.0 (ArC), 43.5 (butyl-NC), 43.4 (butyl-NC), 31.1

(butyl-C), 31.0 (butyl-C), 23.7 (CH_3), 23.6 (CH_3), 20.5 (butyl-C), 20.4 (butyl-C), 14.0 (butyl-C), 13.9 (butyl-C); HRMS (TOF MS): m/z calculated $C_{37}H_{32}N_2O_2$ $[M+1]^+$ 537.2464, found 537.2538.

2-(4-(1,2-Diphenylprop-1-en-yl)phenyl)-6-((2-hydroxyethyl)amino)-1*H*-benzo[*de*]isoquiolin e-1,3(2*H*)-dione (17)

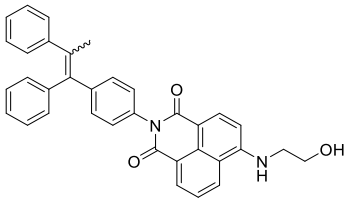

Yellow solid, *E/Z* : 1/3; Yield 63 %; mp: 232-235 ^oC; ^1H NMR (500 MHz, $CDCl_3$): δ 8.63-8.43 (m, 3H, ArH), 8.18-8.15 (m, 1H, ArH), 7.70-7.58 (m, 2H, ArH), 7.46-7.35 (m, 3H, ArH), 7.32-7.28 (m, 4H, ArH), 7.23-7.20 (m, 4H, ArH), 7.17-7.10 (m, 3H, ArH), 7.0 4-7.02 (m, 3H, ArH), 6.96-6.93 (m, 2H, ArH), 6.79-6.71 (m, 1H, ArH), 5.79 (br, s, 2H, OH), 4.45 (br, s, 1H, NH), 4.05 (br, s, 2H, ethyl-OCH_2), 3.97 (br, s, 1H, ethyl-OCH_2), 3.58 (br, s, 3H, ethyl-NCH_2), 2.23 (s, 3H, CH_3), 2.16 (s, 3H, CH_3); ^{13}C NMR (100 MHz, $CDCl_3$): δ 165.0, 164.8, 164.4, 164.3, 144.9, 144.8, 144.6, 144.5, 144.2, 144.1, 143.8, 143.7, 143.3, 143.0, 142.8, 132.0, 131.6, 131.2, 131.0, 130.2, 130.1, 129.4, 128.2, 128.1, 128.0, 127.9, 127.8, 127.7, 127.3, 126.7, 126.6, 126.4, 126.0, 123.0, 120.5, 114.7, 114.3, 110.4, 110.3, 104.6, 104.5 (ArC), 60.5 (CH_2OH), 60.4 (CH_2OH), 45.4 (NCH_2), 45.3 (NCH_2), 23.5 (CH_3), 23.4 (CH_3); HRMS (TOF MS): m/z calculated $C_{35}H_{28}N2O_3$ $[M+1]^+$ 525.2100, found 525.2173.

6-(Allylamino)-2-(4-(1,2-diphenylprop-1-en-1yl)phenyl)-1*H*-benzo[*de*]isoquinoline-1,3(2*H*)-dione (18)

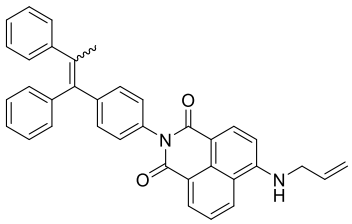

Yellow solid, *E/Z* : 1/1.8; Yield 72 %; mp: 230-234 ^oC; ^1H NMR (500 MHz, $CDCl_3$): δ 8.65-8.57 (m, 2H, ArH), 8.52-8.44 (m, 2H, ArH), 8.18-8.11 (m, 2H, ArH), 7.70-7.63 (m, 2H, ArH), 7.41-7.35 (m, 4H, ArH), 7.31-7.28 (m, 5H, ArH), 7.23 (m, 3H, ArH), 7.17-7.16 (m, 3H, ArH), 7.03-7.02 (m, 3H, ArH), 6.96-6.93 (m, 2H, Ar H), 6.79-6.74 (m, 2H, ArH), 6.04 (br, s, 2H, NH), 5.45-5.37 (m, 2H, allyl-CH), 5.35-5.27 (m, 2H, allyl-CH_2), 5.19-5.17 (d, *J* = 10.15 Hz, 1H, allyl-CH_2), 4.80-4.73 (m, 1H, allyl-CH_2), 4.11-4.02 (m, 4H, allyl-NCH_2), 2.23 (s, 3H, CH_3), 2.16 (s, 3H, CH_3); ^{13}C NMR (100 MHz, $CDCl_3$): δ 165.0, 164.8, 164.5, 164.4, 164.2, 163.9, 144.1, 143.7, 143.4, 143.3, 142.9, 142.8, 138.8, 138.6, 136.4, 134.8, 134.7, 134.6, 134.2, 133.5, 133.0, 131.6, 131.5, 131.3, 131.1, 130.9, 130.2, 129.9, 129.4, 128.5, 128.2, 128.1, 127.9, 127.7, 127.5, 126.7, 126.6, 126.4, 126.3, 126.2, 125.9, 125.0,

124.9, 124.8, 123.4, 123.3, 123.1, 120.5, 120.4, 120.3, 118.1, 118.0, 117.1, 110.7, 110.6 (ArC), 46.2 (allyl-NC), 46.1 (allyl-NC), 23.7 (CH_3), 23.6 (CH_3); HRMS (TOF MS): m/z calculated $C_{36}H_{28}N_2O_2$ $[M+1]^+$ 521.2151, found 521.2277.

6-(Benzylamino)-2-(4-(1,2-diphenylprop-1-en-yl)phenyl)-1*H*-benzo[*de*]isoquinoline-1,3(2*H*)-dione (19)

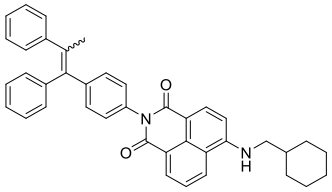

Yellow solid, *E/Z* : 1/1.2; Yield 65 %; mp: 244-248 ^oC; ^1H NMR (400 MHz, $CDCl_3$): δ 8.65-8.62 (d, *J* = 7.30 Hz, 1H, ArH), 8.59-8.57 (d, *J* = 7.25 Hz, 1H, ArH), 8.51-8.49 (d, *J* = 8.35 Hz, 1H, ArH), 8.45-8.41 (d, *J* = 8.35 Hz, 1H, ArH), 8.18-8.12 (m, 2H, ArH), 7.69-7.62 (m, 2H, ArH), 7.43-7.35 (m, 13H, ArH), 7.31-7.28 (m, 5H, ArH),7.23-7.20 (m, 4H, ArH), 7.17-7.11 (m, 5H, ArH), 7.03-7.00 (m, 4H, ArH), 6.96-6.92 (m, 3H, ArH), 6.83-6.77 (m, 2H, ArH), 5.62 (br, s, 1H, NH), 5.55 (br, s, 1H, NH), 4.65-4.61 (m, 4H, benzyl-NCH_2), 2.23 (s, 3H, CH_3), 2.16 (s, 3H, CH_3); ^{13}C NMR (100 Hz, $CDCl_3$): δ 165.0, 164.8, 164.4, 164.2, 144.0, 143.7, 143.4, 143.3, 142.9, 142.8, 138.8, 138.6, 137.1, 136.4, 134.9, 134.7, 134.2, 133.4, 131.6, 131.5, 131.1, 130.9, 130.2, 129.4, 129.2, 129.1, 128.2, 128.1, 127.9, 127.6, 127.5, 126.7, 126.6, 126.5, 126.3, 125.9, 125.1, 125.0, 123.3, 120.5, 120.4, 110.7 (ArC), 48.0 (benzyl-CH_2), 47.9 (benzyl-CH_2), 23.7 (CH_3), 23.6 (CH_3); HRMS (TOF MS): m/z calculated $C_{40}H_{30}N_2O_2$ $[M+1]^+$ 571.2307, found 571.2381.

2-(4-(1,2-Diphenylprop-1-en-1-yl)phenyl)-6-((4-fluorophenyl)amino)-1*H*-benzo[*de*]isoquinoline-1,3(2*H*)-dione (20)

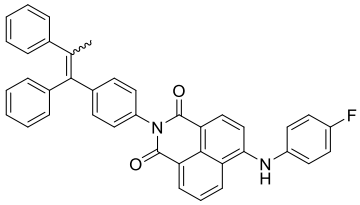

Yellow solid, *E/Z* : 1/4.8; Yield 61 %; mp: 232-234 ^oC; ^1H NMR (400 MHz, $CDCl_3$): δ 8.70-8.58 (m, 2H, ArH), 8.45-8.38 (m, 1H, ArH), 8.09-8.03 (m, 1H, ArH), 7.90-7.82 (m, 1H, ArH), 7.40-7.27 (m, 7H, ArH), 7.24-7.21 (m, 3H, ArH), 7.16-7.10 (m, 5H, ArH), 7.05-6.93 (m, 6H, ArH), 6.66-6.63 (m, 2H, ArH), 6.35-6.33 (d, *J* = 8.40 Hz, 1H, ArH), 3.13 (br, s, 1H, NH), 3.10 (br, s, 1H, NH), 2.21 (s, 1H, CH_3), 2.16 (s, 1H, CH_3); 13C NMR (100 Hz, $CDCl_3$): δ 163.8, 163.8, 163.8, 163.7, 155.8, 144.9, 144.6, 144.5, 144.2, 144.1, 143.7, 143.7, 143.6, 143.4, 143.3, 139.3, 139.1, 138.5, 136.7, 136.6, 134.7, 134.0, 132.6, 132.6, 132.4, 132.0, 131.8, 131.8, 131.7, 131.6, 131.3, 131.3, 131.2, 131.0, 130.2, 130.2, 130.1, 129.4, 129.4, 129.4, 129.3, 128.3, 128.3, 128.2, 128.2, 128.1, 128.0, 128.0, 127.9, 127.8, 127.7, 127.5, 127.5, 127.3,

126.8, 126.7, 126.6, 126.6, 126.4, 126.0, 125.9, 125.7, 114.7, 114.3 (ArC), 23.6 (CH_3), 23.6 (CH_3); HRMS (TOF MS): m/z calculated $C_{39}H_{27}FN_2O_2$ $[M+1]^+$ 575.2057, found 575.2131.

2-(4-(1,2-Diphenylprop-1-en-1-yl)phenyl)-6-(pyrimidin-2-ylamino)-1*H*-benzo[*de*]isoquino line-1,3(2*H*)-dione (21)

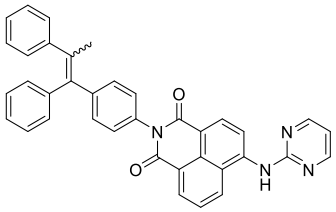

Yellow solid, *E/Z* : 1/1.5; Yield 67 %; mp: 232-235 ^oC; ^1H NMR (500 MHz, $CDCl_3$): δ 8.71-8.42 (m, 5H, ArH), 7.80-7.76 (m, 3H, ArH), 7.45-7.29 (m, 9H, ArH), 7.21-7.12 (m, 6H, ArH), 7.10-7.05 (m, 5H, ArH), 7.03-7.01 (m, 5H, ArH), 6.95-6.92 (m, 3H, ArH), 2.21 (s, 2H, CH_3), 2.15 (s, 3H, CH_3); ^{13}C NMR (100 Hz, $CDCl_3$ + DMSO- d_6): δ 164.9, 164.8, 164.3, 164.2, 160.8, 143.6, 143.3, 143.2, 142.8, 142.7, 138.5, 136.3, 134.2, 134.1,133.4, 131.8, 131.5, 131.1, 130.7, 130.1, 129.7, 129.6, 129.3, 128.4, 128.2, 128.0, 127.8, 127.7, 127.4, 126.6, 126.5, 126.2, 125.9, 125.3, 125.2, 123.1, 123.0, 122.3, 113.4, 110.2, 110.1 (ArC), 23.6 (CH_3), 23.5 (CH_3); HRMS (TOF MS): m/z calculated $C_{37}H_{26}N_4O_2$ $[M+1]^+$ 559.2056, found 559.2130.

CHAPTER 4
BENZOTHIAZOLE APPENDED NAPHTHALIMIDES

4.1 Introduction

Benzothiazole, a heterocyclic ring system containing a thiazole moiety fused with a benzene ring, has attracted significant attention in anticancer activity.[104] The biosynthetic pathway of native benzothiazole has been a popular target for the therapeutic intervention in anticancer drug design; for example, tiazofurin, the first thiazole-containing compound, is employed to treat cancer effectively.[105] Benzothiazole induce cell apoptosis by inhibiting the signaling pathways or enzymes such as TOPO-II, Tyrosine Kinase, which mediate cell growth. Researchers have attempted to modify the benzothiazole core to improve their anticancer activities but ineffective to bring novel drug for the clinic.

On the other hand, naphthalimides have immense pharmacological significance as anticancer agents. Several subsets of structurally related compounds have been synthesized and evaluated extensively for their cytotoxic effect. Rao *et al*. have synthesized naphthalimide-benzothiazole/cinnamide derivatives as active anticancer agent against lung and colon cancer cell lines as well as inhibiting the topoisomerase-II activity,[44] whereas Lu *et al*. reported a series of C-4 naphthalimide-benzothiazole conjugates with potent inhibitory activity towards murine melanoma cell lines.[45] Further, due to their unique properties, 1,8-naphthalimides are major candidates for chemical probes, fluorescent sensors, sensing of biologically relevant proteins, dyes etc.[106] The photophysical and anticancer properties of naphthalimide derivatives are governed by the nature of substituents and the pattern of substitution to its core.[107] Introducing electron-donating and electron-withdrawing groups at the phenyl ring of naphthalimide core at its 4-position make this moiety ideal fluorescent candidate for sensing.[108] Therefore, to develop novel anticancer agents and HSA biomarkers, we synthesized naphthalimides appended with benzothiazole.

Human serum albumin (HSA) and bovine serum albumin (BSA) are two negatively charged, multifaceted, and most ample plasma proteins found in blood.[109] HSA is a 66.5 kDa protein which is composed of 585 amino acid residues of known sequence.[110-111] Owing to its diverse physiological functions, HSA plays important role in regulation of oncotic pressure[112] and transportation and deposition of exogenous and endogenous substances to specific target

organs.[113] It is exclusively synthesized in liver and deteriorated in kidney.[114] With serving as carrier, it is a prominent antioxidant, anti-inflammatory and free radical scavenger.[115] The reference range of HSA in blood plasma is 35-50 g/L and in urine is 2.2-25 mg/L.[116] Presence of elevated level of albumin in plasma (> 50 g/L) causes hyperalbuminemia which is accompanied by dehydration. However, low level of albumin (< 35 g/L) leads to hypoalbuminemia.[117-118] Abnormal concentration of HSA is associated with liver cirrhosis,[119] coronary heart disorder,[120] kahler's disease,[121] diabetes mellitus (hypoglycemia),[122] renal damage[123] and neurometabolic disorder.[124] Therefore, human serum albumin is useful as early biomarker of various diseases.[125] Clinically, developing new methods for accurate quantification and selective detection of HSA is of great interest.

To date, several detection methods have been employed to detect HSA such as enzyme-immunoassay,[126] radioimmuno assay,[127] LC-MS proteomics,[128] surface enhanced Raman scattering,[129] capillary electrophoresis,[130] electrochemistry[131] and colorimetric methods (bromocresol green assay).[132] However, these methods exhibit low sensitivity, low selectivity, high cost, time-sensitive character and laborious procedures.[133-134] Over the several years, extensive developments on fluorescence probes for the detection of human serum albumin have been reported.[135] Fluorescent probe based assays offer high selectivity, sensitivity, high-throughput and rapid response.[136] A number of 1,8-naphthalimide based probes for HSA detection has also gained the attention because of their high quantum yield and good photostability.[137] For instance, Sun *et al.* investigated the interaction between naphthalimide and human serum albumin where detection limit (LOD) was found to be 1.37 x 10^{-10} M for HSA and 1.84 x 10^{-10} M for BSA.[138] Cheng *et al*. have reported the interaction between naphthalimide – based antitumor drugs and HSA with LOD 1.3 x 10^{-6} M.[139] Wei *et al.* reported the fluorescence

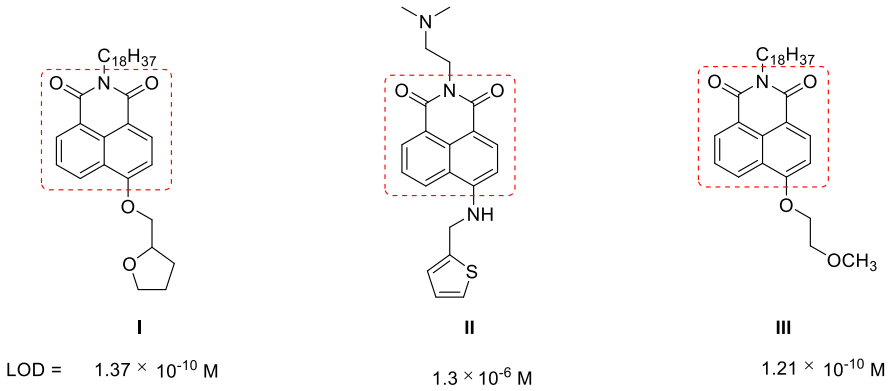

Figure 1: Naphthalimide probes as biomarkers/sensors of human serum albumin

quenching of HSA by naphthalimide dyes and the formation of Dye–HSA complex where the LOD was 1.21 x 10^{-10} M (**Figure 1**).[140] Owing to all these features, newer probes are synthesized in view of their high demand for clinical diagnosis.

4.1.1 Designing of benzothiazole appended naphthalimides

With continuation of our efforts to develop effective anticancer agents, we targeted to attain the rigidity of naphthalimide at *N*-position and C4-position. When naphthalimide possessing EDG/EWG is excited, it exhibits fluorescence due to internal charge transfer (ICT). When the phenomenon of ICT comes into play, it enhances the probability of radiative transition on account of EDG/EWG attached at C-4 position and imide group (EWG) in naphthalimide scaffold which led to push-pull/pull-pull electron system.[141] The rigid organic molecule having push-pull system exhibited strong fluorescence emission as compared to compound with pull-pull system. Keeping this in mind, we have designed a fluorescence probe with high rigidity i.e. by substituting aromatic amine (2-aminobenzothiazole) at *N*-position of naphthalimide which favours the phenomenon of fluorescence.

In this context, we have synthesized 2-(benzo[*d*]thiazol-2-yl)-1*H*-benzo[*de*]isoquinoline-1,3(2*H*)-dione derivatives with various aryl substituents at 4-position of naphthalimide ring and evaluated for their anticancer activity; as well as studied for selective detection of serum albumin (**Scheme 1**). Among these, probes **8** and **12** containing strong electron-donating and -withdrawing groups were selected to determine their binding affinity with serum albumins. Under physiological conditions, *in vitro* studies using UV-visible, fluorescence and circular-dichroism spectroscopies were undertaken to determine the binding interaction between naphthalimides and serum albumins (HSA and BSA). Drug displacement competitive studies of probes **8** and **12** to HSA were also performed to determine the specific binding site. The selectivity of these probes to HSA among various bioanalytes was investigated through competitive experiments. Molecular docking was performed to understand the mechanism of binding interaction and complex stabilization at molecular level. In addition, distance between probes and human serum albumin was determined by Förster energy transfer principle. Furthermore, the anticancer activity of naphthalimides with selected panel of cancer cell lines has also been investigated using standard method. Significantly, these data demonstrate the valuable information about the binding mechanism of naphthalimides to HSA as well as therapeutic effect of these newly synthesized probes in pharmacodynamics and pharmacology.

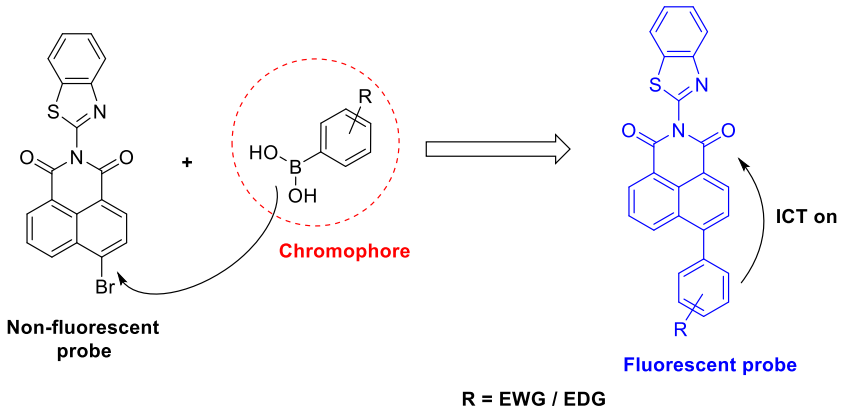

Scheme 1: Schematic representation of fluorescent probe containing naphthalimide conjugated with benzothiazole.

4.2 Chemistry

A route to synthesize naphthalimide analogues **5-18** has been depicted in **Scheme 2**. Commercial available acenaphthene (**1**) was treated with *N*-bromosuccinimide at room temperature for 2.5 h to give 6-bromo-1*H*,3*H*-benzo[*de*]isochromene-1,3-dione (**2**). 4-Bromonaphthalic anhydride (**3**) was prepared according with literature report using 6-bromo-1*H*,3*H*-benzo[*de*]isochromene-1,3-dione and potassium dichromate in acetic acid at 110 ^{o}C for 4 h.[103] Further, the key starting material 2-(benzo[*d*]thiazolyl-2-yl)-6-bromo-1*H*-benzo[*de*]isoquinoline-1,3(2*H*)-dione (**4**) was prepared by microwave irradiation of 4-bromonaphthalic anhydride (**3**) with 2-aminobenzothiazole (synthesized by treatment of 2-aminobenzothiophenol with KSCN and Br_2 in acetic acid at 0-5 ^{o}C)[142] in the presence of zinc acetate and pyridine for 5 min. Intermediate **4** was confirmed by the appearance of aromatic protons of benzothiazole ring in the region 7.59-7.49 and 8.13 ppm. A Suzuki-Miyaura cross coupling reaction of intermediate **4** with corresponding aryl boronic acids in the presence of $Pd(PPh_3)_4$ and potassium carbonate (K_2CO_3) in acetonitrile under inert atmosphere of argon for 24 h furnished 2-(benzo[*d*]thiazol-2-yl)-6-(aryl)-1*H*-benzo[*de*]isoquinoline-1,3(2*H*)-diones (**5-16**). Derivatives **17-18** were tried to synthesize with nucleophilic substitution reaction with secondary amines in the presence of K_2CO_3 in acetonitrile but the reaction was not successful due to the conjugation of bromo with π-electrons of naphthyl ring through resonance efffect. So, derivatives **17-18** were synthesized *via* Buchwald reaction using key intermediate **4** with piperidine or morpholine in the presence of $PdCl_2(PPh_3)_2$ and K_2CO_3 in acetonitrile at reflux temperature for 12 h. All the synthesized derivatives were characterized by NMR, and mass spectrometry. The increase of five aromatic

protons of phenyl ring at the region of δ 7.59 and 7.78 ppm in ^{1}H NMR spectrum confirmed the formation of analogue **5**. On the other hand, ^{1}H NMR of compound **17** showed four protons of triplet, four protons of multiplet and two protons of multiplet of piperidine at δ value of 3.31, 1.94 and 1.78 ppm, respectively. The mass spectra of compounds **5** and **17** exhibited molecular ion peaks of m/z 407.09 and 414.12, respectively which also agreed with their proposed structures.

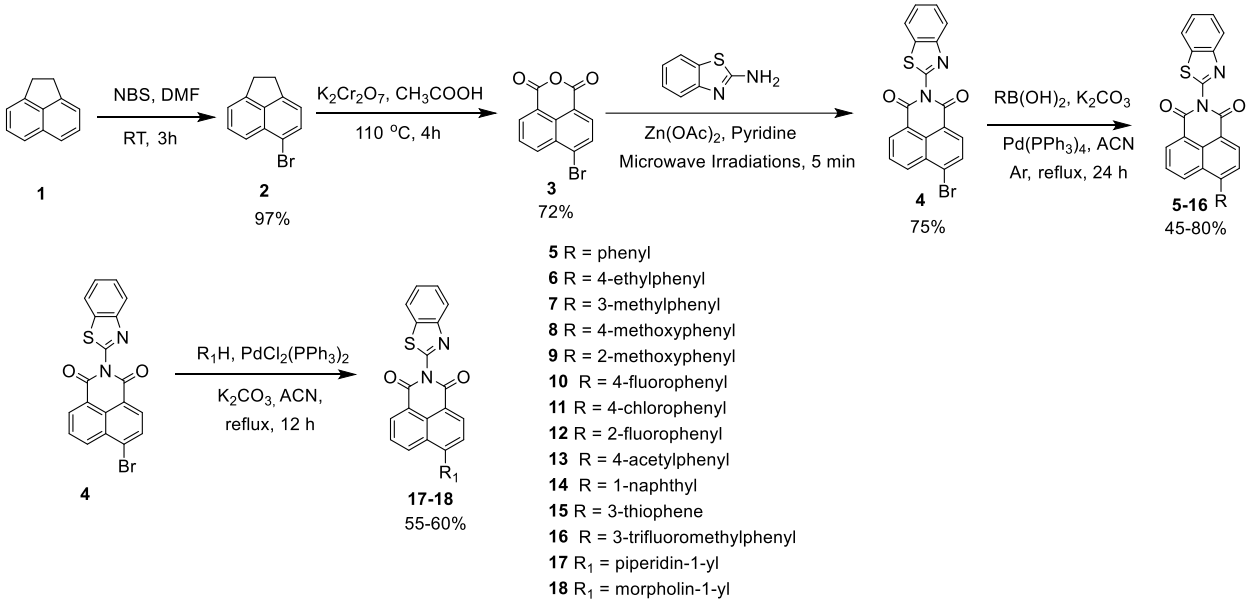

Scheme 2: Synthesis of 2-(benzo[*d*]thiazol-2-yl)-6-subsituted-1*H*-benzo[*de*]isoquinoloine-1,3-(2*H*)-dione

4.3 *In vitro* antiproliferative activity

The cytotoxicity of naphthalimide-benzothiazole derivatives **5-8**, **10-12** and **17-18** against 60 human cancer cell lines at single dose concentration (10 μM) were studied.[76] It has been observed that analogue with the appendage of 2-fluorophenyl ring (**12**) showed good inhibitory effect in most of the cancerous cell lines (**Figure 2**). Compound **12** exhibited potent cytotoxicity against K-562 and SR cancer cell lines of leukemia, HCT-15 cell line of colon, UAAC-62 cell line of melanoma and UO-31 cell line of renal cancer with percentage growth inhibition (%GI) of 54.3, 70.1, 54.8, 57.5 and 55.4, respectively which were found to be better than that of 5-fluorouracil. The order of growth inhibition of derivatives were **12** > **7** > **8** against K-562, SR and UO- 31 cell lines, indicating that cytotoxic effect decreases with the increase in electron donating effect **(Table 1)**. On the other hand, cytotoxicity of **17** is slightly better on comparing

with the cytotoxic effect of aryl substitution except compound **12**. It was also observed that electron withdrawing effect at *ortho* position (**12**) displayed promising activity as compared to the *para* position (**10**) of phenyl ring. These cytotoxic results revealed that the nature and position of substituents attached to phenyl ring may influence the binding affinity of compounds.

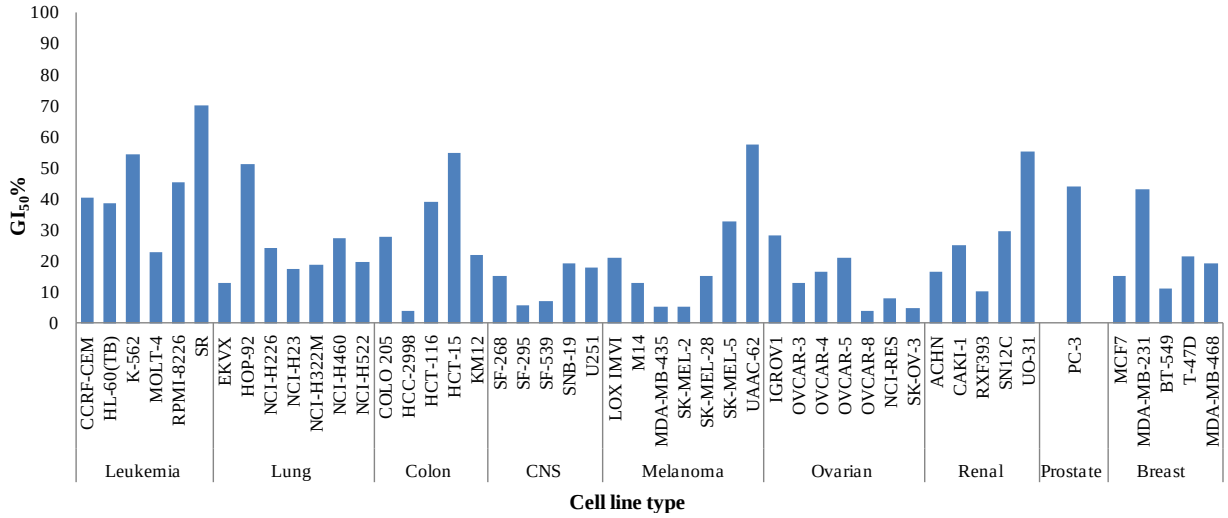

Figure 2: Growth inhibition percentages (GI %) of analogue **12** against sensitive cancer cell lines at one dose concentration (10 μM).

Table 1: Anticancer activity of compounds at one dose concentration (10 μM) with selected cell lines

Panel	Cell line	5	6	7	8	10	11	12	17	18	5-FU
Leukemia	CCRF-CEM	5.18	-	15.3	4.89	-	3.52	**40.5**	19.9	-	**57.1**
	HL-60(TB)	-	-	-	0.90	-	-	**38.5**	19.3	6.36	**47.9**
	K-562	12.3	1.54	15.3	8.51	-	3.84	**54.3**	**32.3**	-	**42.3**
	MOLT-4	-	-	-	5.64	-	-	22.9	18.2	-	**43.1**
	RPMI-8226	7.44	-	15.9	6.57	5.20	6.63	**45.5**	22.5	-	**41.4**
	SR	10.7	3.22	29.1	15.5	1.13	0.14	**70.1**	23.4	4.08	24.8
Lung	HOP-62	7.25	-	26.3	14.5	18.6	12.1	-	5.96	1.84	**52.2**
	HOP-92	22.2	19.5	17.1	25.1	-	7.20	**51.0**	24.6	-	**50.6**
	NCI-H226	3.09	5.39	-	7.24	4.76	9.00	24.3	21.2	8.18	**69.5**
	NCI-H322M	12.4	7.41	-	1.26	11.6	7.16	18.9	27.5	17.5	**40.5**
	NCI-H460	9.67	5.96	-	4.20	7.22	-	27.3	3.78	-	NT
	NCI-H522	10.2	0.37	19.5	13.8	5.33	2.73	19.5	**30.7**	16.2	**58.0**
Colon	COLO 205	-	0.66	4.68	-	-	-	27.7	5.89	-	NT
	HCT-116	7.71	0.72	13.2	7.02	-	-	**38.8**	23.4	8.50	17.8
	HCT-15	1.29	-	-	-	-	-	**54.8**	**40.6**	7.48	26.5
CNS	SNB-75	-	5.69	-	11.3	7.79	-	-	27.0	10.7	**65.9**

Melanoma	LOX IMVI	1.64	5.77	6.07	5.28	6.42	12.6	21.2	11.1	4.55	**30.4**
	MALME-3M	2.06	1.21	24.0	**33.9**	23.4	27.3	-	23.7	17.5	**58.2**
	SK-MEL-5	2.13	7.18	5.50	1.76	3.73	4.08	**32.6**	5.18	5.98	**66.3**
	UAAC-62	17.0	5.53	18.2	12.8	9.33	17.5	**57.5**	25.6	23.9	**94.4**
Ovarian	IGROV1	25.2	12.5	13.1	19.2	28.5	17.2	28.1	22.9	6.13	**51.2**
	OVCAR-4	-	-	13.1	-	-	-	16.4	17.4	2.62	**59.4**
Renal	CAKI-1	11.1	14.5	26.0	4.53	20.6	19.2	25.0	19.2	14.6	**60.6**
	TK-10	-	-	-	-	-	17.7	29.5	-	-	**67.1**
	UO-31	**36.9**	26.3	**40.7**	23.6	**36.5**	29.6	**55.4**	**51.4**	**33.7**	**41.3**
Prostate	PC-3	12.4	1.25	25.1	-	15.0	12.2	**44.2**	**41.0**	9.41	**58.2**
Breast	MDA-MB-231	17.5	0.64	27.6	10.0	1.60	17.3	**43.2**	26.49	20.8	**78.1**
	T-47D	0.88	11.3	12.6	-	-	-	21.36	21.78	-	**56.7**

NT – Not Tested. - indicated inactive, **Orange bold** –30-40% GI, **black bold** – 40-50 % GI, **pink bold** – 50-70 % GI, **blue bold** – 70-100 % GI, 5-FU = 5-fluorouracil

4.4 Serum albumin studies

4.4.1 UV-Visible studies

In order to determine the influence of EDG and EWG at naphthalimides with binding affinity of HSA and BSA, compound **8** with strong electron-donating group at 4-position and **12** with strong electron-withdrawing group at 2-position of phenyl ring (two most active compounds) were selected. The UV-visible absorption spectra of HSA and BSA showed an absorption band at 280 nm. The absorption band at 280 nm exhibited enhancement with appearance of new band at 378 nm, and 348 nm with respective incremental additions of **8** and **12** (**Figure 3**), which revealed the changes in polarity around tyrosine, tryptophan and phenylalanine residues.

From UV-Vis spectral studies, the binding constants have been calculated through Benesi-Hildebrand equation,[96] The binding constants calculated for the interaction of HSA were found to be 5.0×10^4 M^{-1} and 7.9×10^4 M^{-1} for derivatives **8** and **12**, respectively (**Figures 4a** and **4b**), while the binding constants with BSA were determined to be 4.3×10^4 M^{-1} and 6.4×10^4 M^{-1} for respective compounds **8** and **12** (**Figures 4c** and **4d**). It has been revealed that moderate binding interactions with HSA and BSA were observed for compounds **8** and **12** which make these compounds ideal for transportation of drug towards the target site.

4.4.2 Fluorescence emission spectroscopy

On excitation of HSA and BSA at 280 nm, a strong fluorescence band with emission maximum (λ_{em}) at 340 nm appeared. Quenching of emission band of HSA at 340 nm with enhancement at 508 nm and 448 nm was observed in case of respective compounds **8** and **12** with isosbestic

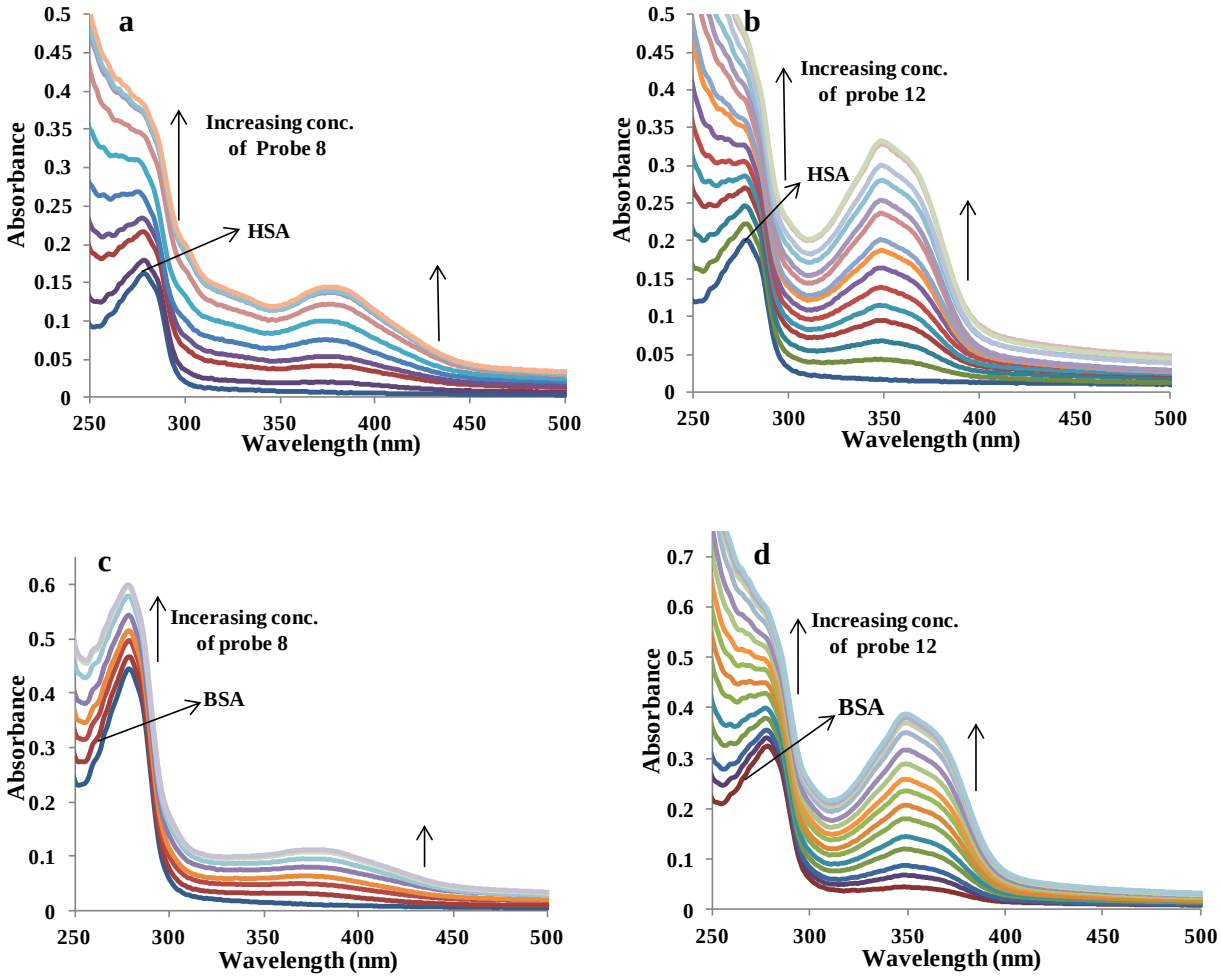

Figure 3: Effect of incremental addition of compounds (a) **8** and (b) **12** on absorption spectra of HSA; (c) **8** and (d) **12** on absorption spectra of BSA in phosphate buffer at *p*H 7.4 and T = 298 K

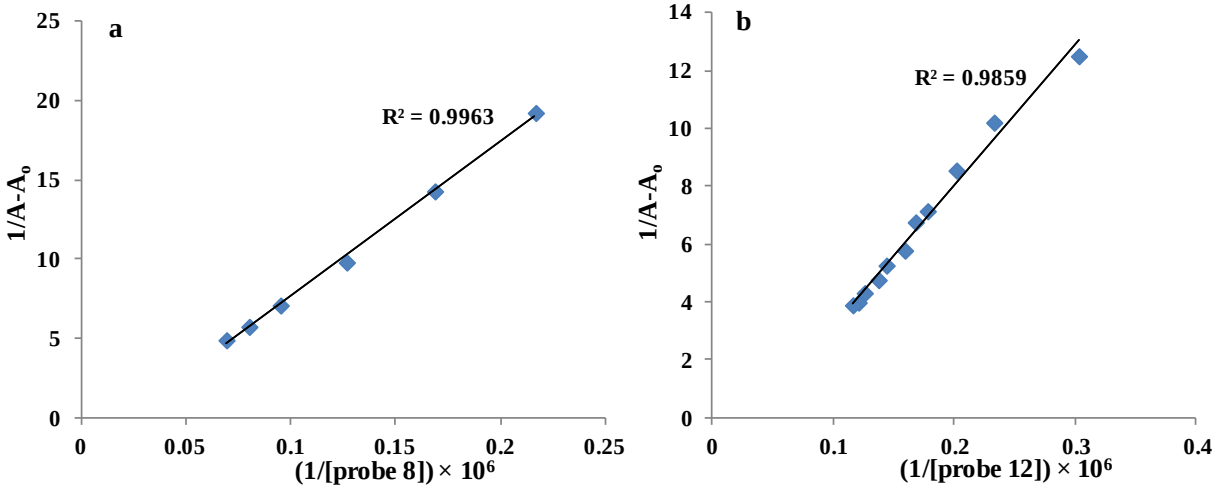

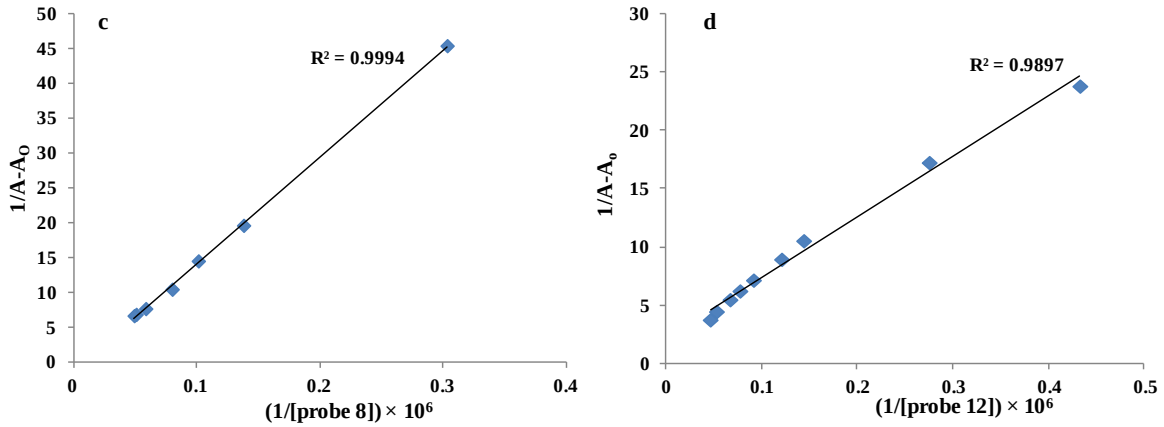

Figure 4: Plots of $1/(A - A_0)$ *vs.* 1/[probe] for absorption spectra of compounds (a) **8** and (b) **12** in the presence of HSA in phosphate buffer; (c) **8** and (d) **12** in the presence of BSA

points at 440 nm and 400 nm, respectively (**Figures 5a-b**). Similarly, fluorescence spectra of BSA showed decrease in emission intensity at 340 nm, accompanied by enhancement of λ_{em} at 508 nm in case of **8** and 448 nm in **12** with clear isosbestic points at 440 nm and 410 nm, respectively (**Figures 5c-d**). A concentration dependent study revealed that there is a linear decrease in fluorescence intensities of HSA and BSA upon addition of compounds **8** and **12**. On increasing the concentrations of compounds **8** and **12**, the bands of HSA and BSA were quenched in both cases. To know the quenching mechanism of HSA and BSA whether it is dynamic (formation of complex of HSA and probe in excited state) or static (complex formed between HSA and probe in ground state), the quenching constants K_q have been calculated with Stern-Volmer equation.[96]

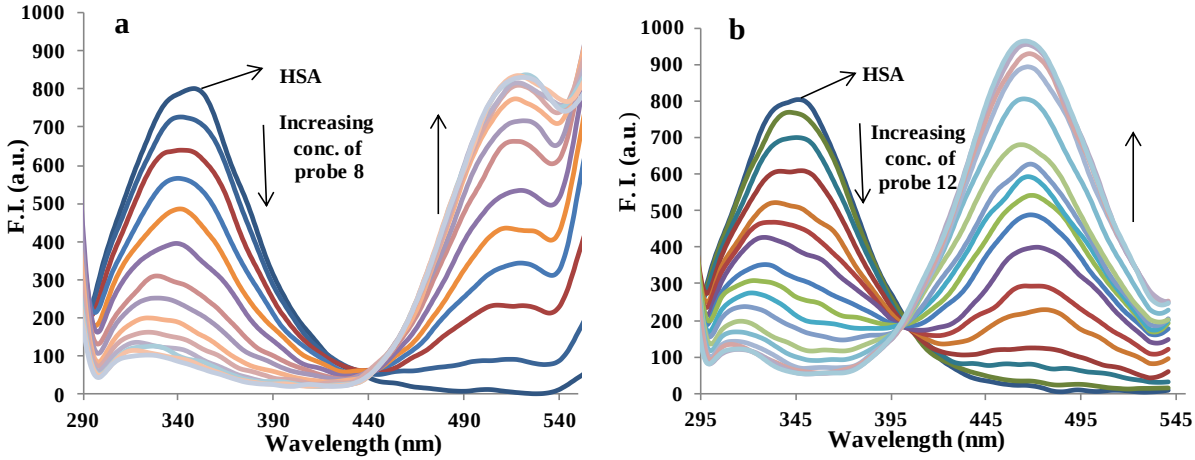

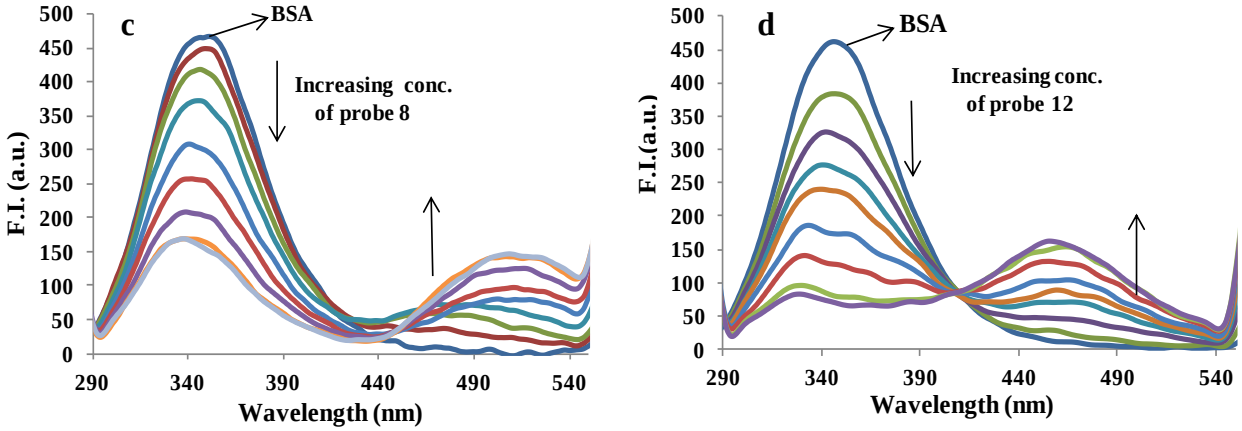

Figure 5: Effect of incremental addition of compounds (a) **8** and (b) **12** on the emission spectra of HSA; (c) **8** and (d) **12** on the emission spectra of BSA and in phosphate buffer at *p*H = 7.4 and T = 298 K

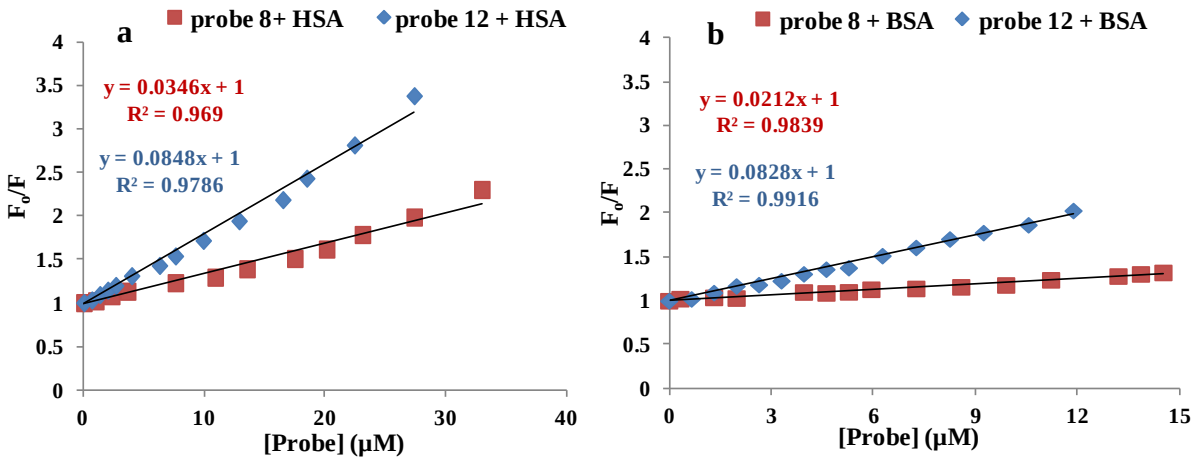

Figure 6: Stern-Volmer plots F_0/F versus [probe] for determination of quenching constant by fluorescence spectrometer titration of (a) HSA and (b) BSA with **8** and **12** in PBS buffer.

Experimentally, the lifetime of the fluorophore (τ_0) i.e. serum albumin was found to be 4.07 ns. The K_q, quenching rate constants of HSA have been determined to be 3.4×10^{12} and 8.4×10^{12} L mol^{-1} s^{-1} and that of BSA were 2.1×10^{12} and 8.2×10^{12} L mol^{-1} s^{-1} for compounds **8** and **12**, respectively (**Figure 6**). These values of K_q were much greater than the standard value assigned for diffusion-limited quenching in water[98] (2×10^{10} L mol^{-1} s^{-1}), which demonstrated that the static quenching is accomplished *via* formation of complex between serum albumin and naphthalimide probes (**8** and **12**) in ground-state.[99] The values of binding constant (K_a) and binding sites (n) for naphthalimide-serum albumin systems were determined using double

logarithmic equation from linear regression plot of log $[(F_0 - F)/F]$ against log $[Q]$[99] represented in **Table 2**. The binding constants for interaction of HSA with **8** and **12** were found to be 1.2×10^5 and 2.3×10^5 L mol^{-1}, respectively. The binding sites (n) were determined to be approximately 1 i.e. 1.09 for **8** and 1.11 in case of **12**. The binding constants exhibited as 0.77×10^5 and 1.8×10^5 L mol^{-1}, and number binding sites (n) with BSA were found to be 1.06 for **8** and 1.09 for **12** (**Figure 7**). It is also observed that values of n are approximately equal to 1, which indicated the existence of only single binding site in serum albumins for both probes (**8** and **12**). These results indicated the existence of strong binding forces for the interaction between the naphthalimide probes, and HSA/ BSA.

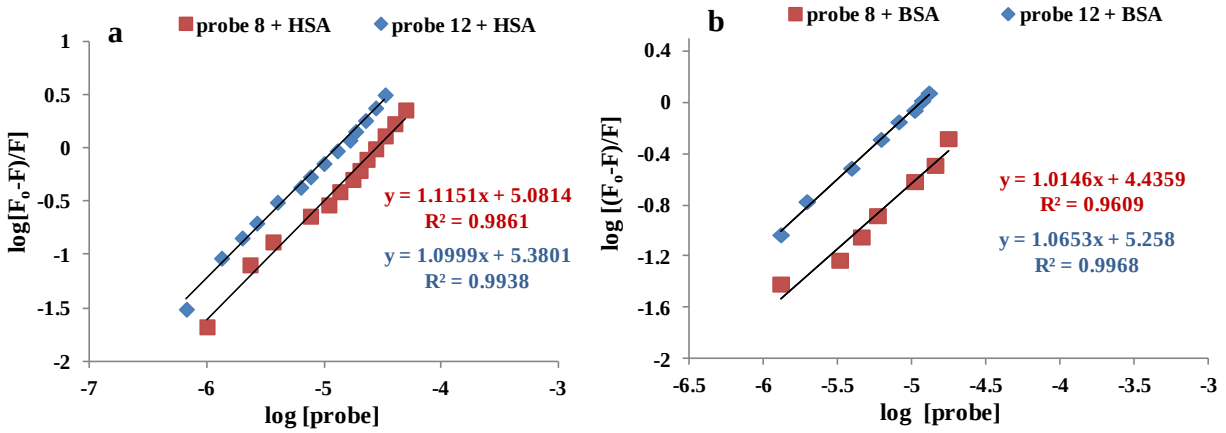

Figure 7: Modified Stern-Volmer plots of log $[(F_o - F)/F]$ versus log [probe] for determination of number of binding sites by fluorescence spectrometer titrations of (a) HSA and (b) BSA with **8** and **12** in PBS buffer.

Table 2: Stern-Volmer quenching constant K_{SV}, bimolecular quenching constant K_q, binding constant K_b, and Gibb's free energy ΔG of HSA-probe and BSA-probe systems.

System	K_{SV} (10^4 L mol^{-1})	K_q (10^{12} L mol^{-1} s^{-1})	K_b (10^5 L mol^{-1})	n	ΔG (kcal mol^{-1})
HSA-**8**	3.4	3.4	1.2	1.09	-6.9
HSA-**12**	8.4	8.4	2.3	1.11	-7.3
BSA-**8**	2.1	2.1	0.77	1.06	-6.6
BSA-**12**	8.2	8.2	1.8	1.09	-7.1

Further, the driving force for binding interaction of probes to HSA may be either spontaneous or non-spontaneous. The Gibb's free energies for the binding of **8** and **12** to HSA were calculated to be -6.9 and -7.3 kcal/mol, respectively. While the free energy changes for

BSA-**8** and BSA-**12** systems were found to be respective values of -6.6 and -7.1 kcal/mol. The negative values of ΔG indicated that the binding of probes **8** and **12** to HSA and BSA are spontaneous. Lower free energy of **8**-HSA and **8**-BSA systems might be due to hydrophilic interactions between methoxy group of **8** and HSA/BSA.

4.4.3 Competitive assay for selectivity

A competitive binding assay was performed to evaluate the selectivity of probes **8** and **12** toward HSA and BSA.[143] **Figure 8** represents the change in the fluorescence intensity of probes **8** (7 μM) and **12** (7 μM) in the presence of various bioanalytes *viz*., HSA, BSA, AMP, ATP, aspartic acid, cysteine, glucose oxidase, glutamic acid, glutathione, histidine, homocysteine, lysine, pepsin, trypsin, urea, Na^+, Ca^{2+}, NH_4^+ and PO_4^{3-}. Remarkably, the presence of other species except HSA and BSA showed negligible change in fluorescence emission bands of compounds **8** and **12**, indicating the selectivity of these compounds toward HSA and BSA in complex samples. Although a slight fluorescence enhancement (~7%) was observed in case of trypsin, its presence seems to be low in the human body. From the concentration-dependent fluorescence data, the limit of detection (LOD) for compounds **8** (7 μM) and **12** (7 μM) with HSA were measured using the formula LOD = 3σ/k and found to be 8.3 μM and 4.3 μM, respectively, while LOD with BSA indicated respective values of 12.98 μM and 5.5 μM for compounds **8** and **12**. The excellent detection range of HSA and BSA spanning 4.3-12.98 μM make these compounds selective in determining the interactions of HSA and BSA in the human body.

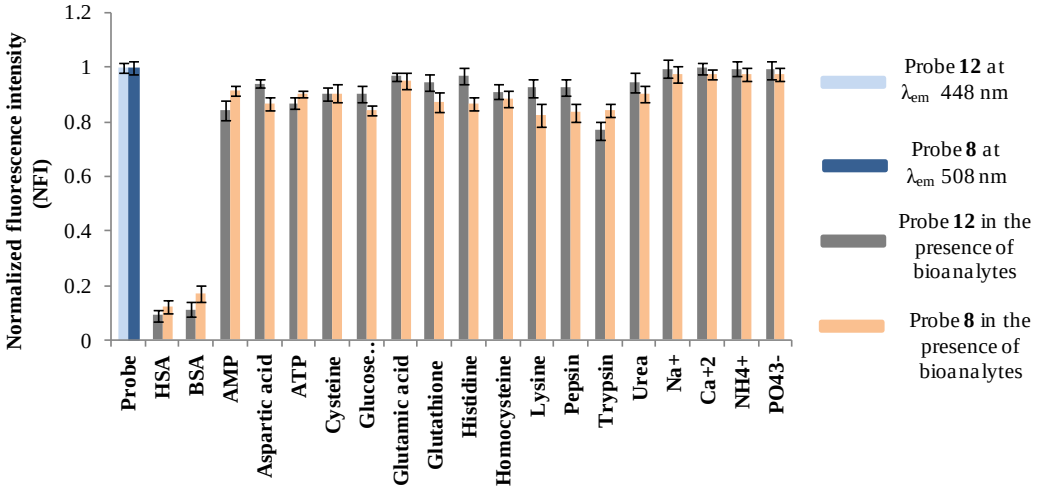

Figure 8: Normalized fluorescence intensity (NFI) of **8** (7 μM, λ_{ex} = 378 nm) and **12** (7 μM, λ_{ex} = 348 nm) in the presence of various bioanalytes; HSA, BSA, AMP, ATP, aspartic acid,

cysteine, glucose oxidase, glutamic acid, glutathione, histidine, homocysteine, lysine, pepsin, trypsin, urea, Na^+, Ca^{2+}, NH_4^+ and PO_4^{3-} at pH 7.4.

4.4.4 Drug displacement studies

To determine the specific binding site for benzothiazole appended naphthalimides on HSA, drug displacement studies were performed with two site markers, i.e., warfarin and ibuprofen. As the warfarin and ibuprofen interacts with HSA through the major drug binding sites, sudlow's site I and sudlow's site II, respectively. The domain IIA comprises suldow's site I, which has a hydrophobic cavity with two hydrophilic centers and the site II is present in domain IIIA which is hydrophilic.[144] With incremental additions of **8** or **12**, the emission bands of complexes of HSA-warfarin and HSA-ibuprofen at 340 nm were quenched (**Figure 9**).

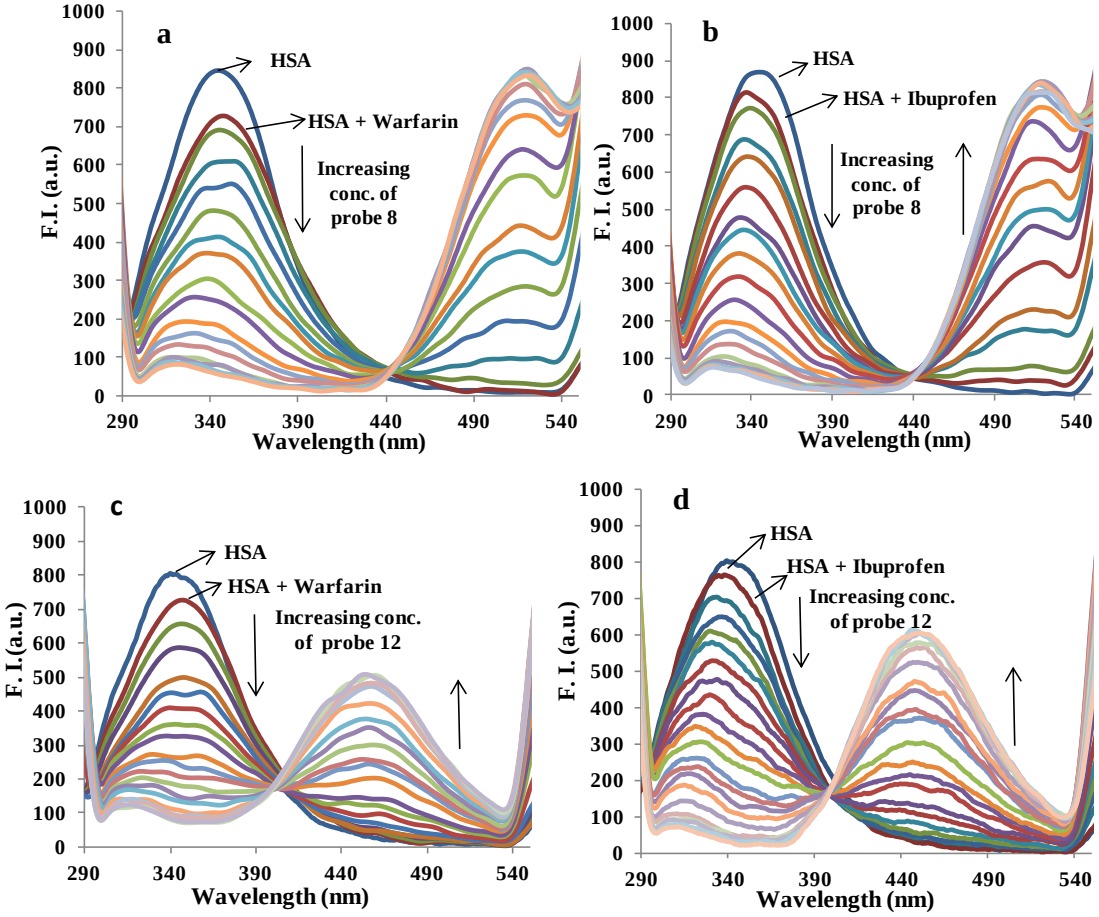

Figure 9: Effect of compound **8** on the emission spectra of (a) warfarin-HSA complex and (b) ibuprofen-HSA complex; effect of compound **12** on the emission spectra of (c) warfarin-HSA complex and (d) ibuprofen-HSA complex, upon excitation at 280 nm.

Table 3: Binding constants K_b of two HSA–probe systems at 298 K in the absence and presence of site markers.

Probe	HSA-**8** system		HSA-**12** system	
	K_b (10^5 L mol^{-1})	n	K_b (10^5 L mol^{-1})	n
Blank	1.2	1.09	2.3	1.11
Ibuprofen	0.22	0.94	2.1	1.09
Warfarin	1.0	1.05	1.23	0.98

From modified Stern-Volmer equation, the binding constants (K_b) for **8**-HSA and **12**-HSA systems in the presence of warfarin were 1.0 × 10^5 and 1.23 × 10^5 L mol^{-1}, respectively (**Figure 10**). On the contrary, in the presence of the drug ibuprofen, the binding constants for **8**-HSA and **12**-HSA systems were found to be 0.22 × 10^5 and 2.1 × 10^5 L mol^{-1}, respectively (**Table 3**). It has been observed that the binding constant of compound **8** has been significantly decreased in the presence of site marker ibuprofen, while in **12**, the binding constant was decreased in the presence of site marker warfarin. These results demonstrated that ibuprofen and warfarin could prevent the binding of compounds **8** and **12**, respectively. It was inferred that compound **8** binds to HSA sudlow's site II and **12** binds through sudlow's site I.

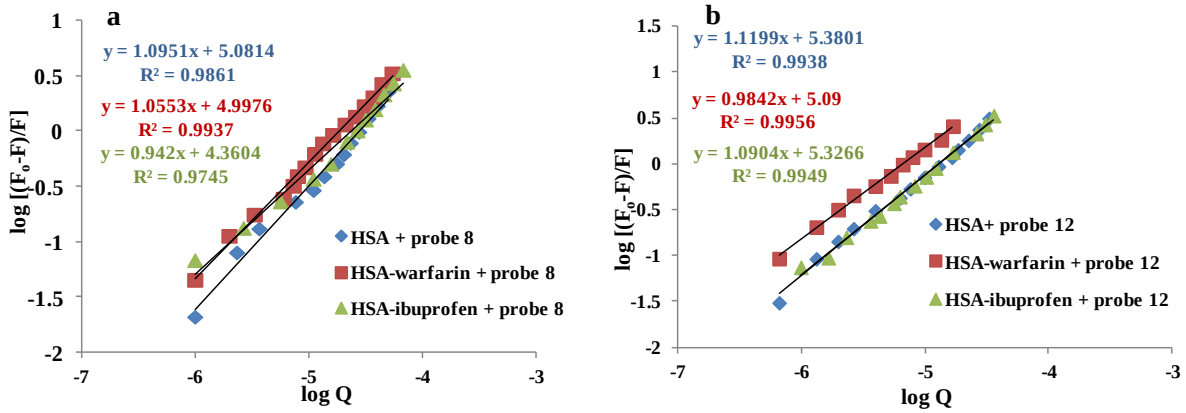

Figure 10: Modified Stern-Volmer plots of log [(F_0 − F)/F] versus log [Q] for determination of binding constant by fluorescence spectrometer titration of HSA with (a) **8** and (b) **12** in PBS buffer.

4.4.5 Circular dichroism studies

Circular dichroism (CD) spectroscopy is a sensitive optical technique which is used to detect changes in confirmation of protein upon drug interactions.[145] CD spectrum of HSA possesses two negative bands; one at 208 nm and another at 222 nm due to π-π* and n-π* transitions of α-

helix, respectively. On addition of compound **8** or **12** to HSA, α-helicity of HSA was decreased which showed unfolding of protein (**Figure 11**). CD results were represented in terms of mean residue ellipticity (MRE).

The α-helical content for HSA was found to be 66.6 % using the above formulae. Upon addition of compound **8** or **12,** the α-helical content is reduced to 55.8 % and 49.3 %, respectively, indicating the significant interaction of compounds with HSA.

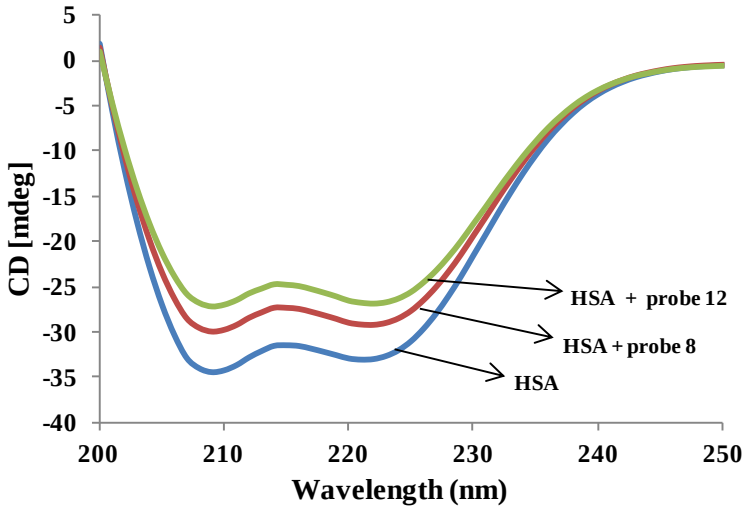

Figure 11: CD spectra of 2.5 μM HSA, in the presence of 3.75 μM of **8** and **12**

4.4.6 Fluorescence resonance energy transfer

Försters principle (FRET) is employed to calculate the binding distance (r_o) between the donor (HSA) and acceptor (naphthalimide analogues) as the emission band of human serum albumin overlaps with the absorption band of compounds **8** and **12**. Försters non-radiative energy theory states that when the small interacting molecule (acceptor) absorbs the excited energy of protein (donor), there is transfer of energy occurs amongst two.[146] The various formulas are used to compute E_{FRET}, i.e. efficiency of energy transfer and calculated to be E_{FRET} = 0.84, $J = 1.15 \times 10^{-18}$ cm^3 L mol^{-1}, R_o = 0.505 nm and r_o = 0.39 nm for compound **8** and E_{FRET} = 0.86, $J = 1.12 \times 10^{-18}$ cm^3 L mol^{-1}, R_o = 0.503 nm and r_o = 0.37 nm for compound **12**. **Figure 12** shows that E_{FRET} is dependent on the distance between donor (human serum albumin) and acceptor (naphthalimide analogues). It has been concluded that **12** (r_o = 0.37 nm) is slightly closer to HSA than **8**. So, there is a strong binding affinity between HSA and **12**. Therefore, the energy is transferred from

human serum albumin to analogues **8** and **12** occurs with high probability. Moreover, the r_o is less than 8 nm, indicates the nature of mechanism is static.[147]

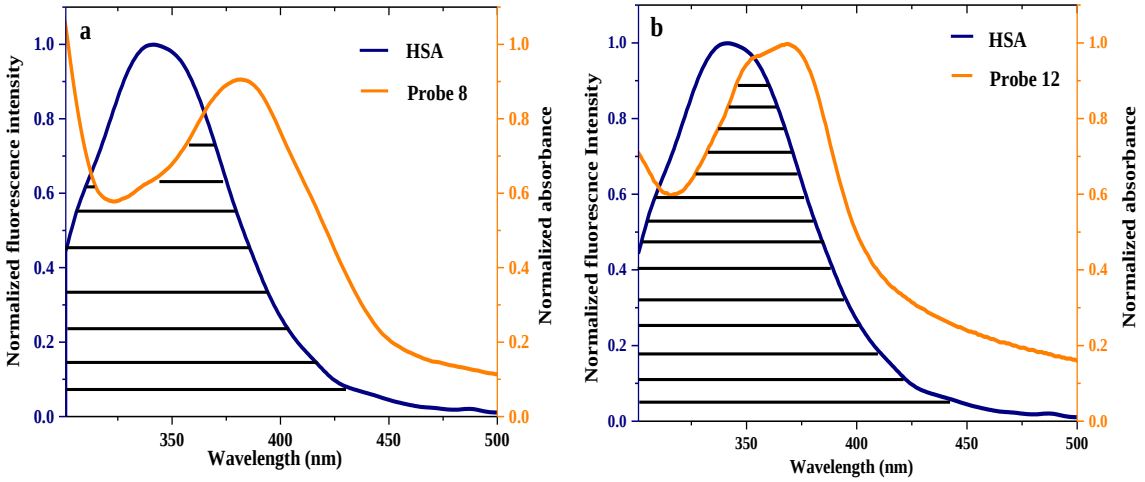

Figure 12: Spectral overlaps of emission spectra of human serum albumin (blue) with absorption spectra of compounds (a) **8** (orange) and (b) **12** (orange); [HSA] = 7 μM, [**8**] = 7 μM, [**12**] = 7 μM.

4.4.7 Lifetime fluorescence technique

To substantiate the mechanism of quenching of HSA by naphthalimides (probes **8** and **12**) whether it is dynamic or static, time-resolved fluorescence studies were carried out. The average fluorescence lifetimes τ_{av} for triexponential iterative fittings were evaluated from the following expression;

$$\tau_{av} = \sum \alpha_i \tau_i$$

Where α_i is the pre-exponential factor and τ_i is the decay time of HSA in free and bound states. Chi-squared (χ^2) valued approaching near unity and were accounted best for the goodness of fit. The time-resolved decay curves for **8**-HSA and **12**-HSA systems were represented in **Figure 13** and the values of other parameters are given in **Table 4**.

The average lifetime of HSA (7 μM) (τ_{av}) with triexponential decay profile was found to be 4.07 ns. Upon addition of probe **8** or **12** to HSA, the lifetime of HSA was decreased from 4.07 ns to 4.03 ns and 3.94 ns, respectively. These findings demonstrated that upon addition of 5 equiv. of naphthalimide probe, a slight reduction in lifetime of HSA is observed. It has been indicated that the static mechanism is responsible for the binding interaction of HSA to naphthalimide probes **8** and **12**.

Table 4: Fluorescence decay profile of HSA and naphthalimide-HSA systems

System	Conc.	τ_1	α_1	τ_2	α_2	τ_3	α_3	τ_{av}	χ^2
HSA		2.84	0.26	6.70	0.47	0.66	0.27	4.07	1.02
HSA-**8**	1:3	3.10	0.26	6.85	0.44	0.67	0.30	4.04	1.04
	1:5	3.26	0.29	6.93	0.42	0.69	0.30	4.03	1.06
HSA-**12**	1:3	3.48	0.30	7.27	0.37	0.70	0.33	3.99	1.09
	1:5	3.28	0.27	7.04	0.40	0.67	0.33	3.94	1.13

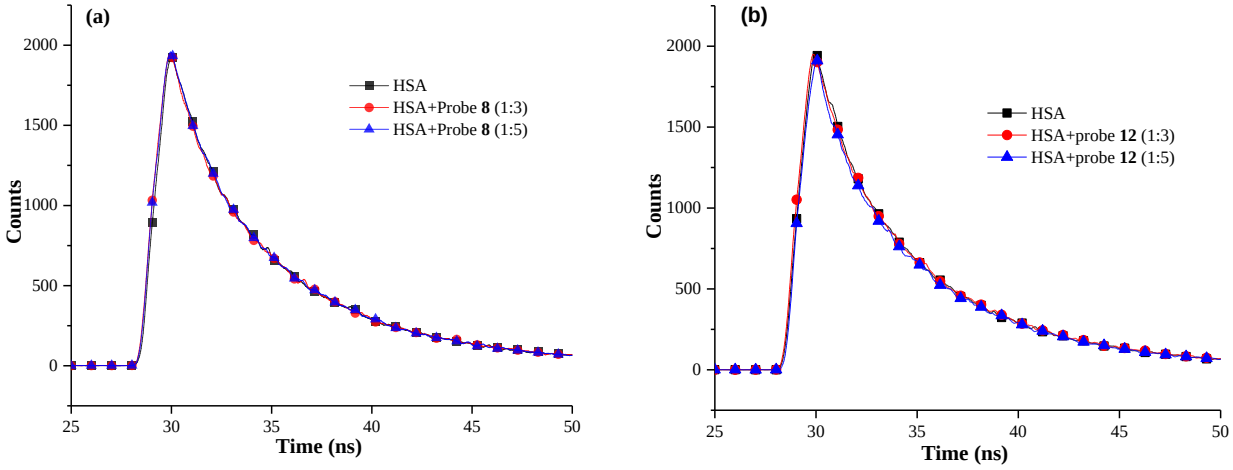

Figure 13: Time-resolved fluorescence spectra of HSA (7.0 μM) in the absence and presence of compounds (a) **8** (0-35 μM) and (b) **12** (0-35 μM)

4.4.8 Sodium dodecyl sulfate studies

Spectroscopic studies demonstrated the probability of denaturation of human serum albumin folds at a higher concentration of probe **8** or **12**. To investigate the reversibility in binding of naphthalimide probes to serum albumins, refolding studies were performed using the anionic surfactant sodium dodecyl sulfate (SDS). SDS is considered as an effective denaturant of protein.[148] However, SDS at lower concentrations refolds the albumin and acts as a protective agent for protein conformation. Therefore, to examine the effect of SDS on refolding of serum albumin denatured by probes **8** and **12**, steady-state fluorescence spectral technique was employed. From spectroscopic studies (discussed above), it is observed that probes **8** and **12** alter the conformation of the serum albumin. The bare structure of HSA can be recovered only if SDS displaces the naphthalimides attached to serum albumin. **Figure 14** showed the fluorescence emission spectra of bare, denaturated, and refolded states of human serum albumin. On addition

of SDS to HSA, which has been denatured by probe **8** (**Figure 14a**) and **12** (**Figure 14b**), the intensity of emission spectrum enhances in the both the cases. It is concluded that addition of SDS strips out probes **8** and **12** from HSA modify the structure of the HSA which was denatured by probes **8** and **12**. Therfore, it is revealed that the binding of compounds **8** and **12** to HSA is reversible, which showed improved pharmacokinetic properties of these compounds.

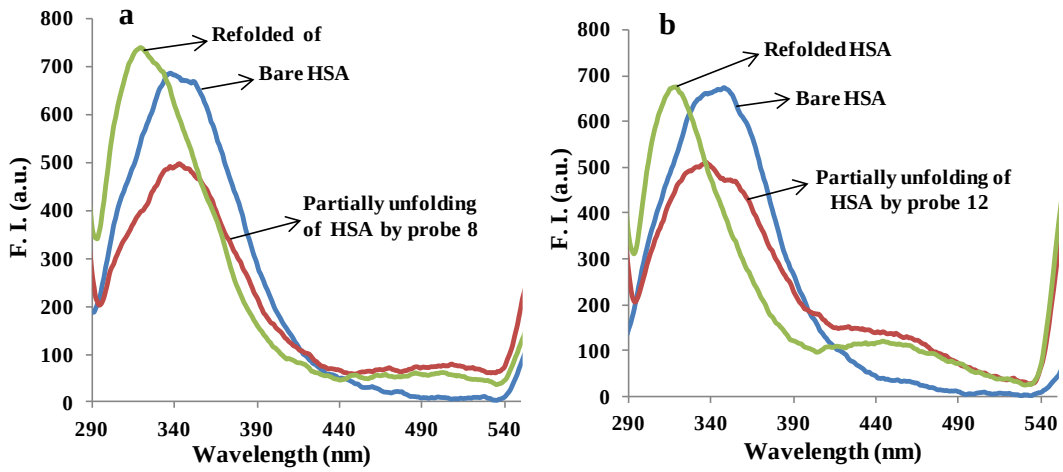

Figure 14: Fluorescence spectra of bare HSA (blue) in the presence of compounds (a) **8** (red) and (b) **12** (red) for unfolding process; and in the presence of sodium dodecyl sulfate (green) for refolding process

4.5 Molecular docking

The complementary application of molecular docking was performed to determine the interactive forces that playing key role in the binding interactions of naphthalimide-benzothiazole conjugates and serum albumin. Structurally, HSA is comprised of three homologous domains; site I (residues 1–195), site II (196–383) and site III (384–585) and each domain possess subdomains. The major regions of drug binding to human serum albumin are present in hydrophobic cavities in subdomains IIA and IIIA of sites I and II. Using AutoDock,[82] the partial binding parameters of conjugate–HSA systems with Pdb : 1H9Z were calculated. The naphthalimide and benzothiazole moieties were well surrounded by binding pockets, and both rings form about 90^{o} angle with each other. It was noteworthy that Trp214 residue of HSA was in close proximity to naphthalimide ring in both the derivatives, while lysine residue (Lys195) interacted with naphthalimide ring in case of **8** and benzothiazole moiety in **12**, indicating the presence of hydrophobic forces between them. The best energy rank has been found to be - 12.9 kcal/mol and -13.4 kcal/mol for compounds **8** and **12**, respectively as shown in **Figure 15**. The

inside wall of pocket of suldow's site I is comprised of hydrophobic amino acids, while the positively charged residue surrounds the entrance of pocket i.e. Ser454, Leu198, Lys199, Leu481, Arg484 and Val344 for compound **8** and Lys199, Leu198, Leu481 and Ala210 for compound **12**. Thus, the above data is proved to be beneficial to explain the quenching of HSA emission band in the presence of naphthalimide-benzothiazole conjugates. These compounds were also interacted through hydrogen bonds between naphthalimide analogues (**8** and **12**) and polar amino acid residues: Ser454 = 3.168 Å (CO), Trp214 = 3.192 Å (S) of **8** and Ser201 = 3.121 Å (F) of **12**. The obtained docking parameters demonstrated that the interaction between naphthalimide-benzothiazole and HSA was conquered by hydrophobic interactions and hydrogen bondings. However, compound **8** binds with BSA; Leu189, Lys431, Tyr451, Ala193, Arg435 residues while probe **12** surrounds the Leu189, Ala193, Arg144, Ile455, Pro110 residues, through only hydrophobic interactions with binding energies of -11.5 kcal/mol and -11.8 kcal/mol, respectively (**Figure 16**), indicated that these compounds showed better interactions with HSA than BSA.

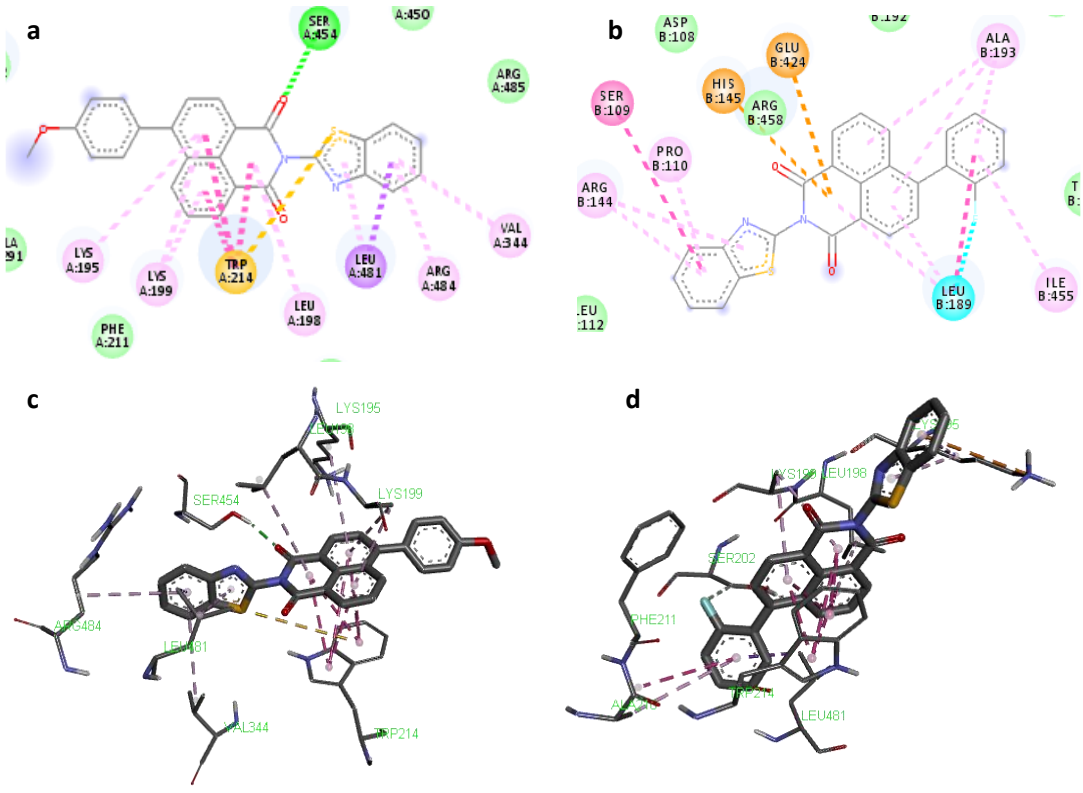

Figure 15: 2-D view of amino acid residues surrounding (a) **8** and (b) **12;** 3-D view conformations of (c) **8** and (d) **12** with HSA (pdb : 1H9Z)

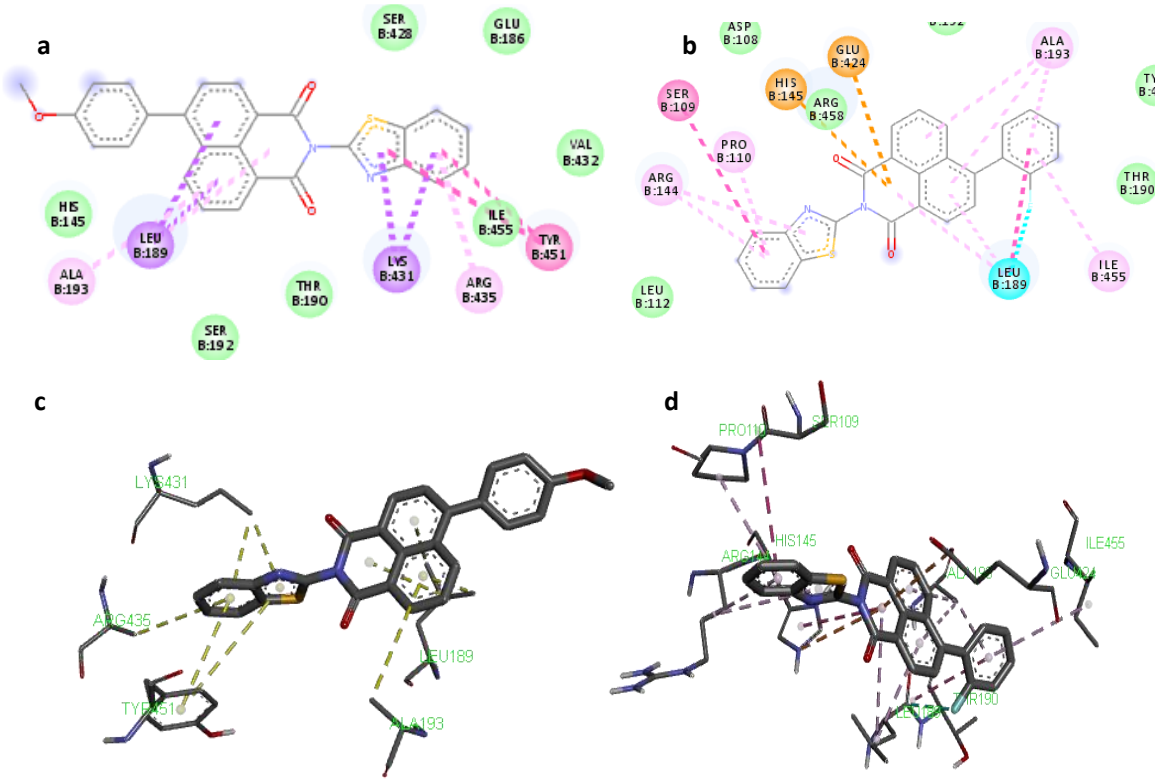

Figure 16: 2-D view of amino acid residues surrounding (a) **8** and (b) **12;** 3-D view conformations of (c) **8** and (d) **12** with BSA (pdb : 3V03)

4.6 Conclusion

In summary, a series of new naphthalimide-benzothiazole based fluorescence probe was synthesized and screened for their anticancer activity against 60 human cancer cell lines. Further, the binding interaction and the selectivity of probes **8** and **12** towards serum albumin were evaluated. Investigation of anticancer activity of synthesized compounds revealed that compound **12** was found to be better cytotoxic against most of the cancer cell lines. The majority of these naphthalimide-benzothiazole analogues selectively inhibited the growth of K-562, SR and UO-31 tumor cell lines. It has also been observed that the non-planar fluorophore **12** exhibited better binding affinity to HSA and BSA as compared to **8**, revealed through various spectroscopic techniques. Compound **12** is highly selective towards the recognizing and detecting HSA and BSA in complex samples containing various interfering biological ions and molecules with detection limits of 4.3 and 5.5 μM, respectively. Importantly, HSA analysis with ibuprofen and warfarin exhibited a potential biomarker for clinical diagnosis. It was also inferred that **8** binds to suldow's site II and **12** through sudlow's site I of HSA. The nature and position of the group

attached to naphthalimide core also strongly affects the binding affinity of analogues with albumin. Overall, these remarkable properties of naphthalimide-benzothiazole make an ideal multifunctional and practically viable probe for various biomedical and molecular biology applications.

4.7 Experimental section

Commercially grade chemicals and solvents were used for the synthesis and purchased from Sigma-Aldrich, TCI, and Spectrochem. Reactions were monitored by TLC (thin layer chromatography) using silica coated plate GF-254 and compounds were further purified by silica gel based column chromatography having mesh size of 60-120. Melting points were determined using micro melting apparatus and were uncorrected. ^{1}H NMR and ^{13}C NMR were recorded on Joel ECS-400MHz spectrometer, using $CDCl_3$ and DMSO-d_6 as solvents. TMS is used as internal reference. Chemical shifts and *J* values were expressed in delta (ppm) and Hertz, respectively. Mass spectra of the synthesized compounds were observed at Water Micromass-Q-T of Micro. CHNS elemental analysis was done using Thermo Scientific (Flash 2000) analyzer. HSA and BSA studies were performed using Shimadzu UV- 2600 and Cary eclipse fluorescence spectrophotometer. The time-resolved lifetime fluorescence experiment was carried out using deltaflex^{TM} spectrometer.

5-Bromo-1,2-dihydroacenaphthylene (2)[102]

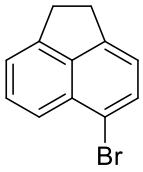

A solution of *N*-bromosuccinimide (11.2 g, 64.8 mmol) in DMF (15 mL) was added to a stirred solution of acenaphthene (10 g, 64.8 mmol) in DMF (15 mL) at room temperature. The reaction mixture was continuously stirred for 3 h at room temperature. After the completion of reaction, the solution was poured into 100 mL of cold water, resulted in separation of yellow colored precipitates. The solution was filtered and vacuum dried. The crude product was recrystallized in ethanol and gave pure product with 97% yield (observed mp: 54-56 ^{o}C, literature mp 52 ^{o}C).

6-Bromo-1*H*,3*H*-benzo[*de*]isochromene-1,3-dione (3)[103]

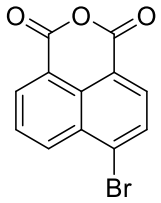

To a solution of 5-bromo-1,2-dihydroacenaphthylene (5 g, 21.4 mmol) in glacial acetic acid (100 mL), potassium dichromate (21 g, 71.38 mmol) was added slowly at 0 ^{o}C for 30 min. The reaction was conducted at 110 ^{o}C for 4 h. On the completion of reaction, the mixture was allowed to cool and 500

mL of cold water was added into it. White colored crude was obtained and the residual chromium salt was removed with boiling water. The resulting solid was recrystallized in acetic acid to give needle shaped crystals (yield = 72%, mp: 221-224 ^{o}C).

2-(Benzo[*d*]thiazolyl-2-yl-6-bromo-1*H*-benzo[*de*]isoquinoline-1,3(2*H*)-dione (4)

In a sealed tube, 6-bromo-1*H*,3*H*-benzo[*de*]isochromene-1,3-dione (**2**) (2 g, 7.2 mmol), 2-amino benzothiazole (**3**) (1.09 g, 7.2 mmol), zinc acetate (1.32 g, 7.2 mmol) and excess of pyridine were irradiated in microwave for 5 min. After completion, the resulting brown solution was poured into cold water; solid was separated out and filtered. The crude product was purified by column chromatography on silica gel with 1:20 ethylacetate: hexane as eluents.

2-(Benzo[*d*]thiazolyl-2-yl-6-bromo-1*H*-benzo[*de*]isoquinoline-1,3(2*H*)-dione (4)

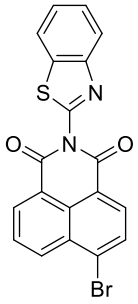

yellow solid; yield: 75%; mp: 248-250 ^{o}C; ^{1}H NMR (400 MHz, $CDCl_3$): δ(ppm) 8.76 (dd, ^{2}J = 7.3 Hz, ^{3}J = 0.92 Hz, 1H, ArH), 8.71 (dd, ^{2}J = 8.6 Hz, ^{3}J = 0.9 Hz, 1H, ArH), 8.51 (d, J = 7.8 Hz, 1H, ArH), 8.13 (t, J = 7.8 Hz, 2H, ArH), 7.98-7.90 (m, 2H, ArH), 7.59-7.49 (m, 2H, ArH); ^{13}C NMR (100 MHz, $CDCl_3$) 155.3 (C=O), 155.3 (C=O), 150.4, 136.8, 134.4, 132.9, 132.0, 131.6, 131.4, 131.0, 128.2, 126.4, 126.2, 124.2, 122.5, 122.5, 121.9, 121.8, 121.6 (ArC).

2-(Benzo[*d*]thiazolyl-2-yl-6-substituted aryl-1*H*-benzo[*de*]isoquinoline-1,3(2*H*)-dione (5-16)

2-(Benzo[*d*]thiazolyl-2-yl-6-bromo-1*H*-benzo[*de*]isoquinoline-1,3(2*H*)-dione (200 mg, 0.4 mmol) was reacted with various substituted aryl boronic acids (0.4 mmol) in the presence of potassium carbonate (101 mg, 0.73 mmol) and $Pd(PPh_3)_4$ (5 mol %) in acetonitrile under inert atmosphere. The reaction was conducted under reflux condition for 24 h. The solvent was vacuum distilled and the product was extracted with chloroform and water. The organic layer was collected and dried over Na_2SO_4. The product was isolated through column chromatography using hexane and ethyl acetate as eluents.

2-(Benzo[*d*]thiazol-2-yl)-6-phenyl-1*H*-benzo[*de*]isoquinoline-1,3(2*H*)-dione (5)

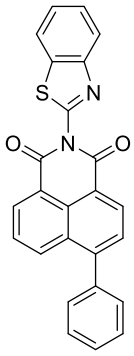

yellow solid; yield: 75%; mp: 240-246 °C; ^{1}H NMR (400 MHz, $CDCl_3$): δ(ppm) 8.74-8.70 (m, 2H, ArH), 8.39 (dd, ^{2}J = 8.6 Hz, ^{3}J = 0.9 Hz, 1H, ArH), 8.17 (d, J = 8.2 Hz, 1H, ArH), 7.98 (dd, ^{2}J = 7.3 Hz, ^{3}J = 0.9 Hz, 1H, ArH), 7.78-7.74 (m, 2H, ArH), 7.59-7.46 (m, 6H, ArH); ^{13}C NMR (100 MHz, $CDCl_3$): δ(ppm) 159.9 (C=O), 159.9 (C=O), 134.8, 134.3, 134.2, 133.3, 132.1, 132.0, 131.9, 131.7, 131.0, 129.7, 128.6, 128.5, 128.4, 128.3, 127.9, 119.3, 118.3 (ArC); MS (EI) : m/z 407.1 (M^{+}+1). Anal. Calc. for $C_{25}H_{14}N_2O_2S$: C, 73.88; H, 3.47; N, 6.89; S, 7.89; Found: C, 73.69; H, 3.61; N, 7.10; S, 7.76.

2-(Benzo[*d*]thiazol-2-yl)-6-(4-ethylphenyl)-1*H*-benzo[*de*]isoquinoline-1,3(2*H*)–dione (6)

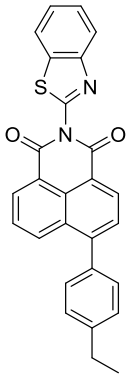

yellow solid; yield: 60%; mp: 260-265 °C; ^{1}H NMR (400 MHz, $CDCl_3$): δ(ppm) 8.73-8.70 (m, 2H, ArH), 8.43 (dd, ^{2}J = 8.6 Hz, ^{3}J = 0.9 Hz, 1H, ArH), 8.17 (d, J = 8.2 Hz, 1H, ArH), 7.99 (dd, ^{2}J = 8.2 Hz, ^{3}J = 0.9 Hz, 1H, ArH), 7.78-7.74 (m, 2H, ArH), 7.59-7.40 (m, 6H, ArH), 2.82 (q, J = 7.8 Hz, 2H, CH_2), 1.37 (t, J = 7.8 Hz, 3H, CH_3); ^{13}C NMR (100 MHz, $CDCl_3$): δ(ppm) 163.88 (C=O), 163.66 (C=O), 155.8, 150.5, 148.3, 145.0, 136.8, 135.8, 134.0, 132.0, 131.7, 130.4, 129.9, 128.2, 128.0, 126.9, 126.3, 126.1, 124.2, 122.2, 121.3, 120.8, (ArC), 28.7 (CH_2-ethyl), 15.5 (CH_3-ethyl); MS (EI) : m/z 435.1 (M^{+}+1); Anal. Calc. for $C_{27}H_{18}N_2O_2S$: C, 74.63; H, 4.18; N, 6.45; S, 7.38; Found: C, 74.39; H, 4.44; N, 7.52; S, 7.17.

2-(Benzo[*d*]thiazol-2-yl)-6-(*m*-tolyl)-1*H*-benzo[*de*]isoquinoline-1,3(2*H*)-dione (7)

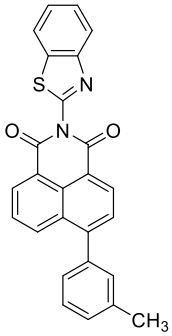

yellow solid; yield: 80%; mp: 248-252 °C; ^{1}H NMR (400 MHz, $CDCl_3$): δ(ppm) 8.73-8.70 (m, 2H, ArH), 8.40 (dd, ^{2}J = 8.2 Hz, ^{3}J = 1.3 Hz, 1H, ArH), 8.17 (dd, ^{2}J = 8.2 Hz, ^{3}J = 1.3 Hz, 1H, ArH), 7.98 (dd, ^{2}J = 8.2 Hz, ^{3}J = 1.3 Hz, 1H, ArH), 7.78-7.74 (m, 2H, ArH), 7.59-7.45 (m, 3H, ArH), 7.36-7.33 (m, 3H, ArH), 2.4 (s, 3H, meth-CH_3); ^{13}C NMR (100 MHz, $CDCl_3$): δ(ppm) 163.8 (C=O), 163.6 (C=O), 155.8, 150.8, 148.3, 138.5, 138.5, 136.8, 133.9, 132.0, 131.8, 130.5, 129.4, 129.2, 128.6, 128.0, 127.0, 126.9, 126.3, 126.1, 124.3, 122.2 , 121.8, 121.0 (ArC), 21.5 (CH_3-methyl); MS (EI) : m/z 421.1 (M^{+}+1)); Anal. Calc. for $C_{26}H_{16}N_2O_2S$: C, 74.27; H, 3.84; N, 6.66; S, 7.62; Found: C, 74.26; H, 3.69; N, 6.88; S, 7.81.

2-(Benzo[*d*]thiazol-2-yl)-6-(4-methoxyphenyl)-1*H*-benzo[*de*]isoquinoline-1,3(2*H*)-d ione (8)

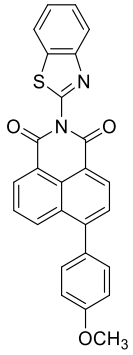

yellow solid; yield: 70%; mp: 260-265 ºC; ^{1}H NMR (400 MHz, $CDCl_3$): δ(ppm) 8.72 (d, *J* = 7.3, 2H, ArH), 8.43 (dd, ^{2}J = 8.7 Hz, ^{3}J = 0.9 Hz 1H, ArH), 8.17 (d, *J* = 7.8 Hz, 1H, ArH), 7.98 (d, *J* = 8.2 Hz, 1H, ArH), 7.78-7.73 (m, 2H, ArH), 7.59-7.48 (m, 4H, ArH), 7.12 (d, *J* = 8.7, 2H, ArH), 3.9 (s, 3H, OCH_3); ^{13}C NMR (100 MHz, $CDCl_3$): δ(ppm) 168.6 (C=O), 163.6 (C=O), 160.1, 147.9, 133.9, 132.0 131.7, 131.1, 130.7, 130.4, 127.9, 126.3, 126.12, 124.2, 122.1, 121.8, 114.0 (ArC), 55.2 (OCH_3); MS (EI) : m/z 437.1 (M^++1); Anal. Calc. for $C_{26}H_{16}N_2O_3S$: C, 71.55; H, 3.69; N, 6.42; S, 7.35; Found: C, 71.44; H, 3.91; N, 6.17; S, 7.52.

2-(Benzo[*d*]thiazol-2-yl)-6-(2-methoxyphenyl)-1*H*-benzo[*de*]isoquinoline-1,3(2*H*)-d ione (9)

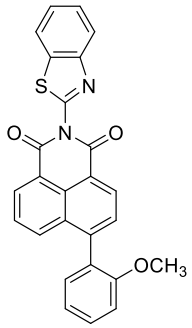

yellow solid; yield: 60%; mp: 255-260 ºC; ^{1}H NMR (400 MHz, $CDCl_3$): δ(ppm) 8.73 (d, *J* = 7.3 Hz, 1H, ArH), 8.69 (dd, ^{2}J = 7.3 Hz, ^{3}J = 0.9 Hz, 1H, ArH), 8.17 (d, *J* = 7.8 Hz, 1H, ArH), 8.07 (dd, ^{2}J = 7.6 Hz, ^{3}J = 1.3 Hz, 1H, ArH), 7.97 (dd, ^{2}J = 7.7 Hz, ^{3}J = 0.9 Hz, 1H, ArH), 7.74-7.68 (m, 2H, ArH), 7.58-7.48 (m, 3H, ArH), 7.34 (dd, ^{2}J = 7.3 Hz, ^{3}J = 1.8 Hz, 1H, ArH), 7.17-7.09 (m, 2H, ArH), 3.72 (s, 3H, OCH_3); ^{13}C NMR (100 MHz, $CDCl_3$): δ(ppm) 164.1 (C=O), 163.6 (C=O), 156.7, 155.8, 150.70, 145.0, 136.8, 134.2, 131.9, 131.6, 131.4, 130.9, 130.6, 130.3, 128.7, 128.6, 127.2, 126.6, 126.3, 126.0, 124.2, 122.0, 121.8, 121.0, 120.8 (ArC); MS (EI) : m/z 437.1 (M^++1); Anal. Calc. for $C_{26}H_{16}N_2O_3S$: C, 71.55; H, 3.69; N, 6.42; S, 7.35; Found: C, 71.32; H, 3.85; N, 6.68; S, 7.49.

2-(Benzo[*d*]thiazol-2-yl)-6-(4-flourophenyl)-1*H*-benzo[*de*]isoquinoline-1,3(2*H*)-dione (10)

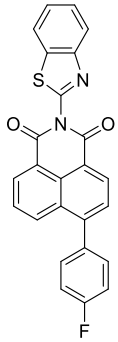

yellow solid; yield: 65%; mp: 265-270 ºC; ^{1}H NMR (400 MHz, $CDCl_3$): δ(ppm) 8.73 (d, *J* = 7.3 Hz, 2H, ArH), 8.34 (dd, ^{2}J = 8.7 Hz, ^{3}J = 0.9 Hz, 1H, ArH), 8.17 (d, *J* = 8.2 Hz, 1H, ArH), 7.98 (d, *J* =7.3 Hz, 1H, ArH), 7.80-7.73 (m, 2H, ArH), 7.59-7.49 (m, 4H, ArH), 7.30-7.28 (m, 2H, ArH); ^{13}C NMR (100 MHz, $CDCl_3$): δ(ppm) 163.8 (C=O), 163.4 (C=O), 155.9, 150.8, 146.9, 136.8, 133.5, 132.1, 131.6, 131.5, 128.1, 127.2, 126.4, 126.1, 124.3, 121.8, 121.2, 116.0, 115.8(ArC); MS (EI) : m/z 425.1 (M^++1); Anal. Calc. for $C_{25}H_{13}FN_2O_2S$: C, 70.74 ; H, 3.09; F, 4.48; N, 6.60; S, 7.55; Found: C, 70.39; H, 3.28; N, 6.38; S, 7.44.

2-(Benzo[*d*]thiazol-2-yl)-6-(4-chlorophenyl)-1*H*-benzo[*de*]isoquinoline-1,3(2*H*)-di one (11)

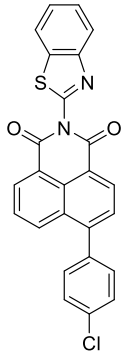

yellow solid; yield: 55%; mp: 260-263 ^{o}C; ^{1}H NMR (400 MHz, $CDCl_3$): δ(ppm) 7.81 (d, *J* = 7.8 Hz, 1H, ArH), 7.72 (d, *J* = 8.2 Hz, 1H, ArH), 7.56 (d, *J* = 7.8 Hz, 2H, ArH), 7.51 (d, *J* = 7.8 Hz, 2H, ArH), 7.42 (t, *J* = 7.3 Hz, 1H, ArH), 7.31-7.24 (m, 4H, ArH), 7.11 (t, *J* = 7.3 Hz, 2H, ArH); ^{13}C NMR (100 MHz, $CDCl_3$): δ(ppm) 163.7 (C=O), 163.5 (C=O), 155.7, 155.3, 150.4, 146.8, 136.7, 134.4, 134.4, 133.5, 132.1, 131.6, 130.4, 129.1, 128.1, 127.0, 126.3, 126.1, 126.1, 124.2, 122.2, 121.8, 121.1, 115.9, 115.7 (ArC); MS (EI) : m/z 441.05 (M^++1);

Anal. Calc. for $C_{25}H_{13}ClN_2O_2S$: C, 68.10; H, 2.97; N, 6.35; S, 7.27; Found: C, 67.95; H, 3.33; N, 6.12; S, 7.48.

2-(Benzo[*d*]thiazol-2-yl)-6-(2-flourophenyl)-1*H*-benzo[*de*]isoquinoline-1,3(2*H*)-di one (12)

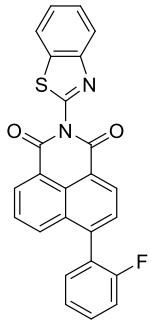

yellow solid; yield: 70%; mp: 268-273 ^{o}C; ^{1}H NMR (400 MHz, $CDCl_3$): δ(ppm) 8.76-8.66 (m, 2H, ArH), 8.15-8.11 (m, 2H, ArH), 7.96 (dd, ^{2}J = 8.2 Hz, ^{3}J = 0.9 Hz, 1H, ArH), 7.78-7.73 (m, 2H, ArH), 7.51-7.42 (m, 4H, ArH), 7.36-7.24 (m, 2H, ArH); ^{13}C NMR (100 MHz, $CDCl_3$): δ(ppm) 163.7 (C=O), 163.5 (C=O), 160.6, 158.6, 155.7, 150.5, 141.8, 133.5, 132.1,131.9, 131.5, 128.9, 127.2, 126.3, 126.1, 124.3, 121.8, 116.2, 116.1 (ArC); MS (EI) : m/z 425.1 (M^++1); Anal.

Calc. for $C_{25}H_{13}FN_2O_2S$: C, 70.74; H, 3.09; N, 6.60; S, 7.55; Found: C, 70.42; H, 3.27; N, 6.36; S, 7.76.

6-(4-Acetylphenyl)-2-(benzo[*d*]thiazol-2-yl)-1*H*-benzo[*de*]isoquinoline-1,3(2*H*)-di one (13)

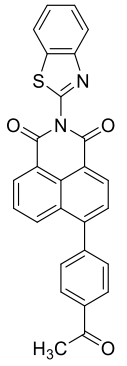

yellow solid; yield: 45%; mp: 275-280 ^{o}C; ^{1}H NMR (400 MHz, $CDCl_3$): δ(ppm) 8.75-8.72 (m, 2H, ArH), 8.31 (dd, ^{2}J = 8.2 Hz, ^{3}J = 0.9 Hz, 1H, ArH), 8.18-8.15 (m, 3H, ArH), 7.98 (dd, ^{2}J = 7.8 Hz, ^{3}J = 1.3 Hz, 1H, ArH), 7.81-7.77 (m, 2H, ArH), 7.67 (d, *J* = 8.2, 2H, ArH), 7.60-7.49 (m, 2H, ArH), 2.72 (s, 3H, acetyl-CH_3); ^{13}C NMR (100 MHz, $CDCl_3$): δ(ppm) 197.5 (C=O), 163.6 (C=O), 163.4 (C=O), 155.6, 150.4, 146.6, 143.1, 137.0, 136.7, 133.2, 131.5, 130.1, 130.0, 129.1, 128.7, 128.0, 127.3, 126.4, 126.1, 124.2, 122.3, 121.8, 121.6 (ArC), 26.8 (CH_3);

MS (EI): m/z 449.1 (M^++1). Anal. Calc. for $C_{27}H_{16}N_2O_3S$: C, 72.31; H, 3.60; N, 6.25; S, 7.15; Found: C, 74.78; H, 5.77; N, 9.36.

2-(Benzo[*d*]thiazol-2-yl)-6-(naphthalen-1-yl)-1*H*-benzo[*de*]isoquinoline-1,3(2*H*)-d ione (14)

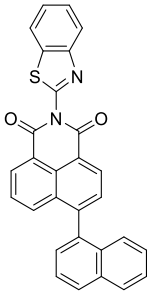

yellow solid; yield: 60%; mp: 268-272 ºC; ^{1}H NMR (400 MHz, $CDCl_3$): δ(ppm) 8.79 (d, *J* = 7.4 Hz, 1H, ArH), 8.69 (d, *J* = 7.2 Hz, 1H, ArH), 8.17 (d, *J* = 8.0 Hz, 1H, ArH), 8.04-7.95 (m, 3H, ArH), 7.88 (d, *J* = 8.4 Hz, 1H, ArH), 7.84 (d, *J* = 7.4 Hz, 1H, ArH),7.66-7.48 (m, 6H, ArH), 7.38-7.24 (m, 2H, ArH); ^{13}C NMR (100 MHz, $CDCl_3$): δ(ppm) 163.8 (C=O), 163.6 (C=O), 156.0, 150.4, 146.5, 136.7, 136.0, 134.1, 133.5, 132.2, 132.1, 131.6, 131.6, 129.1, 129.1, 128.5, 127.8, 127.0, 126.8, 126.4, 126.3, 126.1, 125.7, 125.3, 124.3, 122.2, 121.8, 121.6; MS (EI) : m/z 457.10 (M^++1); Anal. Calc. for $C_{29}H_{16}N_2O_2S$: C, 76.30; H, 3.53; N, 6.14; S, 7.02; Found: C, 76.57; H, 3.67; N, 6.35; S, 6.90.

2-(Benzo[*d*]thiazol-2-yl)-6-(thiophen-3-yl)-1*H*-benzo[*de*]isoquinoline-1,3(2*H*)-dio ne (15)

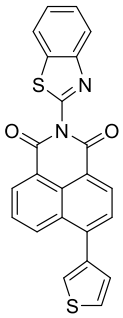

yellow solid; yield: 45%; mp: 258-260 ºC; ^{1}H NMR (400 MHz, $CDCl_3$): δ(ppm) 8.76-8.72 (m, 2H, ArH), 8.70 (dd, *J* = 7.3 Hz, 1H, ArH), 8.17 (dd, ^{2}J = 8.2 Hz, ^{3}J = 1.3 Hz, 1H, ArH), 7.98 (dd, ^{2}J = 7.3 Hz, ^{3}J = 0.9 Hz, 1H, ArH), 7.90 (d, *J* = 7.8 Hz, 1H, ArH), 7.85-7.81 (m, 1H, ArH), 7.61-7.49 (m, 3H, ArH), 7.44-7.40 (m, 1H, ArH), 7.30-7.28 (m, 1H, ArH); ^{13}C NMR (100 MHz, $CDCl_3$): δ(ppm) 163.7 (C=O), 163.4 (C=O), 155.5, 150.4, 140.3, 139.3, 136.8, 133.5, 132.2, 131.5, 129.2, 128.7, 128.0, 127.3, 126.4, 126.1, 124.1, 122.2, 121.9, 121.1 (ArC); MS (EI) : m/z 413.1 (M^++1); Anal. Calc. for $C_{23}H_{12}N_2O_2S_2$: C, 66.97; H, 2.93; N, 6.79; S, 15.54; Found: C, 67.30; H, 2.75; N, 6.98; S, 15.37.

2-(Benzo[*d*]thiazol-2-yl)-6-(3-(triflouromethyl)phenyl)-1*H*-benzo[*de*]isoquinoline-1,3(2*H*)-dione (16)

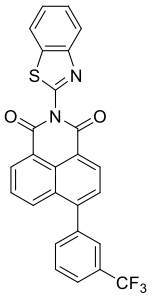

yellow solid; yield: 55%; mp: 255-258 ºC; ^{1}H NMR (400 MHz, $CDCl_3$): δ(ppm) 8.76-8.73 (m, 2H, ArH), 8.27 (dd, ^{2}J = 8.2 Hz, ^{3}J = 1.3 Hz, 1H, ArH), 8.17 (dd, ^{2}J = 7.3 Hz, ^{3}J = 0.9 Hz, 1H, ArH), 7.98 (dd, ^{2}J = 7.3 Hz, ^{3}J = 0.9 Hz, 1H, ArH), 7.83-7.72 (m, 6H, ArH), 7.60-7.50 (m, 2H, ArH); ^{13}C NMR (100 MHz, $CDCl_3$): δ(ppm) 163.6 (C=O), 163.4 (C=O), 155.5, 150.4, 146.0, 139.2, 136.7, 133.0, 132.2, 131.5, 130.1, 129.3, 129.1, 128.2, 127.5, 126.5, 126.4, 126.1, 124.2, 122.4, 122.3, 121.8, 121.7 (ArC); MS (EI) : m/z 475.1 (M^++1); Anal. Calc. for $C_{26}H_{13}F_3N_2O_2S$: C, 65.82; H, 2.76; N, 5.90; S, 6.76; Found: C, 65.98; H, 2.51; N, 6.19; S, 6.59.

2-(Benzo[*d*]thiazolyl-2-yl-6-substituted amine-1*H*-benzo[*de*]isoquinoline-1,3(2*H*)–dione (17-18)

2-(Benzo[*d*]thiazolyl-2-yl-6-bromo-1*H*-benzo[*de*]isoquinoline-1,3(2*H*)-dione (200 mg, 0.4 mmol) and selected amine (0.6 mmol) were refluxed in the presence of $PdCl_2(PPh_3)_2$ (5 mol %) and K_2CO_3 (101 mg, 0.73 mmol) in CH_3CN (5 ml) for 12 h. On completion of the reaction, CH_3CN was vacuum distilled. The product was extracted with ethyl acetate. The extract was then dried over anhydrous sodium sulfate, filtered and concentrated to get the crude product. The residue was purified using column chromatography on silica gel to obtain the desired product.

2-(Benzo[*d*]thiazol-2-yl)-6-piperdin-1-yl-1*H*-benzo[*de*]isoquinoline-1,3(2*H*)-dione (17)

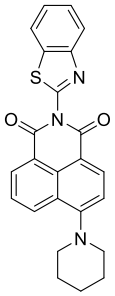

yellow solid; yield: 55%; mp: 290-294 ^oC; ^1H NMR (400 MHz, $CDCl_3$): δ(ppm) 8.65 (dd, , ^2J = 7.3 Hz, ^3J = 1.4 Hz 1H, ArH), 8.57 (d, J = 8.2 Hz, 1H, ArH), 8.48 (dd, ^2J = 8.2 Hz, ^3J = 1.4 Hz, 1H, ArH), 8.15 (dd, , ^2J = 7.8 Hz, ^3J = 1.8 Hz, 1H, ArH), 7.95 (dd, ^2J = 7.3 Hz, ^3J = 0.9 Hz, 1H, ArH), 7.74-7.70 (m, 1H, ArH), 7.57-7.46 (m, 2H, ArH), 7.22 (d, J = 8.2, 1H, ArH), 3.31 (t, J = 5.0, 4H, pip-CH_2), 1.94-1.92 (m, 4H, pip-CH_2), 1.78-1.72 (m, 2H, pip- CH_2); ^{13}C NMR (100 MHz, $CDCl_3$): δ(ppm)164.1 (C=O), 163.9 (C=O), 158.4, 150.5, 155.5, 136.7, 133.5, 131.9, 131.8, 126.2, 125.9, 125.4, 124.1, 121.7, 114.8 (ArC), 54.5 (pip-NCH_2), 26.1 (pip-CH_2), 24.2 (pip-CH_2); MS (EI) : m/z 414.1 (M^++1); Anal. Calc. for $C_{24}H_{19}N_3O_2S$: C, 69.71; H, 4.63; N, 10.16; S, 7.75; Found: C, 69.88; H, 4.38; N, 10.01; S, 7.95.

2-(Benzo[*d*]thiazol-2-yl)-6-morpholino-1*H*-benzo[*de*]isoquinoline-1,3(2*H*)-dione (18)

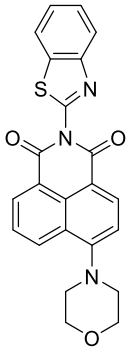

yellow solid; yield: 60%; mp: 285-290 ^oC; ^1H NMR (400 MHz, $CDCl_3$): δ(ppm) 8.76 (dd, ^2J = 7.3 Hz, ^3J = 0.9 Hz 1H, ArH), 8.60 (d, J = 7.7 Hz, 1H, ArH), 8.52 (dd, ^2J = 8.7 Hz, ^3J = 0.9 Hz 1H, ArH), 8.15 (d, J = 8.2 Hz, 1H, ArH), 7.96 (dd, ^2J = 8.7 Hz, ^3J = 1.3 Hz, 1H, ArH), 7.78-7.74 (m, 1H, ArH), 7.57-7.47 (m, 2H, ArH), 7.29 (d, J = 7.8, 1H, ArH), 4.06 (t, J = 4.0 Hz, 4H, mor-CH_2), 3.34 (t, J = 4.6 Hz, 4H, mor-CH_2); ^{13}C NMR (100 MHz, DMSO-d_6): δ(ppm) 168.7 (C=O), 168.1 (C=O), 162.1, 161.5, 155.2, 141.8, 137.9, 136.8, 135.3, 131.6, 131.4, 131.3, 131.2, 128.5, 128.0, 127.9, 127.6, 120.4, 120.4 (Ar-C), 71.3 (CH_2-O morph), 58.2 (CH_2-N morph); MS (EI) : m/z 416.13 (M^++1). Anal. Calc. for $C_{23}H_{17}N_3O_3S$: C, 66.49; H, 4.12; N, 10.11; S, 7.72; Found: C, 66.64; H, 4.27; N, 9.96; S, 7.78.

PROTOCOLS FOR VARIOUS STUDIES

(I) Procedure for in *vitro* anticancer screening

The human tumor cell lines of cancer screening panel were grown in RPMI 1640 medium containing 5% fetal bovine serum and 2 mM L-glutamine. Cells were inoculated into 96 well microtiter plates in 100 ml at plating densities ranging from 5,000 to 40,000 cells/well depending on the doubling time of individual cell lines. The microtiter plates were then incubated at 37 °C, 5% CO_2, 95% air and 100% relative humidity for 24 h.

After 24 h, two plates of each cell line were fixed *in situ* with TCA, to represent a measurement of the cell population for each cell line. Experimental drugs were solubilized in DMSO at 400-fold the desired final maximum test concentration and stored frozen prior to use. At the time of drug addition, an aliquot of frozen concentrate was thawed and diluted to twice the desired final maximum test concentration with complete medium containing 50 μg/ml gentamicin. Additional four, 10-folds or ½ log serial dilutions were made to provide a total of five drug concentrations plus control. Aliquots of 100 μL of these different drug dilutions were added to the appropriate microtiter wells, resulting in the required final drug concentrations. Following drug addition, the plates were incubated for an additional 48 h at 37 °C, 5% CO_2, 95% air, and 100% relative humidity. For adherent cells, the assay was terminated by the addition of cold TCA. Cells were fixed *in situ* by the gentle addition of 50 μL of cold 50% (w/v) TCA and incubated for 60 min at 4 °C. The supernatant was discarded, and the plates were washed five times with tap water and air dried. Sulforhodamine B (SRB) solution (100 μL) at 0.4% (w/v) in 1% acetic acid is added to each well, and plates were incubated for 10 min at room temperature. After staining, unbound dye was removed by washing five times with 1% acetic acid and the plates were air dried and then subsequently solubilized with 10 mM trizma base, and the absorbance was read on an automated plate reader at a wavelength of 515 nm. Using the seven absorbance measurements [time zero (T_z), control growth (C), and test growth in the presence of drug at the five concentration levels (T_i)], the percentage growth is calculated at each of the drug concentration levels. Percentage growth inhibition is calculated as: $[(T_i - T_z)/(C - T_z)] \times 100$ for concentrations for which $T_i \geq T_z$; $[(T_i - T_z)/T_z] \times 100$ for concentrations for which $T_i < T_z$. Three dose response parameters were calculated for each experimental agent. Growth inhibition of 50% (GI_{50}) was calculated from $[(T_i - T_z)/(C - T_z)] \times 100 = 50$. The drug concentration resulting in

total growth inhibition (TGI) was calculated from Ti = Tz. The LC50 was calculated from $[(T_i - T_z)/T_z] \times 100 = 50$.

(II) MTT assay

The cytotoxicity of synthesized derivatives was determined using MTT assay. Hek293 human embryonic kidney cells were seeded in 96 well plates at the density of $1x10^{-5}$ cells/well in low glucose Dulbecco's modified Eagle's medium (DMEM) containing 10% fetal bovine serum (FBS), 50 mM glutamine, 100 U/ml penicillin and 100 mg/ml streptomycin. Cells were incubated at 37 ^oC in an atmosphere of 5% CO_2 incubator. Cells were treated with compounds at five different concentrations (10^{-4}, 10^{-5}, 10^{-6}, 10^{-7}, 10^{-8} M) for 24 h at 37 ^oC. To each well, 10 μl of MTT (prepared in PBS buffer) from 5 mg/ml stock was added and incubated at 37 ^oC for 4 h in dark. The formazan crystals were dissolved using 100 μl of DMSO. Further by using Bio-Red ELISA plate reader, the amount of formazan crystal formation was measured as the difference in absorbance at 570 nm reference wavelength. The experiments were performed three times in triplicates. The relative cell toxicity (%) related to control wells containing culture medium without test material was calculated by using the formula:

$$\%\ cell\ toxicity = \frac{OD\ (compound\ treated\ wells)}{OD\ (untreated\ wells)} \times 100$$

(III) Topoisomerase-II assay

Relaxation of supercoiled plasmid DNA by TOPO-IIα was assayed in 20 μL of buffer (0.5 M Tris-HCl (pH 8.0), 1.5 M NaCl, 100 mM $MgCl_2$, 20 mM ATP, 5 mM dithiothreitol, 300 μg/mL BSA) containing drug solution, 4 U of DNA topoisomerase-IIα and 500 ng of supercoiled pHOT1 plasmid DNA and incubated at 37 ^oC for 30 min. Reactions were terminated by the addition of 2 μL of solution containing 10% sodium dodecyl sulfate (SDS) and 0.5 mg/mL of proteinase K and incubated at 37 ^oC for 30 min. Then, 1μL of loading buffer (50% glycerol and 0.25% bromophenol blue) was added. The samples were electrophoresed in 1% agarose gel with TAE buffer (100 mL of 10 stock solution-4.8 g of tris base, 1.14 mL acetic acid, and 0.37 g EDTA, pH 8.1) for 4 h and then the DNA was stained with ethidium bromide and photographed under UV illuminator.

(IV) HPLC chromatography

To analyze the ratios of *E*- and *Z*-isomers of the triphenylethylene derivatives/TPE-naph, reversed-phase high-performance liquid chromatography (RP-HPLC) has been performed using Ultimate 3000 HPLC (Thermofisher Scientific) system, equipped with C-18 column (250 × 4.6 mm, 5 mm) and UV-Vis detector. The stock solution of *E*/*Z*-triphenylethylene/TPE-naph derivative of concentration 1 mM was prepared in acetonitrile and protected from direct light. The stock solution was then diluted to produce a solution of compound in acetonitrile (2.3×10^{-4} M). First, the prepared sample was filtrated using 0.22 μm cellulose filtrate. Then, 20 μl of the filtered sample was injected into the column with an injection loop.

(V) Molecular Docking

Molecular docking studies were employed to authenticate the interaction between ligand and TOPO-II/HSA/BSA using software AutoDock 4.0. The three-dimensional structure of topoisomerase-II/HSA/BSA was obtained from the protein data bank. To setup ligand –protein interaction, AutoDock tools 1.5.6rc3 was accomplished to remove the water molecules and add the polar hydrogen atoms. As well gasteiger charges were computed and hydrogen atoms which are non-polar were merged to carbon atoms. The 3D structures of the molecules were kept in pdb format with aid of Gaussian 09 W program. Using ADT package (version 1.5.6rc3), the pdb file was further modified for partial charges. The charges of the non-polar hydrogen atoms have been assigned to the atom to which hydrogen is attached and file was saved as Pdbqt file. The docking files were generate by using the AutoDockTools program. A cubic grid dimension with various dimensions with the grid points along the x, y and z axes and a grid spacing of 0.375 Å was used. The optimized cluster was classified with minimum energy level in the best suitable conformation of TOPO-II/protein-ligand modeled structure. The molecular structures were analyzed using Discovery studio.

(VI) Materials and preparation of solutions

Human serum albumin and bovine serum albumin were purchased from TCI. All reagents and other chemicals were bought from sigma Aldrich chemicals, spectrochem and HI-Media. Ultrapure water was used throughout the experiment. The stock solutions of ligands of 10^{-3} M were prepared in DMSO. All the samples of concentration 10^{-3} M were prepared by solubilizing in phosphate buffer (0.1 M) at *p*H 7.4. Concentrations were calculated by UV-Vis absorbance

measurements using molar extinction coefficients of 38700 $M^{-1}cm^{-1}$ for HSA at 280 nm and BSA 43824 $M^{-1}cm^{-1}$ at 280 nm, ibuprofen 346 $M^{-1}cm^{-1}$ at 272 nm and warfarin 13900 M^{-1} cm^{-1} at 308 nm.

(VII) Absorbance measurements

Interactions of compounds were investigated with HSA (7.0 μM) and BSA (7.0 μM) in phosphate buffer (0.1 M, *p*H = 7.4). UV-Vis spectra of HSA and BSA were recorded in range 200-800 nm in the absence and presence of incremental additions of probes/ligands. To calculate the binding constant between human serum albumin and ligand, Benesi Hildebrand equation (1) equation was employed.

$$\frac{1}{A - A_o} = \frac{1}{A_{max} - A} + \frac{1}{((A_{max} - A)K_b\,[Q])} \quad (1)$$

Where A_o and A are the absorbance of human serum albumin in the absence and presence of compound/ligand; A_{max} is the absorbance at saturation; Q is the concentration of compound/ligand.

(VIII) Fluorescence measurements

To a solution of 7 μM HSA and BSA, ligands were added with successive additions. Titrations were done manually by using micro-injector. The fluorescence emission spectra were measured at 298 K in wavelength range 200-800 nm. The quenching constant k_q and Stern-Volmer constant K_{sv} between HSA and ligand have been calculated using Stern-Volmer equation-2 where F_o and F are the fluorescence intensities in the absence and presence of ligand; τ_o is the lifetime of human serum albumin and calculated to be 5.06 ns.

$$\frac{F_0}{F} = 1 + K_q\,\tau_0\,[Q] \quad (2)$$

From the fluorescence emission spectra, binding constant K_b has been calculated using modified Stern-Volmer equation (3), where n is the number of binding site and Q is the concentration of ligand.

$$\log\left(\frac{F_0 - F}{F}\right) = logK_b + nlog[Q] \quad (3)$$

(XI) Gibb's free energy calculation

To determine the spontaneity for formation of complex between ligand and HSA, change in free energy has been calculated by employing following equation, where R is the gas constant (1.9872 $calK^{-1}mol^{-1}$), T is the room temperature (298K) at which experiment is performed and K_b is the calculated binding constant.

$$\Delta G = -RTlnK_b \quad (4)$$

(X) Life-time fluorescence technique

The efficient energy transfer between naphthalimides and serum albumin can also be determined from the lifetime fluorescence studies of serum albumin. The decay of serum albumin (7 μM) in excited state was recorded in the absence and presence of incremental addition of ligands by modulator time-resolved fluorescence system on deltaflex^{TM} spectrometer using inbuilt Horiba EZ time software. The average lifetime of HSA can be calculated by employing following equation 5:

$$\tau_{avg} = \alpha_1\tau_1 + \alpha_2\tau_2 + \alpha_3\tau_3 \quad (5)$$

(XI) Competitive assay for selectivity

A competitive binding assay was performed to evaluate the selectivity of compounds towards HSA and BSA, wherein emission spectra of compounds (7 μM) were recorded in the presence of various bioanalytes *viz*. HSA, BSA, AMP (Adenosine monophosphate), ATP (Adenosine triphosphate), aspartic acid, cysteine, glucose oxidase, glutamic acid, glutathione, histidine, homocysteine, lysine, pepsin, trypsin, urea, Na^+, Ca^{2+}, NH_4^+ and PO_4^{3-}.

(XII) Drug displacement studies

The fluorescence emission has been recorded at 200-800 nm and was excited at λ_{max} of 280 nm. To reduce the non-specific interactions, the equimolar concentration of site markers (7 μM) and serum albumin (7 μM) have been taken and compounds were added with successive additions. The parameters like excitation wavelength, region of emission wavelength, excitation and emission bandwidth are same as in fluorescence emission spectrum.

(XIII) Circular dichroism (CD) experiments

CD experiments (200-250 nm) were conducted using spectropolarimeter (JASCO-J 815) calibrated with ammonium (+)-10-Camphorsulfonate. Three scans were run at a scan rate of 50

nm/min under nitrogen. Far-UV CD spectrum of 2.5 μM HSA in PBS (0.1 M, *p*H = 7.4) was recorded at wavelength 200-250 nm in the absence and presence of analogues (benzothiazole appended naphthalimides). The CD results were represented in terms of mean residue ellipticity (MRE) with following formulae.

$$MRE = \frac{Observed\ CD\ (\ m\ degree)}{C_p nl\ \times 10} \tag{6}$$

Where C_p , the concentration of HSA; n, number of amino acids (585) of protein; l, path length of glass cuvette (1 mm). The α-helix contents of free human serum albumin and the albumin bound gto drugs **8** and **12** were determined from mean residue ellipticity values at 208 nm using the following equation (eqn 6):

$$\alpha - helix\ \% = \frac{-MRE_{208} - \ 4000}{33000 - 4000} \times 100 \tag{7}$$

. Where, MRE_{208} is the observed MRE value at 208 nm, 4000 is the MRE of the β-sheet and random coil conformation at 208 nm, and 33,000 is the MRE for pure α-helix at the same wavelength

(XIV) Fluorescence resonance energy transfer studies

The estimation of the extent of energy transfer and the donor-acceptor binding distance (r) were executed by using the Forster theory. The analysis was done by measuring the fluorescence emission spectrum of the donor, in 200-800 nm regions with excitation wavelength 280 nm; and UV-Vis absorption spectrum of equimolecular acceptor probe in the range of 200-800 nm under the same experimental conditions. The following formulae (eq. 6-8) were used to compute $E_{FRET.}$

$$E_{FRET} = 1 - \frac{F_o}{F} = \frac{R_o^6}{R_o^6 - r_o^6} \tag{8}$$

Where F_o and F are the emission intensities of human serum albumin in the absence and presence of naphthalimide analogues**,** respectively. R_o is the Forster distance when E_{FRET} is 50% and r_o is the distance between HSA and compounds. R_o is computed through equation 2:

$$R_o^6 = 8.79\ \times\ 10^{-25}\ K^2 n^{-4} \varphi J \tag{9}$$

Where K^2 = 2/3, spatial orientation factor; n = 1.33, refractive index of the medium; φ = 0.118 fluorescence quantum yield of protein (HSA); *J*, integral overlap of the emission spectrum of human serum albumin and absorption band of analogues which is evaluated using equation 3:

$$J = \frac{\int_0^\infty F(\lambda)\varepsilon(\lambda)\,\lambda^4 d\lambda}{\int_0^\infty F(\lambda)\,d\lambda} \qquad (10)$$

Where F(λ) = fluorescence intensity of human serum albumin at wavelength λ; ε(λ) = molar extinction coefficient of compounds at wavelength λ.

(XV) Sodium dodecyl sulfate (SDS) studies

Sodium dodecyl sulfate (SDS) is a denaturant of protein, and useful to examine the reversibility in binding of compounds **8** and **12** to HSA. The emission spectrum of HSA in PBS (*p*H = 7.4) at λ_{exc} 280 nm was recorded in the absence and presence of an equimolar concentration of ligands. To HSA-ligand complex system, three equivalents of sodium dodecyl sulfate solution were added.

References

1. F. Bray, J. Ferlay, I. Soerjomataram, R. L. Siegel, L. A. Torre, A. Jemal, Global cancer statistics 2018: GLOBOCAN estimates of incidence and mortality worldwide for 36 cancers in 185 countries, *CA Cancer J. Clin.*, **2018**, *68*, 394-424.
2. J. Ferlay, M. Colombet, I. Soerjomataram, C. Mathers, D. M. Parkin, M. Pineros, A. Znaor, F. Bray, Estimating the global cancer incidence and mortality in 2018: GLOBOCAN sources and methods, *Int. J. Cancer*, **2019**, *144*, 1941-1953.
3. WHO available from :< https://www.who.int/cancer/PRGlobocan2020Final.pdf
4. A. Jemal, F. Bray, M. M. Center, J. Ferlay, E. Ward, D. Forman, Global Cancer Statistics, *CA Cancer J. Clin.*, **2011**, *61*, 69-90.
5. M. L. Lazaro, Two preclinical tests to evaluate anticancer activity and to help validate drug candidates for clinical trials, *Oncoscience*, **2015**, *2*, 91-98.
6. S. R. Hengel, M. A. Spies, M. Spies, Small-molecule inhibitors targeting DNA repair and DNA repair deficiency in research and cancer therapy, *Cell Chem. Biol.*, **2017**, *24*, 1101-1119.
7. X. Liang, Q. Wu, S. Luan, Z. Yin, C. He, L. Yin, Y. Z. Yuan, L. Li, X. Song, M. He, C. Lv, W. Zhang, A comprehensive review of topoiomerase inhibitors as anticancer agents in the past decade, *Eur. J. Med. chem.*, **2019**, *171*, 129-168.
8. A. Udristioiu, D. Nica-Nadea, Autophagy dysfunctions associated with cancer cells and their therapeutic implications, *Biomed. Pharmacother.*, **2019**, *115*, 108892-108897.
9. S. Wang, W. J. Placzek, J. L. Stebbins, S. Mitra, R. Noberini, M. Koolpe, Z. Zhang, R. Dahl, E. B. Pasquale, M. Pellecchia, Novel targeted system to deliver chemotherapeutic drugs to EphA2-expressing cancer cells, *J. Med. Chem.*, **2012**, *55*, 2427-2436.
10. C. Viegas-Junior, A. Danuello, V. D. S. Bolzani, E. J. Barreiro, C. A. M. Fraga, Molecular hybridization: A useful tool in the design of new drug prototypes, *Curr. Med. Chem.*, **2007,** *14*, 1829-1852.
11. L. Xie, P. E. Bourne, Developing multitarget therapeutics to fine-tune the evolutionary dynamics of cancer ecosystem, *Front. Pharmacol.*, **2015**, *6*, 209-213.
12. Shagufta, I. Ahmad, Tamoxifen a pioneering drug: An update on the therapeutic potential of tamoxifen derivatives, *Eur. J. Med. Chem.*, **2018**, *143*, 515-531.

13. M. D. Tomczyk, K. Z. Walczk, 1,8-Naphthalimide based DNA intercalators and anticancer agents. A systematic review from 2007 to 2017, *Eur. J. Med. Chem.*, **2018**, *159*, 393-422.
14. R. Dua, S. Shrivastava, S. Sonwane, S. Srivastava, Pharmacological significance of synthetic heterocycles scaffold: A review, *Adv. Biol. Res.* **2011,** *5*, 120-144.
15. V. C. Jordan, B. W. O'Malley, Selective estrogen-receptor modulators and antihormonal resistance in breast cancer, *J. Clin. Oncol.*, **2007**, *25*, 5815-5824.
16. W. Shelly, M. W. Draper, V. Krishnan, M. Wong, R. B. Jaffe, Selective estrogen receptor modulators: An update on recent clinical findings, *Obstet. Gynecol. Surv.*, **2008**, *63*, 163-181.
17. J. Iqbal, O. M. Ginsburg, T. D. Wijeratne, A. Howell, G. Evans, I. Sestak, S. A. Narod, Endometrial cancer and venous thromboembolism in women under age 50 who take tamoxifen for prevention of breast cancer: A systematic review, *Cancer Treat. Rev.*, **2012**, *38*, 318-328.
18. R. Tandon, V. Luxami, H. Kaur, N. Tandon, K. Paul, 1,8-Naphthalimide: A potent DNA intercalator and target for cancer therapy, *Chem. Rec.*, **2017**, *17*, 956-993.
19. M. S. Christodoulou, N. Fokialakis, D. Passarella, A. N. Garcia-Argaez, O. M. Gia, I. Pongratz, L. D. Via, S. A. Haroutounian, Synthesis and biological evaluation of novel tamoxifen analogues, *Bioorg. Med. Chem.*, **2013**, *23*, 4120-4131.
20. M. S. Christodoulou, M. Zarate, F. Ricci, G. Damia, S. Pieraccini, F. Dapiaggi, M. Sironi, L. L. Presti, A. N. Garcia-Argaez, L. D. Via, D. Passarella, 4-(1,2-diarylbut-1-en-1-yl)isobutyranilide derivatives as inhibitors of topoisomerase II, *Eur. J. Med. Chem.*, **2016**, *118*, 79-89.
21. M. S. R. Marty, M. R. Katiki, J. B. Nanubolu, S. Garimella, S. Polepalli, N. Jain, S. K. Buddana, R. S. Prakasham, Synthesis and biological evaluation of novel tamoxifen-1,2,4-triazole conjugates, *Mol. Divers.*, **2016**, *20*, 687-703.
22. T. Shoda, M. Kato, R. Harada, T. Fujisato, K. Okuhira, Y. Demizu, H. Inoue, M. Naito, M. Kurihara, Synthesis and evaluation of tamoxifen derivatives with a long alkyl side chain as selective estrogen receptor down-regulators, *Bioorg. Med. Chem.*, **2015**, *23*, 3091-3096.
23. G. Kaur, M. P. Mahajan, M. K. Pandey, P. Singh, S. R. Ramisetti, A. K. Sharma, Design, synthesis, and anti-breast cancer evaluation of new triarylethylene analogs bearing short alkyl- and polar amino-/amido-ethyl chains, *Bioorg. Med. Chem. Lett.*, **2016**, *26*, 1963-1969.

24. L. M. Zhao, H. S. Jin, J. Liu, T. C. Skaar, J. Ipe, W. Lv, D. A. Flockhart, M. Cushman, A new Suzuki synthesis of triphenylethylenes that inhibit aromatase and bind to estrogen receptors *α* and *β*, *Bioorg. Med. Chem.*, **2016**, *24*, 5400-5409.
25. W. Lv, J. Liu, T. C. Skaar, E. O'Neill, G. Yu, D. A. Flockhart, M. Cushman, Synthesis of triphenylethylene bisphenols as aromatase inhibitors that also modulate estrogen receptors, *J. Med. Chem.*, **2016**, *59*, 157-170.
26. N. S. Ahmed, N. H. Elghazawy, A. K. ElHady, M. Engel, R. W. Hartmann, A. H. Abadi, Design and synthesis of novel tamoxifen analogues that avoid CYP2D6 metabolism, *Eur. J. Med. Chem.*, **2016**, *112*, 171-179.
27. N. H. Elghazawy, M. Engel, R. W. Hartmann, M. M. Hamed, N. S. Ahmed, A. H. Abadi, Design and synthesis of novel flexible-ester containing analogs of tamoxifen and their evaluation as anticancer agents, *Future Med. Chem.*, **2016**, *8*, 249-256.
28. L. Zhang, Y. C. Yao, M. Y. Gao, R. X. Rong, K. R. Wang, X. L. Li, H. Chen, Anticancer activity and DNA binding property of the trimers of triphenylethylene–coumarin hybrids, *Chin. Chem. Lett.*, **2016**, *27*, 1708–1716.
29. S. Kumar, L. Gub, G. Palma, M. Kaur, A. S. Pillay, P. Singh, V. Kumar, Design, synthesis, anti-proliferative evaluation and docking studies of 1*H*-1,2,3-triazole tethered Ospemifene-isatin conjugates as selective estrogen receptor modulators, *New J. Chem.*, **2018**, *42*, 3703-3713.
30. E. Catanzaroa, F. Seghettib, C. Calcabrinia, A. Rampa, S. Gobbi, P. Sestili, E. Turrini, F. Maffei, P. Hrelia, A. Bisi, F. Belluti, C. Fimognari, Identification of a new tamoxifen-xanthene hybrid as pro-apoptotic anticancer agent, *Bioorg. Chem.*, **2019**, *86*, 538-549.
31. M. I. Ahmad, S. Dixit, R. Konwar, P. G. Vasdev, A. K. Yadav, S. Tripathi, M. M. Gupta, A. Sharma, A. Gupta, Syntheses of conformationally restricted benzopyran based triarylethylenes as growth inhibitors of carcinoma cells, *Bioorg. Med. Chem. Lett.*, **2017**, *27*, 5040-5045.
32. G. Luo, M. Chen, W. Lyu, R. Zhao, Q. Xu, Q. You, H. Xiang, Design, synthesis, biological evaluation and molecular docking studies of novel 3-aryl-4-anilino-2*H*-chromen-2-one derivatives targeting ER*α* as anti-breast cancer agents, *Bioorg. Med. Chem. Lett.*, **2017**, *27*, 2668-2673.

33. A. F. Palermo, M. Diennet, M. E. Ezzy, B. M. Williams, D. C. White, S. Mader, J. L. Gleasona, Incorporation of histone deacetylase inhibitory activity into the core of tamoxifen - A new hybrid design paradigm, *Bioorg. Med. Chem.*, **2018**, *26*, 4428-4440.
34. N. M. O'Boyle, G. Ana, P. M. Kelly, S. M. Nathwani, S. Noorani, D. Fayne, S. A. Bright, B. Twamley, D. M. Zisterer, M. J. Meegana, Synthesis and evaluation of antiproliferative microtubule-destabilising combretastatin A-4 piperazine conjugates, *Org. Biomol. Chem.*, **2019**, *17*, 6184-6200.
35. M. Carr, A. J. S. Knox, D. K. Nevin, N. O'Boyle, S. Wang, B. Egan, T. McCabe, B. Twamley, D. M. Zisterer, D. G. Lloyd, M. J. Meegan, Optimisation of estrogen receptor subtype-selectivity of a 4-Aryl-4*H*-chromene scaffold previously identified by virtual screening, *Bioorg. Med. Chem.*, **2020**, *28*, 115261-115277.
36. D. Dheer, C. Behera, D. Singh, M. Abdullaha, G. Chashoo, S. B. Bharate, P. N. Gupta, R. Shankar, Design, synthesis and comparative analysis of triphenyl-1,2,3-triazoles as anti-proliferative agents, *Eur. J. Med. Chem.*, **2020**, *207*, 112813-112825.
37. M. Xin, J. H. Wei, C. H. Yang, G. B. Liang, D. Su, X. L. Ma, Y. Zhang, Design, synthesis and biological evaluation of 3-nitro-1,8-naphthalimides as potential antitumor agents, *Bioorg. Med. Chem. Lett.*, **2020**, *30*, 127051-127056.
38. R. X. Rong, S. S. Wang, X. Liu, R. F. Li, K. R. Wang, Z. R. Cao, X. L. Li, Lysosomes-targeting imaging and anticancer properties of novel bis-naphthalimide derivatives, *Bioorg. Med. Chem. Lett.*, **2018**, *28*, 742-747.
39. P. Q. Espinoza, P. M. Acosta, A. Amesty , P. M. Rodriguez, I. L. Castrillejo, L. F. Perez, F. Machin, A. E. Braun, 5-Ethynylarylnaphthalimides as antitumor agents: Synthesis and biological evaluation, *Bioorg. Med. Chem*, **2017**, *25*, 1976-1983.
40. Z. Ou, M. Xu, Y. Gao, R. Hu, Q. Li, W. Cai, Z. Wang, Y. Qian, G. Yang, Synthesis, G-quadruplex binding properties and cytotoxicity of naphthalimide-thiourea conjugates, New *J. Chem.*, **2017**, *41*, 9397-9405.
41. A. D. Johnson, R. Zammit, J. Vella, M. Valentino, J. A. Buhagiar, D. C. Magri, Aminonaphthalimide hybrids of mitoxantrone and amonafide as anticancer and fluorescent cellular imaging agents, *Bioorg. Chem.*, **2019**, *93*, 103287-103296.

42. M. Li, Y. Wang, C. Ge, L. Chang, C. Wang, Z. Tian, S. Wang, F. Dai, L. Zhao, S. Xie, Synthesis and biological evaluation of novel alkylated polyamine analogues as potential anticancer agents, *Eur. J. Med. Chem.*, **2018**, *143*, 1732-1743.
43. A. Wu, Y. Xu, X. Qian, Novel naphthalimide–indomethacin hybrids as potential antitumor agents: Effects of linkers on hypoxic/oxic cytotoxicity and apoptosis-inducing activity, *Monatsh. Chem.*, **2010**, *141*, 893-899.
44. N. S. Rao, N. Nagesh, V. L. Nayak, S. Sunkari, R. Tokala, G. Kiranmai, P. Regur, N.Shankaraiah, A. Kamal, Design and synthesis of DNA-intercalative naphthalimide-benzothiazole/cinnamide derivatives: Cytotoxicity evaluation and topoisomerase-IIα inhibition, *MedChemComm.*, **2019**, *10*, 72-79.
45. R. X. Rong, Q. Sun, C. L. Ma, B. Chen, W. Y. Wang, Z. A. Wang, K. R. Wang, Z. R. Cao, X. L. Li, Development of novel bis-naphthalimide derivatives and their anticancer properties, *MedChemComm.*, **2016**, *7*, 679-685.
46. Y. T. Lu, T. L. Chen, K. S. Chang, C. M. Chang, T. Y. Wei, J. W. Liu, C. A. Hsiao, T. L. Shih, Synthesis of novel C4-benzazole naphthalimide derivatives with potent antitumor properties against murine melanoma, *Bioorg. Med. Chem.*, **2017**, *25*, 789-794.
47. I. Singh, V. Luxami, K. Paul, Synthesis of naphthalimide-phenanthro[9,10-*d*]imidazole derivatives: *In vitro* evaluation, binding interaction with DNA and topoisomerase inhibition, *Bioorg. Chem.*, **2020**, *96*, 103631-103642.
48. I. Singh, V. Luxami, K. Paul, Synthesis and *in vitro* evaluation of naphthalimide–benzimidazole conjugates as potential antitumor agents, *Org. Biomol. Chem.*, **2019**, *17*, 5349-5366.
49. Shalini, Pankaj, S. T. Saha, M. Kaur, E. Oluwakemi, P. Awolade, P. Singh, V. Kumar, Synthesis and *in vitro* anti-proliferative evaluation of naphthalimide–chalcone/pyrazoline conjugates as potential SERMs with computational validation, *RSC Adv.*, **2020**, *10*, 15836-15845.
50. G. B. Liang, J. H. Wei, H. Jiang, R. Z. Huang, J. T. Qin, H. L. Wang, H. S. Wang, Y. Zhang, Design, synthesis and antitumor evaluation of new 1,8-naphthalimide derivatives targeting nuclear DNA, *Eur. J. Med. Chem.*, **2021**, *210*, 112951-112963.
51. V. C. Jordan, B. W. O'Malley, Selective estrogen-receptor modulators and antihormonal resistance in breast cancer, *J. Clin. Oncol.*, **2007**, *25*, 5815-5824.

52. V. C. Jordan, Tamoxifen: A most unlikely pioneering medicine, *Nat. Rev. Drug Discov.*, **2003**, *5*, 205-213.
53. V. M. Quirke, Tamoxifen from failed contraceptive pill to best-selling breast cancer medicine: A case-study in pharmaceutical innovation, *Front. Pharmacol.*, **2017**, *8*, 620-635.
54. M. C. Montoy, D. J. Krysan, Repurposing estrogen receptor antagonists for the treatment of infectious disease, *Am. Soc. Microbiol.*, **2018**, *9*, e02272-18.
55. H. Wiseman, Tamoxifen as an antioxidant and cardioprotectant, *Biochem. Soc. Symp.*, **1995**, *61*, 209-219.
56. N. Pavon, M. B. Chontal, F. Correa, B. Y. Sanchez, J. Belmont, L. H. Esquivel, J. S. R. Zavala, E. Chavez, Tamoxifen inhibits mitochondrial membrane damage caused by disulfiram, *Biochem. Cell Biol.*, **2017**, *95*, 556-562.
57. J. S. Shim, R. J. Li, J. Lv, S. Head, E. J. Yang, J. O. Liu, Inhibition of angiogenesis by selective estrogen receptor modulators through blockade of cholesterol trafficking rather than estrogen receptor antagonism, *Cancer Lett.*, **2015**, *362*, 106-115.
58. T. Thomas, M. A. Gallo, T. J. Thomas, Estrogen receptors as targets for drug development for breast cancer, osteoporosis and cardiovascular diseases, *Curr. Cancer Drug Targets*, **2004**, *4*, 483-499.
59. P. Fan, V. C. Jordan, Acquired resistance to selective estrogen receptor modulators (SERMs) in clinical practice (tamoxifen & raloxifene) by selection pressure in breast cancer cell populations, *Steroids*, **2014**, *90*, 44-52.
60. J. Iqbal, O. M. Ginsburg, T. D. Wijeratne, A. Howell, G. Evans, I. Sestak, S. A. Narod, Endometrial cancer and venous thromboembolism in women under age 50 who take tamoxifen for prevention of breast cancer: a systematic review, *Cancer Treat. Rev.*, **2012**, *38*, 318-328.
61. G. Yang, S. Nowsheen, K. Aziz, A, G. Georgakilas, Toxicity and adverse effects of tamoxifen and other anti-estrogen drugs, *Pharmacol. Ther.*, **2013**, *139*, 392-404.
62. C. J. Fabian, B. F. Kimler, Chemoprevention for high-risk women: Tamoxifen and beyond, *Breast J.*, **2001**, *7*, 311-320.
63. F. F. Gao, J. W. Lv, Y. Wang, R. Fan, Q. Li, Z. Zhang, L. Wei, Tamoxifen induces hepatotoxicity and changes to hepatocyte morphology at the early stage of endocrinotherapy in mice, *Biomed Rep.*, **2016**, *4*, 102-106.

64. H. K. Patel, T. Bihan, Selective estrogen receptor modulators (SERMs) and selective estrogen receptor degraders (SERDs) in cancer treatment, *Pharmacol Ther.*, **2018**, *186*, 1-24.

65. R. D. Snyder, J. E. Brown, Evidence for and role of the dimethylamino group in tamoxifen DNA intercalation in intact Chinese hamster V79 cells, *Drug Chem. Toxicol.*, **2002**, *25*, 473-479.

66. M. S, Christodoulou, N. Fokialakis, D. Passarella, A. N. Garcia-Argaez, O. M. Gia, I. Pongratz, L. D. Via, S. A. Haroutounian, Synthesis and biological evaluation of novel tamoxifen analogues, *Bioorg. Med. Chem.*, **2013**, *21*, 4120-4131.

67. I. Larosche, P. Letteron, B. Fromenty, N. Vadrot, A. Abbey-Toby, G. Feldmann, D. Pessayre, A. Mansouri, Tamoxifen inhibits topoisomerases, depletes mitochondrial DNA, and triggers steatosis in mouse liver, *J. Pharmacol. Exp. Ther.*, **2007**, *321*, 526-535.

68. G. Kaur, M. P. Mahajan, M. K. Pandey, P. Singh, S. R. Ramisetti, A. K. Sharma, Design, synthesis, and anti-breast cancer evaluation of new triarylethylene analogs bearing short alkyl- and polar amino-/amido-ethyl chains, *Bioorg. Med. Chem. Lett.*, **2016**, *26*, 1963-1969.

69. A. B. S. Spitmana, J. J. Swena, V. O. Dezentjec, D. J .A. R. Moesa, H. Gelderbloma, H. J. Guchelaara, Clinical pharmacokinetics and pharmacogenetics of tamoxifen and endoxifen, *Expert Rev. Clin. Pharmacol.*, **2019**, *12*, 523-536.

70. V. Agouridas, I. Laıos, A. Cleeren, E. Kizilian, E. Magnier, J. C. Blazejewskia, G. Leclercqb, Loss of antagonistic activity of tamoxifen by replacement of one *N*-methyl of its side chain by fluorinated residues, *Bioorg. Med. Chem.*, **2006**, *14*, 7531-7538.

71. R. P. Tanpure, A. R. Harkrider, T. E. Strecker, E. Hamel, M. L. Trawick, K. G. Pinney, Application of the McMurry coupling reaction in the synthesis of tri- and tetra-arylethylene analogues as potential cancer chemotherapeutic agents, *Bioorg. Med. Chem.*, **2009**, *17*, 6993-7001.

72. M. S. R. Marty, M. R. Katiki, J. B. Nanubolu, S. Garimella, S. Polepalli, N. Jain, A. K. Buddana, R. S. Prakasham, Synthesis and biological evaluation of novel tamoxifen-1,2,4-triazole conjugates, *Mol. Divers.*, **2016**, *20*, 687-703.

73. S. Husain, S. N. Alvi, R. N. Rao, Separation and determination of *E*- and *Z*-isomers of tamoxifen by ion-pair high-performance liquid chromatography, *Anal. Lett.*, **1994**, *27*, 2485-2497.

74. G. R. Bedford, D. N. Richardson, Preparation and identification of *cis* and *trans* isomers of a substituted triarylethylene, *Nature*, **1966**, 212, 733-734.

75. J. Shani, A. Gazit, T. Livshitz, S. Biran, Synthesis and receptor-binding affinity of fluorotamoxifen, a possible estrogen-receptor imaging agent, *J. Med. Chem.*, **1985**, *28*, 1504-1511.

76. M. R. Boyd, B. K. D. Paull, Some practical considerations and applications of the national cancer institute in vitro anticancer drug discovery screen, *Drug Dev. Res.*, **1995**, *34*, 91-109.

77. J. H. Lee, J. M. Berger, Cell cycle-dependent control and roles of DNA topoisomerase II. Genes, **2019**, *10*, 859-877.

78. S. K. Arepalli, C. Lee, S. Sim, K. Lee, H. Jo, K. Y. Jun, Y. Kwon, J. S. Kang, J. K. Y. Jung, H. Lee, Development of 13*H*-benzo[*f*]chromeno[4,3-*b*][1,7]naphthyridines and their salts as potent cytotoxic agents and topoisomerase I/IIα inhibitors, *Bioorg. Med. Chem.*, **2018**, *26*, 5181-5193.

79. G. Vistoli, A. Pedretti, B. Testa, Assessing drug-likeness-what are we missing?, *Drug Discov. Today*, **2008**, *13*, 285-294.

80. U. K. Prajakta, D. G. Manjunath, K. V. Vivek, *In silico* modeling for the design of 2-substitted benzimidazole derivatives, and prediction of activity as procaspase-3 activators and apoptosis inducer, *Lett. Drug Des. Discov.*, **2017**, *14*, 387-397.

81. C. A. Lipinski, F. Lombardo, B. W. Dominy, P. J. Feeney, Experimental and computational approaches to estimate solubility and permeability in drug discovery and development settings, *Adv. Drug Deliv. Rev.*, **2001**, *46*, 3-25.

82. G. M. Morris, R. Huey, W. Lindstorm, M. F. Sanner, R. K. Belew, D. S. Goodsell, A. J. Olson AutoDock 4.0 and AutoDock Tools 4.0: Automated docking with selective receptor flexibility, *J. Comput. Chem.*, **2009**, *30*, 2785-2791.

83. J. C. Wang, Cellular roles of DNA topoisomerase: A molecular perspective, *Nat. Rev. Mol. Cell Biol.*, **2002**, *3*, 430-440.

84. B. H. Schmidt, N. Osheroff, J. M. Berger, Structure of a topoisomerase II- DNA-nucleotide complex reveals a new control mechanism for ATPase activity, *Nat. Struct. Mol. Biol.*, **2012**, *19*, 1147-1152.

85. J. L. Nittis, Targeting DNA topisomerase II in cancer chemotherapy, *Nat. Rev. Cancer*, **2009**, *9*, 338-350.

86. R. J. Sunil, P. Sarbani, A. Jayashree, Molecular hybridization-An emanating tool in drug design, *Med. Chem.* (Los Angeles), **2019**, *9*, 93–95.
87. C. V. Junior, A. Danuello, V. D. S. Bolzani, E. J. Barreiro, C. A. M. Fraga, Molecular hybridization: A useful tool in the design of new drug prototypes, *Curr. Med. Chem.*, **2007**, *14*, 1829-1852.
88. G. Tan, Y. Yao, Y. Gu, S. Li, M. Lv, K. Wang, H. Chen, X. Li, Cytotoxicity and DNA binding property of the dimers of triphenylethylene–coumarin hybrid with one amino side chain, *Bioorg. Med. Chem. Lett.*, **2014**, *24*, 2825-2830.
89. E. Catanzaro, F. Seghetti, C. Calcabrini, A. Rampa, S. Gobbi, P. Sestili, E. Turrini, F. Maffei, P. Hrelia, A. Bisi, F. Belluti, C. Fimognari, Identification of a new tamoxifen-xanthene hybrid as pro-apoptotic anticancer agent, *Bioorg. Chem.*, **2019**, *86*, 538-549.
90. T. Brider, B. Redko, F. Grynszpan, G. Gellerman, Three overlooked chemical approaches toward 3-naphthalimide amonafide *N*-derivatives, *Tetrahedron Lett.*, **2014**, 55, 6675-6679.
91. M. F. Brana, A. Ramos, Naphthalimides as anti-cancer agents: Synthesis and biological activity. *Curr. Med. Chem., Anti-Cancer Agents*, **2001**, *1*, 237–255.
92. M. J. Ratain, R. Mick, F. Berezin, L. Janisch, R. L. Schilsky, N. J. Vogelzang, L. B. Lane, Phase I study of amonafide dosing based on acetylator phenotype. *Cancer Res.*, **1993**, *53*, 2304-2308.
93. W. Hu, X. S. Huang, J. F. Wu, L. Yang, Y. T. Zheng, Y. M. Shen, Z. Li, X. Li, Discovery of novel topoisomerase II inhibitors by medicinal chemistry approaches *J. Med. Chem.*, **2018**, *61*, 8947-8980.
94. S. K. Maddili, R. Katla, V. K. Kannekanti, N. K. Bejjanki, B. Tuniki, C. H. Zhou, H. Gandham, *Eur. J. Med. Chem.*, **2018**, *150*, 228-247.
95. V. D. Suryawanshi, P. V. Anbhule, A. H. Gore, S. R. Patil, G. B. Kolekar, Spectroscopic investigation on the interaction of pyrimidine derivative, 2-amino-6-hydroxy-4-(3,4-dimethoxyphenyl)-pyrimidine-5-carbonitrile with human serum albumin: Mechanistic and conformational study. *Ind. Eng. Chem. Res.*, **2012**, *51*, 95-102.
96. H. A. Benesi, J. H. Hildebrand, A Spectrophotometric investigation of the interaction of iodine with aromatic hydrocarbons *J. Am. Chem. Soc.*, **1949**, *71*, 2703-2707.
97. J. R. Lakowicz, Principles of fluorescence spectroscopy third ed. Springer, New York, 2006.

98. J. R. Lakowicz, G. Webber, Quenching of fluorescence by oxygen. A probe for structural fluctuations in macromolecules *Biochemistry*, **1973**, *12*, 4161-4170.

99. M. R. Eftink, C. A. Ghiron, Fluorescence quenching studies with proteins. *Anal. Biochem.*, **1981**, *114*, 199-227.

100. G. Scatchard, The attraction of proteins for small molecules and ions. *N. Y Ann, Acad. Sci.*, **1949,** *51*, 660-672.

101. L. Zhao, J. Liu, R. Guo, Q. Sun, H. Yang, H. Li, Investigating the interaction mechanism of fluorescent whitening agents to human serum albumin using saturation transfer difference-NMR, multi-spectroscopy, and docking studies. *RSC Adv.*, **2017**, *7*, 27796-27806.

102. S. D. Ross, M. Finkelstein, R. C. Petersen, Solvent effects in the reactions of *N*-bromosuccinimide with toluene, fluorene and acenaphthene; Evidence for a polar mechanism in propylene carbonate. *J. Am. Chem. Soc.*, **1958**, *80*, 4327–4330.

103. P. H. Grayshan, A. M. Kadhim, A. T. Peters, Heterocyclic derivatives of naphthalene-1,8-dicarboxylic anhydride. *J. Heterocyclic Chem.*, **1974**, *11*, 33-38.

104. A. Irfan, F. Batool, S. A. Z. Naqvi, A. Islam, S. M. Osman, A. Nocentini, S. A. Alissa, C. T. Supuran, Benzothiazole derivatives as anticancer agents, *J. Enzym. Inhib. Med. Chem.*, **2020**, *35*, 265-279.

105. S. Jain, S. Pattnaik, K. Pathak, S. Kumar, D. Pathak, S. Jain, A. Vaidya, Anticancer potential of thiazole derivatives: A retrospective review, *Mini Rev. Med. Chem.*, **2018**, *18*, 640-655.

106.G. Saito, D. Velluto, M. Resmini, Synthesis of 1,8-naphthalimide-based probes with fluorescent switch triggered by flufenamic acid, *R. Soc. Open Sci.*, **2018**, *5*, 172137-172148.

107. D. Srikun, E. W. Miller, D. W. Domaille, C. J. Chang, An ICT-Based approach to ratiometric fluorescence imaging of hydrogen peroxide produced in living cells, *J. Am. Chem. Soc.*, **2008**, *130*, 4596-4597.

108. S. Banerjee, E. B. Veale, C. M. Phelan, S. A. Murphy, G. M. Tocci, L. J. Gillespie, D. O. Frimannsson, J. M. Kelly, T. Gunnlaugsson, Recent advances in the development of 1,8-naphthalimide based DNA targeting binders, anticancer and fluorescent cellular imaging agents, *Chem. Soc. Rev.*, **2013**, *42*, 1601-1618.

109. C. Liu, W. Yang, Q. Gao, J. Du, H. Luo, Y. Liu, C. Yang, Differential recognition and quantification of HSA and BSA based on two red-NIR fluorescent probes, *J. Lumin.*, **2018**, 197, 193-199.

110. S. Huang, F. Li, C. Liao, B. Zheng, J. Du, D. Xiao, A selective and sensitive fluorescent probe for the determination of HSA and trypsin, *Talanta*, **2017**, *170*, 562-568.

111. S. A. Yasrebi, R. Takjoo, G. H. Riazi, HSA-interaction studies of uranyl complexes of alkyl substituted isothiosemicarbazone, *J. Mol. Struct.* **2019**, *1193***,** 53-61

112. B. K. Song, W. H. Nugent, P. F. Moon-Massat, R. N. Pittman, Effects of a hemoglobin-based oxygen carrier (HBOC-201) and derivatives with altered oxygen affinity and viscosity on systemic and microcirculatory variables in a top-load rat model, *Microvasc. Res.*, **2014**, *95*, 124-130.

113 D. J. Zheng, J. Xua, M. M. Su, Z. G. Sun, Q. C. Jiao, Y. S. Yang, H. L. Zhu, A small, steady, rapid and selective TICT based fluorescent HSA sensor for pre-clinical diagnosis, *Sens. Actuators B Chem,*. **2018**, *271***,** 82-89.

114. R. E. Wang, L. Tian, Y. H. Chang, A homogenous fluorescent sensor for human serum albumin, *J. Pharm. Biomed.*, **2012**, *63*, 165-169.

115. Z. Luo, B. Liu, K. Zhu, Y. Huang, C. Pan, B. Wang, L. Wang, An environment-sensitive fluorescent probe for quantification of human serum albumin: Design, sensing mechanism, and its application in clinical diagnosis of hypoalbuminemia, *Dyes Pigm.* **2018**, *152*, 60-66.

116. Y. J. Xu, M. M. Su, H. L. Li, Q. X. Liu, C. Xu, Y. S. Yang, H. L. Zhu, A fluorescent sensor for the discrimination of HSA from BSA through selectivity evolution, *Anal. Chim. Acta*, **2018**, *1043*, 123-131.

117. P. B. Soeters, R. R. Wolfe, A. Shenkin, Hypoalbuminemia: Pathogenesis and clinical significance, *J. Parenter. Enter. Nutr.*, **2019**, *43*, 181-193.

118. A. Akirov, H. M. Iraqi, A. Atamna, I. Shimon, Low albumin levels are associated with mortality risk in hospitalized patients, *Am. J. Med.*, **2017**, *130*, 1465.e11-1465.e19.

119. V. Arroyo, R. G. Martinez, X. Salvatell, Human serum albumin, systemic inflammation, and cirrhosis, *J. Hepatol.*, **2014**, *61*, 396-407.

120. Z. Zhao, X. Li, C. Gao, D. Jian, P. Hao, L. Rao, M. Li, Peripheral blood circular RNA hsa_circ_0124644 can be used as a diagnostic biomarker of coronary artery disease, *Sci. Rep.*, **2017**, *7*, 39918.

121. B. Durie, J. L. Harousseau, J. S. Miguel, J. Blade, B. Barlogie, K. Anderson, M. Gertz, M. Dimopoulos, J. Westin, P Sonneveld, H. Ludwig, G. Gahrton, M. Beksac, J. Crowley, A. Belch, M. Boccadaro, I. Turesson, D. Joshua, D. Vesole, R. Kyle, R Alexanian, G. Tricot, M. Attal, G. Merlini, R. Powles, P. Richardson, K. Shimizu, P. Tosi, G. Morgan, S.V. Rajkumar, International uniform response criteria for multiple myeloma, *Leukemia*, **2006,** *20*, 1467-1473.

122. K. Neelofar, J. Ahmad, An overview of *in vitro* and *in vivo* glycation of albumin: A potential disease marker in diabetes mellitus, *Glycoconj J.*, **2017**, *34*, 575-584.

123. T. Zhu, J. Du, W. Cao, J. Fan, X. Peng, Microenvironment-sensitive fluorescent dyes for recognition of serum albumin in urine and imaging in living cells, *Ind. Eng. Chem. Res.*, **2016**, *55*, 527-533.

124. L. Belayev, O. F. Alonso, P. W. Huh, W. Zhao, R. Busto, M. D. Ginsberg, Posttreatment with high-dose albumin reduces histopatholgical damage and imroves neurological deficit following fluid percussion brain injury in rats, *J. Neurotrauma*, **1999**, *16*, 445-453.

125. A. M. Attar, M. B. Richardson, G. Speciale, S. Majumdar, R. P. Dyer, E. C. Sanders, R. M. Penner, G. A. Weiss, Electrochemical quantification of glycated and non-glycated human serum albumin in synthetic urine, *ACS Appl. Mater. Interfaces*, **2019**, 11, 4757-4765.

126. J. Chesham, S. W. Anderton, C. F. Kingdon, Rapid, competitive enzymoimmunoassay for albumin in urine, *Clin. Chem.*, **1986**, *32*, 669-671.

127. V. J. Alino, K. L. Yang, Using liquid crystals as a readout system in urinary albumin assays, *Analyst*, **2011**, *136*, 3307-3313.

128. N. I. Govorukhina, T. H. Reijmers, S. O. Nyangoma, A. G. J. v. Zee, R. C. Jansen, R. Bischoff, Analysis of human serum by liquid chromatography–mass spectrometry: Improved sample preparation and data analysis, *J. Chromatogr. A*, **2006**, *1120*, 142-150.

129. Z. H. Lin, I. C. Chen, H. T. Chang, Detection of human serum albumin through surface-enhanced Raman scattering using gold ‘‘pearl necklace’’ nanomaterials as substrates, *Chem. Commun.*, **2011**, *47*, 7116-7118.

130. S. E. J. Groisman, C. Byland, H. Gerber, Improved sensitivity of capillary electrophoresis for detection of bisalbuminemia, *Clin. Chem.*, **2000**, *46*, 882-883.

131. M. Cieplak, K. Szwabinska, M. Sosnowska, C. Bikram K. C., P. Borowicz, K. Noworyta, F. Souza, W. Kutner, Selective electrochemical sensing of human serum albumin by semi-covalent molecular imprinting, *Biosens. Bioelectron.*, **2015**, *74*, 960-966.

132. B. T. Doumas, W. A. Watson, H. G. Biggs, Albumin standards and the measurement of of serum albumin with bromocresol green, *Clin. Chim. Acta*, **1997**, *258*, 21-30.

133. S. D. Gan, K. R. Patel, Enzyme immunoassay and enzyme-linked immunosorbent assay, *J. Invest. Dermatol.*, **2013**, 133, e12-e14.

134. S. E. Smith, J. M. Williams, S. Ando, K. Koide, Time-insensitive fluorescent sensor for human serum albumin and its unusual red shift, *Anal. Chem.*, **2014**, *86*, 2332-2336.

135. J. Xiong, X. Cao, S. Yang, Z. Mo, W. Wang, W. Zeng, Fluorescent probes for detetion of protein: From bench to bed protein, *Peptide Lett.*, **2018**, *25*, 548-559.

136. Y. R. Wang, L. Feng, L. Xu, J. Hou, Q. Jin, N. Zhou, Y. Lin, J. N. Cui, G. B. Ge, An ultrasensitive and conformation sensitive fluorescent probe for sensing human albumin in complex biological samples, *Sens. Actuators B Chem.*, **2017**, *245*, 923-931.

137. Y. Tian, X. Li, D. Yin, Development of 4-oxime-1,8-naphthalimide as bioorhogonal turn-on probe for fluorogenic protein labeling, *Chem. Commun.*, **2019**, *55*, 12865-12868.

138. Y. Sun, S. Wei, Y. Zhao, X. Hu, J. Fan, Characterization of the interaction between 4-(tetrahydro-2-furanmethoxy)-*N*-octadecyl-1,8-naphthalimide and human serum albumin by molecular spectroscopy and its analytical application, *Appl. Spect.*, **2012**, *66*, 464-469.

139. H. Cheng, T. Zou, Y. Xu, Y. Wang, A. Wu, J. Dai, Y. Zhang, Y. Liu, Investigations on the interactions between naphthalimide-based anti-tumor drugs and human serum albumin by spectroscopic and molecular modeling methods, *Lumin.*, **2016**, *31*, 88-95.

140. S. Wei, Y. Sun, C. Tan, S. Yan, P. Guo, X. Huc, J. Fana, 4-Alkoxyethoxy-*N*-octadecyl-1,8-naphthalimide fluorescent sensor for human serum albumin and other major blood proteins: Design, synthesis and solvent effect, *Lumin.*, **2013**, 2*8*, 318-326.

141. W. Ma, S. Zhang, Z. Tian, Z. Xu, Y. Zhang, X. Xia, X. Chen, Z. Liu, Potential anticancer agent for selective damage to mitochondria or lysosomes: Naphthalimide-modified fluorescent biomarker halfsandwich iridium (III) and ruthenium (II) complexes, *Eur. J. Med. Chem.*, **2019**, *181*, 111599-111608.

142. M. Duran, M. C. Canbaz, *p*Ka determination of newly synthesized *N*-(benzothiazole-2-yl)-2-(4,5-dimethyl-1-(phenylamino)-1*H*-imidazol-2-ylthio)acetamide derivatives, *Ind. Eng. Chem. Res.,* **2013**, *52*, 8355-8360.

143. K. Rajasekhar, C. J. Achar, T. Govindaraju, Red-NIR emissive probe for selective detection of albumin in urine samples and live cells, *Org. Biomol. Chem.*, **2017**, *15*, 1584-1588.

144. J. Ghuman, P. A. Zunszain, I. Petitpas, A. A. Bhattacharya, M. Otagiri, S. Curry, Structural basis of the drug-binding specificity of human serum albumin, *J. Mol. Bio.,* **2005**, *353*, 38-52.

145. S. Huang, S. Peng, W. Su, Z. Tang, J. Cui, C. Huanga, Q. Xiao, *In vitro* interaction investigation between three Ru(II) arene complexes and human serum albumin: Structural influences, *RSC Adv.*, **2016**, *6*, 47043-47054.

146. S. Yasmeen, Riyazuddeen, F. A. Qais, Unraveling the thermodynamics, binding mechanism and conformational changes of HSA with chromolyn sodium: Multispecroscopy, isothermal titration calorimetry and molecular docking studies, *Int. J. Biol. Macromol.,* **2017**, *105*, 92-102.

147. F. L. Cui, J. Fan, D. L. Ma, M. C. Liu, X. G. Chen, Z. D. Hu, A study of the interaction between a new reagent and serum albumin by fluorescence spectroscopy, *Anal. Lett.,* **2003**, *36*, 2151-2166.

148. M. Mathew, S. Sreedhanya, P. Manoj, C. T. Aravindakumar, U. K. Aravind, Exploring the interaction of bisphenol-S with serum albumins: A better or worse alternative for bisphenol A?, *J. Phys.Chem. B,* **2014**, *118*, 3832-3843.

SUMMARY

Cancer is a cluster of diseases that accounts for the leading cause of mortality globally. The incidence of cancer continues to increase in developing as well as developed countries.[1] According to world health organization report, about 17.0 million cancer cases were diagnosed, and 9.5 million died from cancer worldwide in 2018.[2] It was also estimated that over 19.3 million cases of cancer were diagnosed and that 10 million people died from this disease in 2020.[3] The greatest number of deaths are caused due to lung cancer (18.4%), followed by colorectal cancer (9.2%), liver cancer (8.3%), stomach cancer (7.7%), and female breast cancer (6.9%).[3] These new figures indicated that the incidence of cancer and mortality rate is increasing at an alarming rate. In the past decades, researchers have made considerable progress in the field of drug discovery but inefficient in bringing novel drugs for the clinical evaluation.[4] So, despite of many therapeutic successes, cancer still remains as one of the most promising challenges in the 21st century.

At present, the traditional paradigm in cancer therapy is to target DNA or by inhibiting the pathways which mediate and regulate the cell division or replication and transcription of DNA.[5] Although for cancer drug development in pharmaceuticals, inhibition of TOPO-II enzymes has long attracted interest. Type II topoisomerases regulate DNA topology by making a double-stranded break in one DNA duplex, transporting another DNA segment through this break and then resealing it.[6] A number of genetic factors emerged in cancer therapy, between the susceptibility of cancer cells and lack in autophagic machinery.[7] The efficacy of conventional prescribed antineoplastic drugs is often limited due to their high toxicity to normal cells, acquired resistance after long term administration of drug, difficulty in delivering existing drugs to target sites.[8] To improve drug perfusion, potency and oral bioavailability and to develop a new set of potential target with optimal physiochemical profile, immense efforts have been devoted. Chemotherapeutic agents efficiency and specificity towards cancer cells has also been improved by synthesizing the compounds through systematic strategies and molecular hybridization techniques.[9] In the last decades, the “one drug multiple targets” approach has attracted great attention in drug discovery.[10] Several aromatic and heterocyclic functionalities such as triphenylethylene and naphthalimide analogues have been reported in the literature possessing

excellent anticancer activity.[11,12] So, here we have designed potent drugs using various synthetic approaches.

Keeping in view of above points, the following objectives were designed.

1. To synthesize and characterize triphenylethylene derivatives for anticancer activity.
2. To synthesize and characterize naphthalimide derivatives linked to various aromatic / aliphatic groups.
3. *In vitro* evaluation of synthesized compounds for anticancer activity and to develop their structure-activity relationship.

In the quest for potent anticancer agents, we had designed and synthesized triphenylethylene and naphthalimide analogues. These newly synthesized derivatives were evaluated for their anticancer activity against 60 human cancer cell lines. Further, the mechanism of their cytotoxicity has been explored through TOPO-II inhibition. Moreover, the binding interactions of these moieties with human serum albumin and bovine serum albumin were studied through spectroscopy techniques. To determine the interaction of synthesized derivatives with enzymes/serum albumins, molecular docking studies were also performed.

Chapter 2: Triphenylethylene analogues

2.1 Synthesis

To synthesize triphenylethylene scaffolds, a chemical approach was depicted including McMurry coupling and nucleophilic substitution reaction as shown in **Scheme 1**. Cross-coupled product **3** was easily prepared by the reaction of equimolar amount of **1** with acetophenone (**2**) *via* McMurry reaction, in very good yield (80%). Subsequently, treatment of compound **3** with epichlorohydrin in the presence of potassium carbonate afforded cyclized product **4a** and ring-opened product **4b**. The cyclized and open-chain intermediates **4a** and **4b** were obtained in 3.4:1 and 2:1 ratio of *E*- and *Z*-isomers, respectively. Further, the nucleophilic amination was preceded with intermediate **4a** due to its high reactivity as compared to **4b**. Epoxide **4a** was treated with various primary and secondary amines in acetonitrile at reflux temperature. The epoxy ring was opened up to afford corresponding derivatives **5-19** in quantitative yield of 65-85% with varying ratio of *E*- and *Z*-isomers. The statistical mixture of *E*- and *Z*-stereoisomers of triphenylethylene derivatives was obtained and attempts were made to isolate the *E*- and *Z*-isomers but these were unsuccessful due to same R_f value in different solvent systems.

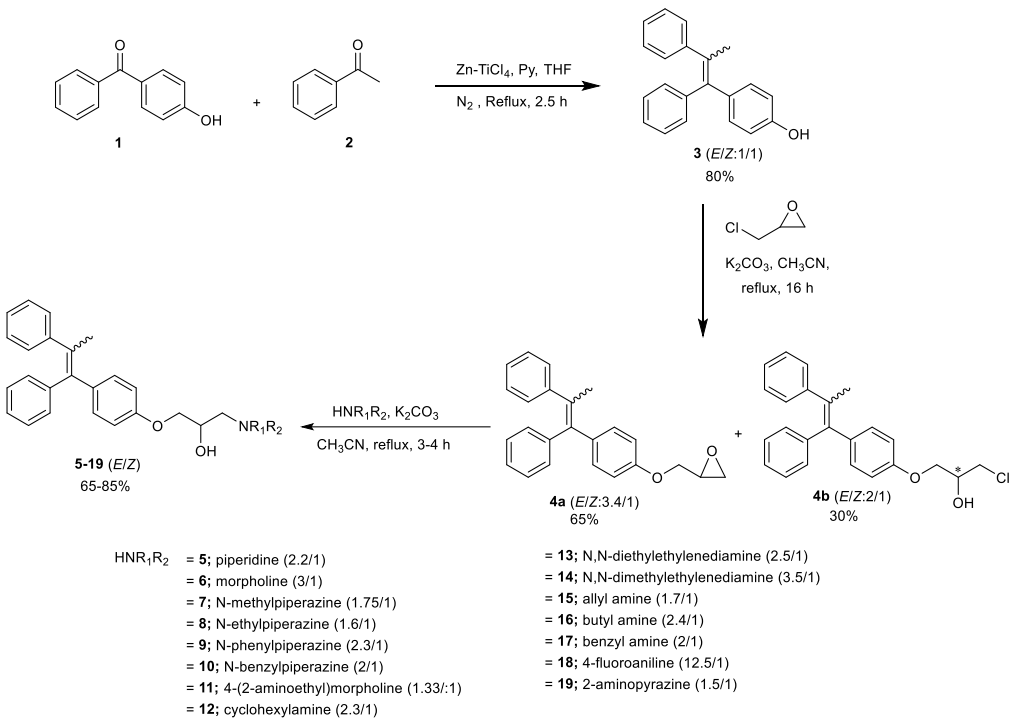

Scheme 1 Synthesis of triphenylethylene analogues with variation of amines (**5-19**) obtained in yield 65 - 85%.

2.2 Characterization

Synthesized triphenylethylene analogues were characterized by NMR and mass spectrometry. The spectrum was recorded on Jeol spectrometer (400 MHz for ^{1}H and 100 MHz for ^{13}C) using $CDCl_3$ as solvent. Mass spectra of synthesized compounds were observed at Water Micromass-Q-T of Micro. Nuclear overhausser effect (NOE) and Co-relation spectroscopy spectrum (COSY) of compound **12** were recorded to assign the *E*/*Z* configuration. The *E*/*Z* ratio of derivatives was confirmed by reverse phase HPLC methodology.

2.3 Biology

2.3.1 *In vitro* antiproliferative activity

The *E*/*Z* derivatives of triphenylethylene series **5-19** were chosen by the National Cancer Institute and the percentages of growth inhibition (% GI) over these cell lines were determined. The analogous with secondary amine substituents were considered to be least effective in the series. Interestingly, derivatives bearing primary amines 4-(2-aminoethyl)morpholine (**11**), cyclohexylamine (**12**), *N*,*N*-diethylethylenediamine (**13**), *N*,*N*-dimethylethylenediamine (**14**) and *N*-butylamine (**16**) render the compounds more active. Compounds **11-13** were evaluated for *in*

vitro antitumor activity against 60 human tumor cell lines at five-dose concentration. It is concluded that compound **11** showed comparable activity as tamoxifen while that compounds **12** and **13** were found to be 2-3 folds more active than tamoxifen. Further, to evaluate the cytotoxic effect of compounds **11**, **12** and **13** on human normal cell line Hek293, a colorimetric assay (MTT assay) was performed. It revealed that the potent compounds **11**, **12** and **13** showed low cytotoxicity against normal cells and selectively kill the cancer cells.

2.3.2 DNA topoisomerase-IIα mediated relaxation activity

To account for possible mechanism of cytotoxicity, the effect of most active compounds **11**, **12** and **13** on relaxation activity of plasmid DNA catalyzed TOPO-IIα was analyzed.

2.4 Physicochemical properties

To determine the properties and drug-like characteristics of compounds **5-19**, we have carried out the theoretical prediction of ADMET parameters using MedChem_designer 5.5 software.

2.5 Molecular docking

Molecular docking studies were performed to understand the intermolecular interactions between topoisomerase-II (PDB code: 1ZXM) and ligands (**11**, **12** and **13**) using AutoDock vina software 4.0 and compare with etoposide.

Chapter 3: Triphenylethylene-naphthalimide conjugates

3.1 Synthesis

A series of triphenylethylene-naphthalimide conjugates was synthesized *via* multistep reactions including molecular hybridization technique (**Scheme 2**). 4-Aminobenzophenone (**1**) was subjected to react with acetophenone *via* McMurry reaction in the presence of Zn and $TiCl_4$ in anhydrous THF to afford cross-coupled product 4-(1,2-diphenylprop-1-en-1-yl)aniline (**2**) in 60% yield. Subsequently, treatment of acenaphthene (**3**) with *N*-bromosuccinimide in DMF at room temperature, furnished intermediate **4** in 97% yield, Further, oxidation of intermediate **4** was accomplished by refluxing of $K_2Cr_2O_7$ in acetic acid to obtain 6-bromo-1*H*,3*H*-benzo[*de*]isochromene-1,3-dione (**5**) in 72% yield. Finally, 6-bromo-2-(4-(1,2-diphenylprop-1-en-yl)phenyl)-1*H*-benzo[*de*]isoquinoline-1,3(2*H*)-di one (**6**) was obtained in quantitative yield on refluxing of compound **2** to a stirred solution of **5** in zinc acetate and ethanol for 15 h. Further, compound **6** was refluxed with primary and secondary amines in the presence of potassium carbonate and DMF for 2-3 h to obtain isomeric products **7-21** in good yields. Attempts were

made to separate *E*- and *Z*-isomers from mixture by column and preparative chromatography were unsuccessful.

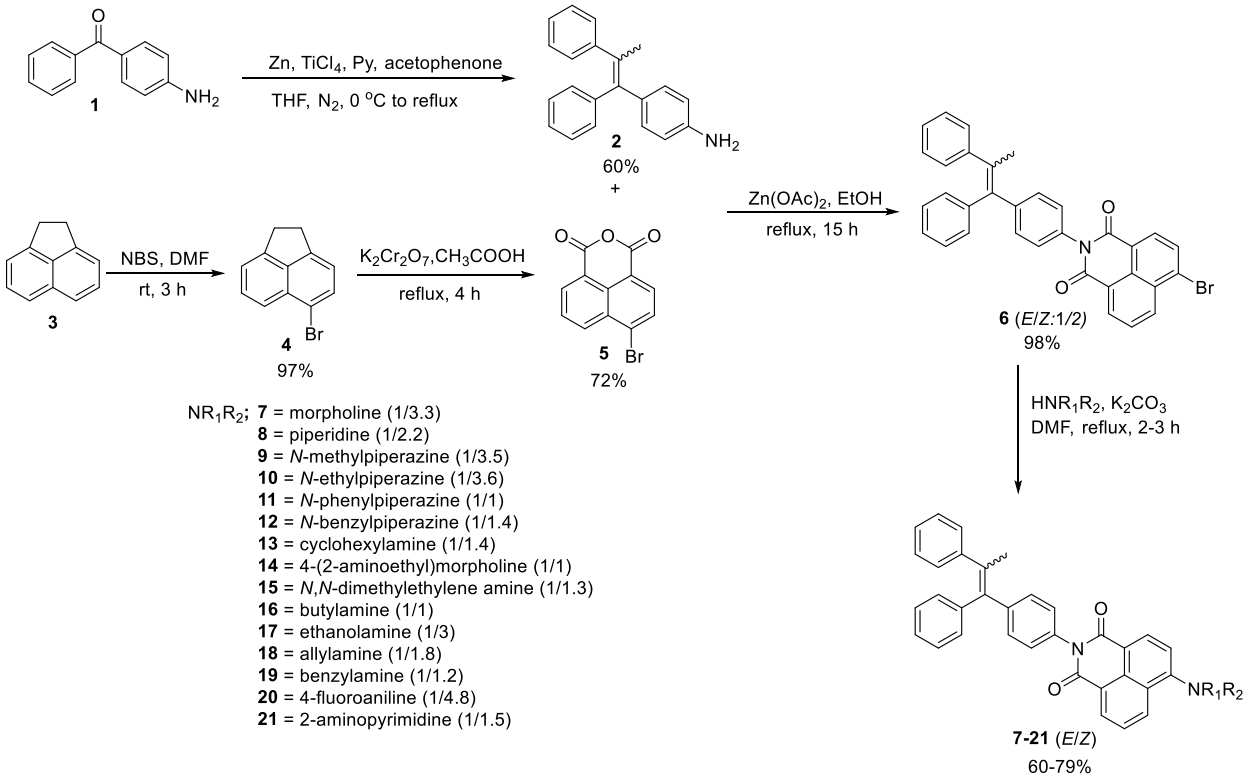

Scheme 1 Synthesis of triphenylethylene-naphthalimide conjugates with variation of amines (**7-21**)

3.2 Characterization

All the synthesiszed compounds were characterized by ^{1}H and ^{13}C NMR, recorded on Jeol spectrometer (400 MHz for ^{1}H and 100 MHz for ^{13}C) using $CDCl_3$ and DMSO-d_6 as solvents. Chemical shifts are reported in parts per million (ppm) with TMS as an internal reference. High Resolution Mass Spectra (HRMS) of the synthesized compounds were observed at Waters Q-TOF of Micromass. The stereochemical assignments of *E*- and *Z*-configurations were given on the basis of Nuclear Overhauser Effect Spectroscopy (NOESY). Reverse-phase high performance liquid chromatography (RP-HPLC) method has been developed for the determination and the separation *E*- and *Z*- isomers of TPE-naphthalimide conjugates.

3.3 Biological Activity

3.3.1 *In vitro* Antiproliferative activity

Preliminary, *in vitro* antiproliferative activity of compounds (*E/Z)* **7-21** at single dose concentration (10 μM) was evaluated against 60 human cancer cell lines by National Cancer Institute (NCI), Bethedsa, USA. Among tested compounds, derivative **7** possessing morpholine group displayed excellent percentage growth inhibition against almost all cancer cell lines. Compound **9** (GI = -9.19%) with methyl piperazine moiety was found to be potent against SR leukemia cancer cell line when compared to amonafide (GI = 91.9%). Compound **7** elicited improve cytotoxic potency towards NCI-H23 (non-small lung), OVCAR-3 (ovarian) and MDA-MB-231 (breast cancer) cell lines in comparison to amonafide. Compound **14** bearing 4-(2-aminoethylene)morpholine was found to be sensitive towards leukemia (K-562, MOLT-4, RPMI-8226, SR), non-small lung (EKVX), colon (HCT-116, HCT- 15), ovarian (OVCAR-4) and breast (MCF-7, T-47D) cancer cell lines with GI > 50%. Analogue **20** with 4-fluoroaniline showed significant activity against leukemia and colon cancer cell lines.

3.3.2 DNA topoisomerase-IIα mediated relaxation activity

To evaluate the mechanism of cytotoxicity of TPE-naph hybrids, we targeted to evaluate the inhibitory effect of analog **7** (with broad-spectrum anticancer activity) on the topoisomerase-IIα using supercoiled pHOT1 plasmid DNA.

3.3.3 Human Serum Albumin (HSA) studies

To analyze the interaction between most active TPE-naph **7** and human serum albumin, *in vitro* studies were carried out *via* UV-visible absorption and fluorescence emission techniques The binding constant (K_b) was calculated using Benesi Hildebrand equation and found to be equal to 1.4×10^4 M^{-1}. It revealed strong binding interaction among HSA and TPE-naph. As well, from the linear plot of regression curve of F_o/F versus [Q], K_{sv} and K_q were calculated to be 6.8×10^4 M^{-1} and 1.6×10^{13} $M^{-1}s^{-1}$, respectively. Fluorescence study suggested that TPE-naph analogue **7** binds with HSA *via* static quenching.

3.3.4 Life-time fluorescence technique

In order to better understanding of quenching mechanism, time-resolved fluorescence experiment was carried out. From steady state and life-time fluorescence experiments, it was inferred that both the static as well as dynamic quenching might be responsible for the interaction of analogue **7** to HSA.

3.4 Molecular docking studies

To better understand the inhibition behavior of *E*- and *Z*-isomers of TPE-naph analogue **7** towards TOPO-II-DNA complex (PDB ID: 5GWK), docking studies were performed using Autodock vina 4.0 software.

Chapter 4: Benzothiazole appended naphthalimides

4.1 Synthesis

A route to synthesize naphthalimide analogues **5-18** has been depicted in **Scheme 1**. On treatment of acenaphthene (**1**) with *N*-bromosuccinamide at room temperature for 2.5 h afforded product **2**. Compound **3** was prepared by refluxing intermediate **2** with potassium dichromate in acetic acid at 110 ^{o}C for 4 h. Further, the key starting material compound **4** was prepared by microwave irradiation of 4-bromonaphthalic anhydride (**3**) with 2-aminobenzothiazole in the presence of zinc acetate and pyridine for 5 min. A Suzuki-Miyaura cross coupling reaction of intermediate **4** with corresponding aryl boronic acids in the presence of $Pd(PPh_3)_4$ and potassium carbonate in acetonitrile under inert atmosphere of argon for 24 h furnished targets **5-16**. Derivatives **17-18** were also synthesized using key intermediate **4** under Buchwald reaction conditions using piperidine or morpholine in the presence of $PdCl_2(PPh_3)_2$ and K_2CO_3 in acetonitrile at reflux temperature for 12 h.

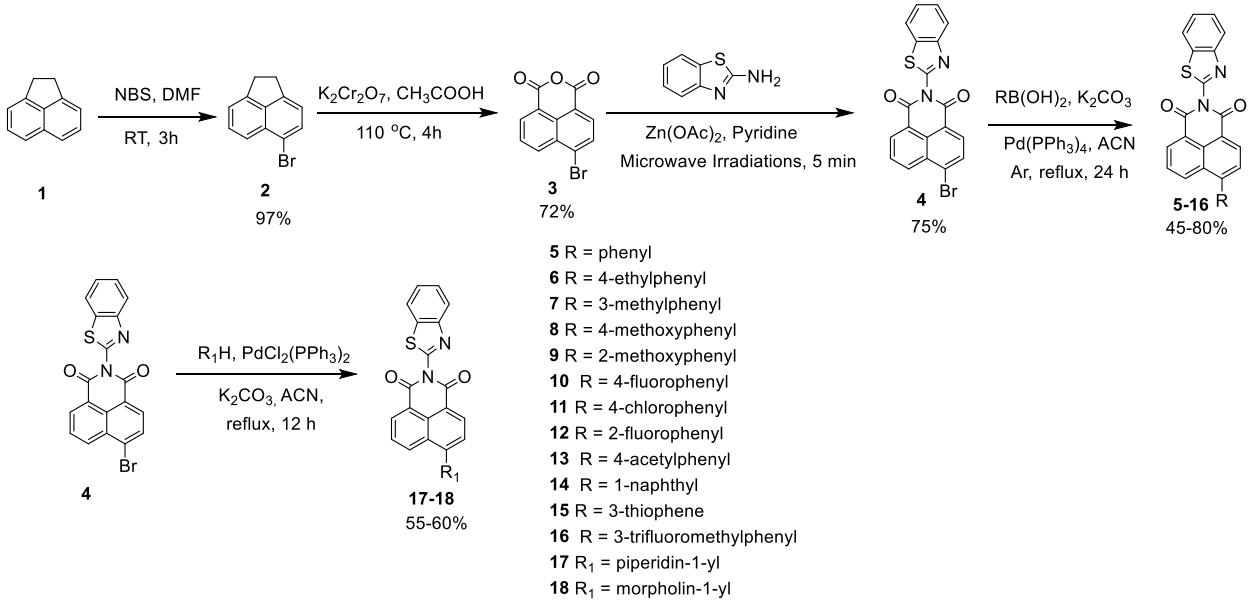

Scheme 1 Synthesis of 2-(benzo[*d*]thiazol-2-yl)-6-subsituted-1*H*-benzo[*de*]isoquinoloine-1,3-(2*H*)-dione

4.2 Characterization

These synthesized compounds were confirmed by ^{1}H and ^{13}C NMR, recorded on Jeol spectrometer (400 MHz for ^{1}H and 100 MHz for ^{13}C) using $CDCl_3$ and DMSO-d_6 as solvents. Chemical shifts are reported in parts per million (ppm) with TMS as an internal reference. Mass spectra of the synthesized compounds were observed at Water Micromass-Q-T of Micro.

4.3 *In Vitro* antiproliferative activity

The cytotoxicity of naphthalimide-benzothiazole derivatives **5-8**, **10-12** and **17-18** against 60 human cancer cell lines at single dose concentration (10 μM) were studied**.** It has been observed that analogue with the appendage of 2-fluorophenyl ring (**12**) showed potent cytotoxicity against leukemia cancer cell line (K-562; GI% = 54.33, SR; GI% = 70.12), colon cancer cell line (HCT-15; GI% = 54.83), melanoma cancer cell line (UAAC-62; GI% = 57.49) and renal cancer cell line (UO-31; GI% = 55.44), which were found to be better than that of 5-fluorouracil. Cytotoxicity of analogue **17** bearing piperidine is slightly increased on comparing with the cytotoxic effect of aryl substitution except compound **12**.

4.4 Serum albumin studies

4.4.1 UV-Visible studies

To determine the influence of EDG and EWG at naphthalimides with binding affinity of HSA and BSA, compound **8** with strong electron-donating group at 4-position and **12** with strong electron-withdrawing group at 2-position of phenyl ring were selected. The UV-visible - absorption spectra of HSA and BSA showed an absorption band at 280 nm. The binding constants calculated for the interaction of HSA were found to be 5.0×10^{4} M^{-1} and 7.9×10^{4} M^{-1} for derivatives **8** and **12**, respectively, while the binding constants with BSA were determined to be 4.3×10^{4} M^{-1} and 6.4×10^{4} M^{-1} for respective compounds **8** and **12.**

4.4.2 Fluorescence emission spectroscopy

The fluorescence spectra of HSA and BSA were recorded on excitation wavelength at 280 nm. The K_q and Ksv were determined using Stern-Volmer equation. The K_q (quenching rate constant) of HSA have been determined to be 3.4×10^{12} and 8.4×10^{12} L mol^{-1} s^{-1} and that of BSA were 2.1×10^{12} and 8.2×10^{12} L mol^{-1} s^{-1} for compounds **8** and **12,** respectively. It demonstrated that the static quenching is accomplished *via* formation of complex between serum albumin and analytes in ground-state. The binding constants were calculated using modified Stern-Volmer equation for interaction of HSA with **8** and **12** and were found to be 1.2×10^{5} and 2.3×10^{5}

L mol^{-1}, respectively. These results indicated the existence of strong binding forces for the interaction between the naphthalimide probe, and HSA/ BSA.

4.4.3 Competitive assay for selectivity

To evaluate the selectivity of compounds **8** and **12** towards HSA and BSA, fluorescence emission spectra of probes **8** (7 μM) and **12** (7 μM) in the presence of various bioanalytes *viz*. HSA, BSA, AMP, ATP, aspartic acid, cysteine, glucose oxidase, glutamic acid, glutathione, histidine, homocysteine, lysine, pepsin, trypsin, urea, Na^+, Ca^{2+}, NH_4^+ and PO_4^{3-} have been recorded.

4.4.4 Drug displacement studies

To determine the specific binding sites for **8** and **12** on HSA, drug displacement studies were performed with two site markers warfarin and ibuprofen.

4.4.5 Circular dichroism studies

To detect changes in confirmation of HSA, the far-UV CD spectrum of 2.5 μM HSA in PBS (0.1 M, *p*H = 7.4) was recorded at wavelength range 200-300 nm in the absence and presence of analogues **8** and **12.**

4.4.6 Fluorescence resonance energy transfer

Försters principle (FRET) is employed to calculate the binding distance (r_o) between donor (HSA) and acceptor (naphthalimide analogues) as the emission band of human serum albumin overlaps with the absorption band of compounds **8** and **12**.

4.4.7 Life-time fluorescence technique

The average fluorescence lifetimes τ_{av} for triexponential iterative fittings were evaluated. It has been indicated that the static mechanism is responsible for the binding interaction of HSA to naphthalimides **8** and **12**.

4.4.8 Sodium dodecyl sulfate studies

It has been revealed that the binding of compounds **8** and **12** to HSA is reversible which showed improved pharmacokinetic properties of these compounds.

4.5 Molecular docking

Molecular docking studies were performed to understand the intermolecular interactions between serum albumins and naphthalimide probes (**8** and **12**) using AutoDock vina software 4.0.

Conclusion

We have successfully designed and synthesized triphenylethylene and naphthalimides analogues using various synthetic approaches. The synthesized compounds were characterized by ^{1}H NMR, ^{13}C NMR and mass spectrometry. These compounds were screened for their *in vitro* anticancer activity towards 60 human cancer cell lines. Many compounds inhibited potent activity towards various cancer cell lines. Structure-activity relationship was studied to find out the activity of these compounds. These compounds were then evaluated for their binding affinity towards HSA. Molecular docking studies demonstrated the existence of various binding forces of these compounds with enzymes/HSA/BSA.

References

1. F. Bray, J. Ferlay, I. Soerjomataram, R. L. Siegel, L. A. Torre, A. Jemal, Global cancer statistics 2018: GLOBOCAN estimates of incidence and mortality worldwide for 36 cancers in 185 countries, *CA Cancer J. Clin.*, **2018**, *68*, 394-424.
2. J. Ferlay, M. Colombet, I. Soerjomataram, C. Mathers, D. M. Parkin, M. Pineros, A. Znaor, F. Bray, Estimating the global cancer incidence and mortality in 2018: GLOBOCAN sources and methods, *Int. J. Cancer*, **2019**, *144*, 1941-1953.
3. WHO Available from :< https://www.who.int/cancer/PRGlobocan2020Final.pdf
4. M. L. Lazaro, Two preclinical tests to evaluate anticancer activity and to help validate drug candidates for clinical trials, *Oncoscience*, **2015**, *2*, 91-98.
5. S. R. Hengel, M. A. Spies, M. Spies, Small-molecule inhibitors targeting DNA repair and DNA repair deficiency in research and cancer therapy, *Cell Chem. Biol.*, **2017**, *24*, 1101-1119.
6. X. Liang, Q. Wu, S. Luan, Z. Yin, C. He, L. Yin, Y. Z. Yuan, L. Li, X. Song, M. He, C. Lv, W. Zhang, A comprehensive review of topoiomerase inhibitors as anticancer agents in the past decade, *Eur. J. Med. chem.*, **2019**, *171*, 129-168.
7. A. Udristioiu, D. Nica-Nadea, Autophagy dysfunctions associated with cancer cells and their therapeutic implications, *Biomed. Pharmacother.*, **2019**, *115*, 108892-108897.
8. S. Wang, W. J. Placzek, J. L. Stebbins, S. Mitra, R. Noberini, M. Koolpe, Z. Zhang, R. Dahl, E. B. Pasquale, M. Pellecchia, Novel targeted system to deliver chemotherapeutic drugs to EphA2-expressing cancer cells, *J. Med. Chem.*, **2012**, *55*, 2427-2436.
9. C. Viegas-Junior, A. Danuello, V. D. S. Bolzani, E. J. Barreiro, C. A. M. Fraga, Molecular hybridization: A useful tool in the design of new drug prototypes, *Curr. Med. Chem.*, **2007,** *14*, 1829-1852.
10. L. Xie, P. E. Bourne, Developing multitarget therapeutics to fine-tune the evolutionary dynamics of cancer ecosystem, *Front. Pharmacol.*, **2015**, *6*, 209-213.
11. Shagufta, I. Ahmad, Tamoxifen a pioneering drug: An update on the therapeutic potential of tamoxifen derivatives, *Eur. J. Med. Chem.*, **2018**, *143*, 515-531.
12. M. D. Tomczyk, K. Z. Walczak, l,8-Naphthalimide based DNA intercalators and anticancer agents. A systematic review from 2007 to 2017, *Eur. J. Med. Chem.*, **2018**, *159*, 393-422.

List of Publications

1. S. Rani, K. Paul, Triphenylethylene analogues: Design, synthesis and evaluation of antitumor activity and topoisomerase inhibitors, *Eur. J. Med. Chem.*, **2020,** *208*, 112775. (**I.F. = 6.514**)
2. S. Rani, V. Luxami, K. Paul, Synthesis of triphenylethylene -naphthalimide conjugates as topoisomerase-IIα inhibitor and HSA binder, *ChemMedChem*, **2021,** *16*, 1822. (**I.F. = 3.466)**
3. S. Rani, K. Raheja, V. Luxami, K. Paul, A Review on Diverse Heterocyclic Compounds as the Privileged Scaffolds in Non-steroidal Aromatase Inhibitors, *Bioorg. Chem.,* **2021,** *113*, 105017. (**I.F. = 5.275)**
4. S. Rani, V. Luxami, K. Paul, A novel target and biomarker benzothiazolyl-naphthalimide probes for precisely and selective detection of serum albumin and anticancer activity. (Under Revision)

Conferences and Workshops

1. Presented a poster in international conference on “Drug Discovery: Biotech and Pharma at Cross Roads” held at Thapar Institute of Engineering and Technology, Patiala, **2018**.
2. Presented a poster in national conference on “Recent Trends in Chemical and Environmental sciences (RTCES)” held at Punjabi University Patiala, **2019**.
3. Presented a poster in Professor Ram Chand Paul symposium on “Emerging Chemical Innovations on Swacch, Swasth and Sarvatra Bharat” held at Panjab University, Chandigarh, **2020**.
4. Workshop on Intellectual Propert Rights and Patenting held at Thapar Institute of Engineering and Technology, Patiala, **2018**.
5. Workshop on “Computational Drug Design using Molecular Docking and Virtual Screening” Thapar Institute of Engineering and Technology, Patiala, **2018**.